

Faculty of Engineering
Department of Civil Engineering



Port Said University

Behavior of Tanks under Static and Cyclic Loading

By

Omar Mohamed Mossad El Gendy

B. Sc. in Civil Engineering
Faculty of Engineering, Suez Canal University, 2008

A Thesis

Submitted for the Partial Fulfillment of the Requirements for the
Degree of Master of Science in Civil Engineering

Under The Supervision of

Prof. Dr. Ibrahim Hassan El Kersh

Prof. of Steel Structures
Dean of Faculty of Engineering
Suez Canal University

Dr. Ibrahim Ahmed El Arabi

Assoc. Prof. of Structural Engineering
Faculty of Engineering
Port Said University

2016

Behavior of Tanks under Static and Cyclic Loading

A Thesis

Submitted for the Partial Fulfillment of the
Requirements for the Degree of
Master of Science
in
Civil Engineering

By

Omar Mohamed Mosad El Gendy
B. Sc. Faculty of Engineering
Suez Canal University, 2008

Under The Supervision of

Prof. Dr. Ibrahim Hassan El Kersh



Prof. of Steel Structures

Dean of Faculty of Engineering

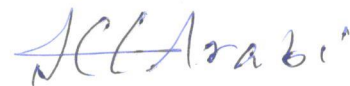
Suez Canal University

Dr. Ibrahim Ahmed El Arabi

Assoc. Prof. of Structural Engineering

Faculty of Engineering

Port Said University



2016

Behavior of Tanks under Static and Cyclic Loading

A THESIS

Submitted in Partial Fulfillment of the
Requirements for the Degree of Master
of Science in Civil Engineering

By

Omar Mohamed Mosad El Gendy
B. Sc. Faculty of Engineering
Suez Canal University, 2008

APPROVED BY

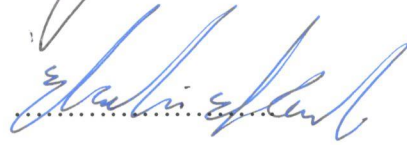
**Prof. Dr. Mostafa Kamel Metwaley
Zedane**

Prof. of Structural Engineering
Faculty of Engineering, Ain Shams
University

.....

Prof. Dr. Ibrahim Hassan Ali El Kersh

Prof. of Steel Structures, Dean of Faculty of
Eng. Suez Canal University

.....

Prof. Dr. Kamal Mohamed Hafez Ismail

Prof. of Soil Mechanics and Foundation
Vice Dean of Faculty of Eng., Suez Canal
University

.....

Dr. Ibrahim Ahmed Ahmed El Arabi

Assoc. Prof. of Structural Engineering
Faculty of Engineering, Port Said University

.....

2016

Abstract

In civil engineering projects, construction on saturated compressible soft soils such as clay and silt is unavoidable. The great problem facing construction on this type of soil is the consolidation settlement, which is a time dependent phenomena. Changes in the soil properties and time dependent loading such as cyclic loading during the consolidation process would affect the rate and amount of the settlement at any particular time.

Cyclic loadings are often applied to clay layers under structures subject to loading and unloading circumstances such as ground water tanks. One of the problems that may be occur is the time-dependent loading and settlement with considering full compatibility between the structure and the soil. In addition, the probability of cracks may take place, which is contrary to the purpose of tanks establishment. Therefore, a numerical analysis based on a cylindrical finite element shell is presented for analyzing circular concrete tanks. The analysis is capable to model circular tanks underlain by multi-layered soil. In addition, a numerical solution for multi-layered soil subjected to any variable stress distribution along the layers height is developed.

In the analysis, the performance of the soil during the consolidation process may be considered as linear, bilinear and nonlinear behavior. The base of the tank may be considered as rigid, elastic or flexible. For analyzing the base of the tank as elastic base, full compatibility between the structure elements and subsoil is taken into account. As a practical application for the developed analysis, a parametric study was carried out to study the behavior of tanks under different variables and conditions using soil data from real sites. The study presents guidelines and diagrams for cylindrical tanks that may be used for this type of soil under static or cyclic loading.

Table of Contents

	Page
Acknowledgement.....	v
Abstract.....	vi
Table of contents	vii
List of Tables.....	x
List of Figures.....	xii
Notations.....	xx
1 Introduction	1
1.1 General	1
1.2 Objectives of the thesis.....	7
1.3 Organization of Thesis	7
2 Literature review	9
2.1 Introduction	9
2.2 Axi-symmetric shells.....	9
2.3 Modeling of foundation-soil interaction.....	11
2.4 Developing the analysis of circular rafts rested on soil.....	12
2.5 Developing models for analyzing cylindrical tanks rested on soil.....	14
2.6 Consolidation of clay under time-dependent and cyclic loading	16
3 Mathematical model.....	21
3.1 Introduction	21
3.2 Finite elements analysis of axi-symmetric shells of revolution	23
3.3 Analysis of water tanks under static loading.....	31
3.4 Analysis of water tanks under cyclic loading.....	51

3.5	Summary of the proposed mathematical models used in the thesis	79
4	Validity of the analysis	85
4.1	Introduction	85
4.2	Tank resting on <i>Winkler's</i> medium.....	86
4.3	Tank with different base thickness resting on half space soil medium	92
4.4	Settlement due to time-dependent loading	98
4.5	Degree of consolidation of clay under trapezoidal cyclic loading	102
4.6	Degree of consolidation of clay under rectangular cyclic loading	105
4.7	Measured settlement of clay under rectangular cyclic loading	107
5	Numerical analysis and discussions of static loads	109
5.1	Introduction	109
5.2	Soil properties and parameters	109
5.3	Effect of the soil type model	120
5.4	Effect of tank location in Port Said	128
5.5	Effect of the thickness of replacement layer on settlement.....	134
5.6	Effect of the roof condition on the flexural behavior of the tank.....	138
6	Numerical analysis and discussions of cyclic loading.....	147
6.1	Introduction	147
6.2	Tanks under time-dependent loading	147
6.3	Tanks under cyclic loading.....	151
7	Conclusions and recommendations.....	188
7.1	Summary.....	188
7.2	Conclusions from the analysis of tanks under static loading	189
7.3	Conclusions from the analysis of tanks under cyclic loading	190

7.4 Recommendations for future works	191
References	192

List of Tables

Table No.	Title	Page
Table 3.1	Numerical calculation methods	31
Table 3.2	Assumptions of cyclic loading model of this study and those of previous studies	82
Table 4.1	Tank material, water unit weight and modulus of subgrade reaction	86
Table 4.2	Comparison between maximum internal forces obtained from analytical solution and those obtained from <i>ELPLA 10</i>	89
Table 4.3	Comparison between maximum internal forces obtained from <i>ABAQUS 6.8</i> and those obtained from <i>ELPLA 10</i>	90
Table 4.4	Tank material and water unit weight.....	93
Table 4.5	Soil data.....	93
Table 4.6	Index and after-compaction properties of the tested soils.....	99
Table 4.7	Data of the test problem	105
Table 4.8	Comparison of the results obtained from <i>LEM</i> with those of <i>VTM</i> ..	106
Table 4.9	Data of Sample number 1	107
Table 5.1	OCR values along the clay layer depth	113
Table 5.2	Maximum allowable safe dimension of tanks in Zone-1	137
Table 5.3	Maximum allowable safe dimension of tanks in Zone-2	137
Table 5.4	Maximum allowable safe dimension of tanks in Zone-3	138
Table 6.1	The time period [days] required to reach <i>SSC</i>	149
Table 6.2	Cyclic loading properties.....	153
Table 6.3	Properties of clay layers for bilinear analysis under cyclic loading..	153
Table 6.4	Properties of clay layer for nonlinear analysis under cyclic loading at Zone-1	154

Table No.	Title	Page
Table 6.5	Properties of clay layer for nonlinear analysis under cyclic loading at Zone-2.....	154
Table 6.6	Properties of clay layer for nonlinear analysis under cyclic loading at Zone-3.....	154
Table 6.7	Effect of loading period to on clay layer behavior	166
Table 6.8	Effect of parameter α_o on clay layer behavior	170
Table 6.9	Effect of parameter β_o on clay layer behavior	174
Table 6.10	Data of the Load-Time schemes for analysis	183

List of Figures

Figure No.	Title	Page
Figure 1.1	Opened concrete storage tank (Wastewater Treatment Plant)	3
Figure 1.2	Concrete storage tank covered with a flat floor	3
Figure 1.3	Concrete storage tank covered with a spherical dome	4
Figure 1.4	Aerial view of two concrete water storage tanks	4
Figure 1.5	Aerial view of wastewater treatment plant	5
Figure 1.6	Cracking in the bottom slab of a circular tank	5
Figure 1.7	Cracks in tanks wall	6
Figure 1.8	Cracking at the wall-base of a circular tank.....	6
Figure 3.1	Aspects treated in <i>ELPLA</i> version 10 [13].....	21
Figure 3.2	Aspects treated in <i>ELPLA</i> version 10 [13].....	22
Figure 3.3	Conical ring shell element.....	24
Figure 3.4	Boundary values for element dimensions	29
Figure 3.5	Tank simulation using thin shell element	30
Figure 3.6	Action between tank base and soil	32
Figure 3.7	Contact pressure distribution for Simple assumption model	33
Figure 3.8	<i>Winkler's</i> model.....	35
Figure 3.9	<i>Winkler/</i> Continuum model.....	39
Figure 3.10	Iteration cycle of the iteration process	41
Figure 3.11	Influence line of elastic displacement in Continuum model.....	42
Figure 3.12	Continuum (elastic base) model.....	43
Figure 3.13	Settlement $s_{i, k}$ of nodal ring i due to contact force Q_k at nodal ring k	44

Figure No.	Title	Page
Figure 3.14	Continuum (rigid base) model	48
Figure 3.15	Continuum (flexible base) model.....	50
Figure 3.16	Stress σ_l under a node k due to a contact pressure q_j at element j	53
Figure 3.17	Constant loading with time	54
Figure 3.18	Linear loading with time	54
Figure 3.19	Behavior of elastic overconsolidated clay ($\sigma'_{max} < \sigma'_{co}$).....	58
Figure 3.20	Behavior of plastic normally consolidated clay ($\sigma'_o > \sigma'_{co}$)	59
Figure 3.21	Consolidation of plastic clay under cyclic loading	61
Figure 3.22	Behavior of <i>NC</i> clay under rectangular cyclic loading	62
Figure 3.23	Determining the value of Δt_N for rectangular cyclic loading	64
Figure 3.24	Rectangular cyclic loading adapted by the superimposing rule.....	65
Figure 3.25	Cyclic loading with virtual times	68
Figure 3.26	Types of cyclic loading	72
Figure 3.27	Effect of the parameter α on the settlement distribution.....	76
Figure 3.28	Available common FE models for such problems	80
Figure 3.29	Axi-symmetric FE shell model used in the present study.....	81
Figure 3.30	Soil representation in this study and that of previous studies	83
Figure 3.31	Settlement in cyclic loading of this study and that of previous studies	84
Figure 4.1	Circular cylindrical tank on isolated springs.....	86
Figure 4.2	Finite element mesh of the tank	87
Figure 4.3	Meridional moment M_s along the wall height.....	88
Figure 4.4	Tangential force N_θ along the wall height.....	88

Figure No.	Title	Page
Figure 4.5	Moment across the base raft M_{base}	89
Figure 4.6	Maximum meridional moment M_s along the wall with varying k_s ...	91
Figure 4.7	Maximum tangential force N_θ along the wall with varying k_s	91
Figure 4.8	Maximum moment M_{base} across the base raft with varying k_s	92
Figure 4.9	Circular cylindrical tank resting on an isotropic elastic soil medium	93
Figure 4.10	Finite element mesh of the tank	94
Figure 4.11	Variation of settlement sbase in the base plate	96
Figure 4.12	Variation of moment M_{base} in the base plate	96
Figure 4.13	Meridional moment M_s along the wall height.....	97
Figure 4.14	Tangential force N_θ along the wall height.....	97
Figure 4.15	Horizontal displacement along the wall height.....	98
Figure 4.16	Loading process for soil A	100
Figure 4.17	Settlement versus time for soil A	100
Figure 4.18	Loading process for soil B	101
Figure 4.19	Settlement versus time for soil B	101
Figure 4.20	Loading scheme used in the present verification	103
Figure 4.21	Influence of T_{vo} on degree of consolidation U	103
Figure 4.22	Influence of α_o on degree of consolidation U	104
Figure 4.23	Influence of β_o on degree of consolidation U	104
Figure 4.24	Degree of consolidation $U(t)$ versus time t for 5 cycles	106
Figure 4.25	Settlement s with time t	108
Figure 5.1	Zones under consideration at Port-Said	110

Figure No.	Title	Page
Figure 5.2	Typical soil properties for Zone-1 (Port-Said west)	112
Figure 5.3	OCR values inferred from strength tests (<i>Pelli/ Rossanese (2000)</i>) for Zone-1	113
Figure 5.4	Typical soil properties for Zone-2 (Port-Said south)	115
Figure 5.5	Typical soil properties for Zone-3 (Port-Said east)	118
Figure 5.6	Position of characteristic point for circular foundation.....	120
Figure 5.7	Geometry of the tank used in the soil model comparison.....	121
Figure 5.8	Finite element mesh of the tank used in the soil model comparison	121
Figure 5.9	Variations of the contact pressure q below the tank base for different soil models	123
Figure 5.10	Variations of the base settlement s_{base} for different soil models...	123
Figure 5.11	Variations of radial moment M_{base} for different soil models	124
Figure 5.12	Radial force across the base N_{base}	125
Figure 5.13	Variations of meridional moment M_s along the wall	126
Figure 5.14	Variations of tangential force N_θ along the wall	127
Figure 5.15	Variations of normal displacement w along the wall	127
Figure 5.16	Geometry of the tank used to compare the results of tank location	128
Figure 5.17	FE mesh of the tank used to compare the results of tank location..	128
Figure 5.18	Variations of the contact pressure q below the tank for different zones	130
Figure 5.19	Variations of the base settlement s_{base} for different zones	130
Figure 5.20	Variations of the radial moment M_{base} for different zones.....	131
Figure 5.21	Variations of the radial Normal force N_{base} for different zones	131

Figure No.	Title	Page
Figure 5.22	Variations of meridional moment M_s along the wall for different zones	133
Figure 5.23	Variations of tangential force N_θ along the wall for different zones	133
Figure 5.24	Variations of normal displacement w along the wall.....	134
Figure 5.25	Effect of replacement thickness in Zone-1 on the variations of the settlement at base center s_c	135
Figure 5.26	Effect of replacement thickness in Zone-2 on the variations of the settlement at base center s_c	136
Figure 5.27	Effect of replacement thickness in Zone-3 on the variations of the settlement at base center s_c	136
Figure 5.28	Tank covered with flat or spherical roof.....	139
Figure 5.29	Finite element mesh of the two covered tanks	139
Figure 5.30	Contact pressure q distribution under the tank base	140
Figure 5.31	Settlement of the base s_{base}	141
Figure 5.32	Moment across the base M_{base}	141
Figure 5.33	Radial force across the base N_{base}	142
Figure 5.34	Meridional moment M_s along the wall height.....	143
Figure 5.35	Tangential force N_θ along the wall height.....	143
Figure 5.36	Moment across the roof M_{Roof}	145
Figure 5.37	Membrane forces across the roof N_θ, N_ϕ	145
Figure 5.38	Vertical displacement of the roof \bar{u}	146
Figure 6.1	Loading scheme of the own weight	148
Figure 6.2	Degree of consolidation of linear analysis U with time.....	149

Figure No.	Title	Page
Figure 6.3	Degree of consolidation of nonlinear analysis U_p with time	150
Figure 6.4	Degree of consolidation of nonlinear analysis U_s with time.....	150
Figure 6.5	Time variation of linear settlement of the clay layer at the base center s_{co} due to unit load.	151
Figure 6.6	The main types of cyclic loading with variables t_o , α_o and β_o	152
Figure 6.7	Geometry of the tank subjected to cyclic loading.....	153
Figure 6.8	Degree of consolidation U in Zone-1	156
Figure 6.9	Settlement s at the center of the flexible base in Zone-1	156
Figure 6.10	Settlement s at the characteristic point of the flexible base in Zone-1.....	157
Figure 6.11	Isochrones for excess pore water pressure u with time in Zone-1 ..	157
Figure 6.12	Degree of consolidation U in Zone-2.....	159
Figure 6.13	Settlement s at the center of the flexible base in Zone-2	159
Figure 6.14	Settlement s at the characteristic point of the flexible base in Zone-2.....	160
Figure 6.15	Isochrones for excess pore water pressure u with time in Zone-2 ..	160
Figure 6.16	Degree of consolidation U in Zone-3.....	161
Figure 6.17	Settlement s at the center of the flexible base in Zone-3	162
Figure 6.18	Settlement s at the characteristic point of the flexible base in Zone-3.....	162
Figure 6.19	Isochrones for excess pore water pressure u with time in Zone-3 ..	163
Figure 6.20	Bilinear degree of consolidation U in Zones under consideration..	164
Figure 6.21	Bilinear settlement s_{co} at the flexible base center	165
Figure 6.22	Bilinear settlement s_{co} at the characteristic point.....	165

Figure No.	Title	Page
Figure 6.23	Influence of t_o on the degree of consolidation U in Zone-1	167
Figure 6.24	Influence of t_o on the degree of consolidation U in Zone-2.....	167
Figure 6.25	Influence of t_o on the degree of consolidation U in Zone-3.....	168
Figure 6.26	Influence of t_o on the settlement s_{co} at the flexible base center in Zone-1.....	168
Figure 6.27	Influence of t_o on the settlement s_{co} at the flexible base center in Zone-2.....	169
Figure 6.28	Influence of t_o on the settlement s_{co} at the flexible base center in Zone-3.....	169
Figure 6.29	Influence of α_o on the degree of consolidation U in Zone-1	171
Figure 6.30	Influence of α_o on the degree of consolidation U in Zone-2.....	171
Figure 6.31	Influence of α_o on the degree of consolidation U in Zone-3.....	172
Figure 6.32	Influence of α_o on the settlement s_{co} at the flexible base center in Zone-1.....	172
Figure 6.33	Influence of α_o on the settlement s_{co} at the flexible base center in Zone-2.....	173
Figure 6.34	Influence of α_o on the settlement s_{co} at the flexible base center in Zone-3.....	173
Figure 6.35	Influence of β_o on degree of consolidation U in Zone-1	175
Figure 6.36	Influence of β_o on degree of consolidation U in Zone-2.....	175
Figure 6.37	Influence of β_o on degree of consolidation U in Zone-3.....	176
Figure 6.38	Influence of β_o on the settlement s_{co} at the flexible base center in Zone-1.....	176
Figure 6.39	Influence of β_o on the settlement s_{co} at the flexible base center in Zone-2.....	177

Figure No.	Title	Page
Figure 6.40	Influence of β_o on the settlement s_{co} at the flexible base center in Zone-3.....	177
Figure 6.41	Load-Time scheme used in Zone-1.....	178
Figure 6.42	Variations of the contact pressure q	179
Figure 6.43	Variations of the base settlement s_{base}	180
Figure 6.44	Variations of radial moment M_{base}	180
Figure 6.45	Radial force across the base N_{base}	181
Figure 6.46	Variations of meridional moment M_s along the wall.....	182
Figure 6.47	Variations of tangential force N_θ along the wall.....	182
Figure 6.48	Load-Time scheme for rectangular cyclic loading.....	183
Figure 6.49	Variations of the contact pressure q at SSC for different Load-Time schemes.....	184
Figure 6.50	Variations of the base settlement s_{base} at SSC for different Load-Time schemes.....	185
Figure 6.51	Variations of radial moment M_{base} at SSC condition for different Load-Time schemes.....	185
Figure 6.52	Radial force across the base N_{base} at SSC condition for different Load-Time schemes.....	186
Figure 6.53	Variations of meridional moment M_s along the wall at SSC for different Load-Time schemes.....	186
Figure 6.54	Variations of tangential force N_θ along the wall at SSC for different Load-Time schemes.....	187

Notations

x, y, s	Local coordinates for a conical shell element in three dimensions, [m].
x, s	Local coordinates for a conical shell element in two dimensions, [m].
r, z	Cylindrical polar coordinates, [m].
φ	The inclination angle of the conical shell element about the vertical axis, [°].
L, t	Length and thickness of conical shell element, respectively, [m].
A	Area, [m ²].
E	Modulus of elasticity in tension and compression, [kN/ m ²].
D	Flexural rigidity of the shell, [kN.m].
ν	<i>Poisson's</i> ratio, [-]
$\gamma_c, \gamma_s, \gamma_w$	Weight per unit volume for reinforced concrete, soil and water, respectively, [kN/ m ³].
u, v, w	Meridional, tangential and normal displacement components, respectively, [cm].
$\chi_s, (dw/ ds)$	Rotation in meridional direction for a conical shell element, [rad].
\bar{u}, \bar{w}	Axial and horizontal displacement components for a conical shell element, respectively, [cm].
F_z, F_r	Load per unit length components in axial and radial directions in a cylindrical coordinate system, respectively, [kN/ m].
N_s, N_θ	Meridional and tangential normal forces per unit length in the axial and the circumferential directions of a cylindrical shell, respectively, [kN/ m].
M_s, M_θ	Meridional and tangential bending moments per unit length in the axial and the circumferential directions of a cylindrical shell, respectively, [kN.m/ m].
Q_s, Q_θ	Transverse shearing forces per unit length parallel to the radial axis in an axial section and a section perpendicular to the axis of a cylindrical shell, respectively, [kN/ m].
K_{ij}	The overall stiffness matrix element of the structure.
k'_{ij}	The individual values of the elements of local stiffness matrices.
q_i	The contact pressure around the nodal ring i , [kN/ m ²].
r_{i1}, r_{i2}	the outer and inner radii of the annular element i , respectively, [m].

Q_i	Equivalent force at the nodal ring i , [kN].
A_i	Annular area corresponding to the nodal contact i , [m ²].
N	Resultant force on the tank, [kN].
A_b	Area of the tank base, [m ²].
$k_{s i}$	The modulus of subgrade reaction at the nodal ring i , [kN/ m ³].
s_i	The settlement at the nodal ring i , [m].
η	The accuracy of the analysis, which is represented by the difference between settlement calculated from the soil and the tank at the same nodal ring. [-].
$c_{i, k}$	The flexibility coefficient, [m/ kN].
w_o	Rigid body translation of the raft at the centroid, [m].
χ_o	Rigid body rotation of the raft at the centroid, [m].
E_s	Modulus of compressibility in loading and constant load phases, [kN/ m ²].
C_c, C_r, C_s	Compression, recompression and swelling indices, [-].
γ_{sat}	Saturated unit weight of the soil, [kN/m ³].
Z	The depth calculated in the clay layer from the surface, [m].
w	Water content, [%].
I_P	Plasticity Index, [%].
I_L	Liquidity Index, [-].
OCR	Over-consolidation ratio, [-].
C_v, C_{vr}	The coefficient of consolidation in the vertical direction for loading and unloading phases, respectively, [kN/m ²].
k_v	Coefficient of permeability, [m/ yr].
m_v, m_r	Coefficient of volume change for loading and reloading, respectively, [m ² /kN].
ξ	The ratio between the stress due to the tank to the initial vertical effective stress, [-]
L_D	The limit depth, [m].
d, a, t, H	Tank diameter, radius, thickness and height, [m].
H_c	Clay layer thickness, [m].
H_d	Length of the drainage pass, [m].
S_{base}	Settlement at the base, [cm]

k_s	Modulus of subgrade reaction, [kN/ m ³].
M_{base}	Radial bending moment at the base of the tank per unit length, [kN.m/ m].
A_j	Area around node j , [m ²].
D_j	The elements of the diagonal square matrix $[D]$ at $t \geq t_c$.
D^*_j	The elements of the diagonal square matrix $[D^*]$ at $t \leq t_c$.
e_i	Void ratio at time t of layer i , [-].
$f_{l,j}$	Stress coefficient of node l due to contact force at node j on the surface, [1/m ²].
h_i	Thickness of layer i , [m].
m, m_i	Number of grid nodes and number of sub-layers in a layer i , [-].
n	Number of function terms (Number of studied nodes).
Q_j	Contact force at node j , [kN].
r	Total number of studied nodes of clay layers, [-].
t	Time in real time scale, [Days].
t'	Virtual time corresponding to real time t , [Days].
Δt_N	Time portion for cycle number N in the real time scale, [Days].
$T_{vi}, T_{vc i}$	Time factor for layer i at times t and t_c , respectively, [-].
T'_{vi}	Time factor for layer i at time t in the virtual time scale, [-].
ΔT_N	The time factor of time Δt_N for cycle number N in the real time scale, [-].
$u(z, t)$	Excess pore water pressure at any vertical depth z and time t , [kN/m ²].
U_p, U_s	Degree of consolidation at the required time t in terms of stress and settlement, respectively, [%].
z_i	Vertical coordinate of layer i , [m].
σ'_i	Effective stresses at time t of layer i , [kN/m ²].
$\sigma'_{o i}$	Initial effective stresses at the middle of layer i , [kN/m ²].
σ'_{ci}	Preconsolidation pressure of a layer i , [kN/m ²].
ω_j	Index of the exponential functions in matrix $[E_v]$.
Δu_i	Average excess pore water pressure at time t in layer i , [kN/m ²].
Δz_i	Depth increment in sub-layer i , [m].
$\Delta \sigma'_i$	Increment of vertical stress at time t in a layer i , [kN/m ²].

$\Delta\sigma(t)_i$	The average stress in a layer i at time t .
α	Coefficient of volume change parameter, [-].
α_o	Loading and unloading parameter, [-].
β	Virtual time factor or coefficient of consolidation parameter, [-].
β_o	Cycle parameter, [-].
t_o	Time length of the subjected load, [Days].
N	Number of cycles, [-].

Chapter 1

1 Introduction

1.1 General

Reinforced concrete cylindrical tanks are very commonly used to store liquids such as water reservoirs and wastewater plants (Figure 1.3 to Figure 1.5). Most of these tanks are either carried up to some depth into the soil or rest on top of the soil, and both problems are generally treated the same way for analysis. Design codes of practice provide methods to calculate design forces in the wall and base plate of such tanks. These methods neglect self-weight of the tank material and assume extreme, namely fixed and hinged conditions for the wall bottom. However, when founded on deformable soil, the actual condition at the wall bottom is neither fixed nor hinged. Further, the self-weight of the tank does affect the design forces. Analytical methods based on fundamental equations of shells were presented by many authors. Numerical methods of analyses using finite elements taking into account soil structure interaction were also introduced. Some of these methods represent the soil as isolated springs depending on *Winkler's* assumption. Others, treat the soil as isotropic elastic half space medium. Soil in reality consists of many layers with different soil materials. Thus, it is required to offer better insight of the combined effect of deformable soil and base plate stiffness on the design forces induced in such cylindrical concrete tanks. The most common problem with concrete storage tanks is the leakage caused by fractures at the base, the wall and the junction between the wall and the base (Figure 1.6, Figure 1.7 and Figure 1.8 respectively).

To avoid such failure both the interactions between the soil and the base foundation, and between the base foundation and superstructure (the tank wall) must be considered for the analysis and design of such storage tanks. Depending on the rigidities of the foundation-soil system and the tank wall, a high concentration of moment may occur at the junction between the foundation and the wall or at the center of the base plate, which if not accounted for may lead to a failure at this interface.

Other point of view which should be taken into consideration for circular concrete tanks rested on layered soil containing saturated clay layers, is the cyclic loading of filling and emptying of tanks with liquids. Since the settlement of the saturated fine grain soil layers is a time dependent phenomenon, changes in the soil properties and time dependent loading such as cyclic loading during the consolidation process would affect the rate and value of the settlement at any particular time. The clay state if normally or overconsolidated under cyclic loading should be taken into consideration, where the behavior of clay is different in one case from the other. Besides, cyclic loading type (rectangular, triangular, and trapezoidal) has a great effect on the settlement changes with time.

All previous studies that presented analytical or semi-analytical methods for cyclic loading on soil had considered the initial pore water pressure distribution along the soil height as uniform for simplicity. Most of these studies have focused on overconsolidated clay, where the case of the normally consolidated clays under cyclic loadings, consolidation computation will be more complicated and the solution for consolidation partial differential equation will be more difficult too.

The present thesis deals with the behavior of structures such as:

- 1- Water storage tanks
- 2- Thermal energy tanks that are used in hospitals, schools, universities, gas plants ... etc.
- 3- Tanks used in wastewater treatment plant which consists of a system of tanks, are often constructed near the sea for discharging the wastewater to the sea.

The analysis in this thesis will focus on available soil properties of soft clay layers. These parameters are required for analyzing tanks of different geometries by different soil models taking into account cycling loading.

A numerical model for analyzing cylindrical tanks using cylindrical finite element shells with different subsoil models was developed. Then, a parametric study was carried out to study the behavior of cylindrical tanks under different variables and conditions. Full compatibility among the tank wall, tank base and the soil is considered in the analysis. The study presented guidelines and diagrams for cylindrical tanks under static and cyclic loading. To achieve this task, the soil data of three different zones were considered. These zones are suitable for constructing these types of tanks.



Figure 1.1 Opened concrete storage tank (Wastewater Treatment Plant)

(<http://wastewatertreatmentplants.wordpress.com>)



Figure 1.2 Concrete storage tank covered with a flat floor

(<http://www.dntanks.com/concrete-storage-tank-galleries.htm>)



Figure 1.3 Concrete storage tank covered with a spherical dome

(<http://www.dntanks.com/concrete-storage-tank-galleries.htm>)



Figure 1.4 Aerial view of two concrete water storage tanks

(<http://www.dntanks.com/concrete-storage-tank-galleries.htm>)



Figure 1.5 Aerial view of wastewater treatment plant

(<http://www.newton.pt/pt/blog/201111/analise-depositos-circulares-betao-grandes-dimensoes.aspx>)



Figure 1.6 Cracking in the bottom slab of a circular tank

(<http://www.newton.pt/pt/blog/201111/analise-depositos-circulares-betao-grandes-dimensoes.aspx>)



Figure 1.7 Cracks in tanks wall

(http://crystalclearqld.com.au/water-tank-repairs/concrete_tank)



Figure 1.8 Cracking at the wall-base of a circular tank

(<http://www.newton.pt/pt/blog/201111/analise-depositos-circulares-betao-grandes-dimensoes.aspx>)

1.2 Objectives of the thesis

The main aim of the present research is to study the behavior of circular storage tanks rested on soil under static and cyclic loading considering the compressibility parameters of the soil. To achieve the above aim, the following studies have been carried steps:

- 1- Choosing a suitable numerical model to analyze circular storage concrete tanks considering soil-structure interaction.
- 2- Compiling available subsoil information to get the soil parameters. Those can be used in numerical analysis of circular storage tanks.
- 3- Presenting the effect of cyclic loading on the consolidation process whatever the distribution of the initial stress is.
- 4- Carrying out a parametric study to evaluate the effects of tank height, diameter, the roof condition (flat, spherical, without roof), replacement layer thickness and the zone of construction on the internal forces and settlements under static loading.
- 5- Carrying out a parametric study to evaluate the effect of the duration of loading-unloading-no loading phases, soil model type (linear or nonlinear), soil state (normally or overconsolidated), cyclic loading type (rectangular, triangular, trapezoidal) and the zone of construction on the consolidation rate and settlements under cyclic loading.

1.3 Organization of Thesis

The thesis contains seven chapters as follow:

Chapter (1): Introduction.

It presents a brief summary of the contents of each chapter.

Chapter (2): Literature review.

It presents some of the available literature related to the scope of the thesis. This chapter presents general idea about axi-symmetric shells of revolution theories, modeling of foundation-soil interaction, methods of analyzing circular rafts and tanks rested on soil, and finally consolidation of clay under time-dependent and cyclic loading.

Chapter (3): Mathematical model.

It describes mathematical models used in the analysis, including: the bases of analysis of axi-symmetric shells using FEM for representing the tank wall and base, the available models that represent the soil and used for analyzing tanks under cyclic loading. *ELPLA* 10 [12] program was used in the analysis in this

thesis after adding the FE axi-symmetric shells model and the soil model used for analyzing tanks under cyclic loading after the agreement of the program developer.

Chapter (4): Validity of the analysis.

This chapter presents a set of verification examples to test the accuracy of the mathematical models used in the analysis. Verifications on both static and cyclic loadings are presented.

Chapter (5): Numerical analysis and discussions of static loading.

In this chapter, numerical parametric study is presented, through the analysis of cases with different parameters such as the tank height, diameter, the roof condition (flat, spherical, without roof), replacement layer thickness and the zone of construction to investigate its effect on the internal forces and settlements under static loading.

Chapter (6): Numerical analysis and discussions of cyclic loading.

In this chapter, a parametric study is presented, through the analysis of cases with different parameters such as the tank height, diameter, the duration of loading-unloading-no loading phases, soil model type (linear or nonlinear), soil state (normally or overconsolidated), cyclic loading type (rectangular, triangular, trapezoidal) and the zone of construction to investigate its effect on the consolidation rate and settlements under cyclic loading.

Chapter (7): Conclusions and recommendations.

The summary, conclusions, guide lines and recommendations derived from studies were presented in this chapter followed by some recommendation for future work.

Chapter 2

2 Literature review

2.1 Introduction

This Thesis highlights the circular concrete tanks resting directly on soil, where a Finite Element model for axisymmetric shells is developed to represent the wall and base of tanks. This Finite element model converts the axisymmetric shells problem from a 3-D problem to a 2-D where the out of plane displacement is neglected. On the other hand the soil is represented using continuum layered model with more realistic soil parameters to get accurate results for soil-structure interaction problems. The tanks were analyzed under static and cyclic loading to study the consolidation rate and settlement of tanks. In this chapter, a brief historical outlines of the development of theories used to achieve this study is presented.

2.2 Axi-symmetric shells

The most common shell theories are those based on linear elasticity concepts. Linear shell theories predict adequately stresses and deformations for shells exhibiting small elastic deformations. It is assumed that the equilibrium equation conditions for deformed shell surfaces are the same as if they were not deformed. There are two different classes of shells: *thick shells* and *thin shells*. A shell is called thin if the maximum value of the ratio t/R (where R is the radius of curvature of the middle surface) can be neglected in comparison with unity. Thin shells are modeled as 2 dimensional structures, where the geometry is fully defined by the shape of the middle surface and the thickness.

2.2.1 Linear thin shell theories

The study of shells of revolution is divided into two separate theories; *membrane theory* and *bending theory*. The two theories describe the in plane membrane forces and the effects of edge disturbances, respectively. In certain cases, the stress and deformation states of the shell can be determined solely by the membrane solution. However, *membrane theory* cannot, in all instances, provide solutions compatible with the actual conditions of deformation. For most practical purposes both theories are required to capture the total load-carrying behavior of the shells. Hence a total analytical solution consists of a combination of the two theories. *Ventsel* and *Krauthammer* (2001) presented a historical brief outlines of development of the linear shell theories in the nineteenth and twentieth centuries. The coming references for axi-symmetric shells were cited from *Ventsel* and *Krauthammer* (2001). The problem of shell was first attacked from the point of view of the three-dimensional equations of linear elasticity by *H. Aron* (1874). His analysis contained some questionable approximations.

The first adequate linear theory of elastic thin shells was given by *Love* (1888) and is also described in detail in *Love's* famous treatise on the mathematical theory of elasticity. *Love* employs certain special assumptions analogous to *Kirchhoff's* (1850); these assumptions are sometimes referred to as the *Kirchhoff-Love* assumptions. The *Love's* theory of thin elastic shells is also referred to as the first order approximation shell theory.

Reissner (1912) presented a classical formulation of the bending problems for a shell of revolution and studied a spherical shell under axisymmetric bending.

Meissner (1915) was able to generalize *Reissner's* results to symmetrical deformation of shells of revolution of an arbitrary shape and having a variable thickness.

Flügge (1932) derived the governing differential equations for circular cylindrical shells in terms of displacements.

Flügge (1934) and *Byrne* (1944) independently developed a more general set of shell equations by retaining all the first approximation assumptions of *Love* on thinness.

Reissner (1941) developed the linear theory of thin shells where some inadequacies of *Love's* theory were eliminated.

Parkus (1951) derived the equations for a cylinder of an arbitrary cross section.

Hoff (1955) analyzed circular conical shells under an arbitrary loading.

Sanders (1959) also developed the first order approximation shell theory from the principle of virtual work and by applying the *Kirchhoff-Love* assumptions.

Timoshenko's theory (1959) of thin shell was very close to the *Love's* theory.

It should be noted that radial simplifications underlying the relations and equations of the general theory of cylindrical shells were introduced by *Donnel* (1976), *Dishinger* (1935), *Hoff* (1954), and *Vlasov* (1964).

Novozhilov (1964) derived the governing differential of the general theory of cylindrical shells of an arbitrary shape using complex variables and pointed out some possible simplifications of these equations.

2.2.2 Analysis of axi-symmetric shells using the FEM

The first approach to the finite element solution of axi-symmetric shells was presented by *Grafton* and *Strome* (1963). In this approach, the element are simple conical frustra and a direct approach via displacement functions is used.

Refinements in the derivation of element stiffness are presented in *Popov et al. (1964)*; *Jones and Strome (1966)*, were elaborated in *Percy et al. (1965)*.

In axi-symmetric shells, in common with all other shells, both bending and in-plan or membrane forces will occur. These will be specified uniquely in terms of the generalized strains, which now involve extensions and curvatures of the middle surface. If the displacement of each point of the middle surface is specified, such strains and the internal stress resultants or simply stresses can be determined by formulae available in standard texts dealing with shell theory.

2.3 Modeling of foundation-soil interaction

Foundation is the base of the structure that transmits its loads to the soil. Usually, foundation is strained with action moments and forces. Although every structure is founded on soil, most of the practical analyses of the structure and its foundation, do not take into account the influence of the subsoil behavior below or around the foundation. In times, when there no computers were available, simplified methods were used. The methods consider as low as possible computation effort to receive the results with acceptable accuracy. In some publications, such as that of *Kany (1974)*, extensive and refined calculation methods were proposed and applied only for few cases in the practice.

Computers with programming and memory possibilities are developed increasingly. This result is revolutions of the calculation practice. Now the programming and extensive computation effort can expand considerably to achieve the results as perfect as possible to the reality. These methods are considered particularly for the analysis of mostly deformation-sensitive large structures.

The subsoil models for analysis of foundations (standard models) can be divided into three main groups:

- Simple assumption model,
- *Winkler's* model,
- Continuum model.

Simple assumption model does not consider the interaction between the foundation and the soil. The model assumes a linear distribution of contact pressures beneath the foundation. *Winkler's* model (1876) is the oldest and simplest one that considers the interaction between the foundation and the soil. The model represents the soil as elastic springs. Continuum model is the complicated model. The model considers also the interaction between the foundation and soil. It represents the soil as a layered continuum medium or isotropic elastic half-space soil medium. In continuum model surface deflections will occur not only immediately under the loaded region but also within certain limited zones outside the loaded region. Generally, the distribution of displacement and stresses in such media remain continuous under the action of external force systems. Continuum model provides a better physical representation of the supporting soil.

Most of available soil models even the complicated one, continuum model, represent the soil as an elastic medium with an elastic modulus. In this case, analyzing foundation on elastic soil layers may be carried out using flexibility coefficients-technique. In contrast, for foundation resting on a consolidated soil, the analysis is preferred to carry out by stress coefficients-technique. In this case, compression index of the soil is used to define the consolidation characteristics of the clay. *El Gendy* (2006) derived closed form equations for determining the increment of non-linear stress in sub-layers of the thick clay deposit caused by unknown contact pressure generated at the interface of the raft. These equations enable modeling a numerical procedure to determine consolidation settlement under the raft of an arbitrary shape on multi-clay layers of any thickness. He also presented an iterative method for analyzing rigid and elastic rafts on clay layers using stress coefficients.

2.4 Developing the analysis of circular rafts rested on soil

In foundation engineering circular slabs are widely used, for example, as bases for cylindrical liquid storage tanks on the ground, as footings for chimneys, circular columns or the shafts of water towers. The foundation slab in these case can be either solid or annular and can have either constant or varying thickness. For proper design of circular foundations on soil, it is necessary to consider the interaction of the slab with the underlying soil. It is known that the bending moment in the slab as well as the deformation (settlement) not only depends on the flexibility of the slab, but also on the soil behavior. The behavior of real soil media is very complex and attempts have been made to develop several idealized models to represent the soil. One of the most widely used models for soil is the elastic continuum in which the soil is assumed to be perfectly elastic, isotropic and homogeneous or anisotropic and nonhomogeneous. Several investigations have studied the contact problem of a rigid solid or annular slab subjected to an axisymmetric load and supported on a homogeneous isotropic elastic half-space or a layer of finite thickness resting on a rigid rough base using the integral transform method.

The analysis of circular plates on the *Winkler* foundation model have been reported extensively by many authors such as (*Schleicher* (1926); *Reissmann* (1954); *Conway* (1955); *Brotchie* (1957); *Leonards and Harr* (1959); *Timoshenko and Krieger* (1959); *Rodriguez* (1961); *Richart and Zia* (1963); *Volterra and Gaines* (1974); *Selvadurai* (1979); *Celep* (1988); *Celep and Turhan* (1990); *Guler and Celep* (1995)). In such analysis, a deformation discontinuity appears between loaded and unloaded parts of the foundation surface. In reality, the foundation soil surface generally does not show any type of discontinuity. In order to eliminate this deficiency of the *Winkler* model, circular plates have been analyzed by representing the foundation soil by improved foundation models in the past (*Browicka* (1936); *Zemochkin* (1939); *Ishkova* (1947); *Benito* (1948); *Reissner* (1955); *Galletly* (1959); *Korenev* (1960); *Palmov* (1960); *Kerr* (1964); *Valzov* and

Leontiev (1966); *Wen-da* and *Shu* (1987); *Al-Sanad* et al. (1993); *Fwa* et al. (1996); *Wang* et al. (2001)).

Other literatures have done to study the soil structure interaction for circular plates resting on soil as:

Cheung and *Zienkiewicz* (1965) have suggested a method of solving the interaction of plates on soil by combining the FEM with the *Boussinesq* solution for point loads.

Brown (1969) has studied the interaction of a circular raft subjected to an axisymmetrical load, resting on an isotropic elastic layer of finite thickness by making use of *Burmister's* solution for point loads or *Sneddon's* solution.

Hooper (1974) has used a total FEM to solve the interaction of a circular raft bonded to a thick elastic layer and has emphasized the difficulty of applying this method for large ratios of the modulus of elasticity of raft to soil.

Desai and *Reese* (1970) have studied the load-deformation characteristics of circular footing on layered soil, by taking a non-linear stress-strain relation for the soil, using the FEM.

Laermann (1981) has studied the interaction of a circular slab on an isotropic elastic layer of finite thickness by using combined photoelastic and *Moiré* methods.

Melerski (1994) extended the method of *Cheung* and *Zienkiewicz* (1965) to study the interaction of a circular slab on cross anisotropic soil.

Chandrashekhara and *Joseph Antony* (1997) presented an elastic interaction analysis of annular slab with soil in which the soil has been modelled as either homogeneous isotropic half-space or multilayered half-space. They solved the interaction problem using a combined approach (hybrid method) in which the FEM has been used to obtain the stiffness matrix for the annular slab while for the elastic half-space soil models, the stiffness matrix has been obtained using an analytical solution. The combined stiffness matrix of the annular slab-elastic half-space has been obtained using the displacement continuity condition at the interface.

El Gendy (2003) developed a numerical analysis to consider the actual contact pressure distribution under the rigid circular raft with an eccentric load. The analysis considers the compatibility between the settlement caused by cohesive soil consolidation and the raft displacement. In which, a direct numerical solution without iteration is derived to obtain the nonlinear soil stress under the rigid circular raft.

2.5 Developing models for analyzing cylindrical tanks rested on soil

Clarifier tank is one of the important components of wastewater treatment plant. Clarifier tank in most cases is a cylindrical concrete tank. Its function is to facilitate settlement of solids. The founding level of treatment units in the wastewater treatment plant is dictated by the overall hydraulics. The clarifiers are usually required to be founded near grade level. At grade level, firm foundation may not be available, and thus in most cases the clarifier tank rests on deformable soils.

The design tables available such as in the Portland cement association publication (PCA, 1993) are popular references for the design of cylindrical concrete tanks. In these tables, and in most other design handbooks, the analysis is simplified by taking ideal boundary conditions at the base of the wall. It is a common practice to analyze the tank wall assuming a fixed base and a hinged base for calculating vertical moment and hoop tension, respectively. The effects of the base raft and its interaction with the underlying soil, are usually neglected to limit complexity of the analysis. Further, self-weight of the tank is also neglected. Such approximations often lead the designers to be excessively conservative, and in some cases, may lead to inadequate designs. Many standard books and researches have worked on the issues related to circular water tanks and flexible nature of soil.

Davies (1962) described a method to predict the elastic behaviour of cylindrical concrete tanks under different support conditions. He assumed the contact pressure distribution on the tank floor to be in the form of a cylinder plus or minus a parabolic curve for granular and cohesive soils, respectively.

Smith (1970), while presenting the FEM for analyzing axisymmetric soil-foundation interaction problems, discussed its application to cylindrical storage tanks. He suggested the application of fixed end moments at the tank wall-foundation junction in the form of an external couple at the edge of an isolated circular foundation subjected to uniformly distributed loading due to liquid pressure and to ring load resulting from the wall.

Selvadurai (1979) described the basic concept of elastic analysis of soil-foundation interaction as well as a detailed literature review up to 1978. The notable methods suggested include the power series solution of *Borowicka* (1936), the integro-collocation method of *Brown* (1965), the finite element solution of *Cheung/Zienkiewicz* (1965), and the energy method of *Selvadurai* (1979).

Booker and *Small* (1983) have presented a flexibility-type approximate analysis procedure, assuming a series function for the reaction distribution of the soil that accounts for the interaction between the tank wall and the plate foundation-soil system. They examined the behavior of cylindrical storage tanks resting on deep

homogeneous elastic layer. Tanks having different wall types, including walls consisting of several different sections, were analyzed.

Cheung and Zienkiewicz (1965), Booker and Small (1983), and Mahmood (1984) have applied the finite element method to analyze such soil-structure interaction problems.

Issa and Zaman (1986) analyzed cylindrical tank-foundation-half-space interaction using an energy method. Circular foundations with radii larger than the tank can also be analyzed with this approach.

Kelkar and Sewell (1987) presented analytical solution for a circular tank in which flexibility of tank raft is considered.

Faruque/ Zaman (1983) and Zaman (1988) have provided an energy-based solution technique for this problem.

Zaman and Koragappa (1989) developed an analytical formulation to analyze the flexural behavior of rectangular and square foundations supporting cylindrical storage tanks or circular columns and resting on an isotropic elastic half-space. Their procedure is based on the principle of minimum potential energy and takes into account the interaction effects between various components, namely, tank wall, foundation, and elastic half-space. The wall-foundation interaction is incorporated by satisfying the compatibility conditions applicable to the wall-foundation junction. The proposed procedure is computationally inexpensive compared to the FE technique.

Melerski (1991) presented a computer program for elastic analysis of axisymmetric cylindrical storage tanks under various axisymmetric support and static loading conditions. It applies to tanks resting on unyielding circular line supports and/ or elastic media represented by either *Winkler* springs or an elastic half-space; linear elastic vertical constraints also being admissible.

Malik (1993) have proposed a differential quadrature solution for the problem of a plate resting on an elastic half space.

Kukreti et al. (1993) proposed analytical procedure by using energy methods to predict the behavior of liquid storage tank resting on elastic soil medium, which is modeled as elastic isotropic half space.

Kukreti and Siddiqi (1997) presented the differential quadrature method to predict the flexure behavior of cylindrical storage tanks with the circular plate foundations resting on top of an isotropic elastic half space.

El Mezaini (2006) presented effects of soil-structure interaction on the analysis of cylindrical tanks using computer software. The method given by him brought out the importance of sub grade interaction on design forces and settlement of such tanks. Effect of self-weight, which is usually neglected, was also considered in his method.

Ziari and Kianoush (2008) investigated effect of direct tension on crack width in reinforced concrete members and pointed out that exceeding the direct tension beyond permissible limit can cause leakage.

Vichare and Inamdar (2010) compared an analytical solution with corresponding computer simulation using the commercial program *ABAQUS* 6.8 and they observed that the range of soil is different from suggested by design codes. This is because, the soil type nature is not able to give completely "fixed" or "hinged" condition at the wall bottom as assumed in design codes.

Mistriková and Jendželovský (2012) compared different types of soil structure-interaction models, they introduced the elastic subsoil model using three basic subsoil models: half-space model, two-parametric model and one-parametric (*Winkler*) subsoil model. They used programs depending on FEM as *ANSYS* 2009 and *NEXIS* 2006 to simulate a tank – soil model and the output is compared with the analytical solutions for the *Winkler's* medium, half space medium and the experimentally measurements of the settlement.

2.6 Consolidation of clay under time-dependent and cyclic loading

In geotechnical engineering, soils beneath several structures are imposed to complicated cyclic loading paths. Among these structures are silos and tanks that undergo filling and discharging, highways, airports and railways, roadbed soils and embankments that are subjected to moving axle loads, and ocean banks subjected to wave action.

Schiffman (1958) was the first to obtain a general solution of soil consolidation considering loading increase linearly with time. In 1967 *Schiffman* developed a computer code to estimate consolidation settlements due to the time-dependent loading by dividing the continuous loading into a series of step load and used the principles of superposition to combine the corresponding settlement for each step of instantaneous loading.

Alonso and Krizek (1974) considered the settlement of elastic soft soil under stochastic loading.

Wilson and El gohary (1974) reported a theoretical solution for the progress of consolidation of a saturated soil layer subjected to cyclic loading. Consolidation under cyclic loading was found to be slower than consolidation under an equivalent sustained loading because positive and negative pore-water pressures produced during the loading and unloading portion of the cycle, cause flow of water from and into the soil. Equilibrium consolidation ratio was dependent on the pattern of loading cycle. Further, it was not possible to reach 100% consolidation under cyclic loading. In this study, curves showed that, in the early stage of consolidation the soil adjacent to the drainage boundary was consolidating, while the soil adjacent to the impervious boundary had not experienced any change in the effective stress. As consolidation proceeded, the positive pore water pressures during periods of the load application decreased and the negative pressures during periods of load removal increased. Finally, after infinite time, the consolidation ratio reached a maximum value throughout the layer; which means that the pore pressure reaches an equilibrium condition. The change in the positive and negative pore pressure when the soil was loaded and unloaded were found to depend upon the thickness, soil properties and cyclic loading characteristic.

Olson (1977) presented a mathematical solution for one-dimensional consolidation of homogeneous soil layer due to a single ramp load.

Baligh and Levadoux (1978) developed a simple method for prediction of behavior of an inelastic (nonlinear) clay layer initially in a normally consolidated state and subjected to one dimensional consolidation under cyclic loading. In a load cycle, the settlement reached a maximum value at the end of the loading (N odd) and a minimum value at the end of the unloading (N even). After a sufficiently large number of cycles (N) a steady –state condition was reached.

Favaretti and Mazzucato (1994) introduced some simple prediction methods for consolidation of elastic and inelastic soils under time-dependent loading.

Favaretti and Soranzo (1995) presented a simplified consolidation theory under cyclic loading conditions, based on *Terzaghi's* one-dimensional consolidation theory. The theory not only allowed estimation of settlement fluctuation with time but also evaluation of the time necessary to reach steady state conditions. Number of load cycles necessary to produce steady state conditions for low values of time factor were much higher in comparison with that of high values of time factor.

Yang et. al. (1995) suggested a one dimensional consolidation model for layered soils subjected to cyclic loading. The consolidation equation for time dependent loading was directly solved by means of *Laplace* transform and a general solution was derived. Based on the general solution, analytical solutions for different type of cyclic loading were obtained using the inverse transform.

Rahal and Vuez (1998) presented solutions for consolidation under time-dependent loading of types linear and sinusoidal loading for elastic clay.

Liang et al. (2002) suggested an one-dimensional consolidation model of saturated soil with semi-pervious boundaries and under the time-varying loading using Laplace Transform. The solution for change in degree of consolidation and effective stress ratio of stratified soil with single-pervious boundaries under cyclic loading were given on the basis of *Terzaghi's* one dimensional consolidation theory.

Xie and Zhuang (2005) presented a semi-analytical method to solve one-dimensional linear consolidation problem by taking consideration of varied compressibility of multi-layered soil under trapezoidal cyclic loading. The compression of each soil layer could be judged by the effective stress of the layer. From the results it was found that the rate of consolidation under cyclic loading was greater than the one predicted by conventional consolidation theory.

Xie et. al. (2006) presented an analytical solution for one-dimensional consolidation of soft soil under some common types of cyclic loading such as trapezoidal cyclic loading. The consolidation degree and pore water pressure values were found to increase during the loading, but decrease during the unloading. After certain cycles, the fluctuation was minimum and reached the stable conditions.

Conte and Troncone (2006) presented an analytical solution for the analysis of one-dimensional consolidation of saturated soil layers subjected to general time-dependent loading. The solution is based on Fourier series for practical applications by choosing a suitable period for both single loads and cyclic loads. The results using this solution give a good agreement with other compared solutions.

Yildirim and Ersan (2007) studied consolidation settlements of soft clay caused by cyclic loading highlighting various factors such as number of cycles and stress level on the behavior of soil. As a result of this study, it was concluded that soft clays subjected to undrained cyclic loading and drainage cycles exhibit more resistance against subsequent cyclic shear stresses. The consolidation settlement, pore pressure and shear strain were found to decrease after each stage of cyclic loading.

Xie et. al. (2008) presented a semi-analytical method of one-dimensional consolidation equation of over-consolidated soil under time-dependent loading. The consolidation behavior of over-consolidated soil was different from that described by *Terzaghi's* theory. From the results, it was found that the magnitude of load, pre-consolidation pressure, and the loading rate had a significant effect on the rate of excess pore water pressure dissipation to developing settlement.

Toufigh and Ouria (2009) presented a semi analytical solution for one dimensional consolidation problem of inelastic clays under cyclic loading considering the effect of the change of the consolidation coefficient of the soil layer. A method based on the time variable exchange along with the super imposing rule was employed. Changes in the consolidation coefficient were applied in the solution of this study by modifying the loading and unloading durations introducing a Virtual Time. Based on the super imposing rule a set of continuous static loads in specified times were used instead of the cyclic load in the transformed time space. Each full cycle of loading was replaced by a pair of static loads with different signs. A set of laboratory consolidation tests under cyclic load and numerical analysis were performed in the study in order to verify the method.

Geng et al. (2009) presented a parametric study to investigate the axisymmetric consolidation of a semi-infinite transversely isotropic saturated clay under various time-dependent loading. A general solution was derived by applying the *Laplace-Henkel* transform technique. Based on this study, it was found that besides the anisotropic parameters of the soil, the types of external loadings and the loading history also have significant influences on the pore pressure dissipation. The amount of pore pressure dissipation was decreased with the increase of the depth. For the ramp loading case, the pore pressure dissipation and the surface settlement increased gradually with time and would reach the peak almost at the end of the construction. The pore pressure dissipation in the soil under the ramp loading and the constant loading were being similar. Moreover, the change of soil surface settlement always lags behind the loading period under cyclic loading, which generates a negative pore water pressure.

François et al. (2010) used a long-term accumulation model for soils under repeated low-amplitude loading to analyze the redistribution of stress and the differential of foundation settlements. The numerical method, although it has the advantage of analyzing the subsoil settlement under complicated stress conditions, also has its shortcomings, such as long calculation time and uncontrollable cumulative calculation errors, which limit its practical use in engineering.

Yazdani and Toufigh (2012) I and II derived a system of two nonlinear partial differential equations to predict the consolidation characteristics of normally consolidated (NC) and overconsolidated (OC) soft clays subjected to cyclic loading by utilizing void ratio-effective stress and void ratio-permeability relationships. This study show that the ratios between the slopes of $e-\log\sigma'$ and $e-\log k$ lines in the NC and OC states play a major role in the consolidation process. The critical assumptions made in the analytical discussion are experimentally verified in a companion other paper and a numerical study is carried out in order to examine the proposed theory.

Hanna et al. (2013) extended *Terzaghi's* one-dimensional consolidation theory to constant rate of loading, where a simple expression relating average degree of consolidation and time factor is derived. This expression is used to assess *Terzaghi's* approximation that the ramp load can be assumed as an instantaneous load, applied at $t_o = 2$, where t_0 is the duration of loading. It is shown that this assumption overestimates the degree of consolidation by approximately 10%.

Abbaspour (2014) performed an experimental study to investigate the consolidation behavior of clay subjected to triangular cyclic loading. Also, he improved linear and non-linear consolidation's theories for triangular cyclic loading with performing the finite difference. The results from linear theory and non-linear theory was compared with experimental results.

Herrmann and *El Gendy* (2014) proposed a Layer Equation Method (*LEM*) for analyzing time-dependent settlement problems. *LEM* depends on selecting a number of nodes in the clay layers along the z -axis. Consequently, a better representation for applied stress on soil layers can be represented. The method is also ideal for using a stress coefficient technique, which may be extended to study the interaction of irregular loaded areas on the surface or contact pressure due to foundation rigidity. *LEM* requires fewer equation terms, in which fewer terms are sufficient to give excellent results compared to the available closed-form solution of time-dependent settlement problems. However, algebraic equations of clay layers are developed from an initial stress applied to a specified number of grid nodes, which can represent the excess pore water pressure at any node on the layers. This method is extended in this thesis to study the behavior of tanks on clay under cyclic loading.

Ouria et al. (2015) presented a simplified solution for consolidation of plastic clays under cyclic loading in disturbed state concept (DSC) framework. DSC can be adapted to this kind of problem using propitious state functions describing the changes in clay state. In the study, an analytical solution of a consolidation partial differential equation was used to obtain a general state function. The state function is used to describe the gradual change in state of the clay from OC to NC during successive cycles. Then the solutions of the problem in two elastic conditions of NC and OC states are interpolated using a derived state function to obtain the solution of the plastic problem. The validity of this method is ensured by a series of numerical and experimental tests.

Chapter 3

3 Mathematical model

3.1 Introduction

In this thesis, the structural behavior of circular cylindrical tanks resting on any layered compressible soil is investigated. In the developed mathematical models, tanks maybe subjected to static or cyclic loading with considering the relation between load and settlement as a time dependent problem. Most of all numerical models of this research are new introduced in the program *ELPLA* 10 [13]. *ELPLA* was developed before to analyze floor slabs, shear walls, grids, frames, rafts and piled rafts using beam and plate elements as shown in Figure 3.1. Figure 3.2 shows the recent version of *ELPLA* 10 including the new aspect concerning the icon "Analysis of rotational shells". An axi-symmetric shell finite element formulation is added to analyze circular cylindrical tanks. The idea of using axi-symmetric shell finite element is to simulate the tank wall, tank base and subsoil as one unit taking into account the soil-structure interaction effect. Using the conditions of axial symmetry, enables to convert the completed three dimensional problem of super structure, foundation and soil into axi- symmetry problem.

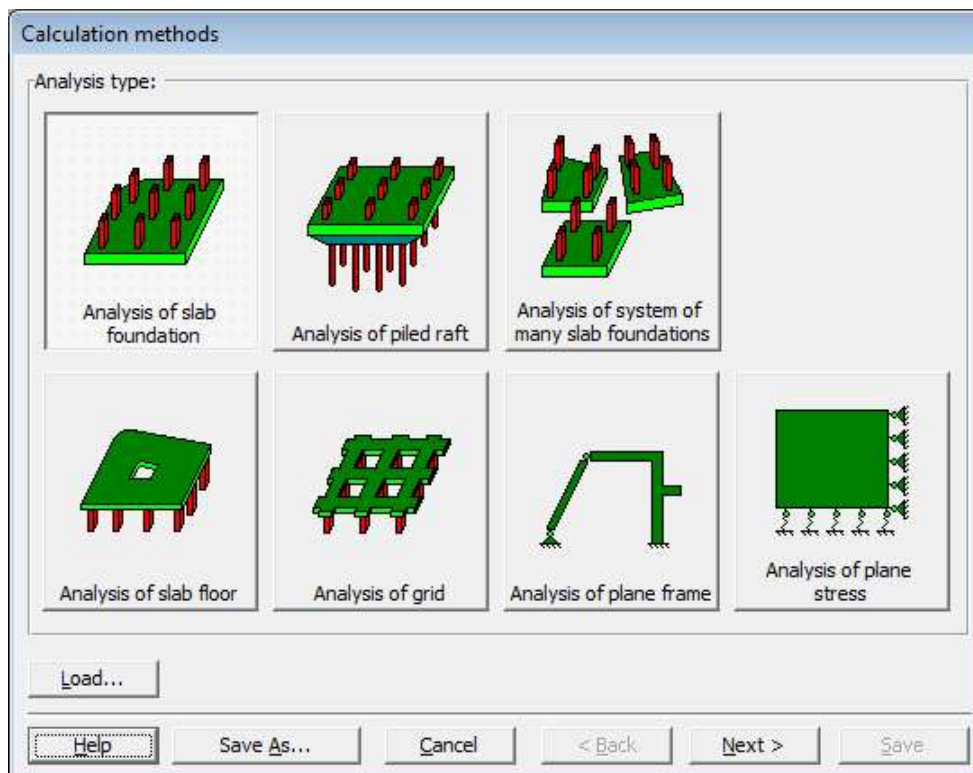


Figure 3.1 Aspects treated in *ELPLA* version 10 [13]

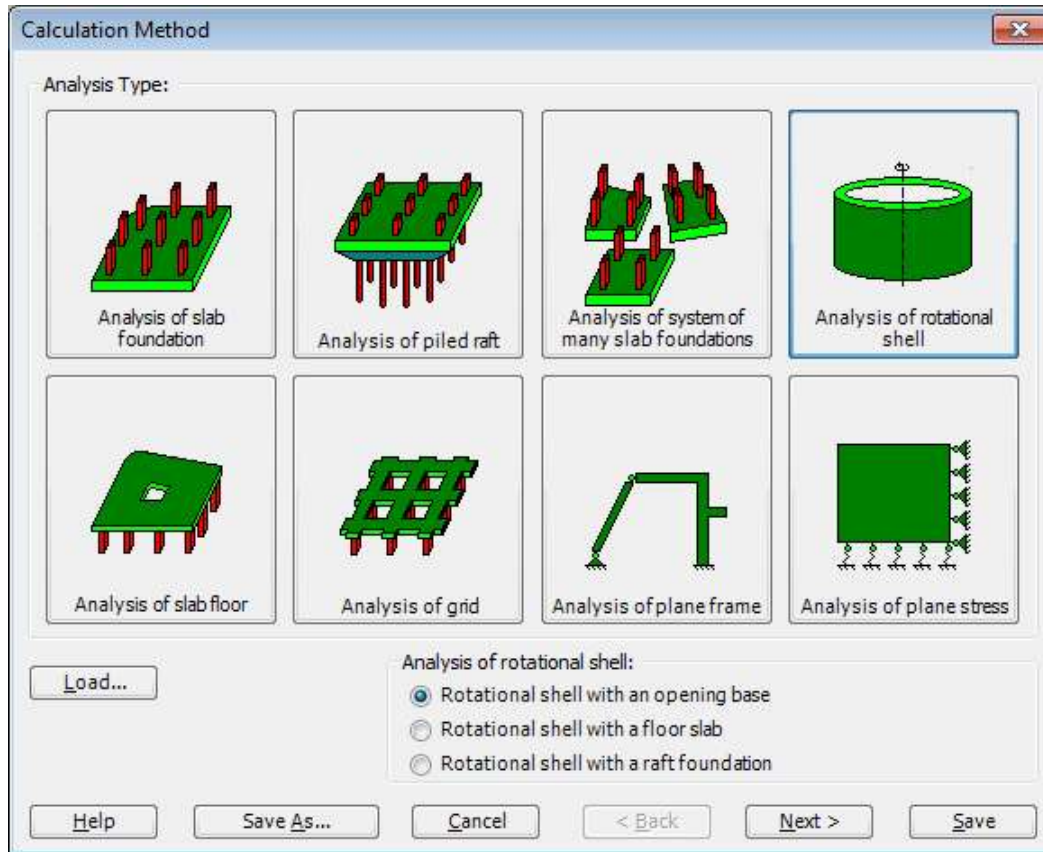


Figure 3.2 Aspects treated in *ELPLA* version 10 [13]

In addition, a numerical modification is carried out on the semi-analytical solution of *Toufigh and Ouria (2009)* to be applicable for multi-layered soil subjected to any variable stress along the depth of the soil using the layer equation method (*LEM*) of *El Gendy and Herrmann (2014)*. The developed solution is used for normally or overconsolidated clays subjected to any type of cyclic loading. It takes into account the structure rigidity with the subsoil layers at any cyclic period. Besides, the actual contact pressure under the tank can be obtained at any cyclic period. The solution is applied for water tanks as a structure subjected to cyclic loading. Base of the tank may be considered as rigid, elastic or flexible. For analyzing the base of the tank as elastic base, full compatibility between the structure elements and subsoil is occurred. Besides adding new formulations in *ELPLA 10*, a series of *MS Excel* sheets were used to confirm the accuracy of the developed *LEM* in static and cyclic loading.

3.2 Finite elements analysis of axi-symmetric shells of revolution

3.2.1 Introduction

Circular cylindrical shells analysis may be considered as an axi-symmetric shell structure problem. An axi-symmetric shell structure can be idealized by a series of conical frustum-shaped elements as shown in Figure 3.3. This element was first suggested by *Grafton* and *Strome* (1963) and later its use was extended by *Percy* et al (1965). It may be noted that this single element has two ring nodes. Since both in-plan and out of plan displacements and forces have to be considered in shell structures, the displacement vector for each node contains axial and radial movements as well as rotation as shown in Figure 3.3 - b). Finite element analysis of axi-symmetric shells in the simplified approach of *Grafton* and *Strome* (1963) are presented by many authors. Some of them are *Zienkiewicz/ Taylor* (1967), *Rockey et al* (1975), *Szilard* (1986), and *Melerski* (2000). *Szilard* (1986) presented a more extensive analysis of axi-symmetric shell structure with a computer program code. The following steps of the FE analysis of axi-symmetric shell structure depends on that of *Rockey et al* (1975) and *Szilard* (1986).

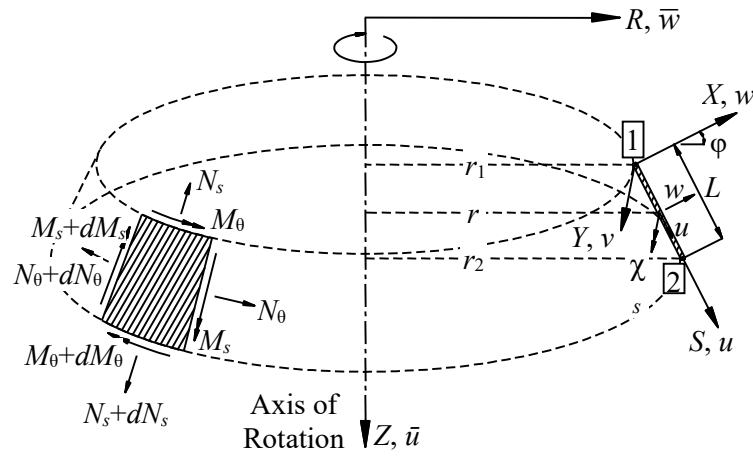
3.2.2 Stiffness matrix formulation

It is convenient to use cylindrical polar co-ordinates (r, z) as shown in Figure 3.3. Considering nodes (1) and (2) in Figure 3.3, the nodal displacement and force vectors for the conical shell element are written respectively as:

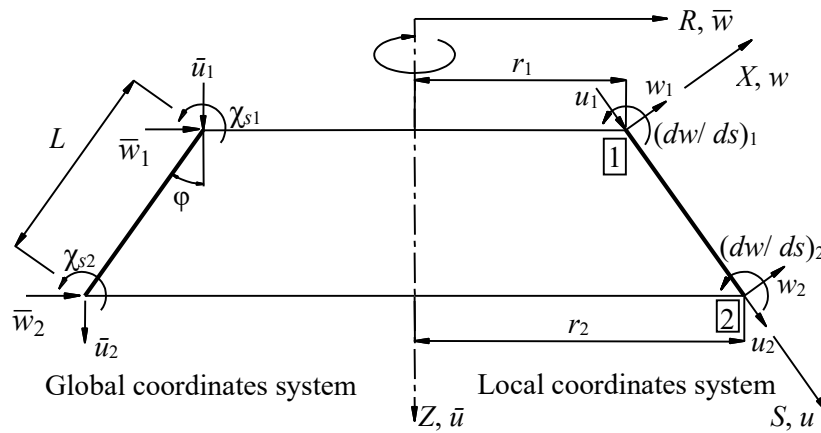
$$\{\delta^e\} = \begin{Bmatrix} \{\delta_1\} \\ \{\delta_2\} \end{Bmatrix} = \begin{Bmatrix} \bar{u}_1 \\ \bar{w}_1 \\ \chi_{s1} \\ \bar{u}_2 \\ \bar{w}_2 \\ \chi_{s2} \end{Bmatrix} \quad (3.1)$$

$$\{F^e\} = \begin{Bmatrix} \{F_1\} \\ \{F_2\} \end{Bmatrix} = \begin{Bmatrix} F_{z1} \\ F_{r1} \\ M_{s1} \\ F_{z2} \\ F_{r2} \\ M_{s2} \end{Bmatrix} \quad (3.2)$$

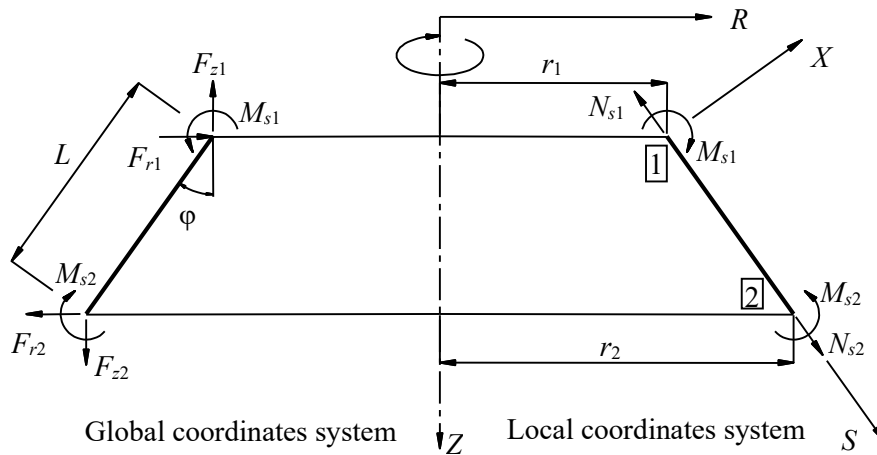
where \bar{u} is the axial displacement in global co-ordinates, \bar{w} is the horizontal radial displacement in global co-ordinates, χ_s is the meridional rotation, F_z is the axial force in global co-ordinates, F_r is the radial force in global co-ordinates and M is the meridional bending moment.



a) Internal forces for conical shell element



b) Deformations at the nodes in the local (right) and global (left) coordinate systems



c) Forces at the nodes in the local (right) and global (left) coordinate systems

Figure 3.3 Conical ring shell element

Thus each axi-symmetric shell element has six degrees of freedom and the complete element stiffness matrix $[K^e]$ is of size 6×6 .

$$\{F^e\} = [K^e]\{\delta^e\} \quad (3.3)$$

According to *Szillard et al* (1986), the elements of the global stiffness matrix for the general case of any angle φ is:

$$[K^e] = \begin{bmatrix} K_{11} & K_{12} & K_{13} & K_{14} & K_{15} & K_{16} \\ & K_{22} & K_{23} & K_{24} & K_{25} & K_{26} \\ & & K_{33} & K_{34} & K_{35} & K_{36} \\ & & & K_{44} & K_{45} & K_{46} \\ \text{Symm.} & & & & K_{55} & K_{56} \\ & & & & & K_{66} \end{bmatrix} \quad (3.4)$$

where:

$$K_{11} = \frac{\pi}{L} \left(\frac{12}{t^2} D(r_1+r_2) \cos^2 \varphi + \frac{36}{L^2} D(r_1+r_2) \sin^2 \varphi \right) = K_{14}$$

$$K_{12} = \frac{\pi}{L} \cos \varphi \left(\frac{12}{t^2} D(r_1+r_2) \sin \varphi - \frac{12}{t^2} DLv - \frac{36}{L^2} D(r_1+r_2) \sin \varphi \right)$$

$$K_{13} = -\frac{6\pi}{L^2} \sin \varphi (2D(2r_1+r_2) - DLv \sin \varphi)$$

$$K_{15} = -\frac{\pi}{L} \cos \varphi \left(\frac{12}{t^2} D(r_1+r_2) \sin \varphi + \frac{12}{t^2} DLv - \frac{36}{L^2} D(r_1+r_2) \sin \varphi \right)$$

$$K_{16} = -\frac{6\pi}{L^2} \sin \varphi (2D(r_1+2r_2) + DLv \sin \varphi)$$

$$K_{22} = \frac{\pi}{L} \left(\frac{12}{t^2} D(r_1+r_2) \sin^2 \varphi - \frac{24}{t^2} DLv \sin \varphi + \frac{12L^2}{r_1 t^2} D + \frac{36}{L^2} D(r_1+r_2) \cos^2 \varphi \right)$$

$$K_{23} = \frac{6\pi}{L^2} \cos \varphi (2D(2r_1+r_2) - DLv \sin \varphi); K_{24} = -K_{12}$$

$$K_{25} = -\frac{\pi}{L} \left(\frac{12}{t^2} D(r_1+r_2) \sin^2 \varphi + \frac{36}{L^2} D(r_1+r_2) \cos^2 \varphi \right)$$

$$K_{26} = \frac{6\pi}{L^2} \cos \varphi (2D(r_1+2r_2) + DLv \sin \varphi)$$

$$K_{33} = \frac{4\pi}{L} \left(D(4r_1+r_2) - 2DLv\sin\phi + D \frac{L^2}{4r_1} \sin^2\phi \right); K_{34} = -K_{15}; K_{35} = -K_{23}$$

$$K_{36} = \frac{2\pi}{L} (4D(r_1+r_2)); K_{44} = K_{11}; K_{45} = -K_{15}; K_{46} = -K_{16}$$

$$K_{55} = \frac{\pi}{L} \left(\frac{12}{t^2} D(r_1+r_2) \sin^2\phi + \frac{24}{t^2} DLv\sin\phi + \frac{12L^2}{r_2 t^2} D + \frac{36}{L^2} D(r_1+r_2) \cos^2\phi \right)$$

$$K_{56} = -\frac{6\pi}{L^2} \cos\phi (2D(r_1+2r_2) + DLv\sin\phi)$$

$$K_{66} = \frac{\pi}{L} \left(4D(r_1+4r_2) + 8DLv\sin\phi + D \frac{L^2}{r_2} \sin^2\phi \right)$$

Where D is the flexural rigidity and can be written as:

$$D = \frac{E t^3}{12(1-\nu^2)} \quad (3.5)$$

where E is *Young's* modulus of elasticity, ν is *Poisson's* ratio and t is the shell thickness.

3.2.3 Internal stresses and stress-displacement matrix

In the case of shells it is usual to work in terms of the stress resultants, which are the forces and moments per unit length. For this axi-symmetric shell element these resultants consists of N_s , N_θ which are the membrane forces per unit length, and M_s , M_θ , the moments per unit length, as shown in Figure 3.3.

The stress vector is given by:

$$\{\sigma(r, s)\} = \begin{Bmatrix} \{\sigma(r, s)_1\} \\ \{\sigma(r, s)_2\} \end{Bmatrix} = \begin{Bmatrix} N_{s1} \\ N_{\theta 1} \\ M_{s1} \\ M_{\theta 1} \\ N_{s2} \\ N_{\theta 2} \\ M_{s2} \\ M_{\theta 2} \end{Bmatrix} \quad (3.6)$$

After calculating the displacements using equation (3.3), the stresses are determined using the following equation:

$$\{\sigma(r, s)\} = [H]\{\delta^e\} \quad (3.7)$$

Where the stress-displacement matrix $[H]$ is obtained from the following equation:

$$[H] = \frac{Et}{(1-\nu^2)} \begin{bmatrix} \frac{-\cos\varphi}{L} & \frac{\nu}{r_1} - \frac{\sin\varphi}{L} & 0 & \frac{\cos\varphi}{L} & \frac{\sin\varphi}{L} & 0 \\ \frac{-\nu\cos\varphi}{L} & \frac{1}{r_1} - \frac{\nu\sin\varphi}{L} & 0 & \frac{\nu\cos\varphi}{L} & \frac{\nu\sin\varphi}{L} & 0 \\ \frac{t^2\sin\varphi}{2L^2} & \frac{-t^2\cos\varphi}{2L^2} & \frac{-t^2}{3L} - \frac{\nu t^2\sin\varphi}{12r_1} & \frac{-t^2\sin\varphi}{2L^2} & \frac{t^2\cos\varphi}{2L^2} & \frac{-t^2}{6L} \\ \frac{\nu t^2\sin\varphi}{2L^2} & \frac{-\nu t^2\cos\varphi}{2L^2} & \frac{-\nu t^2}{3L} - \frac{t^2\sin\varphi}{12r_1} & \frac{-\nu t^2\sin\varphi}{2L^2} & \frac{\nu t^2\cos\varphi}{2L^2} & \frac{-\nu t^2}{6L} \\ \frac{-\cos\varphi}{L} & \frac{\sin\varphi}{L} & 0 & \frac{\cos\varphi}{L} & \frac{\nu}{r_2} + \frac{\sin\varphi}{L} & 0 \\ \frac{-\nu\cos\varphi}{L} & \frac{\nu\sin\varphi}{L} & 0 & \frac{\nu\cos\varphi}{L} & \frac{1}{r_2} + \frac{\nu\sin\varphi}{L} & 0 \\ \frac{-t^2\sin\varphi}{2L^2} & \frac{t^2\cos\varphi}{2L^2} & \frac{t^2}{6L} & \frac{t^2\sin\varphi}{2L^2} & \frac{-t^2\cos\varphi}{2L^2} & \frac{t^2}{3L} - \frac{\nu t^2\sin\varphi}{12r_2} \\ \frac{-\nu t^2\sin\varphi}{2L^2} & \frac{\nu t^2\cos\varphi}{2L^2} & \frac{\nu t^2}{6L} & \frac{\nu t^2\sin\varphi}{2L^2} & \frac{-\nu t^2\cos\varphi}{2L^2} & \frac{\nu t^2}{3L} - \frac{t^2\sin\varphi}{12r_2} \end{bmatrix} \quad (3.8)$$

3.2.4 Calculation process with axially symmetrical loading

The analysis of axially symmetrical loaded shells of revolution is carried out in the usual way by the finite element method. The structure is converted into a quasi-one-dimensional replacement system using conical ring shell elements. The geometry of this replacement system is defined in a global reference system Z, R by the cylindrical coordinates of the nodes (z_i, r_i) . The Z -axis is selected as the axis of rotation. The origin of the coordinate system is usually set in the vertex of the axi-symmetric shell.

Next, the authorized global nodes deformations are numbered. The overall stiffness matrix of the structure K is set by superposition of the individual values of the stiffness indices.

$$K_{ij} = \sum_{ij} k'_{ij} \quad (3.9)$$

After assembling the overall stiffness matrix, the given boundary conditions should be incorporated. The outer surface loading must be converted into a resultant force acting on the nodes in the vertical or horizontal direction.

3.2.5 Simulation of circular plate

Equations (3.3) and (3.7) represent a conical shell with an arbitrary tangential angle φ . For a circular cylindrical shell, $\varphi = 0$ [°], while for a circular flat plate $\varphi = 90$ [°].

Shells are often closed at the ends like conical shell elements or circular plates. Both cases can be treated with appropriate limits of the element dimensions. At cone vertex (Figure 3.4- a)) r_1 or r_2 may not be exactly zero, because the values of the matrix elements in equation (3.9) would be divided by zero, as r_1 or r_2 are divisors. To avoid such numerical instabilities, the program used in this research (*ELPLA 10*) changes internally the entered zero value with a radius equal to 10^{-3} [m]. Circular plates have to be analyzed also with a fictional small overall height (for example, 10^{-3} [m]) (Figure 3.4 b)). Taking these limitations, walls of the circular cylindrical tank with circular base plate are analyzed using the same shell elements.

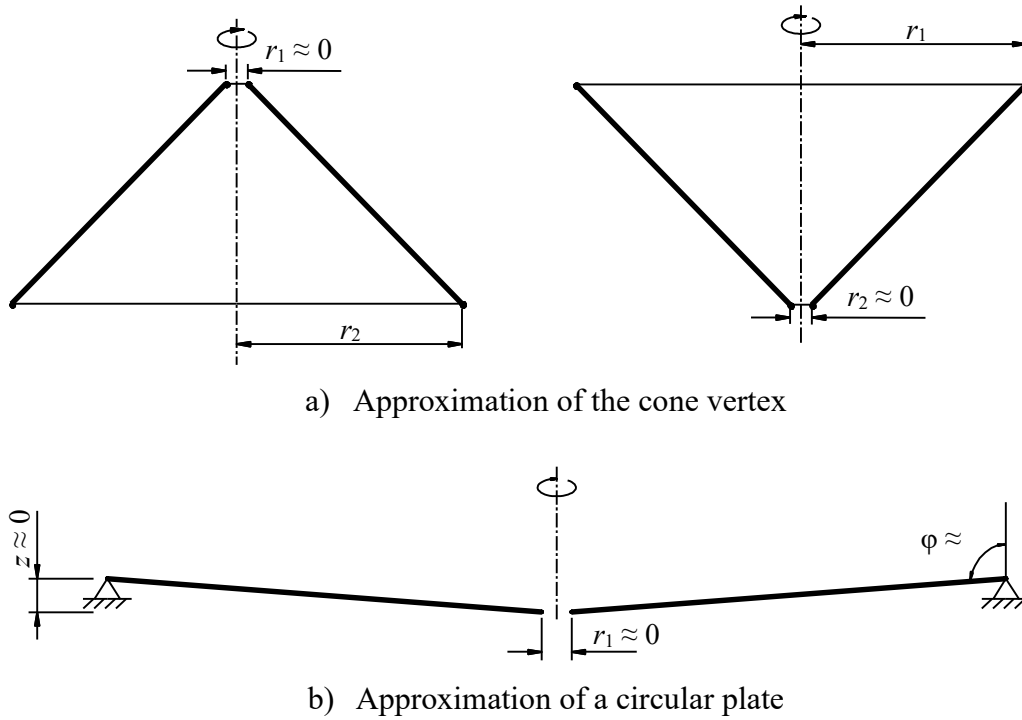


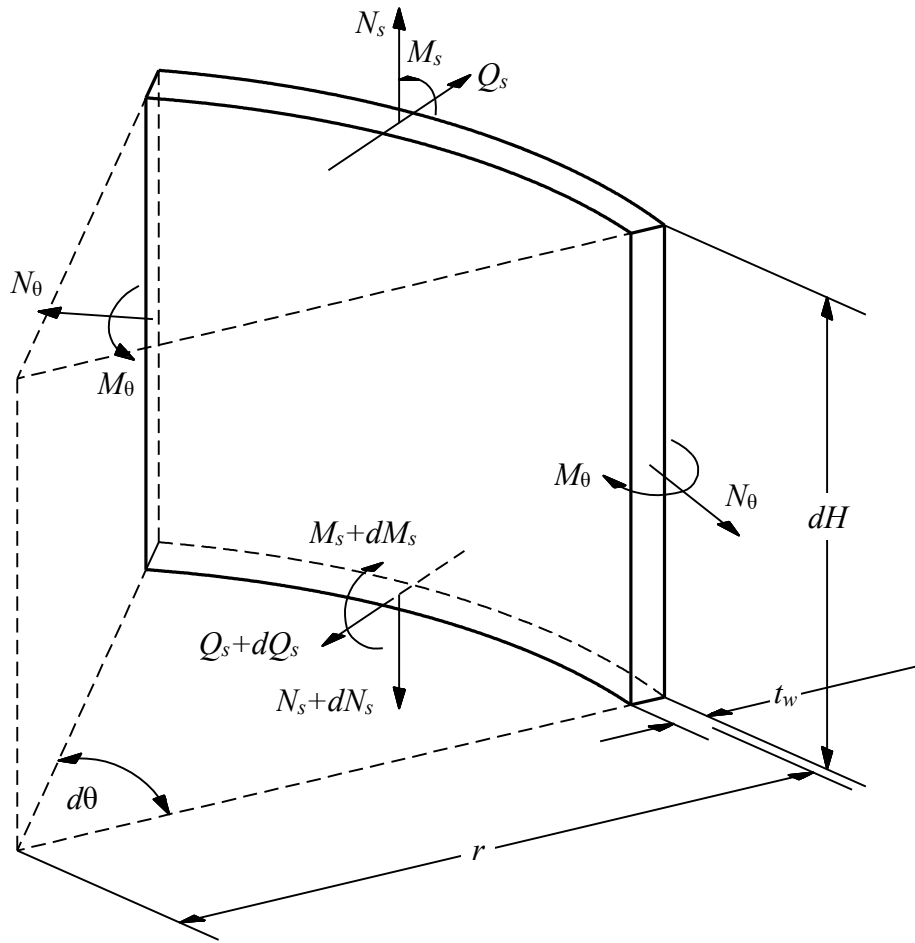
Figure 3.4 Boundary values for element dimensions

3.2.6 Simulation of the tank wall and base using thin shell element

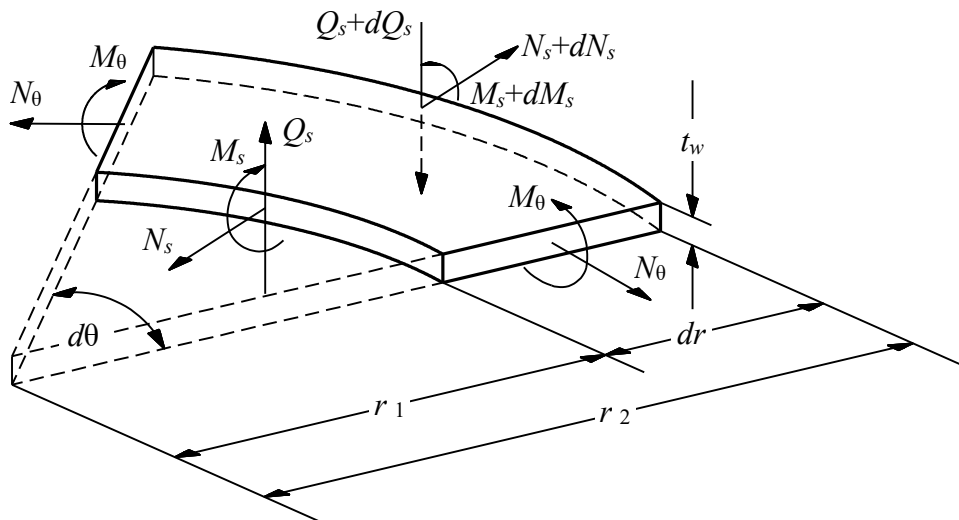
The analysis of the tanks used in this thesis are carried out numerically by *ELPLA* 10, where the circular cylindrical wall and the base were simulated with a thin shell element using finite element method.

Figure 3.5-a shows the internal forces acting on a cylindrical shell element which simulates the wall of the tank, while Figure 3.5-b shows the internal forces acting on a circular flat shell element which simulates the base of the tank.

Considering the two shell elements, the internal forces acting on these elements are the tangential normal force (N_θ), the meridional normal force (N_s), the tangential bending moment (M_θ), the meridional bending moment (M_s) and the transverse shearing force component (Q_s). Due to the axial symmetry, the transverse shearing force component (Q_θ), the tangential shearing force components ($N_{\theta s}$, $N_{s\theta}$) and torsional moments ($M_{s\theta}$, $M_{\theta s}$) will vanish.



a) Internal forces on a wall element



b) Internal forces on a circular flat shell element

Figure 3.5 Tank simulation using thin shell element

3.3 Analysis of water tanks under static loading

3.3.1 Introduction

According to the three standard soil models available in *ELPLA* (simple assumption model - *Winkler's* model - Continuum model), six numerical calculation methods are considered to analyze the tank considering soil structure interaction as shown in Table 3.1.

Table 3.1 Numerical calculation methods

Method No.	Method
1	Simple assumption model
2	<i>Winkler's</i> model
3	<i>Winkler's</i> / Continuum model
4	Continuum model for elastic base
5	Continuum model for rigid base
6	Continuum model for flexible base

The Finite elements-method is used to analyze the tank wall and base for all numerical calculation methods except Continuum model for rigid and flexible bases, which did not obey the elasticity rules. In the Finite elements-analysis, the tank base is represented by annular shell elements according to the dimensional nature of the base.

To formulate the equations of the numerical calculation methods, both the base and the contact area of the supporting medium are divided into annular elements as shown in Figure 3.6. Compatibility between the base and the soil medium in vertical direction is considered for all methods except Simple assumption model.

The fundamental formulation of equilibrium equation for the tank can be described in general form through the following equation:

$$[k_p]\{\delta\} = \{F\} \quad (3.10)$$

Where $\{F\}$ is the vector of forces acting on the tank, $[k_p]$ is the stiffness matrix of the tank and $\{\delta\}$ is the deformation vector.

In principle for all calculation methods, the acting forces are known and equal to the applied forces on the tank wall and base, while the reaction forces (contact forces) are required to be found according to each soil model.

It is assumed that the contact pressure q_i can be replaced by equivalent force Q_i at the various nodal rings. The contact pressure around the nodal ring i is given by $q_i = Q_i / A_i$ over an annular area A_i corresponding to the nodal contact i . According to subsoil models (Simple assumption model - *Winkler's model* - Continuum model), six numerical calculation methods are considered to find the contact pressures q_i , and hence to analyze the tank. The next pages describe the interaction between the tank base and subsoil medium in these methods.

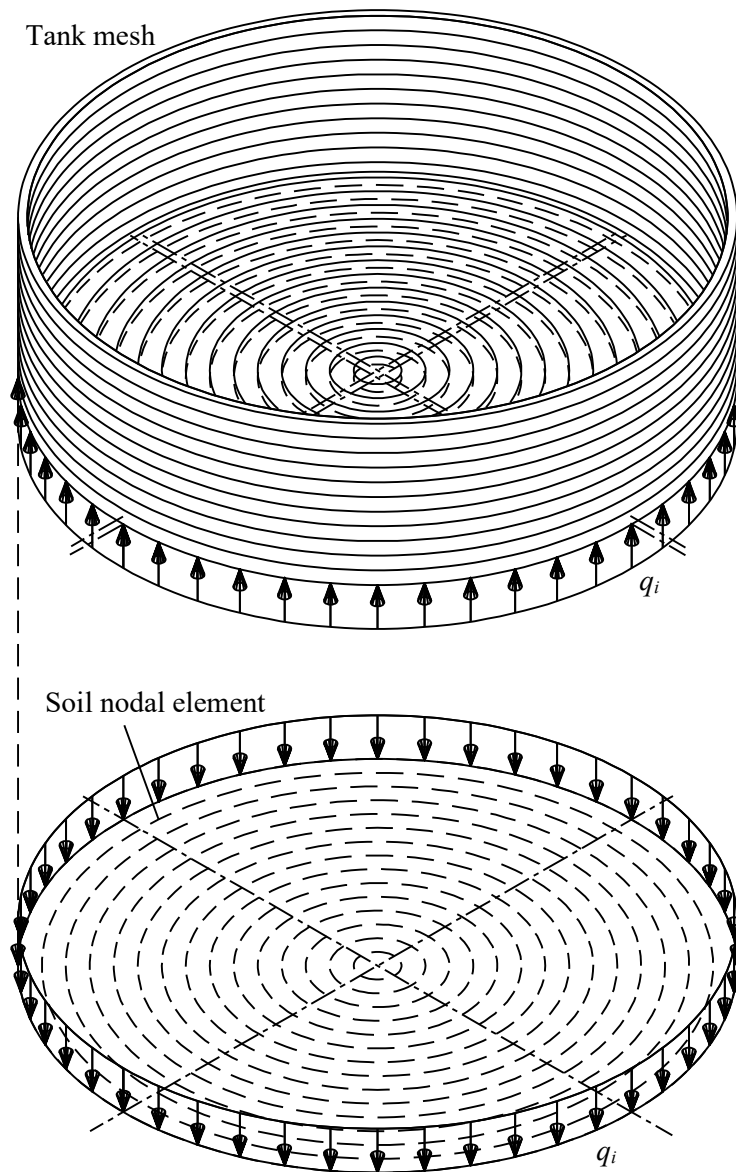


Figure 3.6 Action between tank base and soil

3.3.2 Simple assumption model

This method is the simplest one for determination of the contact pressure distribution under the tank base. The assumption of this method is that there is no compatibility between the tank base deflection and the soil settlement. In the method, it is assumed that the contact pressures are distributed uniformly on the bottom of the base (statically determined) as shown in Figure 3.7, in which the resultant of soil reactions coincides with the resultant of applied loads.

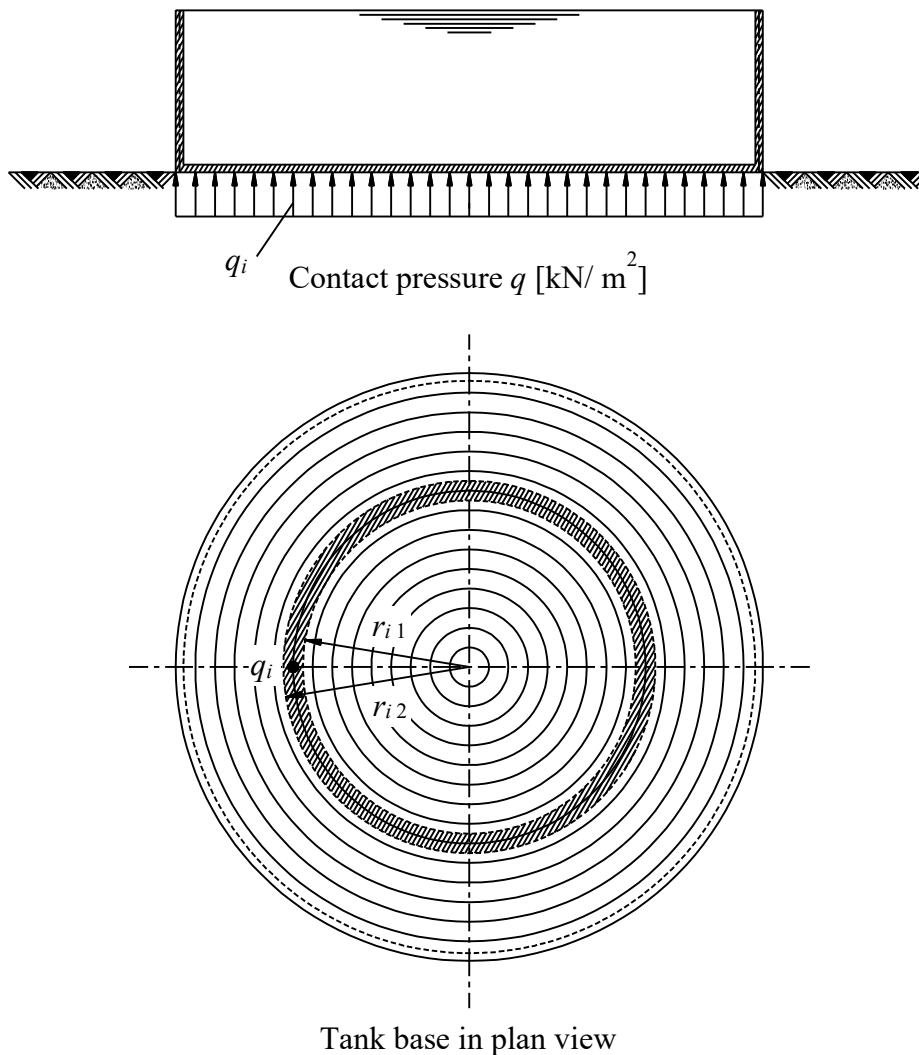


Figure 3.7 Contact pressure distribution for Simple assumption model

For a base without eccentricity the contact pressure q_i will be uniform under the base and is given by:

$$q_i = \frac{N}{A_b} \quad (3.11)$$

where N is the resultant force on the tank and A_b is the area of the tank base.

3.3.2.1 System of equations of Simple assumption model

The tank can be analyzed by calculating the soil reactions at the different nodal rings of the Finite elements-mesh. This is done by obtaining the contact pressure q_i from equation (3.11). Then, the contact force Q_i at ring i is given by:

$$Q_i = q_i (\pi r_{i2}^2 - \pi r_{i1}^2) \quad (3.12)$$

where r_{i1} and r_{i2} are the outer and inner radii of the annular element i , [m].

Considering the entire base, the base will deflect under the action of the total external forces $\{F\}$ due to known applied loads $\{P\}$ and the known soil reactions $\{Q\}$, where:

$$\{F\} = \{P\} - \{Q\} \quad (3.13)$$

The equilibrium of the system is expressed by the following matrix equation:

$$[k_p]\{\delta\} = \{P\} - \{Q\} \quad (3.14)$$

3.3.2.2 Equation solver of linear contact pressure method

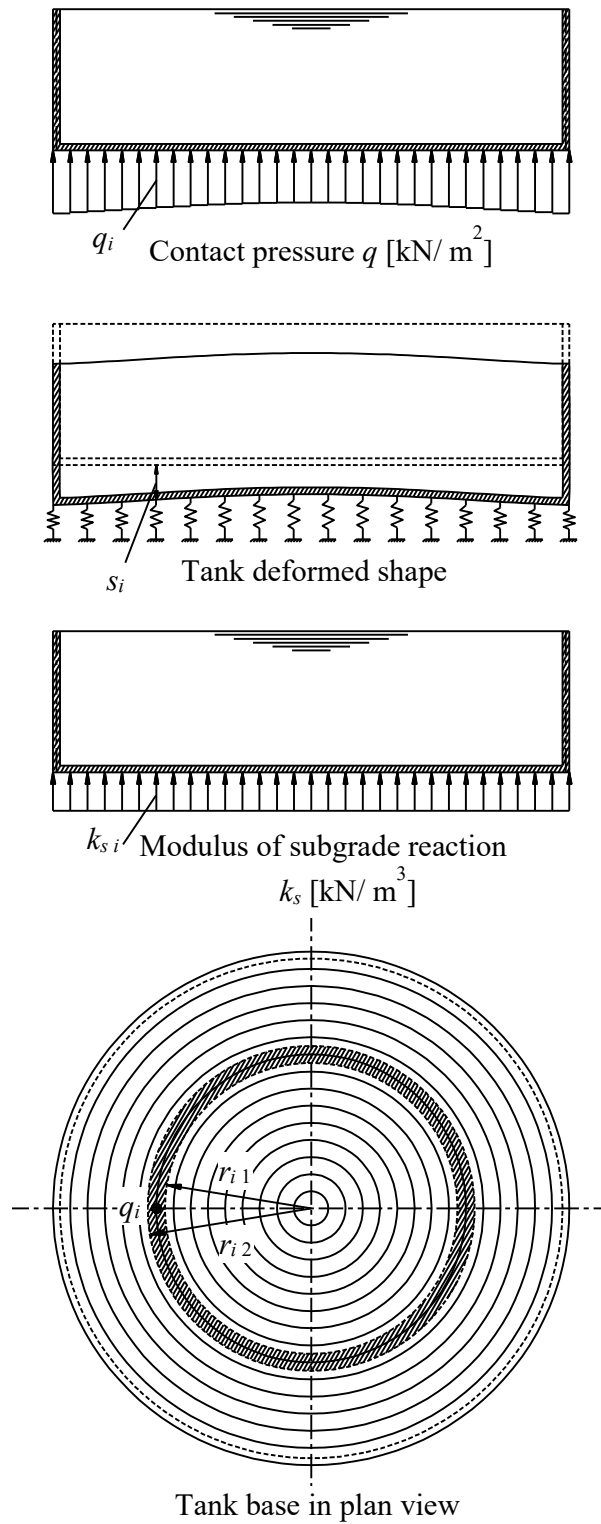
As the stiffness matrix $[k_p]$ in equation (3.10) is a diagonal matrix, the system of linear equations in equation (3.14) is solved by Banded coefficients-technique. The unknown variables are the nodal displacements w_i and the nodal rotations χ_i .

3.3.3 Winkler's model

The oldest method for the analysis of foundation on elastic medium is the modulus of subgrade reaction, which was proposed by *Winkler* (1867). The assumption of this method is that the soil model is represented by elastic springs as shown in Figure 3.8. The settlement s_i of the soil medium at any point i on the surface is directly proportional to the contact pressure q_i at that point and is mathematically expressed as:

$$q_i = k_{si} s_i \quad (3.15)$$

The ratio between the contact pressure q_i [kN/ m²] and the corresponding settlement s_i [m] is termed the modulus of subgrade reaction k_{si} [kN/ m³].

Figure 3.8 *Winkler's model*

3.3.3.1 System of equations of Winkler's model

For a nodal ring i on the Finite elements-mesh, the contact force Q_i is given by:

$$Q_i = (\pi r_{i2}^2 - \pi r_{i1}^2) k_{si} s_i \quad (3.16)$$

It should be noticed that k_{si} is the modulus of subgrade reaction at nodal ring i . It may be constant for the entire base (Constant modulus of subgrade reaction) or variable from a nodal ring to another (Variable modulus of subgrade reaction).

Considering the entire base, equation (3.16) can be rewritten in matrix form as:

$$\{Q\} = [k_s]\{s\} \quad (3.17)$$

3.3.3.2 Complete stiffness formulation of Winkler's model

The base will deflect under the action of the total external forces $\{F\}$ due to known applied loads $\{P\}$ and the unknown soil reactions $\{Q\}$, where:

$$\{F\} = \{P\} - \{Q\} \quad (3.18)$$

The equilibrium of the tank-soil system is expressed by the following matrix equation:

$$[k_p]\{\delta\} = \{P\} - \{Q\} \quad (3.19)$$

Considering the compatibility of deformation between the base and the soil medium, where the soil settlement s_i equal to the base deflection w_i , equation (3.17) for *Winkler's* model can be substituted into equation (3.19) as:

$$[[k_p]+[k_s]]\{\delta\} = \{P\} \quad (3.20)$$

Equation (3.20) shows that the stiffness matrix of the whole tank-base-soil system is the sum of the tank and the soil stiffness matrices, $[k_p]+[k_s]$.

3.3.3.3 Equation solver of Winkler's model

It should be noticed that the soil stiffness matrix $[k_s]$ is a purely diagonal matrix for *Winkler's* model. Therefore, the total stiffness matrix for the tank and the soil is a banded matrix. Then, the system of linear equation (3.20) is solved by Banded coefficients-technique. Since the total stiffness matrix is a banded matrix, the Equation solver equation (3.19) takes short computation time by applying this method.

The unknown variables in equation (3.20) are the nodal displacements w_i ($w_i = s_i$) and the nodal rotations χ_i . After solving the system of linear equations (Eq. 4.76), substituting the obtained settlements s_i in equation (3.17), gives the unknown contact forces Q_i .

3.3.4 *Winkler's/ Continuum model*

This method was proposed by *Ahrens/ Winselmann* (1984), which based on the soil, is represented by variable moduli of subgrade reactions similar to the Continuum model. In the method the base and soil medium are treated separately, the results of one analysis forming the boundary conditions for the subsequent analysis as part of an iterative process. By modifying the variable moduli through the iterative process, the compatibility between the soil and base interface is reached. The obtained results here are similar to those by Continuum model. The method is not only used for analysis of the foundations by Continuum model but also by modulus of subgrade reaction with variable moduli. The first iterative cycle gives an analysis for modulus of subgrade reaction with variable moduli. The results at any intermediate iteration cycle may be considered as acceptable results, which in fact lie between *Winkler's* model with variable moduli and Continuum model. See Figure 3.9.

The iteration process of this method can be described as follows:

i) First, uniform distribution of contact pressure q_o on the bottom of the foundation is assumed as:

$$q_o = \frac{N}{A_b} \quad (3.21)$$

ii) For a set of nodal rings of Finite elements-mesh, the soil settlement s_i at nodal ring i due to contact forces in manner described later for Continuum model is obtained from:

$$s_i^{(j)} = \sum_{k=1}^n c_{i,k} Q_k \quad (3.22)$$

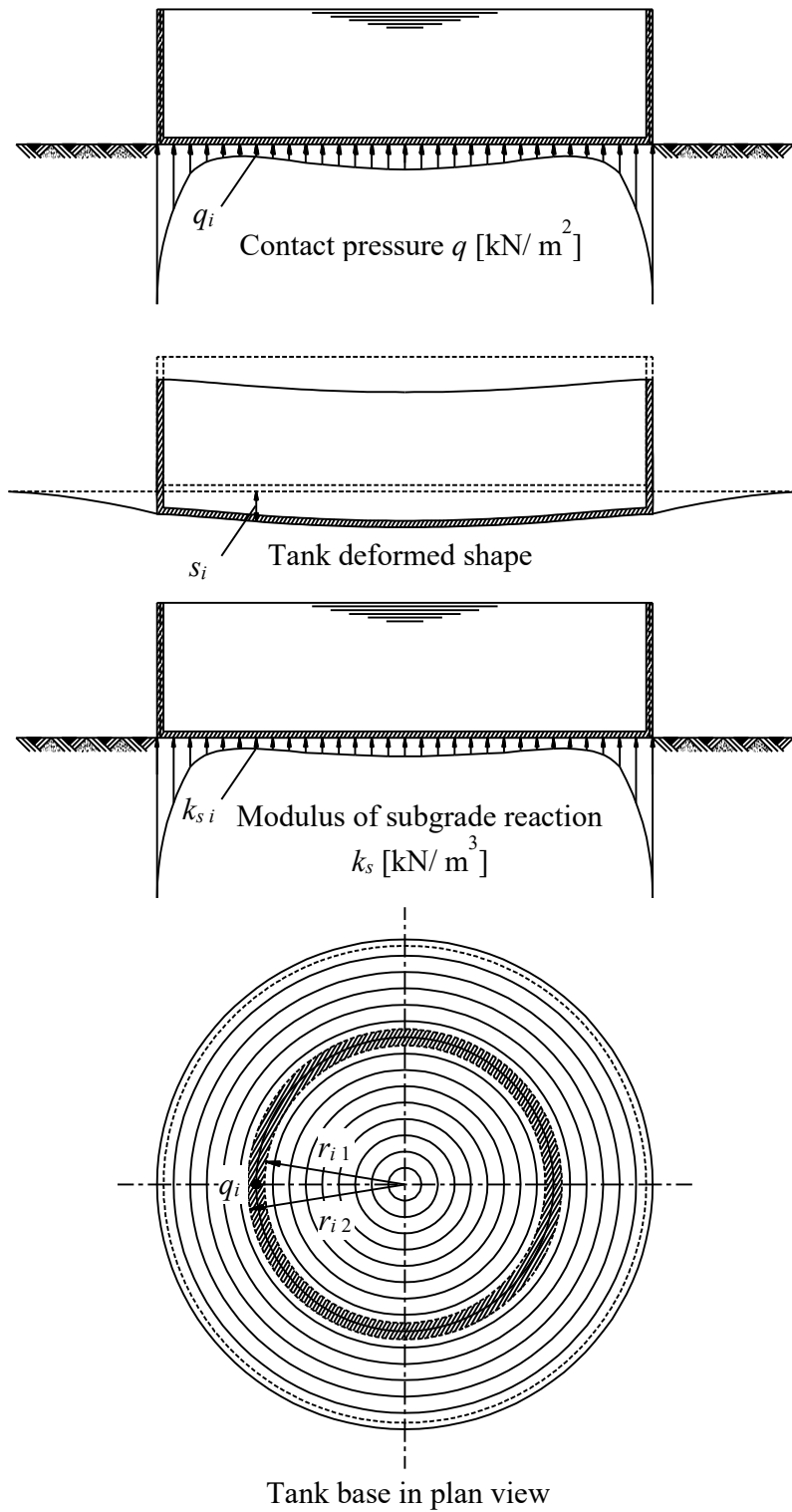
iii) The spring stiffness k_i from the soil settlement s_i and contact force Q_i is computed from:

$$k_i^{(j)} = \frac{Q_i^{(j)}}{s_i^{(j)}} \quad (3.23)$$

iv) The foundation is analyzed as plate on springs, the spring coefficients are used to generate the soil stiffness matrix $[k_s]$. This matrix will be a diagonal matrix. Therefore, adding the soil stiffness matrix $[k_s]$ to the base stiffness matrix $[k_p]$ is easy. Then, the overall matrix for wall-base-soil system becomes a banded matrix. The entire system equation is expressed as:

$$[[k_p]+[k_s]]\{\delta\} = \{P\} \quad (3.24)$$

v) A set of nodal displacements $\{\delta\}$ is obtained by solving the system equation (3.24) using the Banded coefficients-technique.

Figure 3.9 *Winkler/* Continuum model

vi) The soil settlements s_i are compared with the corresponding base deflections w_i , which were computed from the system equation (3.24):

$$\eta = \| s_i - w_i \| \quad (3.25)$$

vii) If the accuracy does not reach to a specified tolerance η a new set of contact forces are obtained using:

$$Q_i^{(j+1)} = k_i^{(j)} w_i^{(j)} \quad (3.26)$$

The steps *ii* to *vii* are repeated until the accuracy reaches to a specified tolerance η , which means that sufficient compatibility between the base deflections w_i and the soil settlements s_i is reached in the base-soil interface. Figure 3.10 shows the iteration cycle of the iteration process.

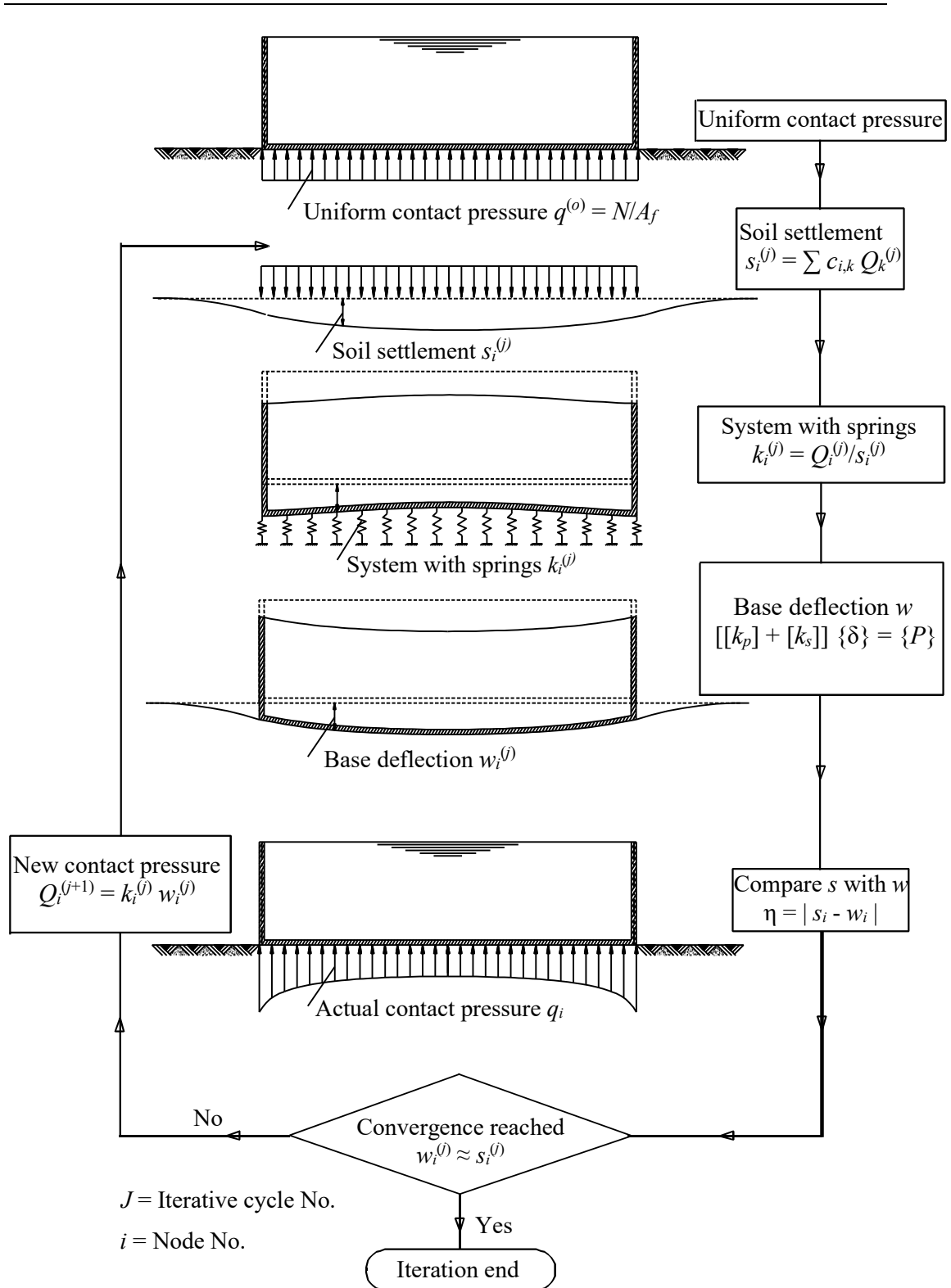


Figure 3.10 Iteration cycle of the iteration process

3.3.5 Continuum model for elastic base

Continuum model was first proposed by *Ohde* (1942), which based on the settlement will occur not only under the loaded area but also outside (Figure 3.11). Otherwise, the settlement at any nodal point is affected by the forces at all the other nodal points.

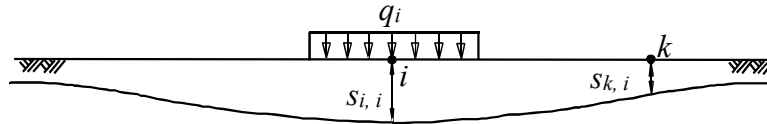


Figure 3.11 Influence line of elastic displacement in Continuum model

Continuum model assumes continuum behavior of the soil, where the soil is represented as isotropic elastic half-space medium or layered medium. Consequently, this model overcomes the assumption of *Winkler's* model, which does not take into account the interaction between the different points of the soil medium. Representation of soil as a continuum medium is more accurate as it realizes the interaction among the different points of the continuum medium. However, it needs mathematical analysis that is more complex. The earliest application for rafts on continuum medium using Finite elements-method related to *Cheung/ Zienkiewicz* (1965). These authors considered the soil as isotropic elastic half-space medium.

The isotropic elastic half-space soil medium bases on *Boussinesq's* solution (1885). The medium in this solution is semi-infinite homogeneous isotropic linear elastic solid subjected to a concentrated force. The force acts normal to the plane boundary at the surface. This basic solution can be used to obtain the surface settlement of isotropic elastic half-space soil medium subjected to a concentrated load acting on the ground surface.

Continuum model for elastic base, which is described here, considers the interaction between the base and soil. It represents the soil as layered soil medium (Figure 3.12).

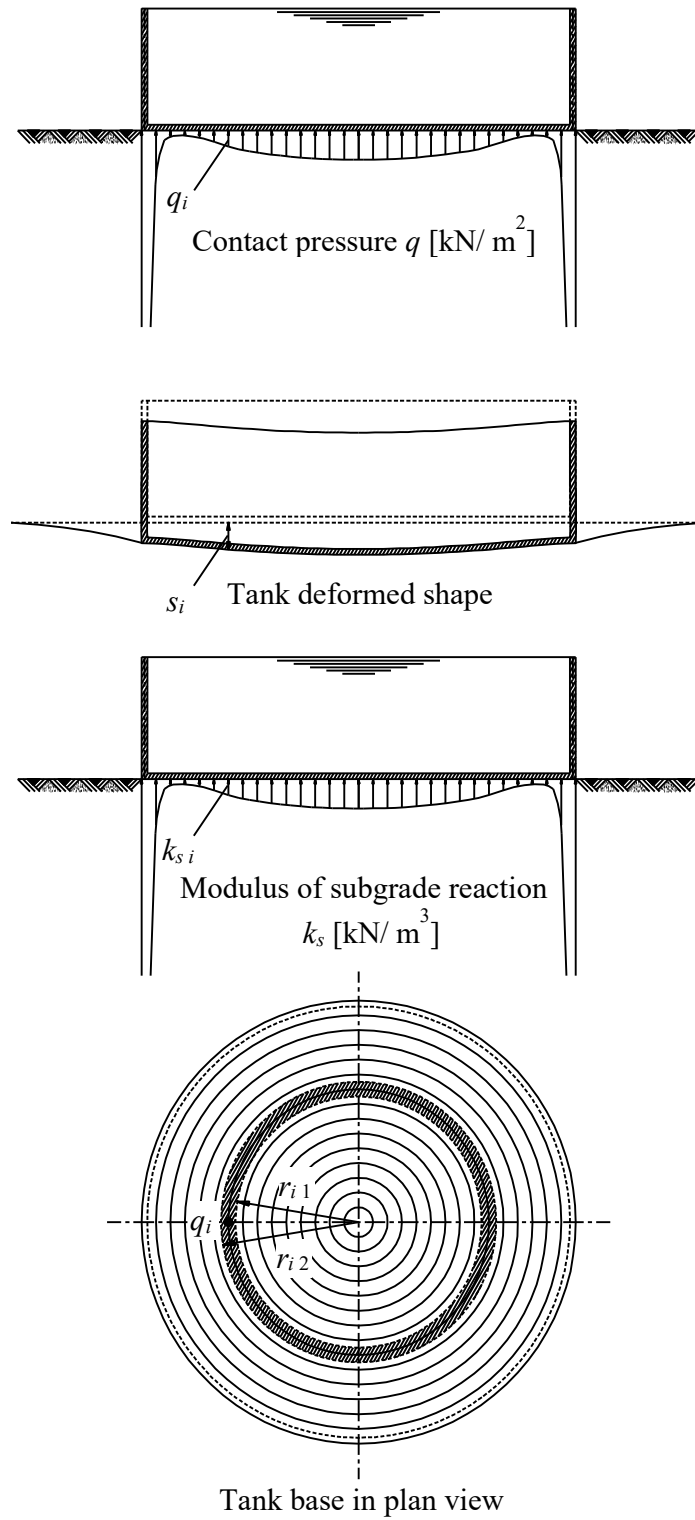


Figure 3.12 Continuum (elastic base) model

3.3.5.1 Formulation of flexibility matrix of soil

The settlement $s_{i, k}$ of the nodal ring i , due to contact force Q_k on nodal ring k , Figure 3.13, can be expressed by:

$$s_{i, k} = c_{i, k} Q_k \quad (3.27)$$

The ratio between the settlement $s_{i, k}$ of nodal ring i and the contact force Q_k at a nodal ring k is termed the flexibility coefficient $c_{i, k}$ [m/ kN]. It can be recognized as the settlement of a nodal ring i due to a unit load at a nodal ring k .

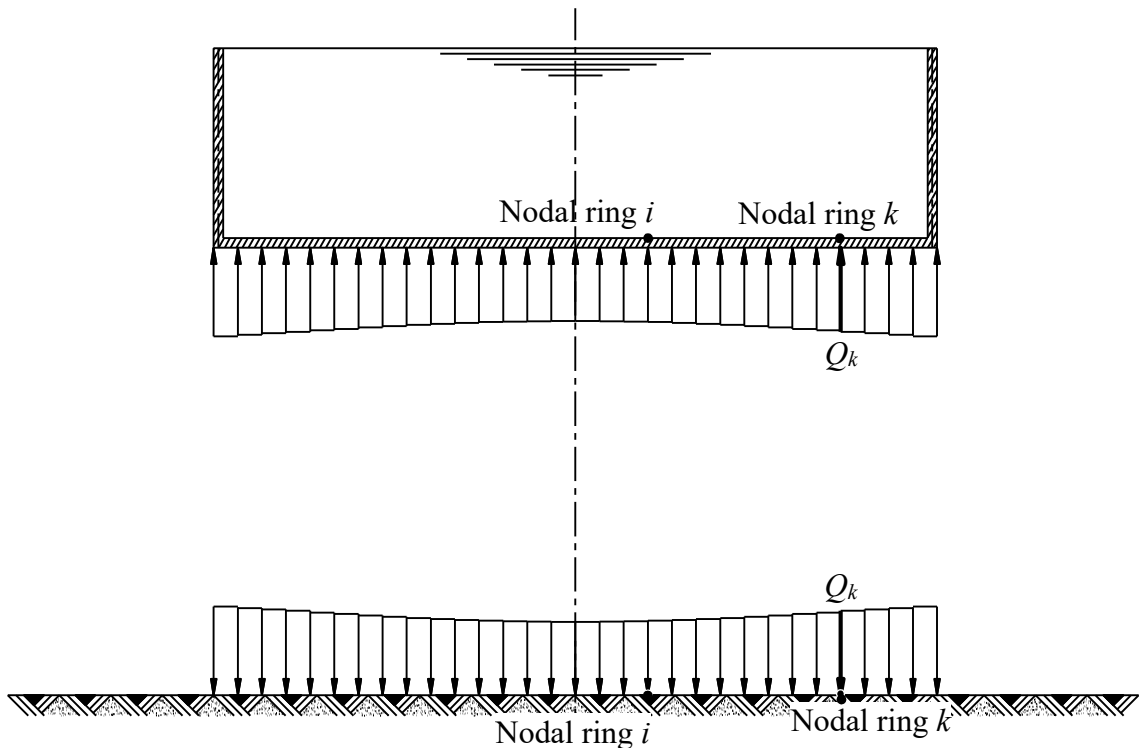


Figure 3.13 Settlement $s_{i, k}$ of nodal ring i due to contact force Q_k at nodal ring k

3.3.5.2 Assembling of the flexibility matrix

To find the settlement s_i at nodal ring i , equation (3.27) is applied for that nodal ring i , while equation (3.28) is applied for the other remaining nodal rings considering contact forces over nodal rings. For a set of nodal rings of Finite elements-mesh, the settlement at nodal ring i is obtained from:

$$s_i = s_{i, 1} + s_{i, 2} + s_{i, 3} + \dots + s_{i, n} = c_{i, 1} Q_1 + c_{i, 2} Q_2 + c_{i, 3} Q_3 + \dots + c_{i, n} Q_n \quad (3.28)$$

Equation (3.29) in series form is:

$$s_i = \sum_{k=1}^n c_{i,k} Q_k \quad (3.29)$$

Equation (3.29) for the entire foundation in matrix form is:

$$\begin{Bmatrix} s_1 \\ s_2 \\ s_3 \\ \vdots \\ s_n \end{Bmatrix} = \begin{bmatrix} c_{1,1} & c_{1,2} & c_{1,3} & \cdots & c_{1,n} \\ c_{2,1} & c_{2,2} & c_{2,3} & \cdots & c_{2,n} \\ c_{3,1} & c_{3,2} & c_{3,3} & \cdots & c_{3,n} \\ \vdots & \vdots & \vdots & \ddots & \vdots \\ c_{n,1} & c_{n,2} & c_{n,3} & \cdots & c_{n,n} \end{bmatrix} \begin{Bmatrix} Q_1 \\ Q_2 \\ Q_3 \\ \vdots \\ Q_n \end{Bmatrix} \quad (3.30)$$

Equation (3.30) is simplified to:

$$\{s\} = [c]\{Q\} \quad (3.31)$$

To assemble the flexibility matrix of the soil $[c]$, each node is loaded by a unit contact force and the resulting settlements in all remaining nodal rings and in the loaded rings are calculated. Inverting the flexibility matrix $[c]$, gives the $[n \times n]$ stiffness matrix of the soil $[k_s]$ corresponding to the contact forces at the n nodal rings such that:

$$\{Q\} = [k_s]\{s\} \quad (3.32)$$

3.3.5.3 Complete stiffness formulation for isotropic elastic half-space soil medium

The base will deflect under the action of the total external forces $\{F\}$ due to known applied loads $\{P\}$ and the unknown soil reactions $\{Q\}$, where:

$$\{F\} = \{P\} - \{Q\} \quad (3.33)$$

The equilibrium of the wall-base-soil system is expressed by the following matrix equation:

$$[k_p]\{\delta\} = \{P\} - \{Q\} \quad (3.34)$$

Considering the compatibility of deformation between the base and the soil medium, where the soil settlement s_i is equal to the base deflection w_i , equation (3.32) for Continuum model can be substituted into equation (3.34) as:

$$[[k_p]+[k_s]]\{\delta\} = \{P\} \quad (3.35)$$

Equation (3.35) shows that the stiffness matrix of the whole wall-base-soil system is the sum of the wall-base and the soil stiffness matrices, $[k_p] + [k_s]$.

It should be noticed that the matrix $[k_s]$ is not compatible with the matrix $[k_p]$, because the degrees of freedom in equation (3.32) differ from that in equation (3.34). To overcome this problem, equation (3.32) can be treated by extending the row and column of matrix $[k_s]$ in the same manner as the matrix $[k_p]$. Consequently, the operation of matrix equations can then be accepted.

3.3.5.4 Equation solver for isotropic elastic half-space soil medium

It should be noticed that the matrix $[k_s]$ is full matrix. Therefore, the total stiffness matrix for the raft and the soil is also full matrix.

The system of linear equations is solved by *Gauss* elimination-technique. Since the total stiffness matrix is a full matrix, the equation solver equation (3.35) takes long computation time by applying this method. The unknown variables in equation (3.35) are the nodal displacements w_i ($w_i = s_i$) and the nodal rotations χ_i . After solving the system of linear equation (3.35), substituting the obtained settlements s_i in equation (3.32), gives the unknown contact forces Q_i .

3.3.6 Continuum model for rigid base

In many practice cases, treating the tank as completely rigid is convenient. In this case, for a tank with symmetrical shape and loading, the unknowns of the interaction problem, Figure 3.14, are:

- n contact pressures q_i .
- Rigid body translation of the raft w_o at the centroid.

3.3.6.1 Formulation of the rigid raft

To describe the method, consider the base shown Figure 3.14. The contact pressure q_i at a nodal ring i under the base is replaced by equivalent contact force Q_i . For a set of nodal rings of elements-mesh, the settlement at a nodal ring i is obtained from:

$$s_i = \sum_{k=1}^n c_{i,k} Q_k \quad (3.36)$$

Considering the entire base, equation (3.36) can be rewritten in matrix form as:

$$\{s\} = [c]\{Q\} \quad (3.37)$$

Inverting the flexibility matrix $[c]$, gives the stiffness matrix of the soil $[k_s]$ corresponding to the contact forces at the n nodal rings such that:

$$\{Q\} = [k_s]\{s\} \quad (3.38)$$

For a tank with symmetrical load and shape, the settlement will be uniform ($s_i = w_o$) and the tank will not rotate ($\chi_o = 0$). Therefore, the unknowns of the problem reduce to n contact pressures q_i and rigid body translation w_o .

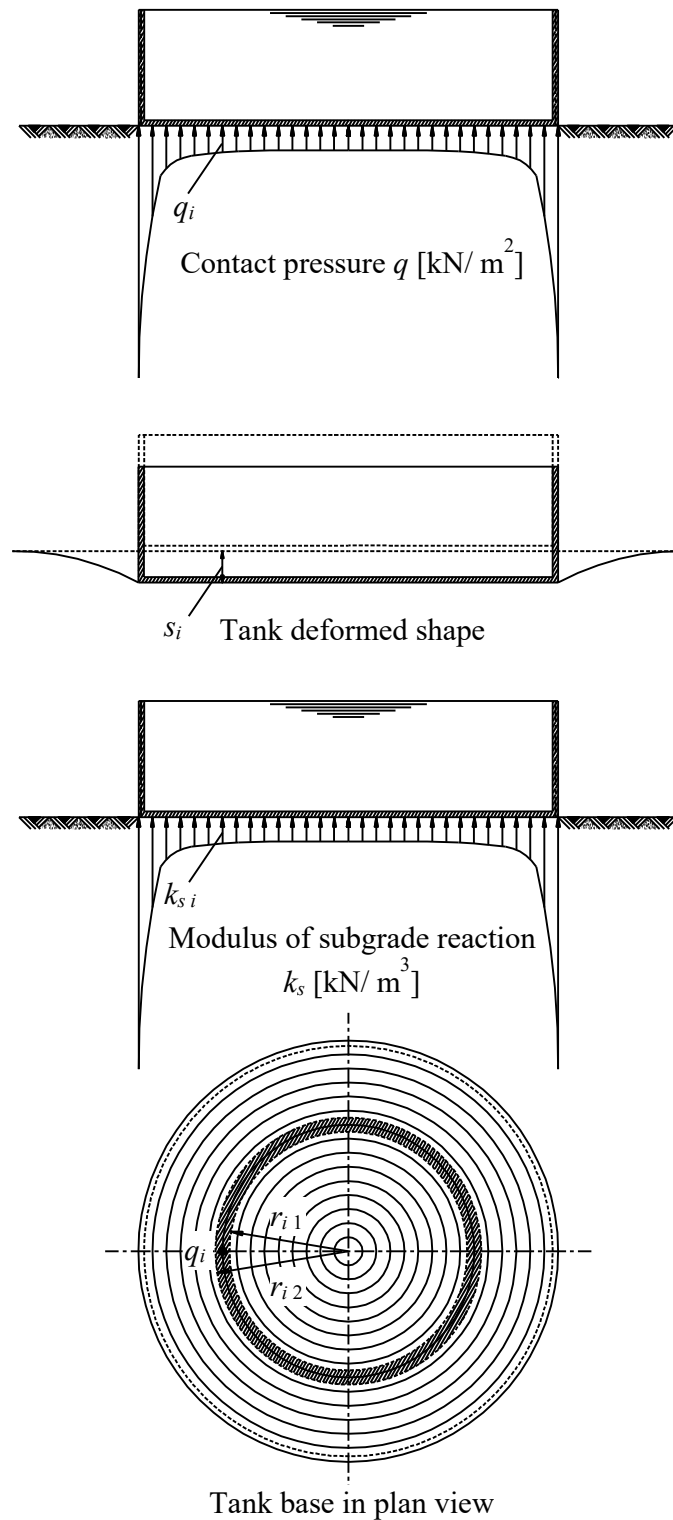


Figure 3.14 Continuum (rigid base) model

3.3.6.2 Derivation of uniform settlement w_o

The derivation of the uniform settlement for the rigid base can be carried out by equating the settlement s_i by uniform settlement w_o for all nodal rings in equation (3.38). In this case, the contact forces can be rewritten as a function in the terms $k_{i,j}$ of the soil stiffness matrix as follows:

$$\left. \begin{aligned} Q_1 &= k_{1,1} w_o + k_{1,2} w_o + k_{1,3} w_o + \dots + k_{1,n} w_o \\ Q_2 &= k_{2,1} w_o + k_{2,2} w_o + k_{2,3} w_o + \dots + k_{2,n} w_o \\ Q_3 &= k_{3,1} w_o + k_{3,2} w_o + k_{3,3} w_o + \dots + k_{3,n} w_o \\ &\vdots \\ Q_n &= k_{n,1} w_o + k_{n,2} w_o + k_{n,3} w_o + \dots + k_{n,n} w_o \end{aligned} \right\} \quad (3.39)$$

Carrying out the summation of the all contact forces:

$$\sum_{i=1}^n Q_i = w_o \sum_{i=1}^n \sum_{j=1}^n k_{i,j} \quad (3.40)$$

The rigid body translation w_o , which equals to the settlement s_i at all nodal rings, is obtained from:

$$w_o = \frac{\sum_{i=1}^n Q_i}{\sum_{i=1}^n \sum_{j=1}^n k_{i,j}} = \frac{N}{\sum_{i=1}^n \sum_{j=1}^n k_{i,j}} \quad (3.41)$$

Substituting this value of w_o in equation (3.38) gives the n unknown contact forces Q_i .

The summation of terms $k_{i,j}$ ($= N/w_o$) may be used to determine the modulus of subgrade reaction k_s .

3.3.7 Continuum model for flexible base

If the tank base is perfectly flexible, then the contact stress will be equal to the gravity stress exerted by the base on the underlying soil. See Figure 3.15.

For the set of nodal rings of the base, the soil settlements are:

$$\{s\} = [c]\{Q\} \quad (3.42)$$

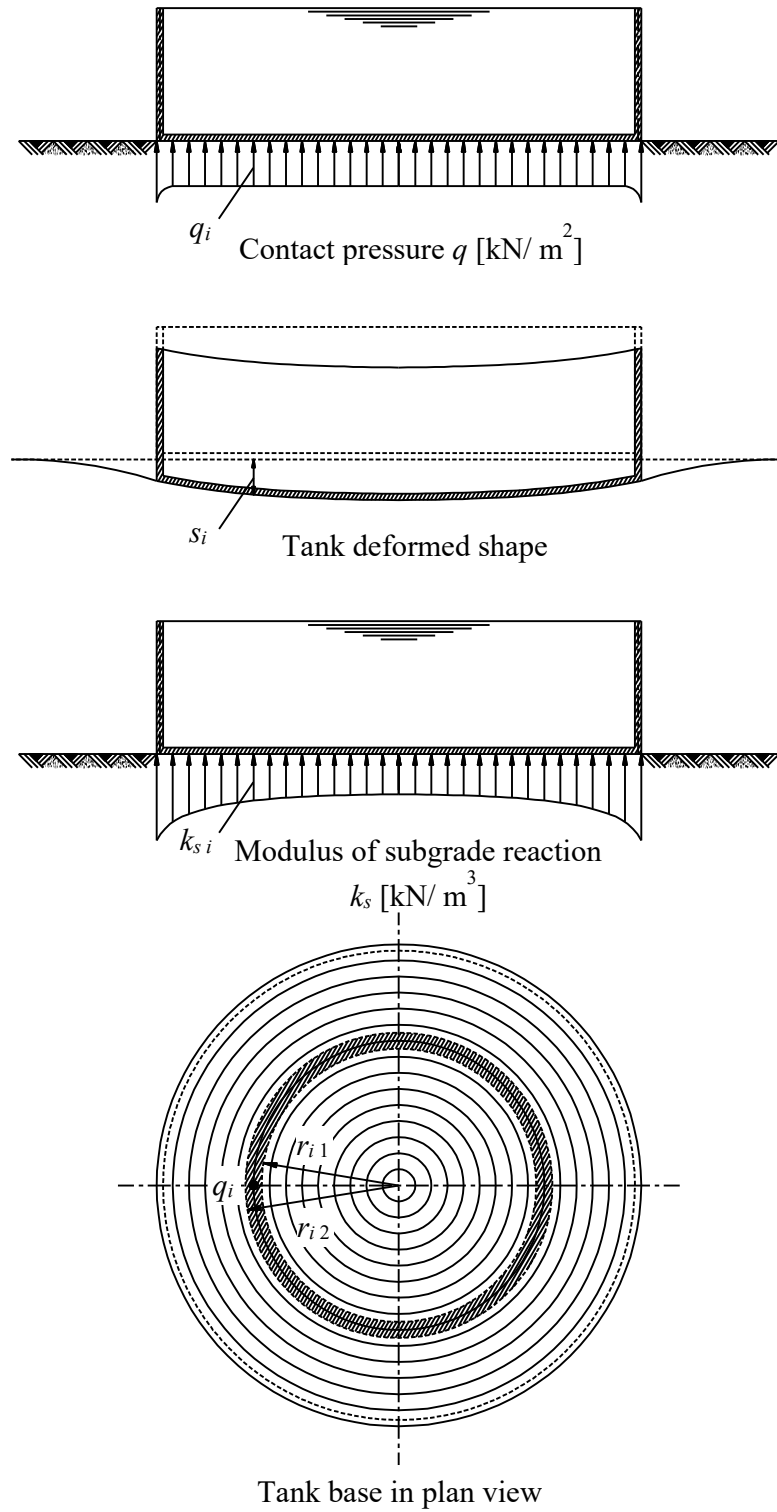


Figure 3.15 Continuum (flexible base) model

3.4 Analysis of water tanks under cyclic loading

3.4.1 Introduction

Consolidation is a time dependent problem. Soil properties and time dependent loading such as cyclic loading during the consolidation process would affect the rate and amount of the settlement at any time. Cyclic loadings are often applied to clay layers under structures subject to loading and unloading circumstances such as ground water tanks. Analyzing water tanks on clay under cyclic loading is a complex task because it is a three-dimensional problem including many difficulties. The main factors that must be considered in the analysis are: the interaction among the wall and base of the tank and the soil, the actual loading and geometry of the tank, to choose a suitable model to idealize the soil, and to treat the problem as a time-dependent settlement problem. In recent years, many authors suggested simplified methods to solve this problem [*Xie and Zhuang (2005)*, *Conte and Troncone (2006)*, *Toufigh and Ouria (2009)*, *Abbaspour (2014)* and *Ouria et al. (2015)*]. Most of the proposed solutions assumed that the subsoil is taken as a single layer subjected to an initial uniform excess pore water pressure along its entire height neglecting the effect of soil structure interaction.

Toufigh and Ouria (2009) presented a semi-analytical method to determine the pore water pressure and degree of consolidation for a rectangular cyclic loading, considering the effect of change of the consolidation coefficient of the clay layer. Changes in the consolidation coefficient are applied by modifying the loading and unloading durations using a virtual time. Based on the superimposing rule a set of continuous static loads in specified times are used instead of the cyclic load in the transformed time space. Each full cycle of loading is replaced by a pair of static loads with different signs. Based on the *Terzaghi's* theory the pore-water pressure distribution and the degree of consolidation are calculated for each static load and the results are superimposed. They verified the solution by carrying out a set of laboratory consolidation tests under cyclic loading. Throughout their solution, *Toufigh and Ouria (2009)* neglect the effect of structure rigidity on the consolidation and they did pay no account for soil stratification. They also assumed that the clay layer is subjected to an initial uniform excess pore water pressure.

In this research, the semi-analytical solution of *Toufigh and Ouria (2009)* is developed to study the behavior of circular storage tanks underlain by multi-layered soil; which is subjected to any variable stress distribution along the layers height by the *LEM* of *El Gendy and Herrmann (2014)*. The interaction between the subsoil layers and the tank structure throughout the entire cyclic load history is taken into consideration. Besides, the actual contact pressure under the tank can be obtained at any load cycle. The solution is applied for water tanks as a structure subjected to cyclic loading. Base of the tank may be considered as rigid, elastic or flexible. For analyzing the base of the tank as elastic base, full compatibility among the structure elements and subsoil is taken into account. The proposed

numerical solution of tanks resting on multi-layered soil and subjected to cyclic loading is described in the next sections.

3.4.2 Formulation of pore water pressure for static loading

To formulate the analysis, the loaded area on the soil surface under the tank is divided into annular circular elements; each of which is subjected to a different intensity of contact pressure q_k , as shown in Figure 3.16. The soil under the loaded area may consist of a system of successive clay layers with different soil parameters; which is divided into n sub-layers with r nodes as shown in Figure 3.16. Stress coefficients for the annular circular elements can be determined as described by *El Gendy* (2006).

For a set of annular elements of m contact pressures q_j at the surface, the vertical stress σ_l at a node located at depth l under the surface node k can be computed as the sum of the stresses caused by all of the contact pressures on that node:

$$\sigma_l = \sum_{j=1}^m f_{l,j} q_j \quad (3.43)$$

where $f_{l,j}$ is the stress coefficient of node l due to the contact pressure at annular element j on the surface. It depends only on the geometry of the loaded area and the soil layer.

Referring to Figure 3.16 every soil layer i has its own soil parameters such as: the coefficient of permeability k_{vi} [m/Year], the coefficient of consolidation c_{vi} [Year/m²], the coefficient of volume change m_{vi} [m²/kN], the depth z_i [m], and the thickness h_i [m]. H [m] is the sum of heights of all clay layers.

At any time $t = 0$, Equation (3.43) can be written in a matrix form for any section along the z -axis passing through point k through the entire clay layers, as:

$$\{\sigma\}_o = [f]\{q\}_o \quad (3.44)$$

where $\{\sigma\}_o$ is the initial vertical stress vector at time $t = 0$, $[f]$ is the stress coefficient matrix and $\{q\}_o$ is the initial contact pressure vector at time $t = 0$.

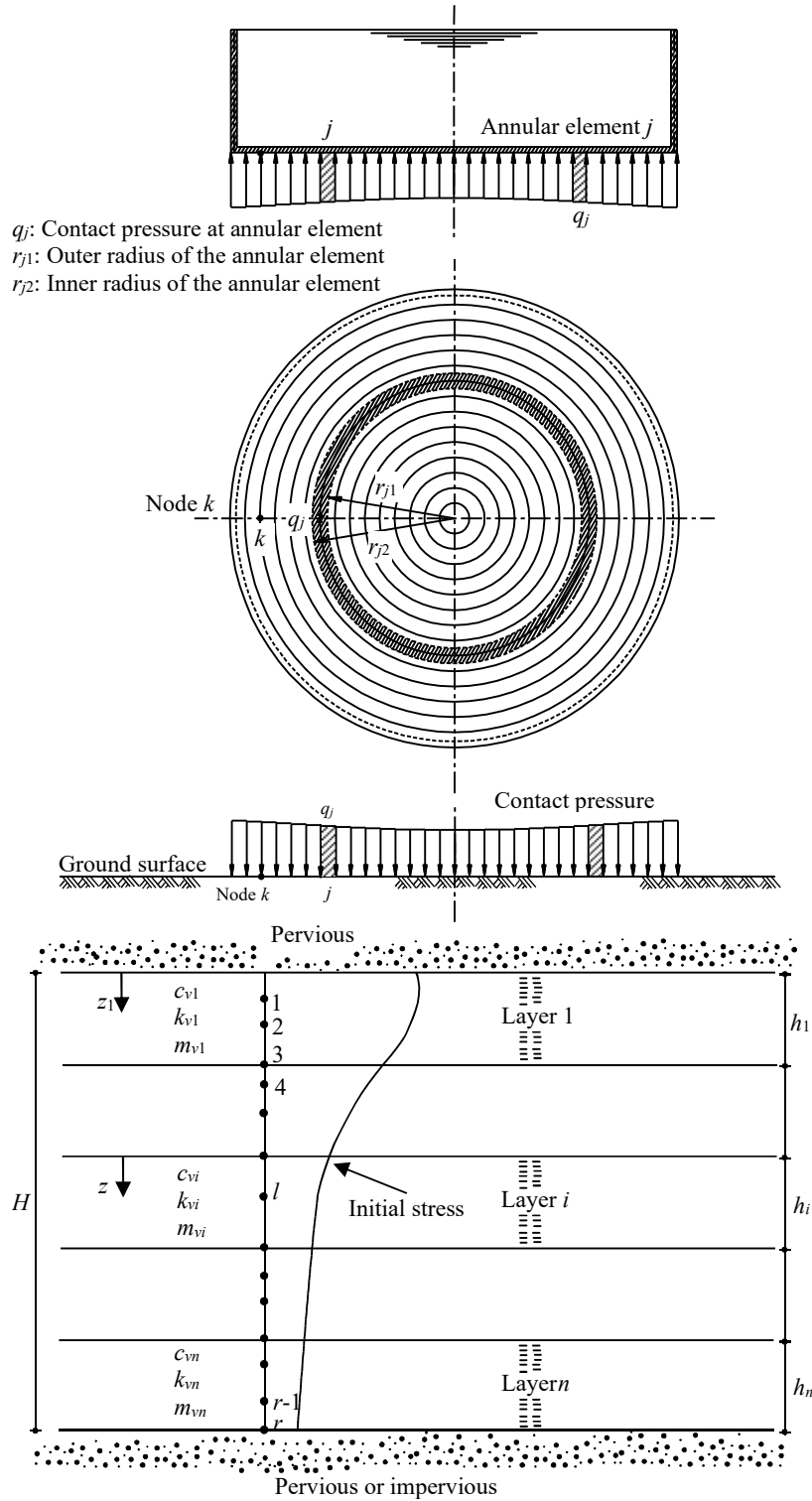


Figure 3.16 Stress σ_l under a node k due to a contact pressure q_j at element j

For a constant loading as described in Figure 3.17, the excess pore water pressure at any time t at a point k on the base of the tank according to *LEM*, is given by:

$$\{u\}_t = [\Phi] [E_v]^t [\Phi]^{-1} \{u\}_o \quad (3.45)$$

where $\{u\}_t$ is the vector of the excess pore water pressure u_i , $i=1$ to r , $\{u\}_o$ is the initial excess pore water pressure, $\{\sigma\}_o$ the initial vertical stress vector, $[\Phi]$ is the matrix of basic functions and $[E_v]$ is the diagonal square matrix of the exponential functions.

Details of the matrices $[\Phi]$ and $[E_v]$ are listed in *El Gendy and Herrmann (2014)*.

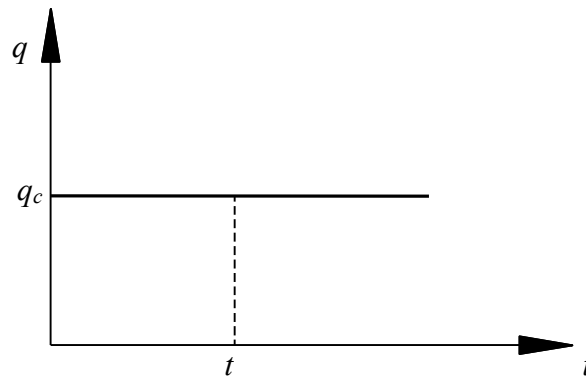


Figure 3.17 Constant loading with time

3.4.3 Formulation of pore water pressure for time-dependent loading

In practice, the total load on clay under a structure may be applied linearly over a period of time. In this case, the total load of construction on the surface q_c can be applied gradually over a time t_c as shown in Figure 3.18.

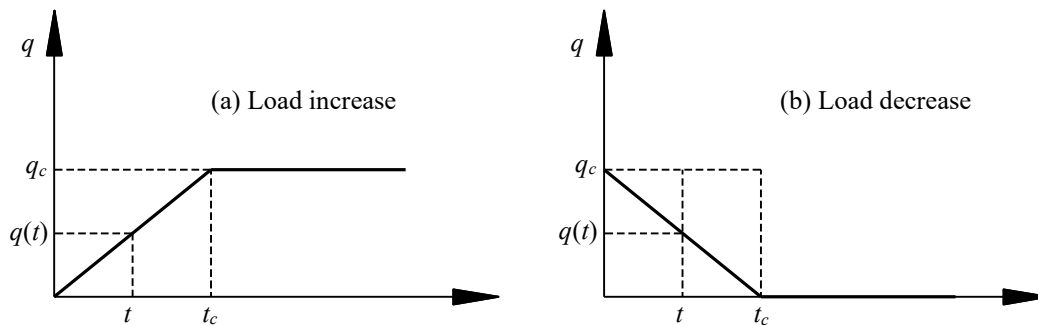


Figure 3.18 Linear loading with time

3.4.3.1.1 Case of $t \geq t_c$

If $t = t_c$ or $t > t_c$, the excess pore water pressure can be found as:

$$\{u\}_t = \pm [\Phi] [E_v]^t [D] [\Phi]^{-1} \{u\}_o \quad (3.46)$$

where $[D]$ is a diagonal square matrix for which the element D_j is given by:

$$D_j = \frac{\exp(\omega_j t_c) - 1}{\omega_j t_c} = \frac{\exp(\lambda_j^2 T_{vc1}) - 1}{\lambda_j^2 T_{vc1}} \quad (3.47)$$

where λ_j is the differential equation operator and T_{vc1} is the time factor at time t_c for layer number 1 in a multilayered soil system. In this case T_{vc1} can be calculated as:

$$T_{vc1} = \frac{C_{v1} t_c}{h_1^2} \quad (3.48)$$

where C_{v1} is the coefficient of consolidation of layer number 1 in a multilayered soil system in [m^2/year], h_1 is the thickness of layer number 1, in [m], and ω_j is a factor given by:

$$\omega_j = \frac{C_{v1}}{h_1^2} \lambda_j \quad (3.49)$$

3.4.3.1.2 Case of $t \leq t_c$

If $t < t_c$, the load is assumed to be proportional to time, then:

$$\frac{q}{q_c} = \frac{t}{t_c} \quad (3.50)$$

The excess pore water can be expressed as:

$$\{u\} = \frac{t}{t_c} [\Phi] [E_v]^t [D] [\Phi]^{-1} \{u\}_o \quad (3.51)$$

In this case, the diagonal elements of the matrix $[D]$ are given as:

$$D_j = \frac{\exp(\omega_j t) - 1}{\omega_j t} \quad (3.52)$$

The excess pore water pressure given in equation (3.46) would have a positive sign for the case of load increase and it would have a negative sign for the case of load decrease.

Equations (3.46) and (3.51) can be combined to express the pore water pressure in a general form as:

$$\{u\} = \pm[\Phi] [E_v]^t [D_j^*] [\Phi]^{-1} \{u\}_o \quad (3.53)$$

In this case, the diagonal elements of the matrix $[D^*]$ are given by:

$$D_j^* = \frac{\exp(\omega_j t) - 1}{\omega_j t_c} = \frac{\exp(\lambda_j^2 T_{v1}) - 1}{\lambda_j^2 T_{vc1}} \quad (3.54)$$

where T_{v1} is the time factor at time t for layer number 1 in a multilayered soil system, and it can be calculated from equation (3.48) by replacing t_c with t .

3.4.4 Degree of Consolidation

3.4.4.1 Degree of consolidation for load increase

For load increase, the degree of consolidation U_p and U_s at time t can be obtained based on either the stress or the settlement. The degree of consolidation U_p can be written as a function of the stress as:

$$U_p = \frac{\sum_{i=1}^n \Delta\sigma(t)_i h_i - \sum_{i=1}^n \Delta u_i h_i}{\sum_{i=1}^n \Delta\sigma_{oi} h_i} \quad (3.55)$$

where Δu_i is the average excess pore water pressure at any time factor in that layer, $\Delta\sigma_{oi}$ is the initial average stress in a layer i and $\Delta\sigma(t)_i$ is the average stress in a layer i at time t .

In this case, the degree of consolidation U_p can be expressed as a function of the applied current load q as:

$$U_p = \frac{q}{q_c} - \frac{\sum_{i=1}^n \Delta u_i h_i}{\sum_{i=1}^n \Delta \sigma_{oi} h_i} \quad (3.56)$$

In the same manner, the degree of consolidation U_s can be written as a function of the settlement as:

$$U_s = \frac{q}{q_c} - \frac{\sum_{i=1}^n m_{vi} \Delta u_i h_i}{\sum_{i=1}^n m_{vi} \Delta \sigma_{oi} h_i} \quad (3.57)$$

where m_{vi} is the coefficient of volume change of a layer i .

3.4.4.2 Degree of consolidation for load decrease

For load decrease, both the stress dependent- and the settlement dependent degree of consolidation, U_p and U_s , respectively, can be expressed as:

$$U_p = \left(1 - \frac{q(t)}{q_c}\right) - \frac{\sum_{i=1}^n \Delta u_i h_i}{\sum_{i=1}^n \Delta \sigma_{oi} h_i} \quad (3.58)$$

$$U_s = \left(1 - \frac{q(t)}{q_c}\right) - \frac{\sum_{i=1}^n m_{vi} \Delta u_i h_i}{\sum_{i=1}^n m_{vi} \Delta \sigma_{oi} h_i} \quad (3.59)$$

3.4.5 Behavior of elastic clay under cyclic loading

If the soft clay layer is overconsolidated (OC) at the beginning of the loading, and the effective stress at the end of every loading phase is smaller than the preconsolidation pressure, the clay will consolidate and expand with the properties of the overconsolidated clay as shown in Figure 3.19. This type of clay is called elastic clay, which remain in the same state under cyclic loading. Figure 3.19-(a) shows the idealized e - $\text{Log}(\sigma')$ relationship, where e_{co} , e_o and e_{min} . [-] are the void ratios corresponding to initial preconsolidation pressure σ'_{co} , initial effective stress caused by the weight of the soil itself at the middle of the layer σ'_o and maximum effective stress at the end of the loading phase σ'_{max} . [kN/m^2], respectively. The slopes of the straight lines in the e - $\text{Log}(\sigma')$ relationship are: the compression index C_c [-], the swelling index C_s [-] and for simplicity it is considered to equal the

recompression index, C_r [-], the slope of reloading line in e - $\text{Log}(\sigma')$ space. On the other hand, according to Figure 3.19-(b), for an overconsolidated clay a similar linear relationship can be presented between void ratio and permeability, where k_{vco} , k_{vo} and $k_{v \text{ min.}}$ are the coefficients of permeability corresponding to initial consolidation pressure, σ'_{co} , initial effective stress, σ'_o , and maximum effective stress at the end of the loading phase, σ'_{max} . [kN/m²], respectively. The slopes of the straight lines in the e - $\text{Log}(k_v)$ relationship are: the permeability index for compression, C_{ck} [-], the permeability index for swelling, C_{sk} [-], and it is equal to the permeability index for recompression C_{rk} [-], the slope of reloading line in e - $\text{Log}(k_v)$ space.

It's obvious from Figure 3.19 that the soil consolidate and expand with the recompression properties at the route (1-2) and (2-1). In elastic clay, the coefficient of consolidation is constant during loading and unloading phases as shown in Figure 3.19-(c). The distribution of the average degree of consolidation for elastic clay subjected to rectangular cyclic load is shown in Figure 3.19-(d).

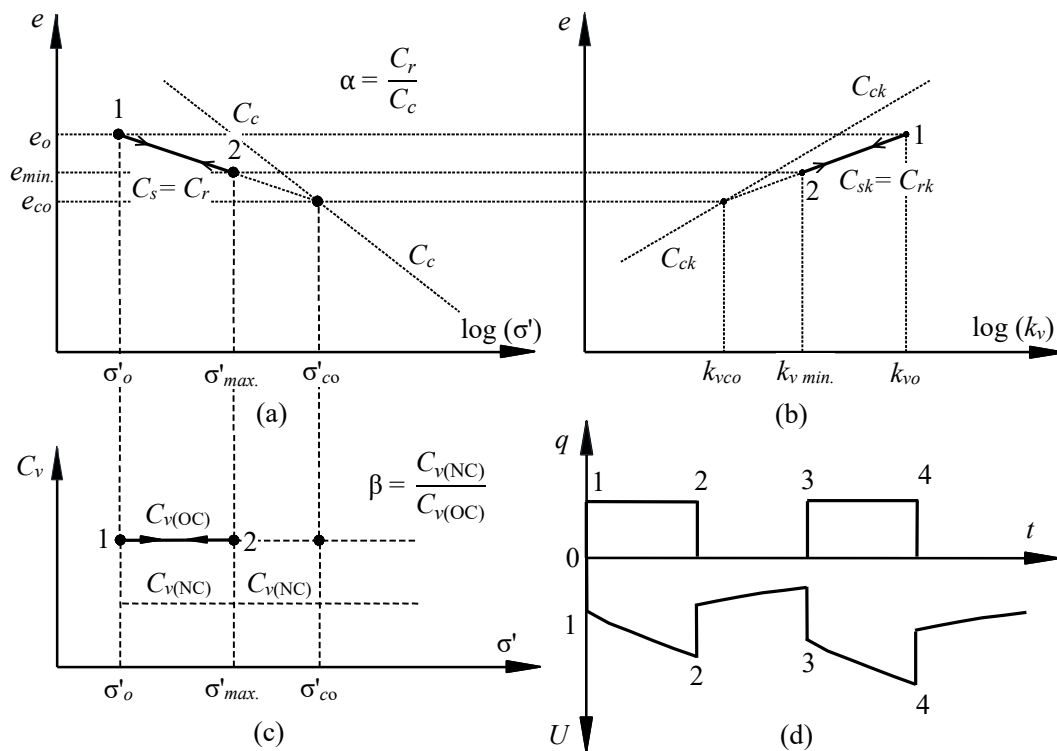


Figure 3.19 Behavior of elastic overconsolidated clay ($\sigma'_{max} < \sigma'_{co}$)

3.4.6 Behavior of plastic clay under cyclic loading

Plastic behavior of soils in a limited stress range under a cyclic of loading can be considered using bilinear model that is shown in Figure 3.20. According to this model, the coefficients of volume change m_v and permeability k_v of plastic clays changes during the loading and unloading phases. Therefore, the coefficient of

consolidation C_v is considered as a function of these parameters and changes in each cycle of loading.

At the beginning of loading, soil is in normally consolidated (NC) state and stress path is according to route [1-2], as shown in Figure 3.20-(a), (b) and (c). During the unloading phase, soil is at OC state and stress path is according to routes [2-3], [5-6] and so on. After the first full cycle, in the next loading phase, stress path will be according to route [3-4-5]. Point 4 is the position of the new preconsolidation pressure σ_{c1} , which is more than the initial preconsolidation pressure σ_{co} . The preconsolidation pressure σ_{cN} increases by increasing number of cycles and reaches to a point where the soil body stays in OC state during the entire loading phases, which is called steady-state condition (SSC).

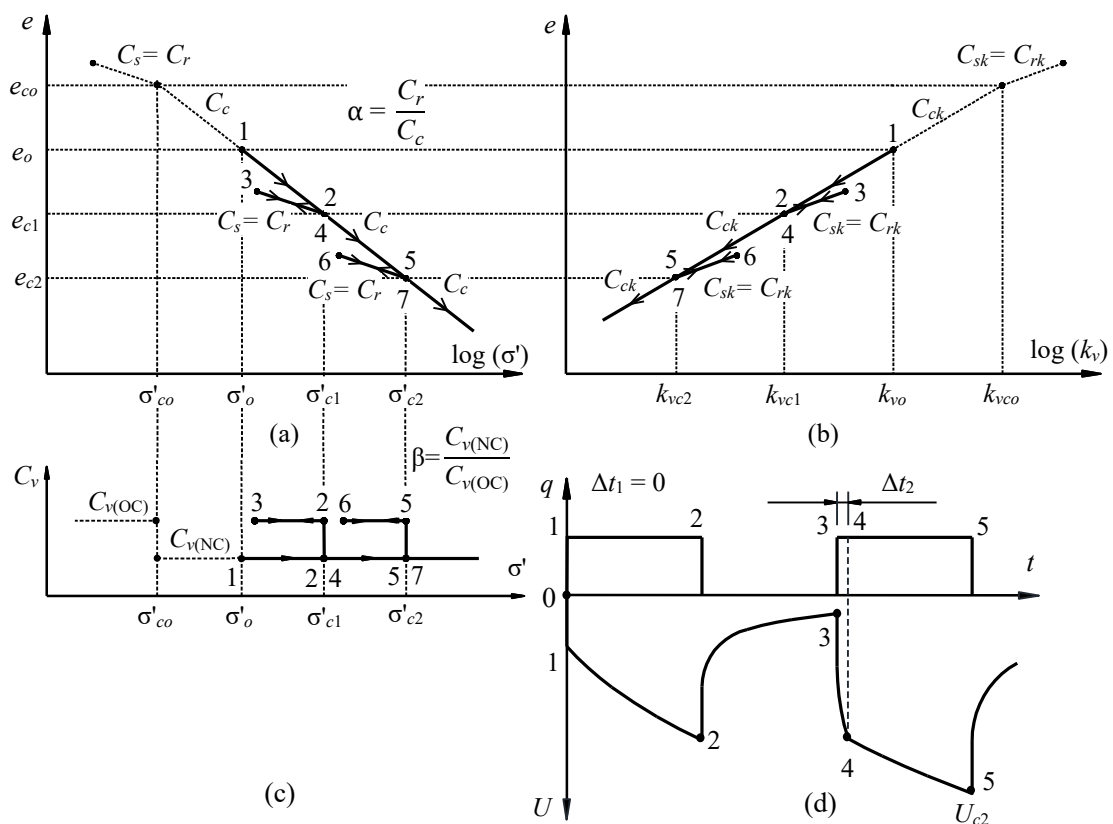


Figure 3.20 Behavior of plastic normally consolidated clay ($\sigma'_{o} > \sigma'_{co}$)

According to the bilinear model shown in Figure 3.20-(c), C_v changes around points 2, 4 and 5, 7. One of the main objectives in this case is to determine the required time to get to points of preconsolidation pressure as points 4 and 7 in every reloading phase.

Points 2 and 5 are located at the beginning of the unloading phase and are known. The soil is in the NC state when the average degree of consolidation is greater than its previous values (according to routes [1-2] and [4-5] in Figure 3.20). It is OC when it does not have the maximum of the previous values (according to routes [2-3-4] and [5-6-7] in Figure 3.20).

In linear analysis of the consolidation process, the coefficient of consolidation C_v is assumed to have only two different values in the state of NC or OC and changes suddenly when the soil changes from NC to OC or vice versa where; $C_{v(\text{NC})} = \beta C_{v(\text{OC})}$ as shown in Figure 3.20-(c). Also the coefficient of volume change m_v has only two values and changes when the soil changes from NC to OC state or vice versa.

According to *Toufigh/ Ouria (2009)* and *Yazdani/ Toufigh (2012)*; the coefficient of volume change or compression index for loading and reloading may be expressed in the ratio α as:

$$\alpha = \frac{m_r}{m_v} = \frac{C_r}{C_c} \quad (3.60)$$

The coefficient of permeability k_v has also two values calculated using the famous equation of *Terzaghi*:

$$C_v = \frac{k_v}{m_v \gamma_w} \quad (3.61)$$

The degree of consolidation for plastic clay subjected to rectangular cyclic load is shown in Figure 3.20-(d). *Yazdani/ Toufigh (2012)* performed a series of experiments in which they reached that making $\alpha = \beta$ is a reasonable result, where β is the ratio between the coefficient of consolidation for loading and reloading states as:

$$\beta = \frac{C_{v(\text{NC})}}{C_{v(\text{OC})}} \quad (3.62)$$

Figure 3.21 shows the degree of consolidation for a clay in elastic and plastic states to illustrate the behavior of plastic clay under cyclic load. This figure presents two elastic conditions for the clay, one with NC parameters of the same material and the other one with OC parameters of the same material. In addition to these two states, a plastic state is also considered for the same clay. For case of compression, only the maximum points of the degree of consolidation curve in each loading cycle are plotted in Figure 3.21.

It can be seen that the curve of plastic problem start similar to the curve of the elastic NC problem because they are both NC at the beginning. As time passes, the curve of the plastic problem approach the curve of the elastic OC problem. After certain number of cycles, the degree of consolidation increases by increasing number of cycles and reaches to a point where the soil body stays in OC state during the entire loading phases, which is called steady-state.

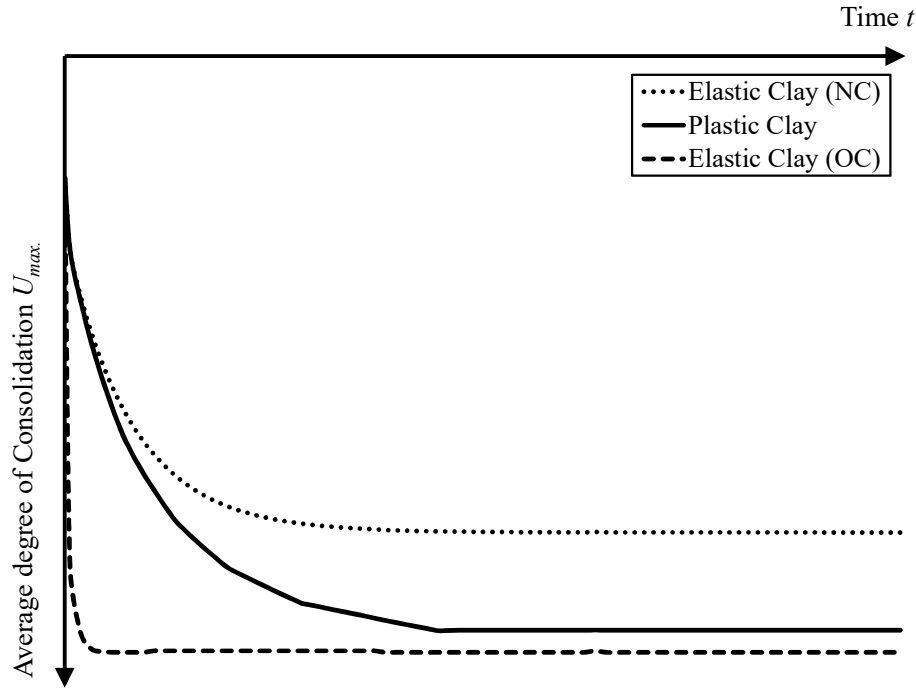


Figure 3.21 Consolidation of plastic clay under cyclic loading

3.4.7 Virtual time method for modeling rectangular cyclic loading

To illustrate the solution of the consolidation of the clay under cyclic loading using the virtual time method in a simple way, consider the bilinear model as shown in Figure 3.22, which describes one cycle of rectangular cyclic loading. In the model, the coefficients of volume change m_v and permeability k_v of the clay changes during the loading and unloading half cycles. The coefficient of consolidation C_v is a function of these parameters and changes in each cycle of loading. The coefficient of consolidation is assumed to have only two different values in the state of normally consolidated NC or overconsolidated OC as indicated before, where $C_{v(\text{NC})} = \beta C_{v(\text{OC})}$.

In Figure 3.22, at the loading phase of the cycle, clay is in NC state and stress path is according to [1-2] route. During the unloading process of all unloading phases, clay is at OC state and stress path is according to [2-3] route. After the first full cycle, in the next loading phase of the cycle, stress path will be according to [3-4-5] route. Position of point 4 is the same as the preconsolidation pressure σ_c application point, which represents the maximum degree of consolidation that the

clay obtained in the previous cycle. This σ_c increases by increasing number of cycles and reaches to a point where the clay stays in OC state during the entire loading phases, which is called steady-state. The clay is in the NC state when the degree of consolidation is greater than its previous values (according to routes [1-2] and [4-5]). It is OC when it does not have the maximum of the previous values (according to the route [2-3-4]).

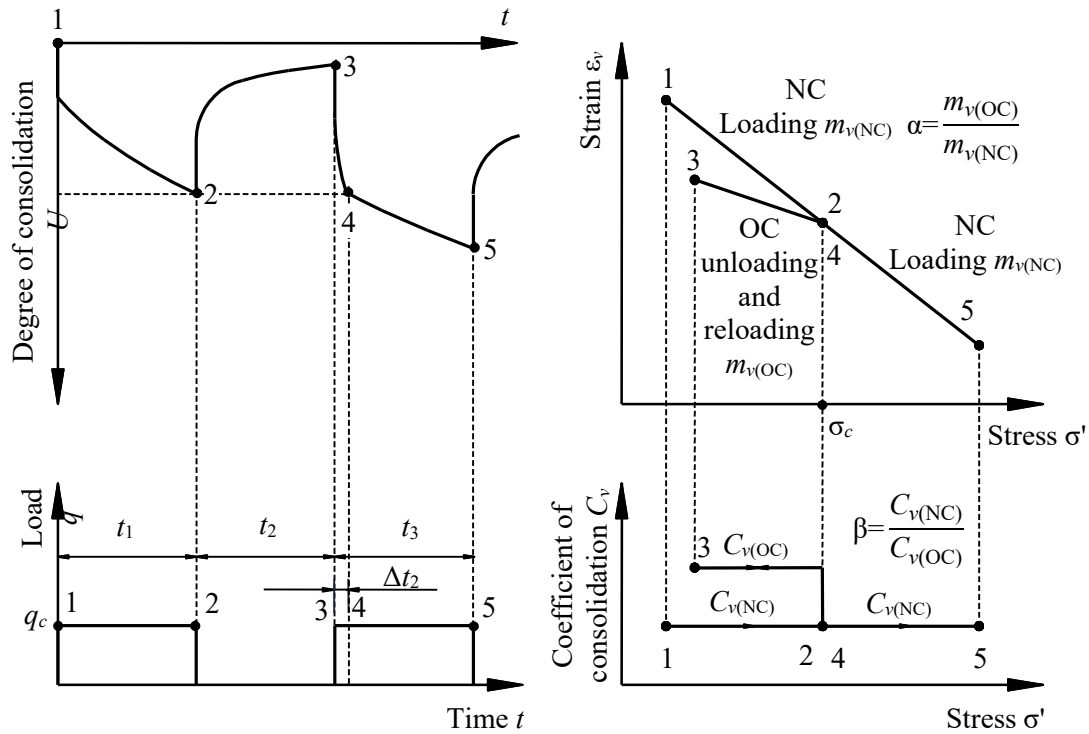


Figure 3.22 Behavior of NC clay under rectangular cyclic loading

Cyclic loading calculation requires to use two different values of coefficient of consolidation, $C_{v(NC)}$ for NC state and $C_{v(OC)}$ for OC state, while elements of the matrices $[\Phi]$ and $[E_v]$ in equation (3.45) are derived from only one C_v for each soil layer at any time during the consolidation process. Therefore, to use this equation in either loading or reloading state a way to keep only one C_v for both states is required.

Since the time factor T_v , is a linear function of coefficient of consolidation C_v and time t , it means that the equal variation of both factors would cause same changes in the results. In order to obtain the results considering the varying C_v , any changes of the C_v is applied to t and C_v is assumed to be constant as described in the following time factor equation:

$$T_v = \frac{(kC_v)t}{H_d^2} = \frac{C_v(kt)}{H_d^2} = \frac{C_v t'}{H_d^2}, \quad t' = kt \quad (3.63)$$

where H_d is the length of the drainage pass, t is the real time, t' is the virtual time and k can be any factor.

This idea introduces a transformation function, where a clay layer in which C_v is variable, constant C_v can be substituted in an adjusted time space. During the time period of the unloading phases, where the clay is in OC state, the value of C_v is different from its value in NC state. In this case, the calculation can be carried out by $C_{v(\text{NC})}$ and a virtual time t' .

Therefore, the equivalent time for unloading phases may be defined as:

$$t'_{2N} = \frac{t_{2N}}{\beta}, \quad N = 1, 2, 3, \dots \quad (3.64)$$

where N is the number of cycles and β is the virtual time factor.

3.4.8 Determining the time portion of each phase

After the first full cycle as indicated in Figure 3.23, the clay is in OC state until the degree of consolidation $U_{\Delta 2}$ reaches the previous maximum degree of consolidation, which is equal to the degree of consolidation at the end of the last loading phase U_{c1} . The time portion of each loading phase Δt_N shown in Figure 3.23 to get points similar to point 4 in every loading phase can be replaced by:

$$\Delta t'_N = \frac{\Delta t_N}{\beta} \quad (3.65)$$

3.4.9 Formulation of pore water pressure for rectangular cyclic loading

Figure 4.4 shows rectangular cyclic loading adapted by the superimposing rule using virtual time according to *Toufig and Ouria (2009)*. In this type of loading, Δt_N is the time portion of each loading phase, in which the clay is in OC state and then becomes NC. In order to define the virtual time transformation function for loading phases, the value of Δt_N must be known. It can be determined through iteration. On the other hand, superimposing rule can be used to replace a cyclic loading by a set of static loads. As shown in Figure 3.24, the cyclic loading system in the real time space is adapted in the virtual time space, each full cycle of cyclic load is replaced by a pair of static loads with plus and minus signs. Then, the vector of pore water pressure for rectangular cyclic loading at any cycle can be easily determined.

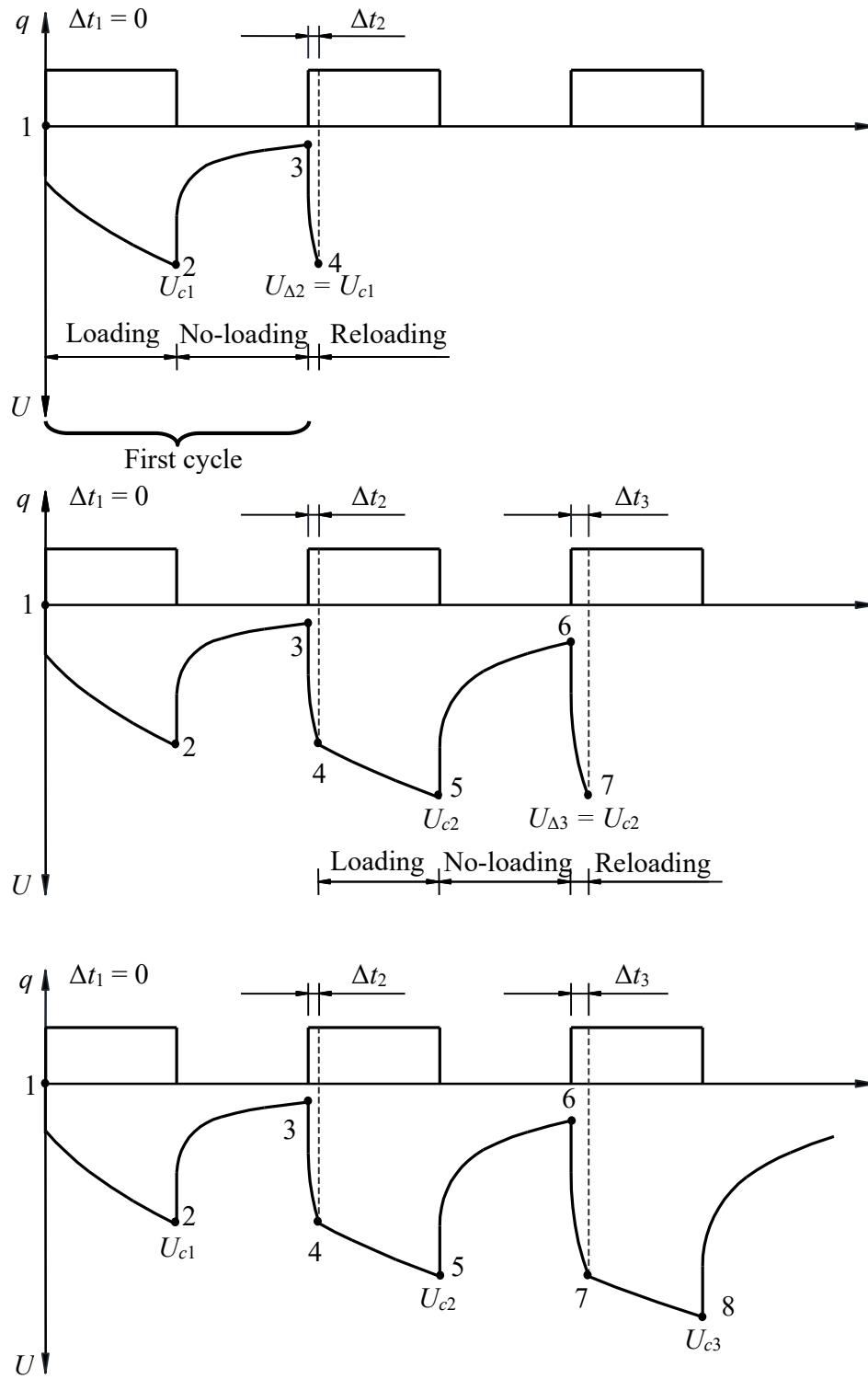


Figure 3.23 Determining the value of Δt_N for rectangular cyclic loading

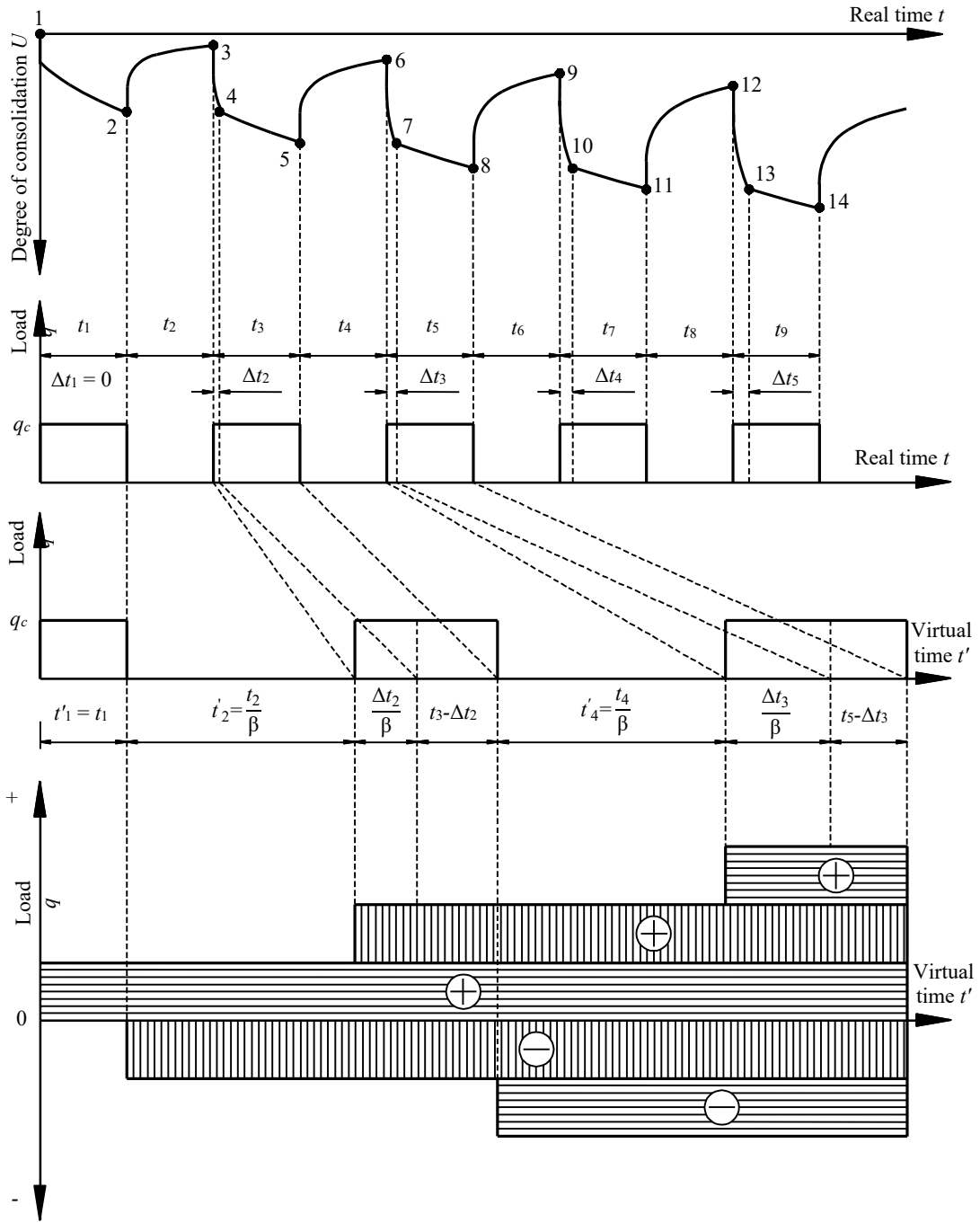


Figure 3.24 Rectangular cyclic loading adapted by the superimposing rule

3.4.10 Cyclic loading for flexible base

To describe the analysis of a water tank under cyclic loading, consider the water tank in Figure 3.16 and the rectangular cyclic loading in Figure 3.24. If the base of the tank is perfectly flexible (when neglecting the tank rigidity), then the contact stress will be equal to the gravity stress exerted by the tank on the underlying soil. In this case, the vector of pore water pressure for rectangular cyclic loading at a period of time $2t_c$ under any point on the base can be determined using *LEM of El Gendy and Herrmann (2014)* as follows:

At the first half cycle (point 2), the pore water pressure vector is:

$$\{u\}_1 = [\Phi] [E_v] \frac{t_c}{2} [\Phi]^{-1} \{u\}_o \quad (3.66)$$

At the second half cyclic (point 3), the pore water pressure vector is:

$$\{u\}_2 = [\Phi] [E_v] \left(\frac{t_c + t_c}{2} \right) [\Phi]^{-1} \{u\}_o - [\Phi] [E_v] \frac{t_c}{2\beta} [\Phi]^{-1} \{u\}_o \quad (3.67)$$

At the end of interval time Δt_2 (point 4), the pore water pressure vector is:

$$\{u\}_3 = [\Phi] [E_v] \left[\left(\frac{t_c + t_c}{2} \right) + \frac{\Delta t_2}{\beta} \right] [\Phi]^{-1} \{u\}_o - [\Phi] [E_v] \frac{t_c + \Delta t_2}{2\beta} [\Phi]^{-1} \{u\}_o + [\Phi] [E_v] \quad (3.68)$$

At the middle of the second cycle (point 5), the pore water pressure vector is:

$$\begin{aligned} \{u\}_4 = & [\Phi] [E_v] \left[\left(\frac{t_c + t_c + \Delta t_2}{2} \right) + \left(\frac{t_c - \Delta t_2}{2} \right) \right] [\Phi]^{-1} \{u\}_o - [E_v] \left[\left(\frac{t_c + \Delta t_2}{2\beta} \right) + \left(\frac{t_c - \Delta t_2}{2} \right) \right] [\Phi]^{-1} \{u\}_o \\ & + [\Phi] [E_v] \frac{\Delta t_2}{\beta} + \left(\frac{t_c - \Delta t_2}{2} \right) [\Phi]^{-1} \{u\}_o \end{aligned} \quad (3.69)$$

At the end of the second cycle (point 6), the pore water pressure vector is:

$$\begin{aligned} \{u\}_5 = & [\Phi] [E_v] \left[\left(\frac{t_c + t_c + \Delta t_2}{2} \right) + \left(\frac{t_c - \Delta t_2}{2} \right) + \frac{t_c}{2\beta} \right] - [\Phi] [E_v] \left[\left(\frac{t_c + \Delta t_2}{2\beta} \right) + \left(\frac{t_c - \Delta t_2}{2} \right) + \frac{t_c}{2\beta} \right] \\ & + [\Phi] [E_v] \frac{\Delta t_2}{\beta} + \left(\frac{t_c - \Delta t_2}{2} \right) + \frac{t_c}{2\beta} [\Phi]^{-1} \{u\}_o - [\Phi] [E_v] \frac{t_c}{2\beta} [\Phi]^{-1} \{u\}_o \end{aligned} \quad (3.70)$$

Equations (3.67) to (3.70) may be rewritten as:

$$\{u\}_2 = [\Phi] \left[[E_v] \left(\frac{t_c + t_c}{2} \right) - [E_v] \frac{t_c}{2\beta} \right] [\Phi]^{-1} \{u\}_o \quad (3.71)$$

$$\{u\}_3 = [\Phi] \left[[E_v] \left(\frac{t_c + \frac{t_c}{2}}{2} + \frac{\Delta t_2}{2\beta} \right) - [E_v] \frac{t_c + \frac{\Delta t_2}{2}}{2\beta} + [E_v] \frac{\Delta t_2}{\beta} \right] [\Phi]^{-1} \{u\}_o \quad (3.72)$$

$$\{u\}_4 = [\Phi] \left[[E_v] \left(\frac{t_c + \frac{t_c}{2} + \frac{\Delta t_2}{\beta}}{2} + \left(\frac{t_c - \Delta t_2}{2} \right) \right) - [E_v] \left(\frac{t_c + \frac{\Delta t_2}{2}}{2\beta} \right) + \left(\frac{t_c - \Delta t_2}{2} \right) \right] [\Phi]^{-1} \{u\}_o \quad (3.73)$$

$$\left[[E_v] \frac{\Delta t_2}{\beta} + \left(\frac{t_c - \Delta t_2}{2} \right) \right]$$

$$\{u\}_5 = [\Phi] \left[[E_v] \left(\frac{t_c + \frac{t_c}{2} + \frac{\Delta t_2}{\beta}}{2} + \left(\frac{t_c - \Delta t_2}{2} \right) + \frac{t_c}{2\beta} \right) - [E_v] \left(\frac{t_c + \frac{\Delta t_2}{2}}{2\beta} \right) + \left(\frac{t_c - \Delta t_2}{2} \right) + \frac{t_c}{2\beta} \right] [\Phi]^{-1} \{u\}_o \quad (3.74)$$

$$\left[+ [E_v] \frac{\Delta t_2}{\beta} + \left(\frac{t_c - \Delta t_2}{2} \right) + \frac{t_c}{2\beta} - [E_v] \frac{t_c}{2\beta} \right]$$

In general, the pore water pressure vector at the end of Δt_{nc} of the n_c cycle is given by (such as point 3):

$$\{u\}_{3n_c-3} = [\Phi] \left[\sum_{i=1}^{2n_c-1} (-1)^{(i+1)} [E_v] \left(T_i - \frac{t_c}{2\beta} - \frac{t_c}{2} + \Delta t_{nc} \right) \right] [\Phi]^{-1} \{u\}_o \quad (3.75)$$

while, the pore water pressure vector at the middle of the n_c cycle is given by (such as point 4):

$$\{u\}_{3n_c-2} = [\Phi] \left[\sum_{i=1}^{2n_c-1} (-1)^{(i+1)} [E_v] \left(T_i - \frac{t_c}{2\beta} \right) \right] [\Phi]^{-1} \{u\}_o \quad (3.76)$$

and the pore water pressure vector at the end of the n_c cycle is given by (such as point 6):

$$\{u\}_{3n_c-1} = [\Phi] \left[\sum_{i=1}^{2n_c} (-1)^{(i+1)} [E_v]^{T_i} \right] [\Phi]^{-1} \{u\}_o \quad (3.77)$$

where:

$$T_i = \left(2n_c(1+\beta) + 2 - \sum_{k=1}^i (1-(-1)^k) - \beta \sum_{k=1}^i (1-(-1)^{(k+1)}) \right) \frac{t_c}{4\beta}$$

$$+ \frac{(1-\beta)}{2\beta} \left(2 \sum_{k=1}^{n_c} \Delta t_k - \sum_{k=1}^i (1-(-1)^{(k+1)}) \Delta t_{\left(\frac{1-(-1)^{(k+1)}}{4} \right) k} \right)$$

3.4.11 Cyclic loading for elastic and rigid bases

To analyze elastic or rigid water tank under cyclic loading, the interval times Δt_{nc} of reloading parts at each cycle nc must be first determined and known in order to define the virtual time transformation function for loading half cycles. On the other hand, superimposing rule can be used to replace a cyclic loading by a set of static loads. To save the time of computation, the interval times Δt_{nc} may be estimated by carrying out the consolidation for cyclic loading under a characteristic point on the base. According to *Grafhoff* (1955), the characteristic point of a uniformly loaded area on the surface is defined as the point of a flexible settlement s_o is identical with the rigid displacement w_o . For a circular base, the characteristic point lies at a distance $r_c = 0.845 R$ from the center of the base, where R is the radius of the base. In the analysis, the own weight of the tank is neglected as the most effects due to this weight occur during the construction of the tank. Carrying out the analysis using the described method of cyclic loading for flexible base at characteristic point, gives the required interval times Δt_{nc} . Once the interval times Δt_{nc} is obtained, the real times of the periods are translated to virtual times t'_i as indicated in Figure 3.25. Then, the compatibility between the base deflections and soil settlements at all nodes can be verified for elastic or rigid water tank through iteration.

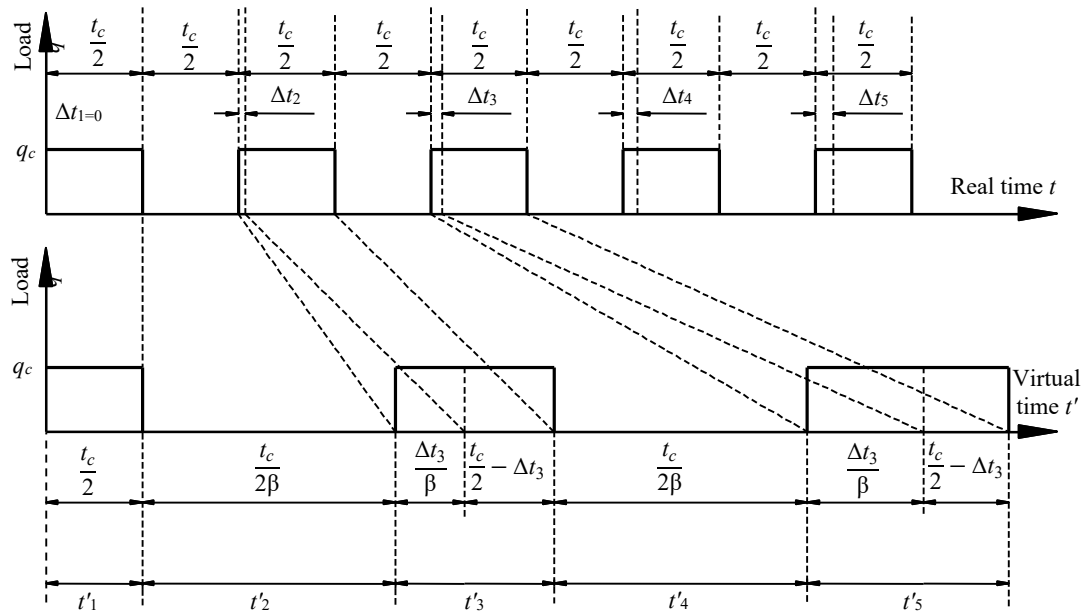


Figure 3.25 Cyclic loading with virtual times

A) Cycle 1

Determining the degree of consolidation, soil settlement and internal forces of the tank at the first half cycle

The pore water pressure under a node on the tank base is given by:

$$\{u\}_1 = [\Phi] [E_v]^{T_1} [\Phi]^{-1} \{u\}_o^{(1)} \quad (3.78)$$

where $\{u\}_o^{(1)}$ is the initial pore water pressure at first cycle and equal to the initial vertical stress $\{\sigma\}_o^{(1)}$ due to the actual contact pressure from the tank on the soil at time $t=0$ and it is unknown.

The actual contact pressure on the tank base can be obtained iteratively through an iteration process described as follows:

1. First, assume a uniform distribution of contact pressure on the base q_o . Then, the pore water pressure under a node on the tank base is determined from equation (3.78). In this case, $\{u\}_o^{(1)}$ is the initial pore water pressure at first cycle and equal to the initial vertical stress due to this assumed uniform contact pressure from the tank on the soil at time $t=0$.
2. Find the soil settlements s_i on all nodes on the base of the tank at the first halve cycle after time T_1 considering the degree of consolidation obtained from the step 1.
3. Simulate the base as a plate on a system of springs. Find the spring stiffness ks_i from the soil settlement s_i and contact pressure q_i .
4. Analyze the entire tank as a wall with a plate on springs, whenever the base is rigid or elastic, according to the previous methods for analyzing water tanks under static loading. The spring coefficients are used to generate the soil stiffness matrix $[k_s]$.
5. Compare the obtained deflections on base nodes w_i from the previous step 4 with the soil settlements s_i obtained from step 2.
6. If the accuracy does not reach to a specified tolerance ε , a new set of contact pressures are determined using spring stiffness ks_i and deflections w_i .

The steps 2 to 6 are repeated until the accuracy reaches to a specified tolerance η , which means that sufficient compatibility between the base deflections w_i and the soil settlements s_i is reached in the base-soil interface.

Determining degree of consolidation, soil settlement and internal forces of the tank at the second half cycle

Now, the actual contact pressure on the base of the tank is determined from the previous steps, which leads to an actual initial pore water pressure at first cycle $\{u\}_o^{(1)}$. Then, the pore water pressure vector can be determined from:

$$\{u\}_2 = [\Phi] [E_v]^{(T_1+T_2)} [\Phi]^{-1} \{u\}_o^{(1)} - [\Phi] [E_v]^{T_2} [\Phi]^{-1} \{u\}_o^{(1)} \quad (3.79)$$

or

$$\{u\}_2 = [\Phi] \left[[E_v]^{(T_1+T_2)} - [E_v]^{T_2} \right] [\Phi]^{-1} \{u\}_o^{(1)} \quad (3.80)$$

B) Cycle 2

At the end of interval time T_3 , the pore water pressure vector is:

$$\begin{aligned} \{u\}_3 = & [\Phi] \left[[E_v]^{(T_1+T_2+T_3)} - [E_v]^{(T_2+T_3)} \right] [\Phi]^{-1} \{u\}_o^{(1)} + \\ & [\Phi] [E_v]^{T_3} [\Phi]^{-1} \{u\}_o^{(2)} \end{aligned} \quad (3.81)$$

where $\{u\}_o^{(2)}$ is the pore water pressure at the half first cycle 2 and equal to the actual contact pressure under the base at time T_3 and is unknown.

Solving equation (3.81) in similar manner to solving (3.78), gives the vector $\{u\}_o^{(2)}$.

At the end of the second cycle 2, the pore water pressure vector is:

$$\begin{aligned} \{u\}_3 = & [\Phi] \left[[E_v]^{(T_1+T_2+T_3+T_4)} - [E_v]^{(T_1+T_2+T_3+T_4)} \right] [\Phi]^{-1} \{u\}_o^{(1)} \\ & + [\Phi] \left[[E_v]^{(T_3+T_4)} - [E_v]^{T_4} \right] [\Phi]^{-1} \{u\}_o^{(2)} \end{aligned} \quad (3.82)$$

The above steps are repeated until the required cycle is reached.

3.4.12 Formulation of pore water pressure for nonrectangular cyclic loading

Figure 3.26 shows different types of cyclic loading. The types may be represented any expected cyclic loading shape. In the figure, there are three parameters t_o , α_o and β_o reflect the properties of the loading. The number of cycle is N . The time t_o represents the time length of the subjected load whatever the load geometry is, while the time $\beta_o t_o$ is the total length of the cycle. The parameter α_o represents the load geometry, where $\alpha_o=0$ creates a rectangular cyclic loading, $\alpha_o = 0.5$ creates a triangular cyclic loading and $0 < \alpha_o < 0.5$ creates a trapezoidal cyclic loading.

3.4.12.1 Plastic clay

The clay is named as plastic clay if the clay changes from a state to another -for example from NC to OC- during the time of the subjected cyclic load. Considering the first cycle of the trapezoidal cyclic load shown in Figure 3.26. The excess pore water pressure for the loading and constant load phases at any time t , where $0 \leq t \leq (t_o - \alpha_o t_o)$ can be calculated using the following equation:

$$\{u_j\}_t = [\Phi][E_v]^t [D_j]^t [\Phi]^{-1} \{u_j\}_o \quad (3.83)$$

where $[D_j]^t$ is a square diagonal matrix with elements D_j . The elements D_j are calculated using Eqns (3.47) and (3.54) for trapezoidal and triangular cyclic load, while for rectangular load the elements are $D_j=1$.

The rest of the first cycle are the unloading and no-loading phases. The excess pore water pressure for these phases at any time t , where $(t_o - \alpha_o t_o) \leq t \leq (\beta_o t_o)$ can be calculated using the following equation:

$$\{u_j\}_t = \left[[\Phi][E_v]^t [\Phi]^{-1} \{u_j\}_{(t_o - \alpha_o t_o)} \right] - \left[[\Phi][E_v]^t [D_j]^t [\Phi]^{-1} \{u_j\}_o \right] \quad (3.84)$$

The constant load phase is considered to continue till time t , while the unloading and no-loading phases -which are the reverse of the loading and constant load phases- are subtracted from the continued values.

Cycle two starts with reloading phase extended to portion time Δt_2 , then the phase is changed to loading phase till reaching the time $\{\beta_o t_o + (t_o - \alpha_o t_o)\}$ as shown in Figure 3.23. The excess pore water pressure at Δt_2 can be calculated using the following equation:

$$\{u_j\}_{\Delta t_2} = \left[[\Phi][E_v]^{\Delta t_2} [\Phi]^{-1} \{u_j\}_{\beta_o t_o} \right] + \left[[\Phi][E_v]^{\Delta t_2} [D_j]^{\Delta t_2} [\Phi]^{-1} \{u_j\}_o \right] \quad (3.85)$$

Substituting from equation (3.85) into equations (3.56) and (3.57) to find the last maximum degree of consolidation. The value of Δt_2 is difficult to be calculated

using closed form solution, so the try and error or iteration methods are successful to get the value of Δt_2 .

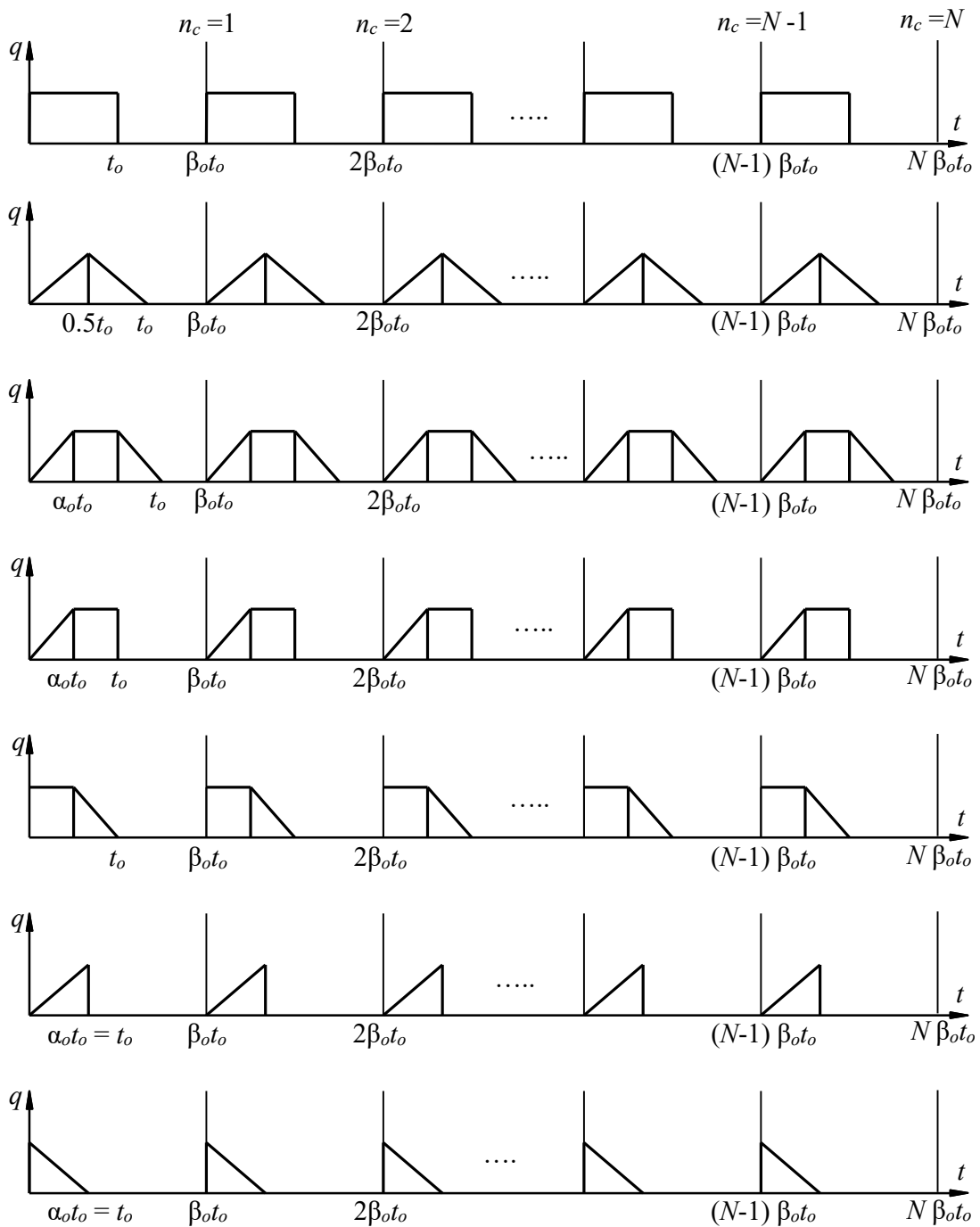


Figure 3.26 Types of cyclic loading

After that, the excess pore water pressure for the loading and constant load phases at any time t , where $\Delta t_2 \leq t \leq \{\beta_o t_o + (t_o - \alpha_o t_o)\}$ can be calculated using the following equation:

$$\{u_j\}_t = \left[[\Phi][E_v]^t [\Phi]^{-1} \{u_j\}_{\beta_o t_o} \right] + \left[[\Phi][E_v]^t [D_j]^t [\Phi]^{-1} \{u_j\}_o \right] \quad (3.86)$$

where the time factor T_v in the square matrix $[E_v]^t$ is calculated according to *Toufigh/ Ouria (2009)* as shown in Figure 3.25 and using the following equation:

$$T'_v = \frac{\Delta T_N}{\beta} + (T_v - \Delta T_N) \quad (3.87)$$

Where T'_v is the time factor of time t in the virtual time scale, ΔT_N is the time factor of time portion Δt_N for cycle number N in the real time scale, β is the virtual time factor and equal $C_v(\text{NC})/C_v(\text{OC})$ and T_v is the time factor of time t in the real time scale, [-].

The rest of the second cycle are the unloading and no-loading phases. The excess pore water pressure for these phases at any time t , where $\{\beta_o t_o + (t_o - \alpha_o t_o)\} \leq t \leq (2\beta_o t_o)$ can be calculated using the following equation:

$$\{u_j\}_t = \left[[\Phi][E_v]^t [\Phi]^{-1} \{u_j\}_{\{\beta_o t_o + (t_o - \alpha_o t_o)\}} \right] - \left[[\Phi][E_v]^t [D_j]^t [\Phi]^{-1} \{u_j\}_o \right] \quad (3.88)$$

For the general case of cyclic loading shown in Figure 3.26, the excess pore water pressure for loading and constant load phases can be determined using the following equation:

$$\{u_j\}_t = \left[[\Phi][E_v]^t [\Phi]^{-1} \{u_j\}_{(N-1)\beta_o t_o} \right] + \left[[\Phi][E_v]^t [D_j]^t [\Phi]^{-1} \{u_j\}_o \right] \quad (3.89)$$

And, the excess pore water pressure for unloading and no-loading phases can be determined using the following equation:

$$\begin{aligned} \{u_j\}_t = & \left[[\Phi][E_v]^t [\Phi]^{-1} \{u_j\}_{\{(N-1)\beta_o t_o + (t_o - \alpha_o t_o)\}} \right] - \\ & \left[[\Phi][E_v]^t [D_j]^t [\Phi]^{-1} \{u_j\}_o \right] \end{aligned} \quad (3.90)$$

While, the excess pore water pressure for reloading phases can be determined using the following equation:

$$\begin{aligned} \{u_j\}_{\Delta t_N} = & \left[[\Phi][E_v]^{\Delta t_N} [\Phi]^{-1} \{u_j\}_{\beta_o t_o} \right] + \\ & \left[[\Phi][E_v]^{\Delta t_N} [D_j]^{\Delta t_N} [\Phi]^{-1} \{u_j\}_o \right] \end{aligned} \quad (3.91)$$

3.4.12.2 Elastic clay

The clay is named elastic clay if the clay remain in the same state -OC- during the time of cyclic loading. In this type of clay, it's not necessary to calculate the portion time Δt_N because the clay remain in the same state if it is subjected to either loading, constant load or unloading, no-load. The excess pore water pressure can be calculated using equations (3.89) and (3.90).

3.4.13 Linear degree of consolidation

The linear average degree of consolidation can be calculated using equation (3.56) for loading, constant load and reloading phases. In other hand, for unloading and no-loading phases, the linear average degree of consolidation can be calculated using equation (3.58).

3.4.14 Formulation of linear settlement

3.4.14.1 Linear settlement of elastic clay

Elastic clay remain in the OC state with loading and unloading phases, so the linear settlement of layer i is calculated using the following equation according to *El Gendy and Hermann (2014)*:

$$s_i = m_{ri}(\Delta\sigma_i - \Delta u_i)h_i \quad (3.92)$$

where s_i is the consolidation settlement of layer i , m_{ri} is the coefficient of volume change of layer i for unloading, no-loading and reloading, $\Delta\sigma_i$ is the increment of vertical stress at time t in a layer i due to the applied load on the surface, Δu_i is the average excess pore water pressure at time t in a layer i and h_i is the thickness height of layer i .

It should be noticed that the coefficient of volume change m_{ri} is constant and equal αm_{vi} .

3.4.14.2 Linear settlement of plastic clay

Plastic clay changes from NC state to OC state or vice versa during the consolidation process. In the NC state, the linear settlement of layer i is calculated using the following equation according to *El Gendy* and *Hermann* (2014):

$$s_i = m_{vi}(\Delta\sigma_i - \Delta u_i)h_i \quad (3.93)$$

where m_{vi} is the coefficient of volume change of layer i for loading and constant load phases.

In OC state, the linear settlement of layer i is calculated using the following equation:

$$s_i = s_c + m_{ri}\{(\Delta\sigma_i - \Delta u_i) - (\Delta\sigma_{ci} - \Delta u_{ci})\}h_i \quad (3.94)$$

where s_{ci} , $\Delta\sigma_{ci}$ and Δu_{ci} are the settlement, the increment in vertical stress and the average excess pore water pressure of layer i at the preconsolidation pressure, or at the last maximum effective stress. The coefficient of volume change m_{ri} is constant and equal αm_{vi} . Figure 3.27 shows the effect of the parameter α on the settlement distribution.

The figure shows that the greater the coefficient of volume change for reloading the greater the difference between maximum and minimum values of the settlement curve, until it reaches the same value of the coefficient of volume change for loading, the distribution of the settlement curve shall be the same as the distribution of the degree of consolidation curve.

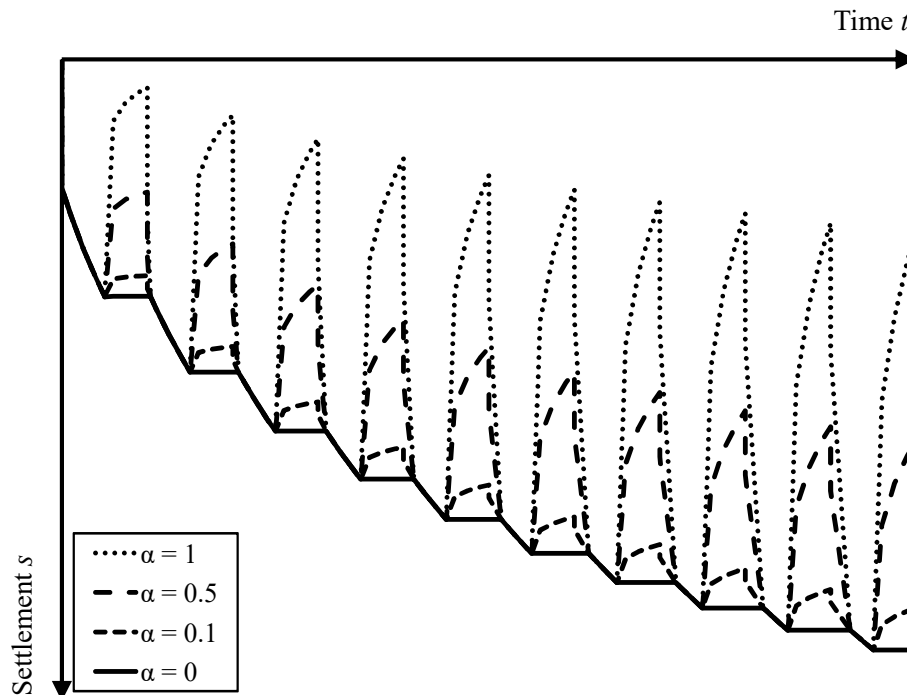


Figure 3.27 Effect of the parameter α on the settlement distribution

3.4.15 Non-linear consolidation of clay subjected to cyclic load

In linear analysis of consolidation of clay, it was considered that the coefficients of consolidation, volume change and permeability have only two values during the consolidation process, one for the NC state, and another one for the OC state. In non-linear consolidation of soft soils these hypotheses are not suitable, as these coefficients are changing with the stresses and time changes. This non-linear model is difficult to be solved with many variables, so the non-linear model is simplified to be solved easily.

From Figure 3.19 and Figure 3.20, there are 4 factors that affect on the coefficients of consolidation C_v , volume change m_v and permeability k_v . These factors are the compression index C_c , the recompression index C_r , the compression index for permeability C_{ck} , and the recompression index for permeability C_{rk} . Based on the laboratory tests, *Yazdani/ Toufigh* (2012) described that the slopes of $e-\text{Log } k$ in the NC and OC states are usually the same ($C_{ck} = C_{rk}$). It means that $e-\text{Log } k$ has usually a unique line during cyclic loading with constant slope C_k . Therefore, the slope of the line can be used to simplify the analysis.

Berry/ Wilkinson (1969) pointed out that the ratio C_c/C_k is about 0.5~2, and mostly between 0.5 and 1, therefore the value of C_c/C_k is selected to be 1 here for simplicity.

The coefficient of volume change factor α has a constant value, where $m_r = \alpha m_v$ and $\alpha = C_r / C_c$. On the other hand, the coefficient of consolidation factor β is not constant, where it's calculated using the following equation:

$$\beta = \alpha(\text{OCR})^{(1-\alpha)} \quad (3.95)$$

where OCR is the overconsolidation ratio, the ratio of the past maximum effective stress of the soil to its current effective stress. If the value of OCR is nearly 1, it could be assumed that $\alpha = \beta$ as in linear consolidation.

It is assumed that the decrease in permeability is proportional to the decrease in compressibility. Therefore, if the coefficient of consolidation is considered as constant during the consolidation process (equation (3.96)), the only soil variable during the consolidation process required for the nonlinear analysis will be the coefficient of volume change.

$$C_{vi} = \frac{k_{vi}}{\gamma_w m_{vi}} = \frac{k_{voi}}{\gamma_w m_{voi}} \quad (3.96)$$

The excess pore water pressure at any time can be calculated using equations (3.89), (3.90) and (3.91) as explained before in linear consolidation.

3.4.16 Non-linear degree of consolidation

The non-linear average degree of consolidation U_p and U_s can be calculated using equations (3.56) and (3.57) respectively for loading, constant load and reloading phases. In other hand, for unloading and no-loading phases, the non-linear average degree of consolidation U_p and U_s can be calculated using equations (3.58) and (3.59) respectively.

3.4.17 Formulation of Non-linear settlement

3.4.17.1 Non-linear settlement of elastic clay

Elastic clay stays in the OC state as explained before, therefore the coefficient of volume change for reloading or unloading is only the needed coefficient to be calculated using the following equation:

$$m_{ri} = \frac{C_{ri}}{(1+e_{oi})(\Delta\sigma_i - \Delta u_i)} \text{Log} \left(\frac{\sigma'_{oi} + \Delta\sigma_i - \Delta u_i}{\sigma'_{oi}} \right) \quad (3.97)$$

where m_{ri} is the coefficient of volume change of layer i for unloading, no-loading and reloading, C_{ri} is the recompression index of layer i , e_{oi} is the initial void ratio of layer i , $\Delta\sigma_i$ is the increment of vertical stress at time t in a layer i due to the applied load on the surface, Δu_i is the average excess pore water pressure at time t

in a layer i and σ'_{oi} is the initial vertical effective stress caused by the weight of the soil itself at the middle of layer i , [kN/m²].

The settlement can be calculated using equation (3.92).

3.4.17.2 Non-linear settlement of plastic clay

Plastic clay changes from NC state to OC state or vice versa during the consolidation process. In the NC state, the coefficient of volume change for loading and constant load is calculated using the following equation:

$$m_{vi} = \frac{C_{vi}}{(1+e_{oi})(\Delta\sigma_i - \Delta u_i)} \text{Log} \left(\frac{\sigma'_{oi} + \Delta\sigma_i - \Delta u_i}{\sigma'_{oi}} \right) \quad (3.98)$$

In the same phases, the non-linear settlement is calculated using equation (3.93), where m_{vi} is variable and calculated using equation (3.98).

In phases of unloading, no-loading and reloading, the non-linear settlement is calculated using either equation (3.94) or the following equation:

$$s_i = s_c + \frac{C_{ri}h_i}{1+e_{ci}} \left[\text{Log} \left(\frac{\sigma'_{oi} + \Delta\sigma_i - \Delta u_i}{\sigma'_{oi}} \right) - \text{Log} \left(\frac{\sigma'_{oi} + \Delta\sigma_{ci} - \Delta u_{ci}}{\sigma'_{oi}} \right) \right] \quad (3.99)$$

$$s_i = s_c + \frac{C_{ri}h_i}{1+e_{ci}} \text{Log} \left(\frac{\sigma'_{oi} + \Delta\sigma_i - \Delta u_i}{\sigma'_{oi} + \Delta\sigma_{ci} - \Delta u_{ci}} \right) \quad (3.100)$$

where e_{ci} is the void ratio of layer i at last maximum effective stress (preconsolidation pressure).

By equating equation (3.94) with equation (3.100), m_{ri} at any time can be expressed as:

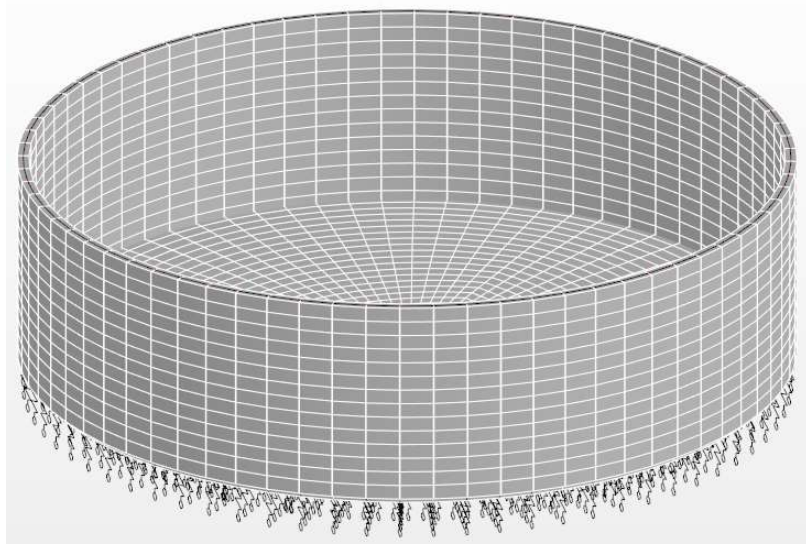
$$m_{ri} = \frac{C_{ri}}{1+e_{ci}\{(\Delta\sigma_i - \Delta u_i) - (\Delta\sigma_{ci} - \Delta u_{ci})\}} \text{Log} \left(\frac{\sigma'_{oi} + \Delta\sigma_i - \Delta u_i}{\sigma'_{oi} + \Delta\sigma_{ci} - \Delta u_{ci}} \right) \quad (3.101)$$

3.5 Summary of the proposed mathematical models used in the thesis

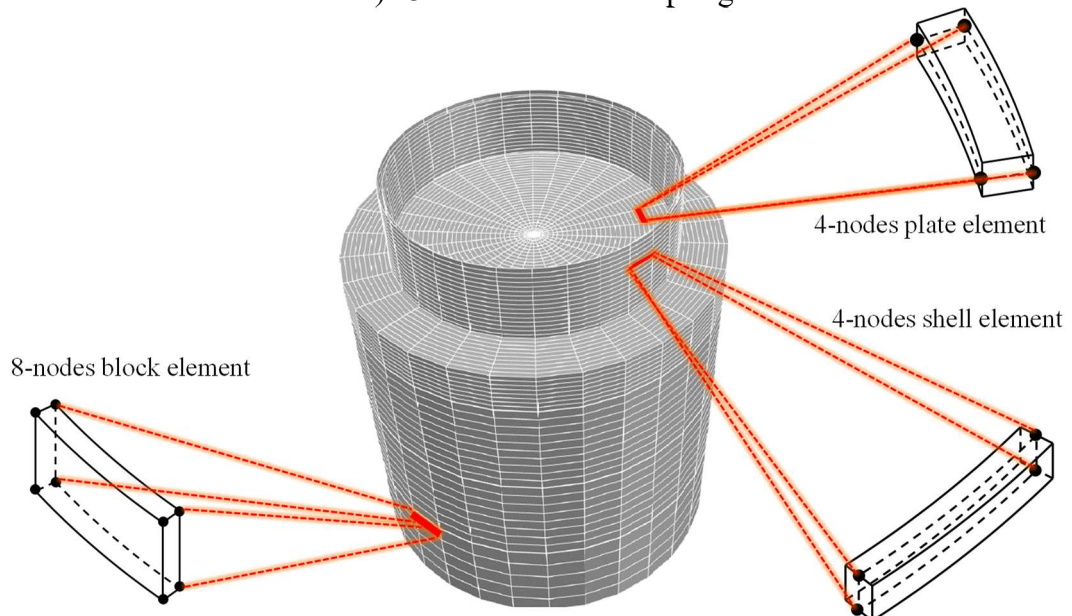
3.5.1 FE shell model of the tank

A numerical analysis based on finite element method using a cylindrical finite element shell is presented to study the behavior of cylindrical tanks resting directly on soil and subjected to static or cyclic loading. The analysis capable to modeling circular cylindrical tanks resting on layered soil medium with real subsoil physical constants. The FE model of the tank consists of a group of frustum-shaped elements each with only two nodes and each node has three degrees of freedom. In this mathematical model, the axi-symmetry of the problem is exploited to transform the problem from a 3-D problem to a 2-D problem to save in memory and time required for calculations. In this mathematical model the classical 3-D analysis has been avoided, in which the base and the wall of the tank besides the soil are divided into a large number of nodes, as well as the time must be divided into small periods. In the classical 3-D analysis the base and the wall of the tank are represented using 3-D shell elements, each element has four nodes, and each node has six degrees of freedom. On the other hand, the soil is represented using block elements, each element has eight nodes, and each node has six degrees of freedom.

This large number of nodes lead to a huge number of equations that need a very long time to be solved. Consequently, round off errors may be generated in the calculations. Therefore, these methods become impractical. Figure 3.28 and Figure 3.29 show the difference between the FE model in the present study and in other available FE models used to analyze the same problem.

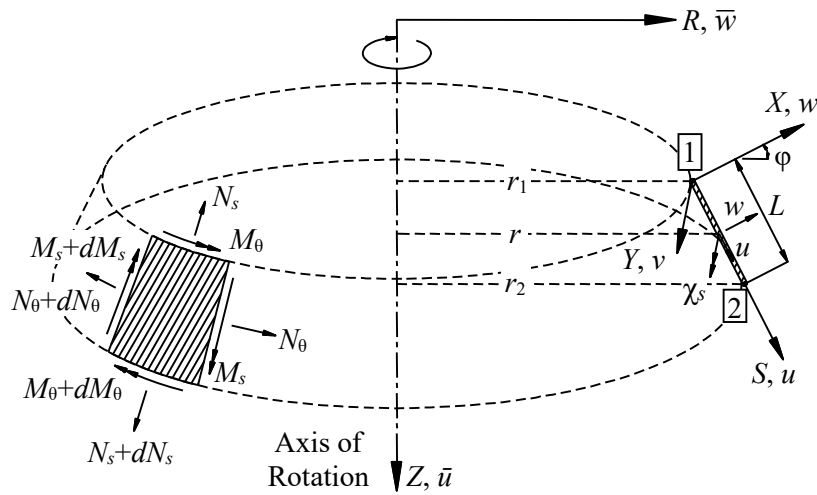


a) 3-D tank rested on springs

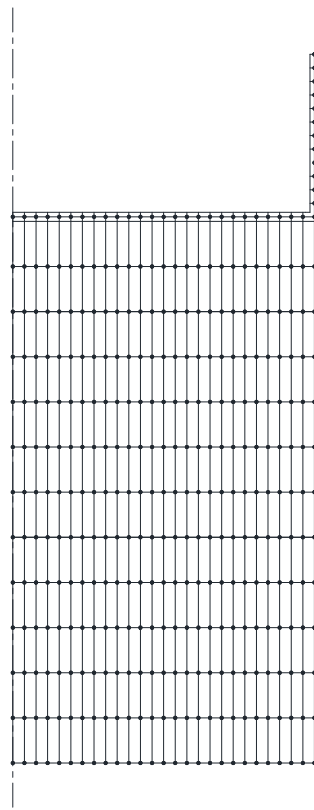


b) 3-D tank with layered soil block elements

Figure 3.28 Available common FE models for such problems



a) Single element of the proposed axi-symmetric FE model



b) The tank-soil axi-symmetric FE model

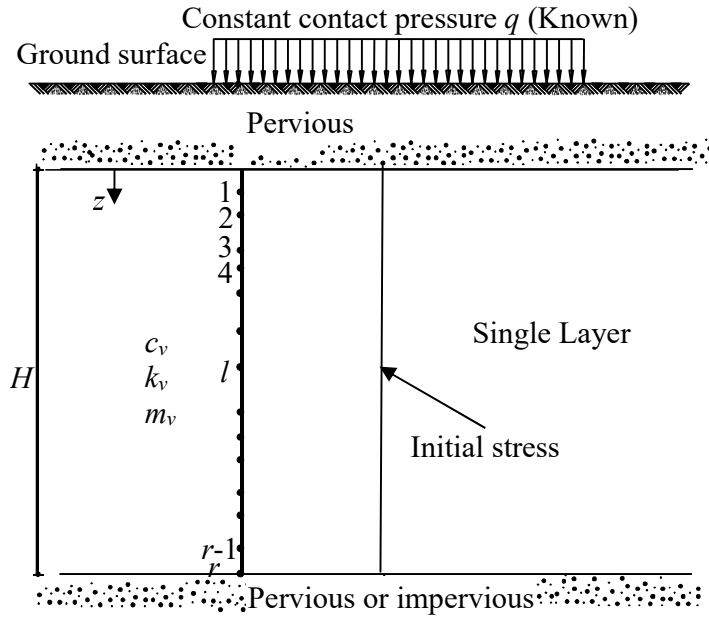
Figure 3.29 Axi-symmetric FE shell model used in the present study

3.5.2 Cyclic loading model

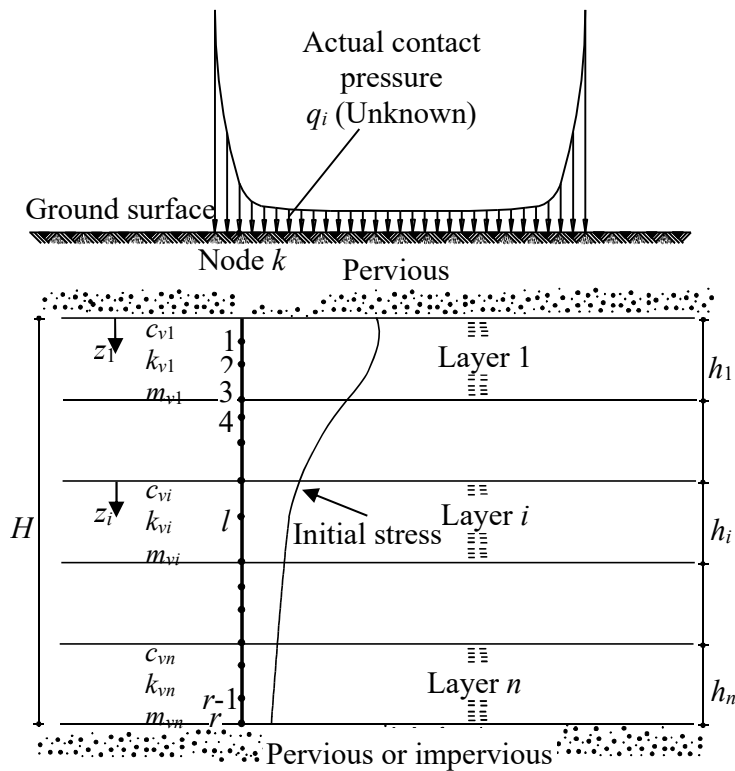
In cyclic loading model, a numerical modification is carried out on the semi-analytical solution of *Toufigh and Ouria (2009)* to be applicable for multi-layered soil subjected to any variable stress along the depth of the soil using *LEM* of *El Gendy and Herrmann (2014)*. The proposed solution is used for normally or overconsolidated clays subjected to any type of cyclic loading. It takes into account the structure rigidity with the subsoil layers at any cyclic period. Besides, the actual contact pressure under the tank can be obtained at any cyclic period. The solution is applied for water tanks as a structure subjected to cyclic loading. Base of the tank may be considered as rigid, elastic or flexible. For analyzing the base of the tank as elastic base, full computability among the structure and subsoil elements, wall, base and subsoil, is occurred. Table 3.2, Figure 3.30 and Figure 3.31 illustrate the difference between the assumptions in this study and those of the most of the previous studies for analyzing consolidation under cyclic loading.

Table 3.2 Assumptions of cyclic loading model of this study and those of previous studies

Item	Assumptions of cyclic loading model	
	Previous studies	This study
Contact pressure q	Uniform and known	Non-uniform and unknown
Initial stress u_o	Uniform along the layer height	Variable along the layer height
Clay layer	Single layer only	Multilayered soil system
Pore water equation	Infinite series	Finite with number of nodes along the clay layer
Settlement	Flexible settlement	Settlement for flexible, rigid and elastic base
Base rigidity	unavailable	Available
Soil-structure interaction	unavailable	Available
Contact area under the base	A point under the base	The entire base



a) Soil model of cyclic loading in previous studies



b) Soil model of cyclic loading in this study

Figure 3.30 Soil representation in this study and that of previous studies

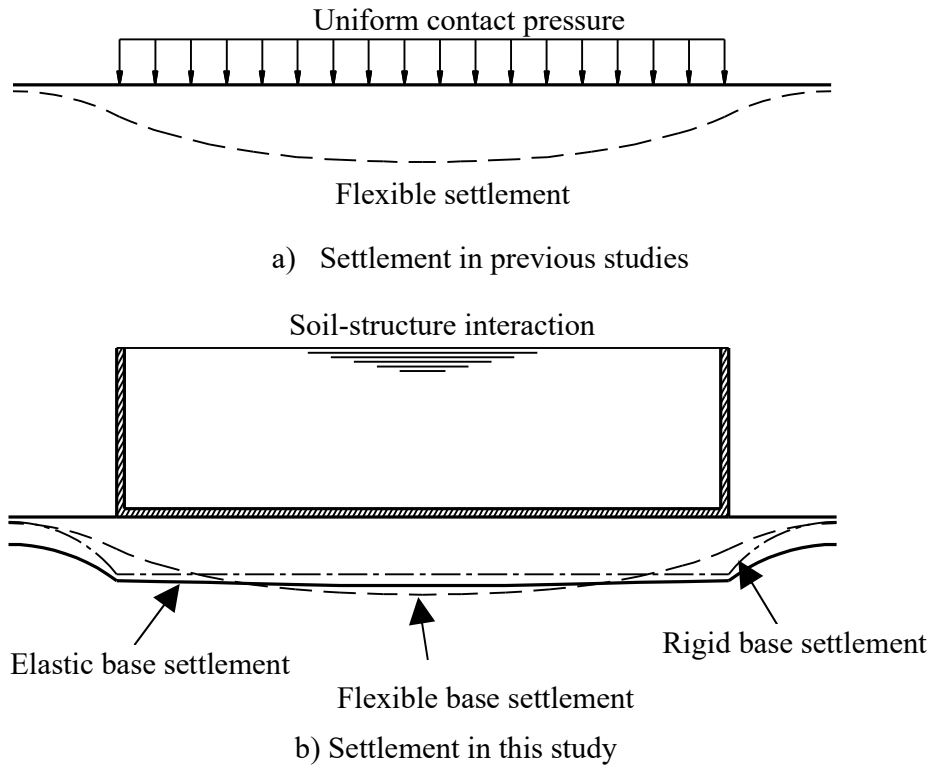


Figure 3.31 Settlement in cyclic loading of this study and that of previous studies

Chapter 4

4 Validity of the analysis

4.1 Introduction

Most of mathematical models used in the analysis of this research such as analysis of circular cylindrical tanks resting on layered soil under static and cyclic loading are new developed in the program *ELPLA 10* [13]. *ELPLA 10* is a user-friendly computer program. It can analyze structures with different types of subsoil models. To verify the validity of this computer program, some results published previously by researchers using different methods of analyses and models are compared with the results obtained by the analysis used in this thesis. A verification study is carried out using the computer program to analyze circular cylindrical tanks of arbitrary shapes with different subsoil models. The mathematical solution of the circular cylindrical tanks is based on the Finite Element Method using circular cylindrical shell elements.

The verification analyses are focused on two parts in 6 test problems. The first part of the verifications is the validity of the structural analysis of circular cylindrical tanks. The mathematical model of the structural analysis is based on the Finite Element Method using circular cylindrical shell elements. Items to be checked under different conditions are internal forces, deformations in the tank wall and base. This part is covered by test problems 1 and 2.

The main effect on the behavior of storage tanks is filling and emptying the liquid in the tank. Therefore, the subsoil analysis under the base of the tank depending on time-settlement and time-loading relations, such as consolidation rate of clay layers, loading and reloading besides cyclic loading, is verified in the second part. Items to be checked under different conditions are settlement, degree of consolidation and pore water pressure. The second part is covered by test problems 3 to 6. The analysis of this part is carried out by layered equation method *LEM*, which is further developed for this research. Results of the subsoil analysis are not only verified with those obtained by previous numerical analysis but also with results obtained by experimental works.

4.2 Tank resting on *Winkler's* medium

4.2.1 Description of the problem

Numerical and analytical analysis for axi-symmetrically circular cylindrical tank resting on elastic foundation using *Winkler's* model is presented by *Vichare/Inamdar* (2010) [55]. To verify analysis of circular cylindrical tank resting on *Winkler's* medium, the internal forces calculated numerically and analytically by *Vichare/Inamdar* (2010) at different cases of modulus of subgrade reaction are compared with those obtained by *ELPLA* 10.

A circular cylindrical tank of an inner diameter of $d = 13$ [m] and a height of $H = 3.5$ [m] is considered as shown in Figure 4.1. Thickness of the wall tank is $t = 0.175$ [m]. The tank is filled with water. The soil under the base of the tank is represented by isolated springs of stiffness k_s , which represent modulus of subgrade reaction. The tank material, unit weight of the water and the modulus of subgrade reaction are listed in Table 4.1.

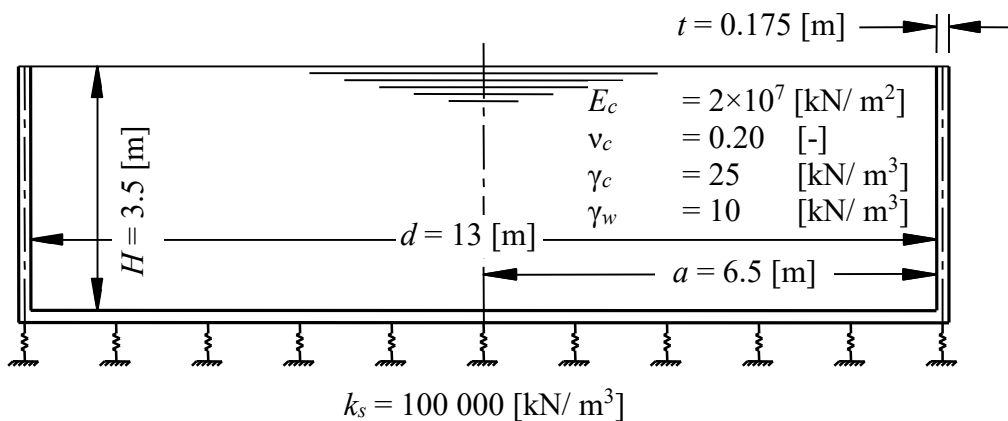


Figure 4.1 Circular cylindrical tank on isolated springs

Table 4.1 Tank material, water unit weight and modulus of subgrade reaction

Modulus of Elasticity of the tank material	E_c	$= 2 \times 10^7$	[kN/ m ²]
<i>Poisson's</i> ratio of the tank material	ν_c	$= 0.2$	[-]
Unit weight of the tank material	γ_c	$= 25$	[kN/ m ³]
Unit weight of the water	γ_w	$= 10$	[kN/ m ³]
Modulus of subgrade reaction	k_s	$= 100\ 000$	[kN/ m ³]

4.2.2 Numerical Analysis

In order to illustrate the comparison between analytical and numerical analysis of *Vichare/Inamdar* (2010) and that of *ELPLA* 9.4, the height of the tank is divided

into 35 equal elements, each of 0.10 [m], as shown in Figure 4.2. The base of the tank is divided into 50 equal elements, each of 0.13 [m].

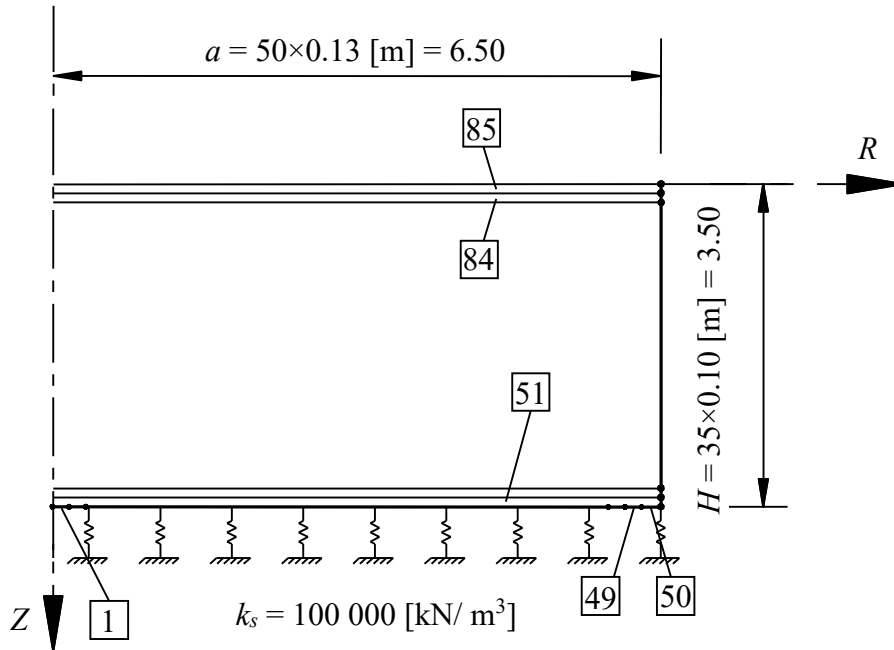


Figure 4.2 Finite element mesh of the tank

4.2.3 Results and discussions

The analysis of the considered tank is carried out numerically by *ELPLA 10*, where the tank wall and the base were simulated with a thin circular cylindrical shell element using finite element method. *Vichare/ Inamdar (2010)* analyzed the same tank first numerically by *ABAQUS 6.8* [25] using three dimensional finite element model, then analytically using equations of *Timoshenko/ Krieger (1959)* [52].

Figure 4.3, Figure 4.4 and Figure 4.5 show a comparison between results of the above analyses for meridional moment M_s along the wall height, tangential force N_θ along the wall height and the moment across the base M_{base} respectively. In these analyses, the modulus of subgrade reaction is chosen to be $k_s = 100\ 000$ [kN/m³].

Table 4.2 shows a comparison between maximum internal forces obtained from analytical solution and those obtained from *ELPLA 10*, while Table 4.3 shows a comparison between maximum internal forces obtained from *ABAQUS 6.8* and those obtained from *ELPLA 10*. From these figures and tables, it can be concluded for the considered tank and soil that the difference in values is not more than 5 % which illustrates a good accuracy for the program used in this research.

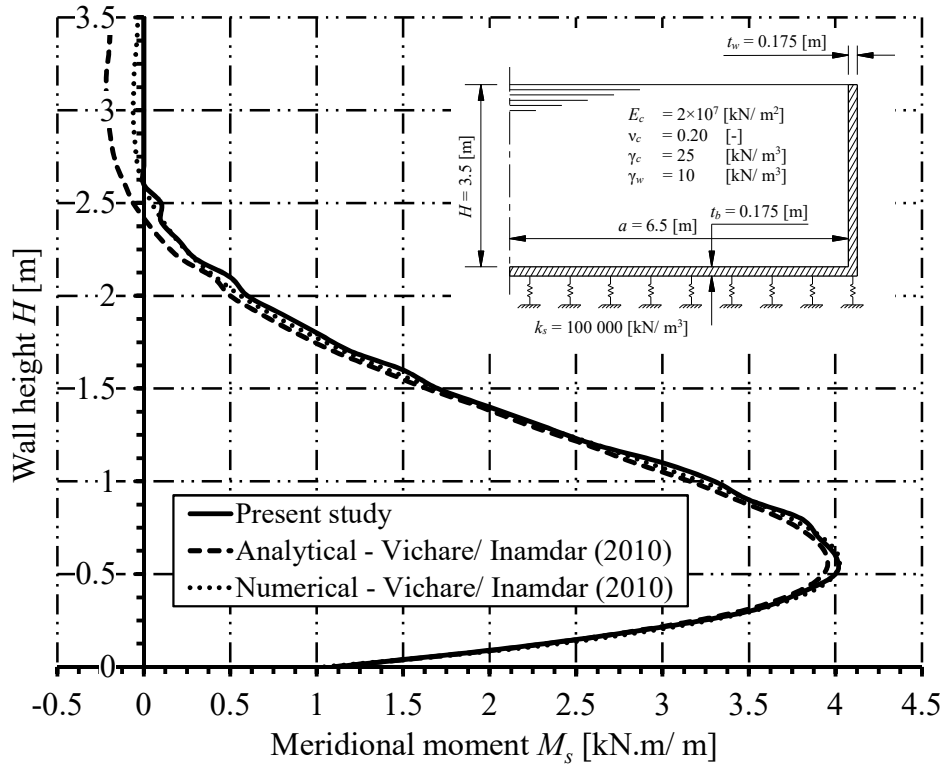


Figure 4.3 Meridional moment M_s along the wall height

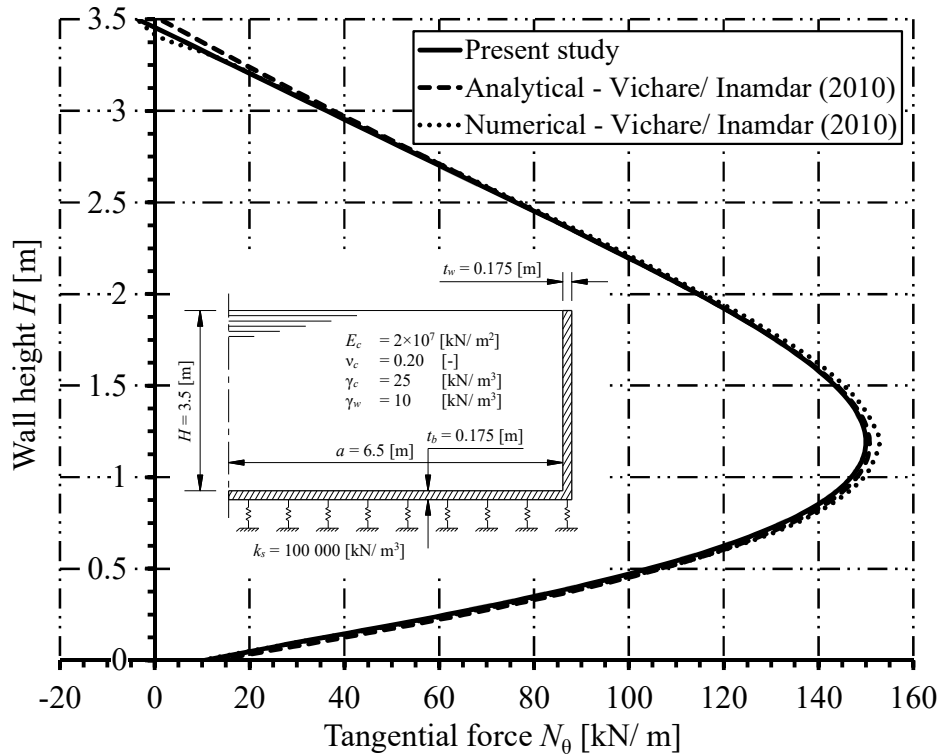
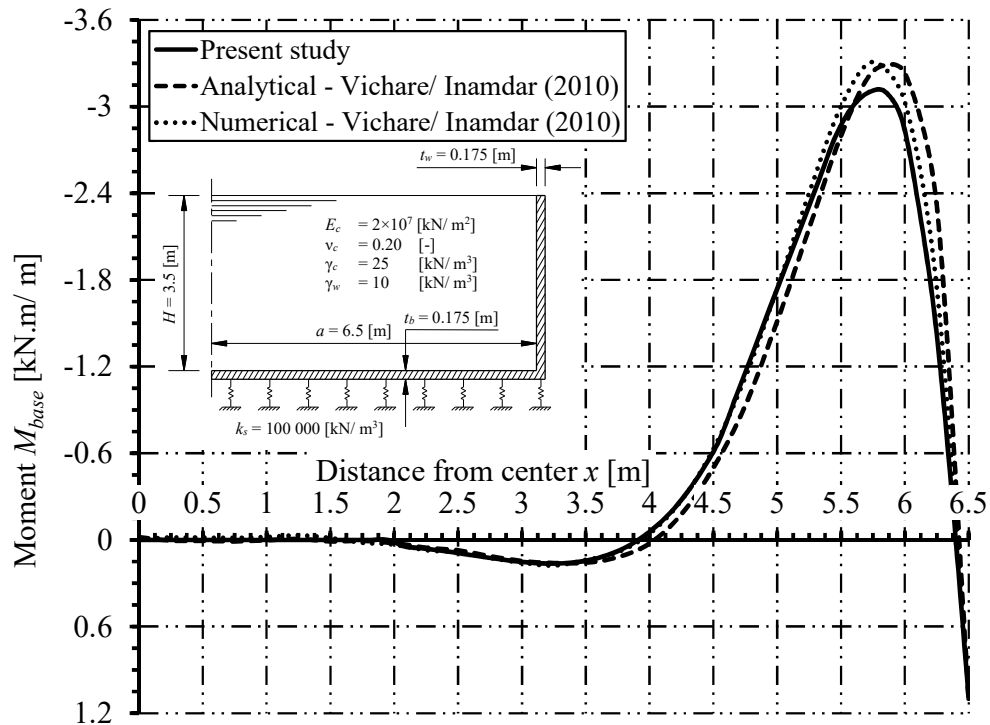


Figure 4.4 Tangential force N_θ along the wall height

Figure 4.5 Moment across the base raft M_{base} Table 4.2 Comparison between maximum internal forces obtained from analytical solution and those obtained from *ELPLA 10*

Result	Type of analysis		Difference
	Analytical	<i>ELPLA 10</i>	
Maximum meridional moment on the wall M_s	M_s	M_s	ΔM_s
	[kN.m/ m]	[kN.m/ m]	[%]
	3.95	3.90	1.27
Maximum tangential force on the wall N_θ	N_θ	N_θ	ΔN_θ
	[kN/ m]	[kN/ m]	[%]
	150.73	146.7	2.67
Maximum moment on the base M_{base}	M_{base}	M_{base}	ΔM_{base}
	[kN.m/ m]	[kN.m/ m]	[%]
	-3.25	-3.1	4.62

Table 4.3 Comparison between maximum internal forces obtained from *ABAQUS* 6.8 and those obtained from *ELPLA* 10

Result	Type of analysis		Difference
	<i>ABAQUS</i> 6.8	<i>ELPLA</i> 10	
Maximum meridional moment on the wall M_s	M_s [kN.m/ m]	M_s [kN.m/ m]	ΔM_s [%]
	4.02	3.9	2.99
Maximum tangential force on the wall N_θ	N_θ [kN/ m]	N_θ [kN/ m]	ΔN_θ [%]
	152.91	146.7	4.06
Maximum moment on the base M_{base}	M_{base} [kN.m/ m]	M_{base} [kN.m/ m]	ΔM_{base} [%]
	-3.31	-3.1	0.21

4.2.4 Conversion of the solution

To show the accuracy of the results of *ELPLA* 10 for different moduli of subgrade reactions, the considered tank is analyzed again for different values of modulus of subgrade reaction k_s ranges from 20 [MN/m³] to 200 [MN/m³].

For this range of k_s values, Figure 4.6 shows the maximum meridional moment M_s in the wall, Figure 4.7 shows the maximum tangential force in the wall and Figure 4.8 shows the maximum moment in the base.

It is observed that with increasing k_s value, the maximum tangential moment and tangential force decrease. For the base, it is observed that the variation of base moment with stiffness is marginal. A little difference in base moment occurred at stiff soil.

In general, the above comparison show that the results of analyzing circular cylindrical tank on elastic foundation using *Winkler's* model are in a good agreement with those obtained analytically or numerically using three dimensional finite element model.

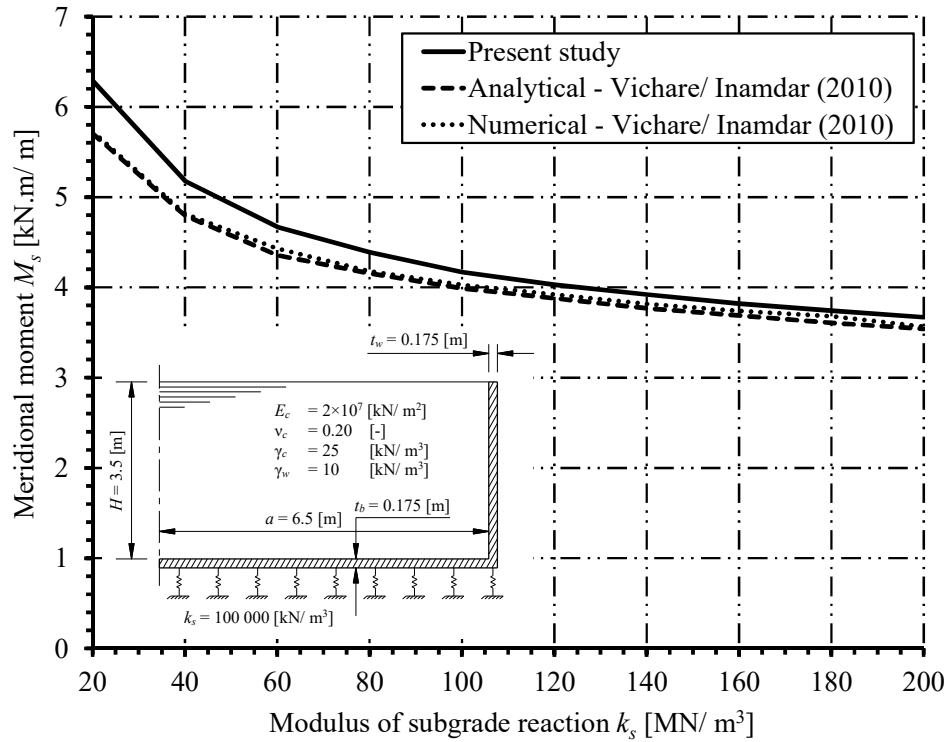


Figure 4.6 Maximum meridional moment M_s along the wall with varying k_s

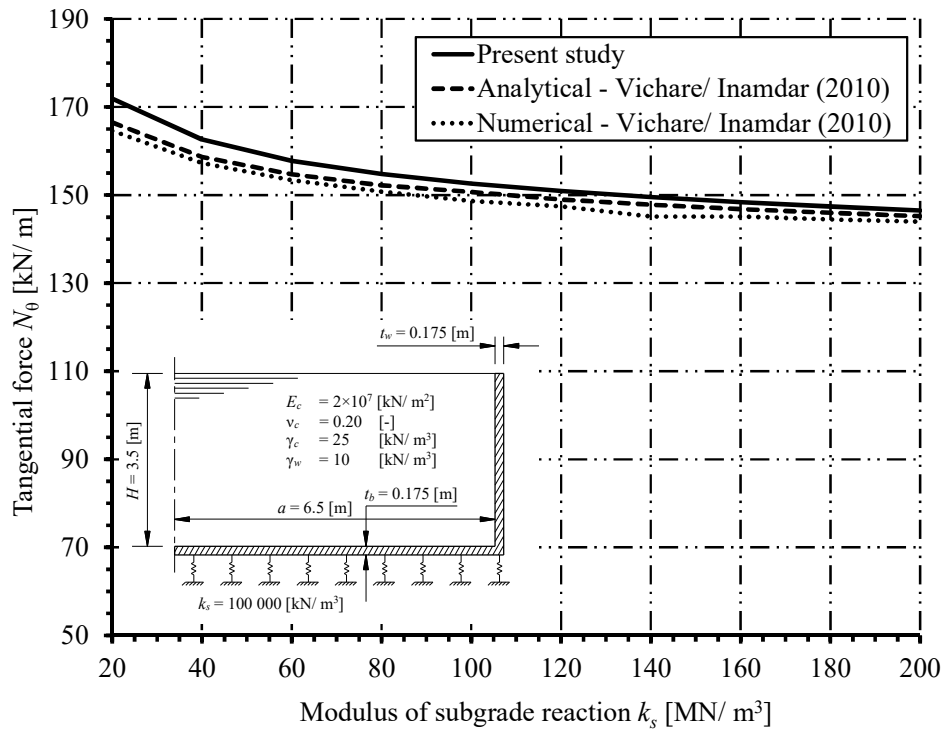


Figure 4.7 Maximum tangential force N_θ along the wall with varying k_s

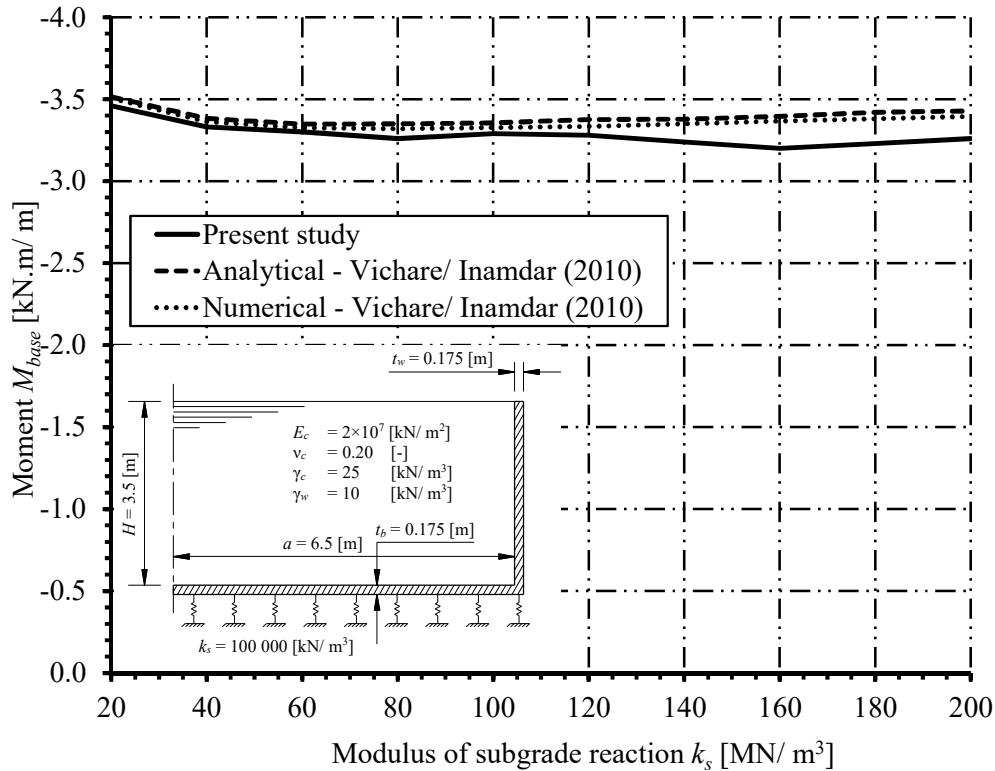


Figure 4.8 Maximum moment M_{base} across the base raft with varying k_s

4.3 Tank with different base thickness resting on half space soil medium

4.3.1 Description of the problem

A finite element analysis for the flexure behavior of a circular cylindrical storage tank resting on an isotropic elastic half space soil medium is presented by *Melerski* (2006) [33]. The solution takes into account the interaction between the tank wall and the base using slope and moment compatibility. It also takes into account the interaction between the base and the soil medium.

To verify analysis of circular cylindrical storage tank resting on half space soil medium, results of the analysis using finite element analysis of *Melerski* (2006) were compared with those obtained by the finite element analysis of *ELPLA 10* using circular cylindrical shell elements.

A circular cylindrical tank of an inner diameter of $d = 20$ [m] and a height of $H = 10$ [m] is considered as shown in Figure 4.9. Thicknesses of the wall and the base are different. The thickness of the tank wall $t_w = 0.2$ [m] and that of the base is $t_b = 0.5$ [m]. The tank is filled with water. Figure 4.9 shows the storage tank, while the tank material and unit weight of the water are listed in Table 4.4. The data of soil medium under the base of the tank are shown in Table 4.5.

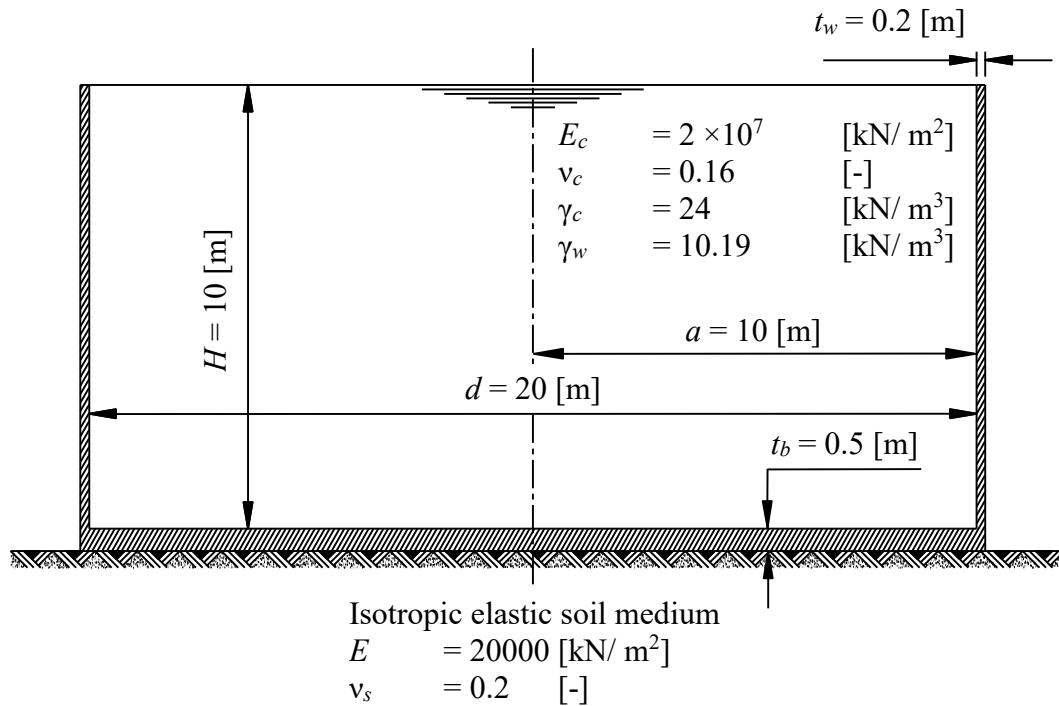


Figure 4.9 Circular cylindrical tank resting on an isotropic elastic soil medium

Table 4.4 Tank material and water unit weight

Modulus of Elasticity of the tank material	E_c	$= 2 \times 10^7$	[kN/ m ²]
Poisson's ratio of the tank material	ν_c	$= 0.16$	[-]
Unit weight of the tank material	γ_c	$= 24$	[kN/ m ³]
Unit weight of the water	γ_w	$= 10.19$	[kN/ m ³]

Table 4.5 Soil data

Modulus of Elasticity of the soil medium	E	$= 20000$	[kN/m ²]
Poisson's ratio of the soil medium	ν_s	$= 0.2$	[-]

4.3.2 Numerical Analysis

In order to illustrate the comparison between analyzing water storage tanks resting on an isotropic elastic half space soil medium and that of *ELPLA 10*, this example shown in Figure 4.9 is analyzed. Internal forces and displacements calculated by *ELPLA 10* were compared with those of *Melerski (2006)*. The height of the tank is divided into 50 equal elements, each of 0.20 [m], as shown in Figure 4.10. The half base of the tank is divided into 50 equal elements, each of 0.20 [m].

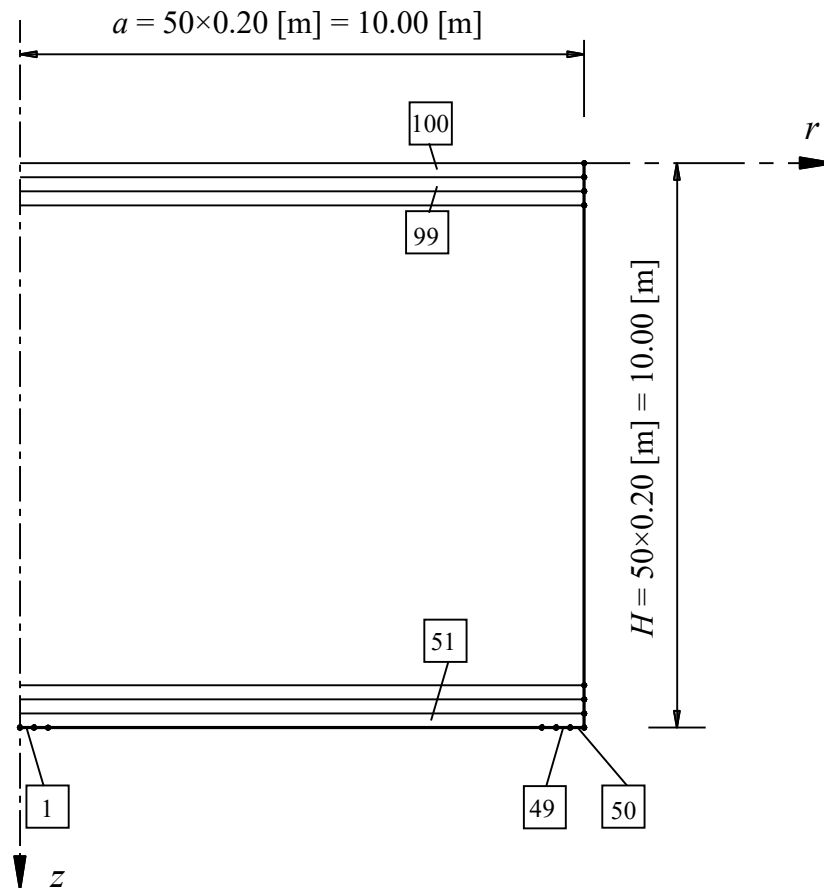


Figure 4.10 Finite element mesh of the tank

4.3.3 Results and discussions

The analysis of the considered tank is carried out by *ELPLA 10*, where the circular cylindrical tank and the base were simulated with a thin circular cylindrical shell element using finite element method. *Melerski* (2006) analyzed the same tank by a finite element method.

The tank is analyzed under the following two load cases:

- (a) Empty tank (self-weight only).
- (b) Full tank (self-weight and liquid pressure).

The base settlement in the two cases of loading are shown in Figure 4.11. They are in close agreement with the finite element solution of *Melerski* (2006). For case (a), the difference at the center is about 13%, while at the edge the value is fewer than *Melerski's* result with nearly 10% difference. For case (b), the values are more compatible, where the value of settlement at the center is greater with approximately 2%, while at the edge the difference becomes 6%.

The base moment is shown in Figure 4.12. Because high concentrations of moment often occur at the base center and at the junction of the tank wall with the base, the prediction of the central moment and the edge moment are of particular interest in structural analysis and design. For case (a), the edge moment obtained from the present analysis is about 7% less than the value of *Melerski* (2006), while the value of the moment at the center equals zero. For case (b), the edge moment is fewer than the value of *Melerski* (2006) with about 6%, while the moment at the center is bigger with about 1.8 %.

The wall meridional moment along the height of the tank is shown in Figure 4.13. For case (a), the moment at the wall-base junction is fewer than the value of *Melerski* (2006) with 1%. For case (b), the moment at the wall-base junction is bigger than the value of *Melerski* (2006), where the moment at the wall-base junction is not equal to the edge moment at the base for *Melerski* (2006) solution.

The tank wall tangential force variations along the height of the tank is shown in Figure 4.14. The results are in close agreement with the finite element solution of *Melerski* (2006).

Figure 4.15 shows the tangential displacement. It has the same diagrams as the tangential force diagrams in the two cases of the analysis, where the tangential displacement equal $w = N_{\theta} \cdot a / E t_w$.

where:

- w Tangential displacement, [m].
- N_{θ} Tangential normal force in the wall, [kN/ m].
- a Tank radius, [m].
- E *Young's* modulus of elasticity, [kN/m²].
- t_w Wall thickness, [m].

From these figures, it can be concluded for the considered tank and soil that the model used in the analysis illustrates a good accuracy for the program used in this research.

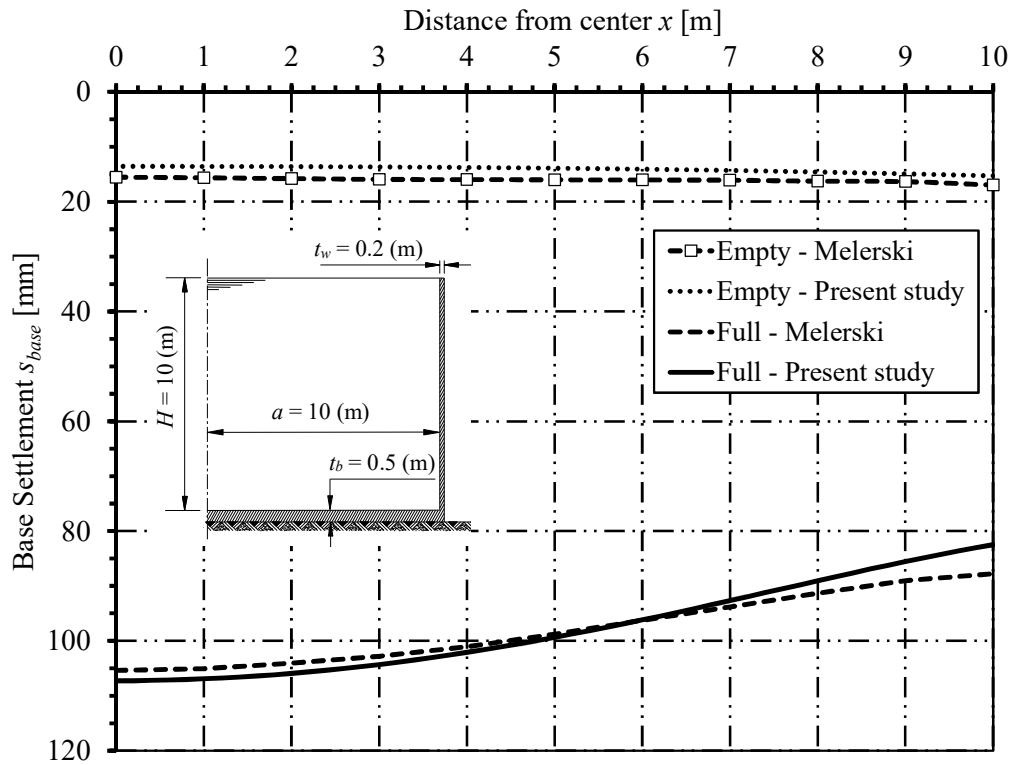


Figure 4.11 Variation of settlement s_{base} in the base plate

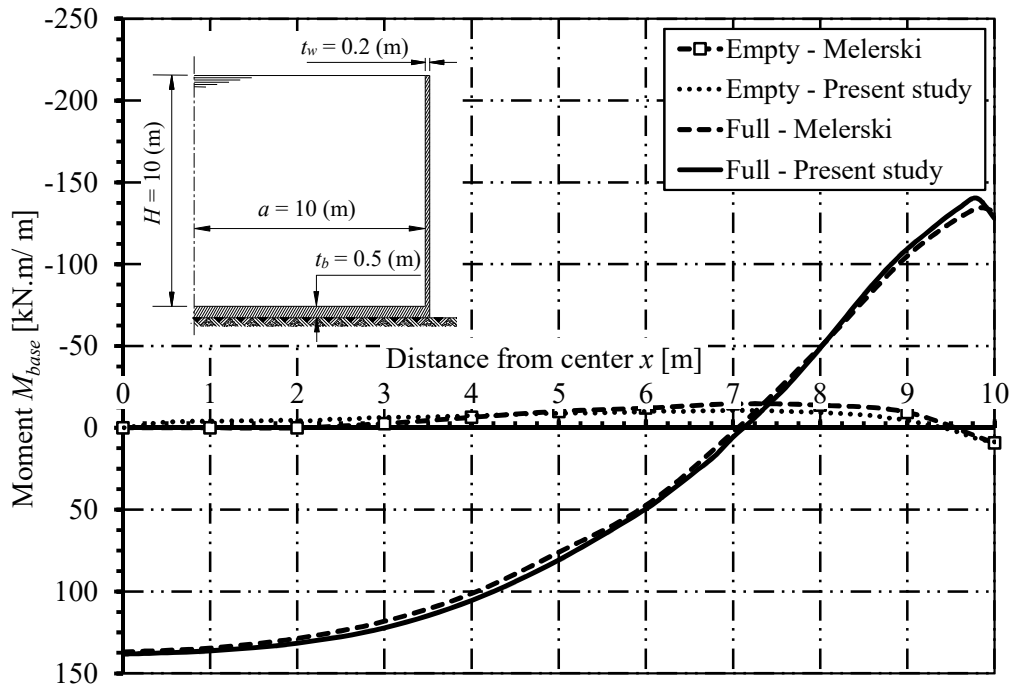
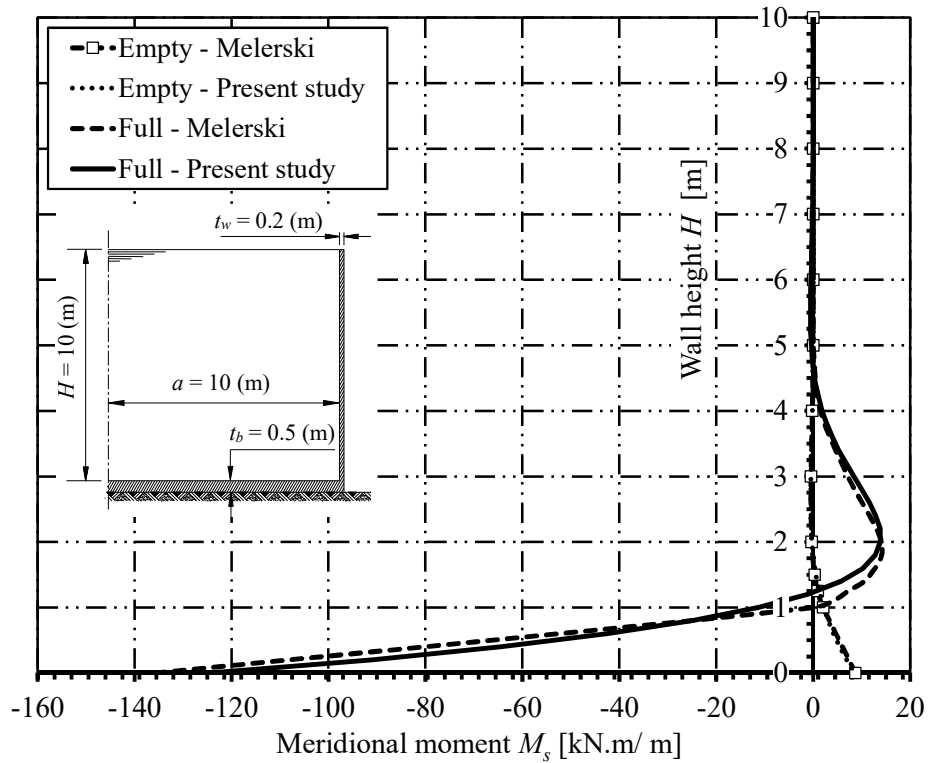
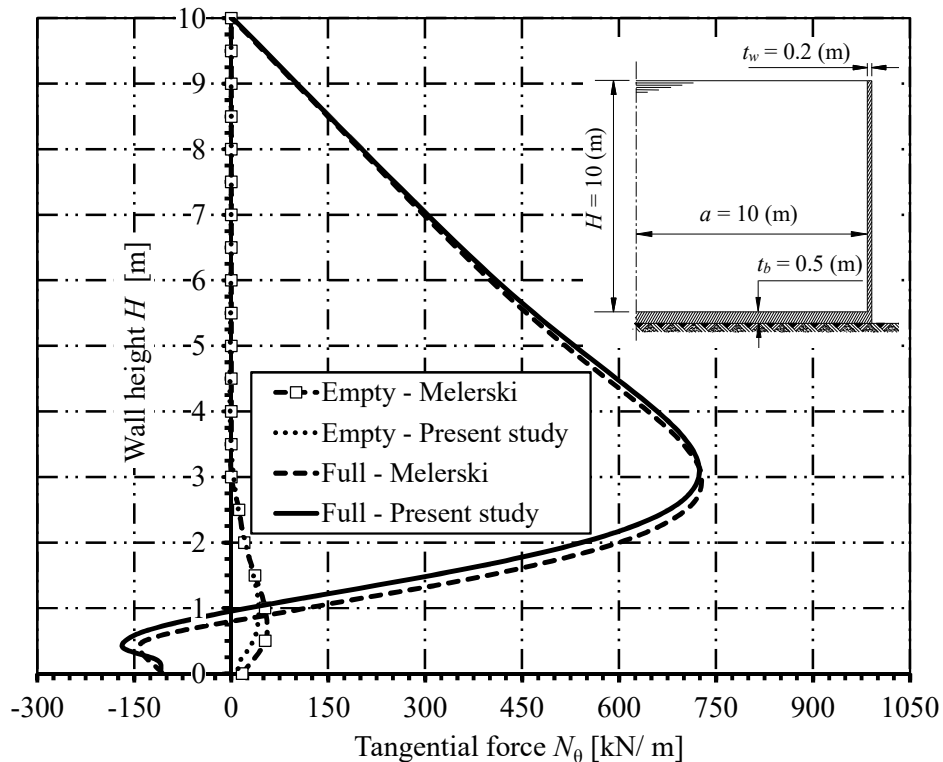


Figure 4.12 Variation of moment M_{base} in the base plate

Figure 4.13 Meridional moment M_s along the wall heightFigure 4.14 Tangential force N_θ along the wall height

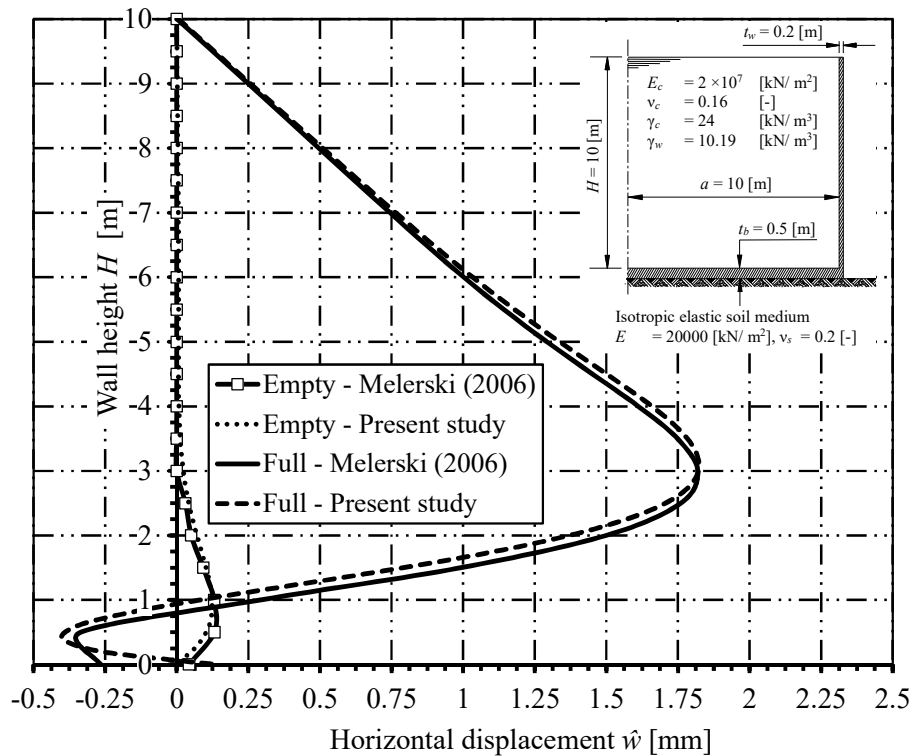


Figure 4.15 Horizontal displacement \bar{w} along the wall height

4.4 Settlement due to time-dependent loading

4.4.1 Description of the problem

Conte and Troncone (2006) [7] presented an analytical solution for the analysis of one dimensional consolidation of saturated soil layers subjected to general time-dependent loading. In the mentioned study, a simple calculation procedure that makes use of the *Fourier* series is proposed for practical applications. They compared their results with experimental results of oedometer tests. The apparatus used for the tests is not conventional and operates on specimens of 100 [mm] diameter and 29 [mm] height. A hydraulic system provides the load whose magnitude is controlled by a pressure regulator. This allows loading and unloading with general time history to be readily applied to the soil specimen. The tests were carried out on two prepared soil mixtures of different particle-size distribution, herein denoted soil *A* and soil *B*. Soil *A* is a sandy silt with clay, and soil *B* is a clayey silty sand. Samples of these soils were compacted at the optimum water content according to the standard Proctor procedure. Table 4.6 summarizes the main index properties of the tested soils and those after compaction. After compaction, the specimens were carefully trimmed and placed in the ring of the oedometer cell, where soil saturation was achieved by applying a backpressure in a way similar to that usually adopted in the triaxial tests. Consolidation tests under

time-dependent loading were then carried out. During these tests, water flow was prevented at the base of the specimen and drainage was allowed at the top.

Table 4.6 Index and after-compaction properties of the tested soils.

Property	Soil <i>A</i>	Soil <i>B</i>
Type	Sandy silt with clay	Clayey silty sand
Liquid limit $L.L$ [%]	37	22
Plastic limit $P.L$ [%]	16	15
Plasticity index I_P [%]	21	7
Specific weight G_s [-]	2.69	2.66
Water content w [%]	14	11
Dry unit weight γ_{dry} [kN/ m ³]	16.9	18.3
Coeff. of volume change m_v [m ² / kN]	7.4×10^{-5}	8.0×10^{-5}
Coeff. of consolidation C_v [m ² / sec.]	1.7×10^{-8}	1.8×10^{-6}

4.4.2 Numerical Analysis

To examine the accuracy of the numerical analysis of consolidation of clay under time-dependent loading using the *LEM* method, the clay layer is divided into 10 equal layers each of 2.9 mm depth, and the time is divided every 90 seconds.

4.4.3 Results and discussions

The loading process for soils *A* and *B* are shown in Figure 4.16 and Figure 4.18, while the settlement curves versus time are shown in Figure 4.17 and Figure 4.19, respectively. From the figures, it seems clear that the results of the *LEM* are applicable to the results of *Conte* and *Troncone* (2006) procedure, and also in a good agreement with the experimental results.

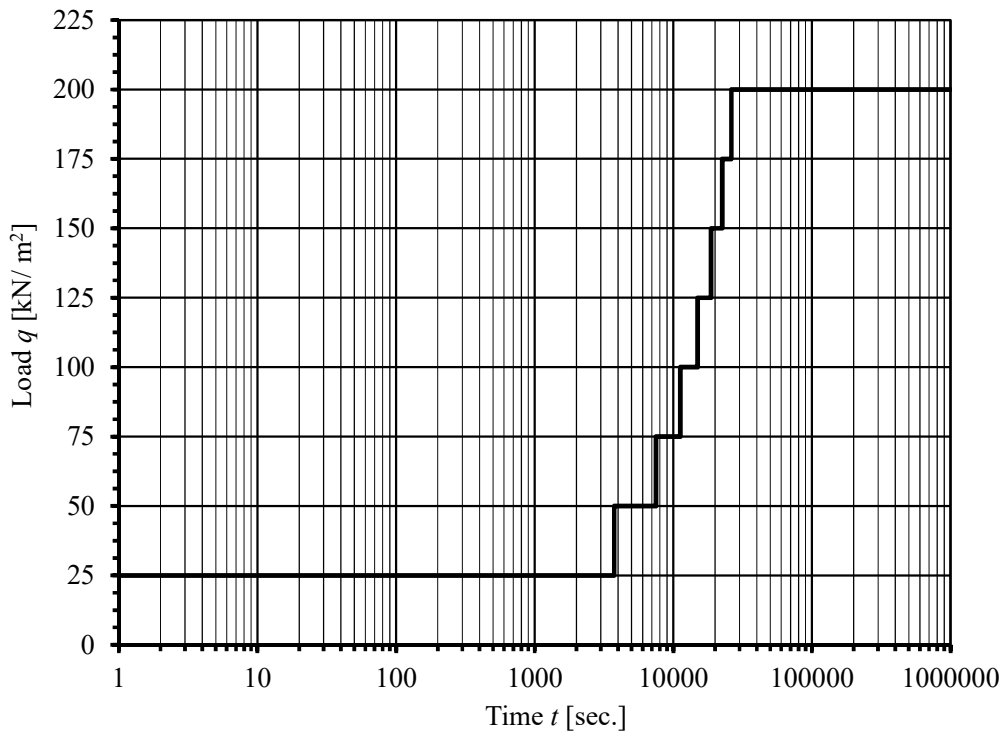


Figure 4.16 Loading process for soil A

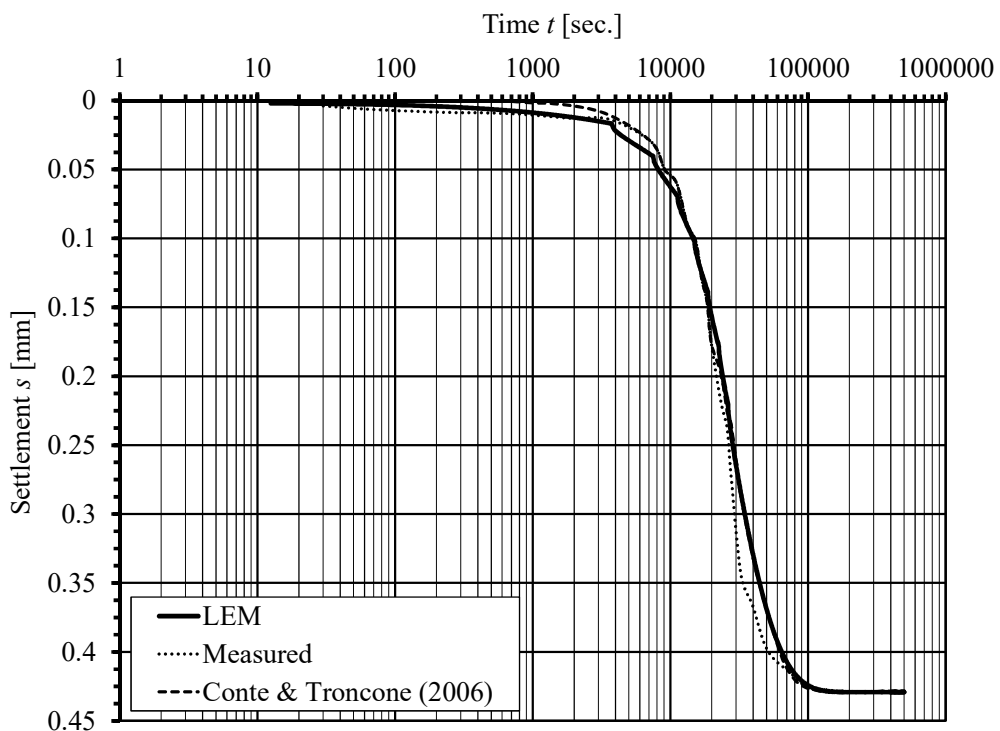


Figure 4.17 Settlement versus time for soil A

Chapter 5

5 Numerical analysis and discussions of static loads

5.1 Introduction

In this chapter, circular cylindrical concrete tanks resting on soil containing clay layers are introduced and studied under static loads using the developed numerical model using cylindrical finite element shells with different subsoil models. The analysis accounts for the soil layers defined by the modulus of compressibility or compression index. This enables considering sand or clay layers with their appropriate properties. Full compatibility between the tank wall, tank base and the soil is considered. Soil conditions for various zones at Port-Said area are considered, in order to study the structural response of circular tanks constructed therein. The results of the study introduced guidelines and diagrams for cylindrical tanks that may be used in Port-Said under static and cyclic loading.

5.2 Soil properties and parameters

Wastewater Treatment Plant, which consists of a system of tanks, are often constructed near to the sea for the purpose of discharging the wastewater to the sea. This thesis investigates the behavior of structures such as tanks used in Wastewater Treatment Plant under static and cycling loading in Port-Said area. Figure 5.1 shows the main industrial zones and the locations most probably appropriate for the construction of circular tanks at Port-Said. The geotechnical studies for Zone-1 which is located at Port-Said west were carried out by *Pelli/ Carletti* (1998) [42]. Zone-1 contains most of the natural gas facilities such as the condensation treatment plant owned by Petrobel Belayim Petroleum Company, Egypt. For Zone-2 which is located at Port-Said south, the geotechnical studies were carried out by *Golder Associates* (1979) [18]. Zone-2 comprises Port-Said water treatment station, a few residential buildings, the southern industrial zone, and agricultural development areas. The geotechnical studies for Zone-3 was taken from the report of *The Consulting Engineering Office* (2012) [6]. Zone-3 is located at the east of Port-Said, which contains Port-Said eastern Harbor.



Figure 5.1 Zones under consideration at Port-Said

5.2.1 Zone-1 at Port-Said west

The resource of the soil data for this zone is taken from the project of construction of a gas and condensate treatment plant owned by the *Petrobel Belayim* Petroleum Company, Egypt. The site of the project lies on the Mediterranean coast about 10 [km] west of Port Said, within the Nile delta area, and is adjacent to the Manzala Lake.

For the project an extensive soil investigation was carried out by *Pelli/ Carletti* (1998) [42] to select and design the most suitable foundation schemes for the plant. *Pelli/ Rossanese* (2000) [43] discussed also the performance of an instrumented landfill resting on soft silty and clayey soils with vertical drains, and presented the results of a numerical back-analysis of the main parameters controlling the consolidation.

The available geotechnical data include 15 borehole logs 50-60 [m] of depth, 7 borehole logs to 15-40 [m], 5 Dutch-cone CPT records to 35-40 [m], 11 CPTU records to 45 [m], 11 CPTU-dissipation test at variable depths, 9 field-vane tests (FV), oedometer tests, UU triaxial compression tests on 'undisturbed' and remoulded samples, CIU triaxial compression tests, pocket-penetrometer (PP) and *torvane* tests (TV), and classification tests.

5.2.1.1 Soil stratification in zone-1

The site is located within the Nile Delta system, where the Holocene delta sediments began accumulating with the rise in sea level at the end of the last glaciation, with an estimated sediment accumulation rate of about 5 [mm] per year. It is characterized by a 30-35 [m] thick deposit of soft clays/silts with sand interlayers, resting on compacted clay layer.

Figure 5.2 shows the typical site stratification in the considered site near Port-Said, which was carried out by *Pelli/ Carletti* (1998) [42] and *Pelli/ Rossanese* (2000) [43] according to several investigated points up to 60 [m] under the ground surface. The stratification is quite constant throughout the plant area.

Subsoil of the considered site can be classified in 5 main layers as follows:

- Silty clay, very soft
- Sand, fine loose to dense
- Clay, soft to firm
- Sand, medium to very dense
- Clay, very stiff to hard

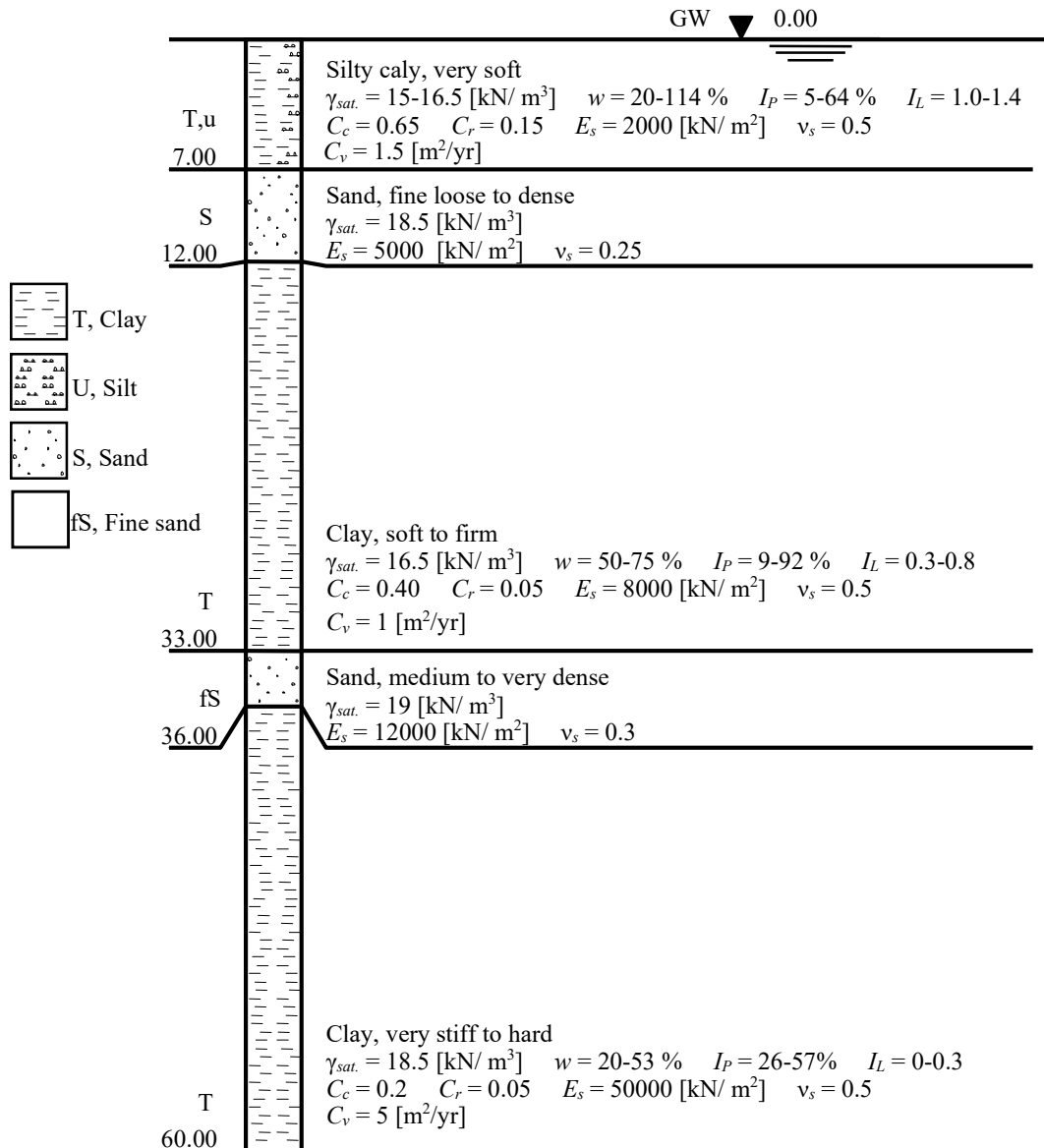


Figure 5.2 Typical soil properties for Zone-1 (Port-Said west)

5.2.1.2 Soil properties in zone-1

5.2.1.2.1 Over-consolidation ratio OCR

The over-consolidation ratio of **layer 1** was obtained from measurements of the undrained shear strength carried out in the laboratory. OCR values inferred from the undrained shear strength c_u and based on the relationship $OCR = (c_u / 0.23 \times \sigma'_{v0})^{1/0.8}$ are shown in Figure 5.3. OCR's larger than one are estimated, with relatively high values close to the ground surface. $OCR \approx 3.9-1.6$ was adopted for **layer 1**. **layer 3** (Pro-delta clay) appears to be essentially normally consolidated. However, due to secondary effects, a limited amount of preconsolidation, difficult to detect

on conventional laboratory specimen, may be present. For **layer 5**, the laboratory tests indicate a preconsolidation pressure in excess of 450 [kN/m²], and therefore the vertical stress increase does not enter the normally consolidated range.

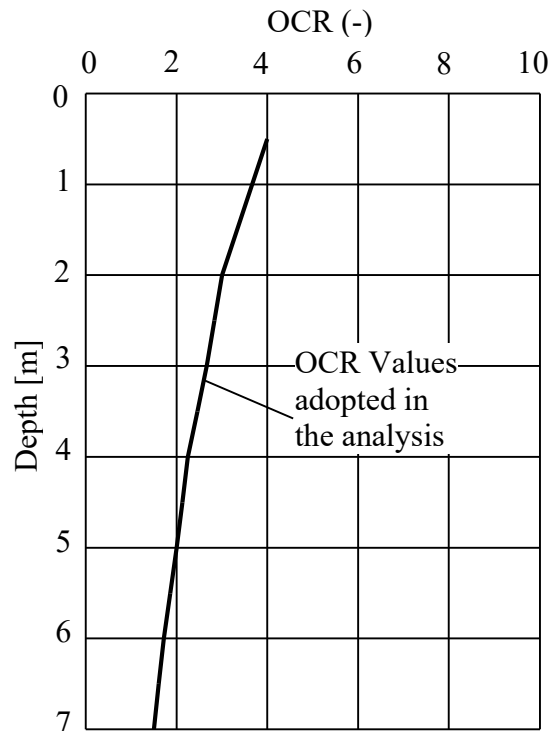


Figure 5.3 OCR values inferred from strength tests (*Pelli/ Rossanese (2000)*) for Zone-1

In Zone-1, the over-consolidation ratio OCR varies with the depth of clay as explained in Figure 5.3. After replacing the surface 2 m soil as mentioned above, the rest of the main 7 m thick-clay layer is divided into five sub-layers, 1 m thick each, in order to get a more accurate analysis. The five sub-layers have the same properties except for the OCR value that varies as given in Table 5.1.

Table 5.1 OCR values along the clay layer depth

Sub-layer No. [-]	Depth from the ground surface [m]	Over consolidation ratio OCR [-]
1	2.5	1.685
2	3.5	1.654
3	4.5	1.541
4	5.5	1.419
5	6.5	1.274

5.2.1.2.2 Void ratio e_o

According to *Nishida* (1956), void ratio e_o as a function in compression index C_c can be expressed as:

$$C_c = 0.54(e_o - 0.35) \quad (5.1)$$

where e_o is the initial void ratio and C_c is the compression index.

The void ratio e_o can be determined from the above equation by substituting the compression index C_c in the equation. $e_o = 1.55, 1.10$ and 0.72 [-] was adopted for **layers 1, 2 and 3**.

5.2.1.2.3 Coefficient of permeability k_v

According to *Terzaghi et al* (1996), the coefficient of permeability can be obtained from the coefficient of volume change through the relation:

$$c_v = \frac{k_v}{\gamma_w m_v} \quad (5.2)$$

where k_v is the coefficient of permeability, γ_w is the unit weight of the water and m_v is the coefficient of volume change ($m_v = 1/E_s$).

$k_v = 0.0074$ [m/ yr] was adopted for **layer 1**, while for **layers 3, 5** $k_v = 0.0013$ and 0.0001 [m/ year], respectively.

5.2.2 Zone-2 at Port-Said south

Zone-2 contains Port-Said water treatment station, a few residential buildings, the southern industrial zone, and agricultural development areas. The resource of soil data for this zone were carried out by *Golder Associates* (1979) according to several deep investigated logs up to 60 [m] under the ground surface.

5.2.2.1 Soil stratification in zone-2

Figure 5.4 shows the typical site stratification in the considered site at the south of Port-Said. The whole area has a thin layer of very soft surface clay of 2 [m] depth. Below the surface clay there is compact dense fine sand with a thickness of about 5.6 [m], the sand grades downward through a transition zone into firm clay. The clay extends to an average depth of about 50 [m] below the ground surface, the clay resting on basal deposits of very hard clay and dense sand.

Subsoil of the considered site can be classified in 6 main layers as follows:

- Clay, very soft
- Sand, dense fine
- Silt
- Clay, firm
- Sand, medium to very dense
- Clay, very stiff to hard

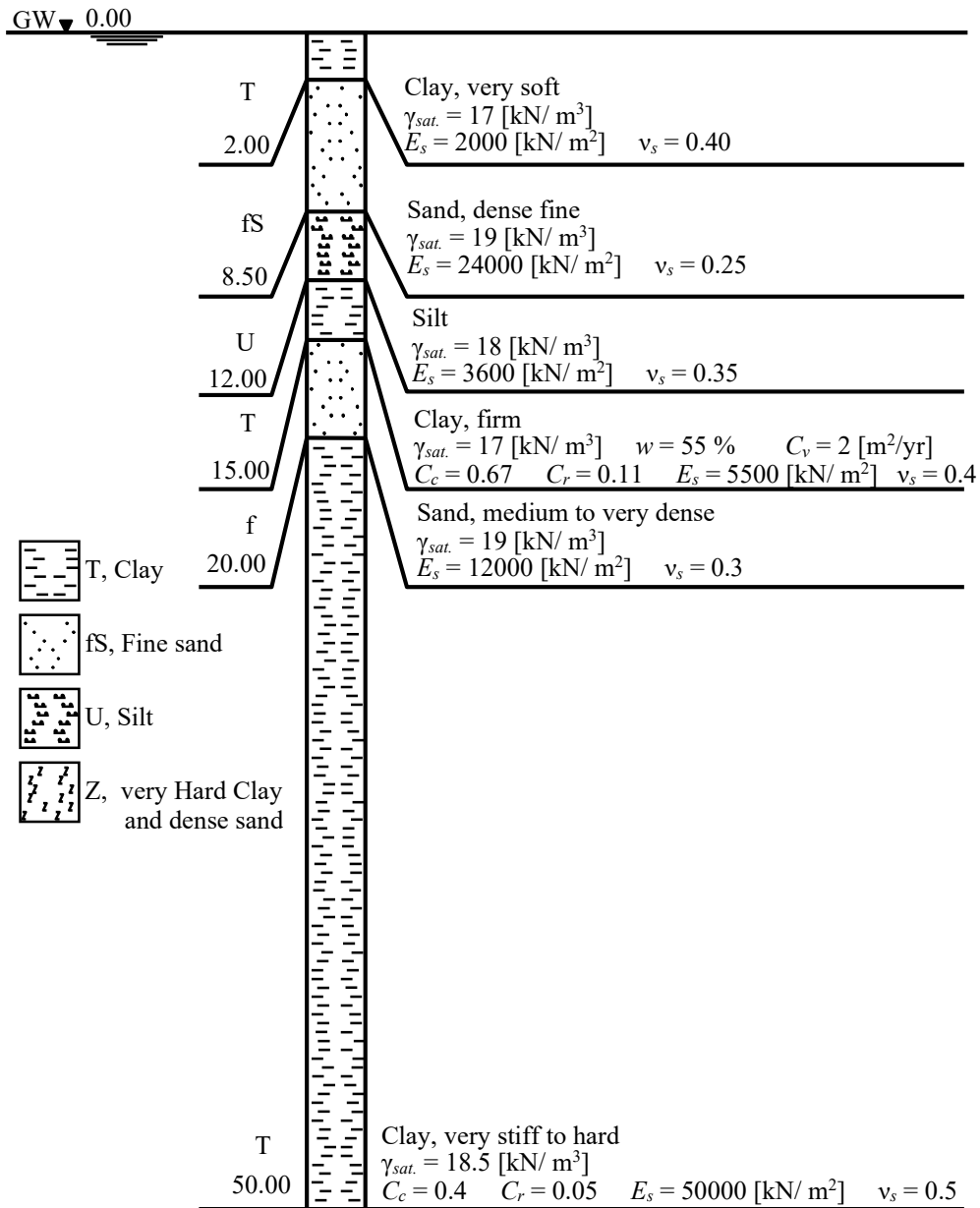


Figure 5.4 Typical soil properties for Zone-2 (Port-Said south)

5.2.2.2 Soil properties in zone-2

5.2.2.2.1 Soil compressibility

The soil compressibility of the cohesive layers was determined either from oedometer tests carried out in the soil laboratory or estimated using empirical equations.

The relationship between compression index and water content according to *Nishida* (1956) may be expressed as:

$$C_c = 0.0054(2.6w - 35) \quad (5.3)$$

where w is the water content.

For layer 4: $C_c = 0.67$ and $C_r = 0.11$ were adopted based on oedometer tests.

5.2.2.2.2 Over-consolidation ratio OCR

The over-consolidation ratio of **layer 4** was obtained from measurements of the cone penetration test (CPTU). $OCR = 1.3$ was adopted for **layer 4**.

5.2.2.2.3 Void ratio e_o

Void ratio e_o as a function in compression index C_c can be expressed as equation (5.1). $e_o = 1.10$ [-] was adopted for **layer 4**.

5.2.2.2.4 Coefficient of permeability k_v

The coefficient of permeability can be obtained from the coefficient of volume change through equation (5.2). $k_v = 0.0044$ [m/ yr] was adopted for **layer 4**.

5.2.3 Zone-3 at Port-Said east

Zone-3 locates at the east of Port-Said, which contains Port-Said eastern Harbor. The resource of soil data for this zone were taken from a technical report on the soil investigation and recommendations of foundation to create a trucks parking in Port-Said East harbor by *The Consulting Engineering Office*. Excavating boring logs and field tests were carried out by *Geo Group Company*, Egypt, while the lab tests were carried out by *Egypt Raymond for Foundation Lab*. 12 borehole logs were constructed to investigate the site, one of them is chosen to represent the soil properties of the eastern side of Port-Said.

The available geotechnical data include 3 borehole logs to 15 [m] of depth, 1 borehole log to 20 [m] and 8 borehole logs to 25 [m], 3 CPTU records to 20 [m], field-vane tests (FV), oedometer tests, UU triaxial compression tests on ‘undisturbed’ and remoulded samples, CIU triaxial compression tests, Standard penetration tests SPT in sandy soil, and classification tests.

5.2.3.1 Soil stratification in zone-3

Figure 5.5 shows the typical site stratification in the considered site at the east of Port-Said. Subsoil of the considered site can be classified in 7 main layers as follows:

- Silty sand, fine
- Sandy silt
- Clay, soft
- Sand, fine
- Silty sand, fine
- Sandy clayey silt
- Clay, soft

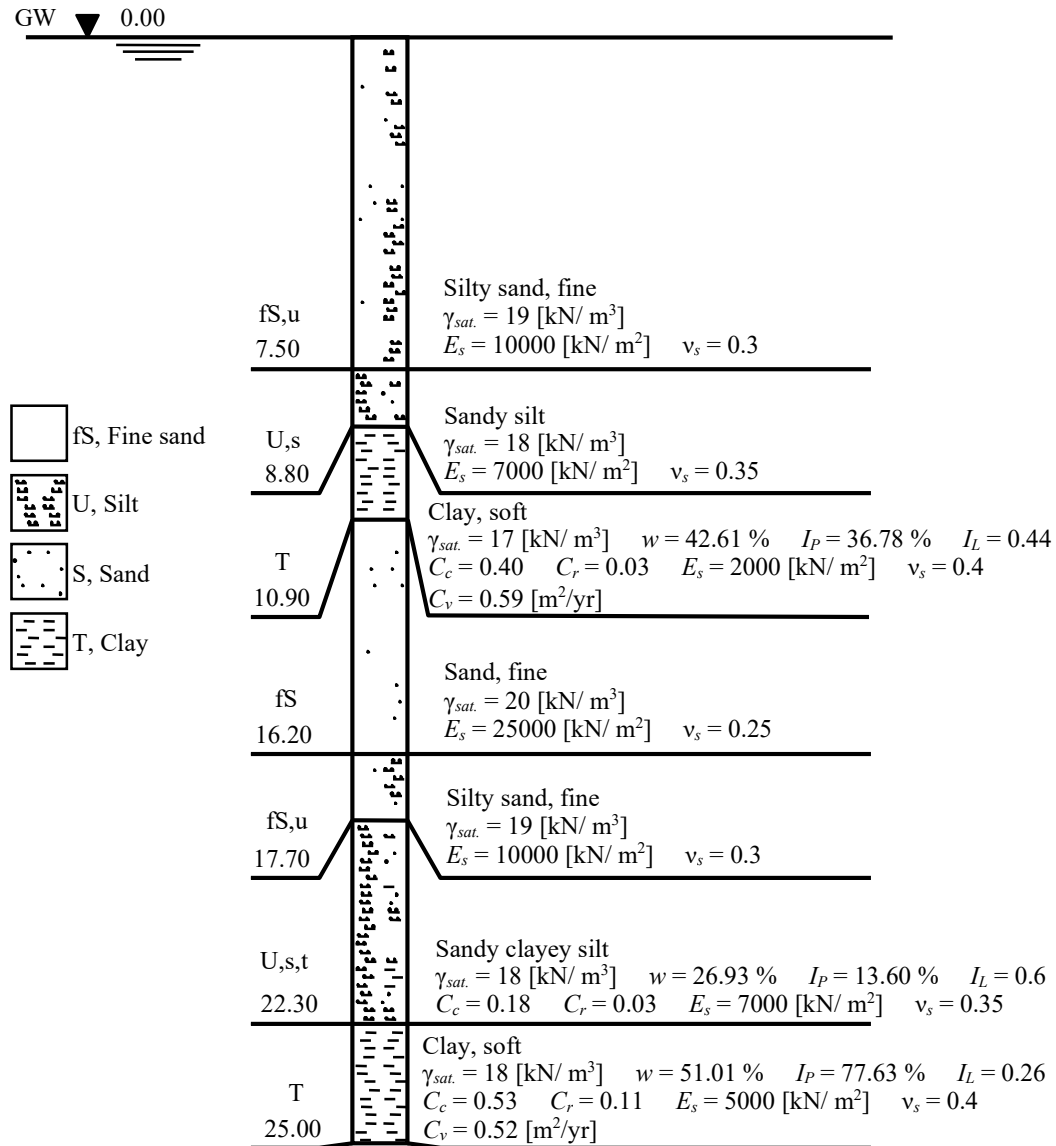


Figure 5.5 Typical soil properties for Zone-3 (Port-Said east)

5.2.3.2 Soil properties in zone-3

5.2.3.2.1 Over-consolidation ratio OCR

The over-consolidation ratio of **layer 3** was obtained from measurements of the cone penetration test (CPTU). $OCR = 1$ was adopted for **layer 3**. **Layer 7** appears to be essentially normally consolidated where $OCR = 0.765$.

5.2.3.2.2 Void ratio e_o

Void ratio e_o as a function in compression index C_c can be expressed as equation (5.1). $e_o = 1.186, 0.764[-]$ were adopted for **layers 3** and **7** respectively.

5.2.3.2.3 Coefficient of permeability k_v

The coefficient of permeability can be obtained from the coefficient of volume change through equation (5.3). $k_v = 0.0045, 0.0010$ [m/ yr] were adopted for **layers 3** and **7** respectively.

5.2.4 Groundwater

Groundwater at the coast in Port-Said lies within 0 to 1.25 [m] from the ground surface. The groundwater level is assumed to lie directly below the tank.

5.2.5 Properties of the replacement soil

Practically, the studied tank cannot be constructed directly on the soft clay of the first layer. Therefore, An assumed of two meter deep from the first layer is replaced by a good soil from gravel and sand. Properties of the replacement soil maybe taken as:

Modulus of compressibility $E_s = 100\ 000$ [kN/m²].

Unit weight of the soil $\gamma_{sat} = 22$ [kN/m³].

5.2.6 Determination of the limit depth L_D

The level of the soil under the tank at which the expected settlement will be very small and can be ignored is determined first as a limit depth of the soil. The limit depth is chosen to be the level at which the stress due to the tank $\Delta\sigma$ reaches the ratio $\xi = 0.1$ of the initial vertical stress σ'_o . The stress in the soil $\Delta\sigma$ may be determined at the characteristic point c or at the center of the circular base. This stress $\Delta\sigma$ is due to the average contact pressure from the tank at the surface q_o [kN/ m²]. At the characteristic point, from the definition of *Graßhoff* (1955), the settlement if the foundation is full rigid, will be identical with that if the foundation is full flexible. The characteristic point c lies at a distance $0.845 r$ from the center of the tank base as shown in Figure 5.6.

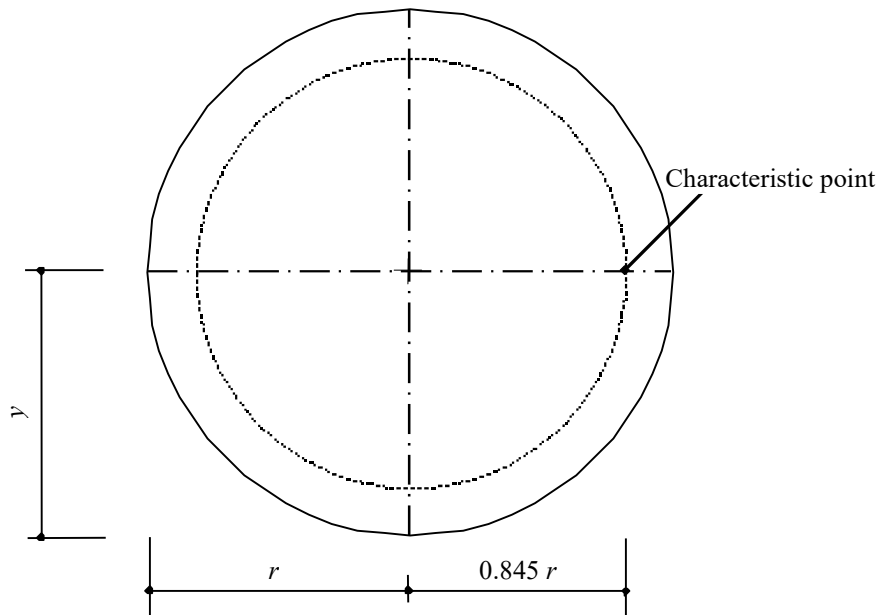


Figure 5.6 Position of characteristic point for circular foundation

5.3 Effect of the soil type model

The tank problem is analyzed with the following five different methods as.

1. Simple assumption model that neglect the soil and the contact pressure is uniform below the base.
2. *Winkler's* model that simulates the soil as isolated springs at nodal rings.
3. Continuum model for elastic base represented by the soil properties of zone-3.
4. Continuum model for flexible base represented by the soil properties of zone-3.
5. Continuum model for rigid base represented by the soil properties of zone-3.

The internal forces are not suggested in models number 4 and 5, the settlement and contact pressure.

5.3.1 Tank geometry and mesh

To study the sensitivity of the analysis results to the type of soil model, the tank shown in Figure 5.7 is assumed to be constructed at Port-Said east (Zone-3). The analysis was carried out by the present axi-symmetric shell finite elements. Figure 5.8 shows the mesh discretization of the tank.

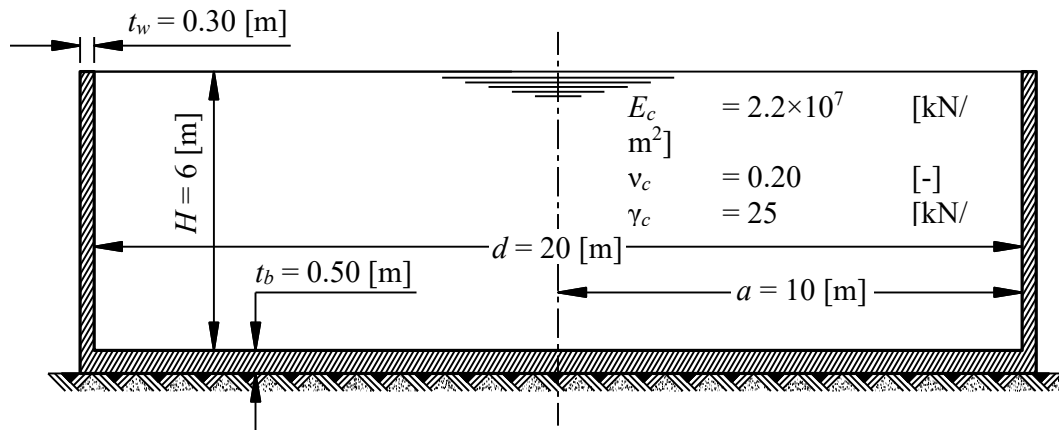


Figure 5.7 Geometry of the tank used in the soil model comparison

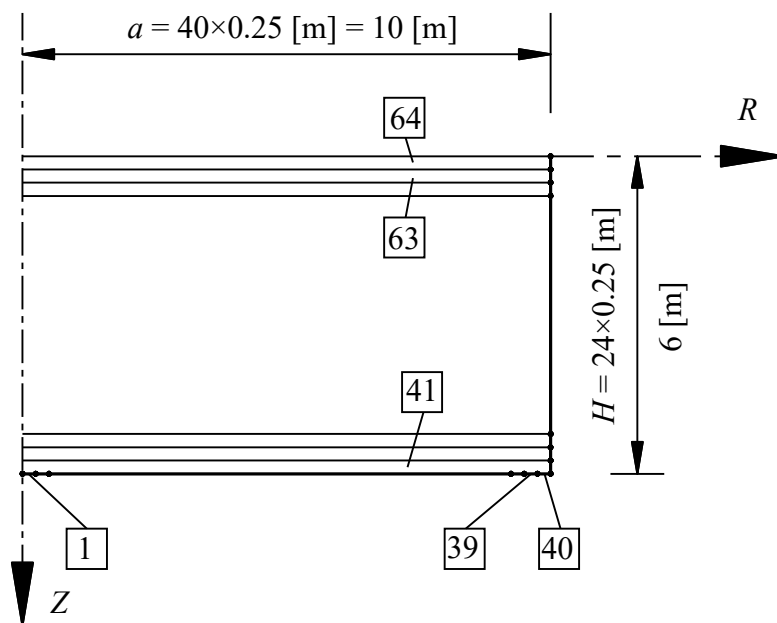


Figure 5.8 Finite element mesh of the tank used in the soil model comparison

5.3.2 Contact pressure q

In this section, it is assumed that the tank described in Figure 5.7 is constructed at Port-Said south (Zone-3). Figure 5.9 shows the radial variations of contact pressure under the tank base plate, for each of the considered soil models. In the first case (Simple assumption model), the contact pressure distribution under the base is uniform and this is due to that it is equal to the tank weight divided by the base area (by assumption), so it can be presented as an average value. The soil interaction with the base is neglected in this case.

In the second case (*Winkler's* model), the distribution of the contact pressure is almost uniform apart from the edge of the base plate, as it is higher 15 % than the contact pressure at the center. The contact pressure at the center is smaller than the average value of the first model with difference 8%, and at the edge the value is higher than the average value with difference 6%.

In the continuum model for elastic base, the contact pressure values are very high on the edge of the tank base and less toward the center with differences 657% and 37% respectively of the average value.

In the continuum model for rigid base, the contact pressure distribution is close to that of the continuum model for elastic base with differences 628% and 52% respectively with the average value. These results agree with the analytical solution for the contact pressure that tends to infinity at the edge according to *Boussinesq's* hypothesis.

In the continuum model for flexible base, the contact pressure is uniform below the base except at the edge below the wall. The uniform pressure is equal to the water pressure and the weight of the base, while the pressure below the walls equal the weight of the walls only. The uniform pressure is smaller than the average value with 11%, while the edge contact pressure is bigger than the average value with 215%.

5.3.3 Base settlement s_{base}

Figure 5.10 shows the radial variation of settlements in the base plate (positive when downward). For *Winkler's* model, this variation follows the contact pressure variation, as the contact pressure is equal to the settlement multiplied by the constant modulus of subgrade reaction k_s . The biggest settlement values occur in the flexible base, while the settlement in the rigid base is constant at any position. In continuum model for elastic base, the settlement at the edge of the base plate is less than the central settlement; and the settlement curve lies between the rigid and flexible base settlement curves. At the center of the base, the elastic settlement is smaller than the flexible settlement with a difference of 7%, and bigger than the rigid settlement with difference of 16%. On the other hand, the elastic settlement at the edge is bigger than the flexible settlement with difference of 5%, and smaller than the rigid settlement with difference of 10%. The settlements in *Winkler's* model are smaller than the elastic settlements with differences 50 % and 27% at the center and the edge of the base, respectively.

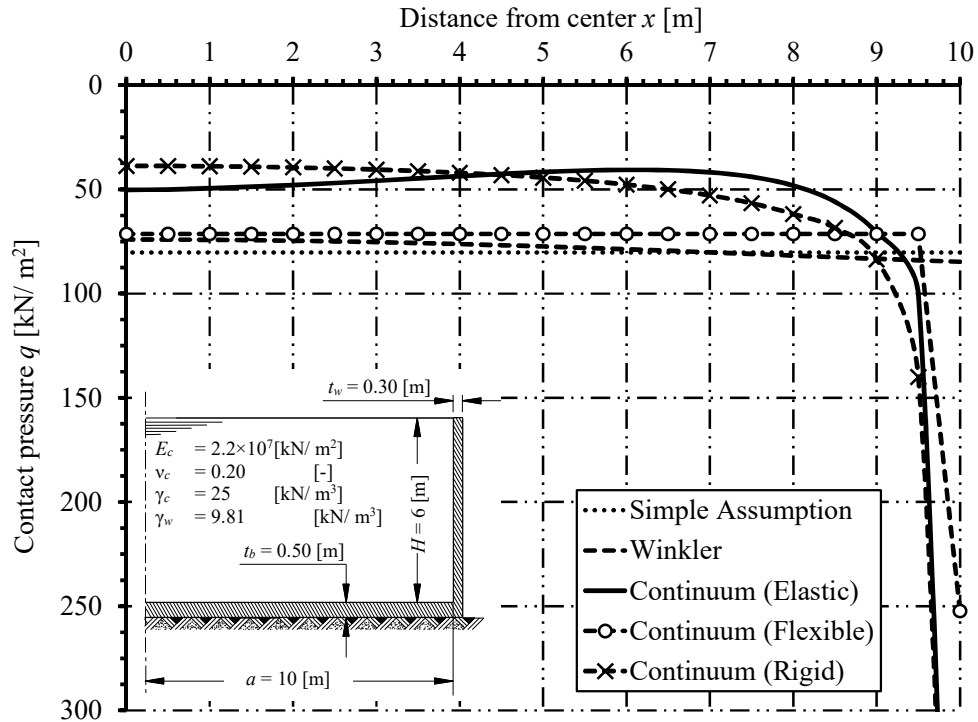


Figure 5.9 Variations of the contact pressure q below the tank base for different soil models

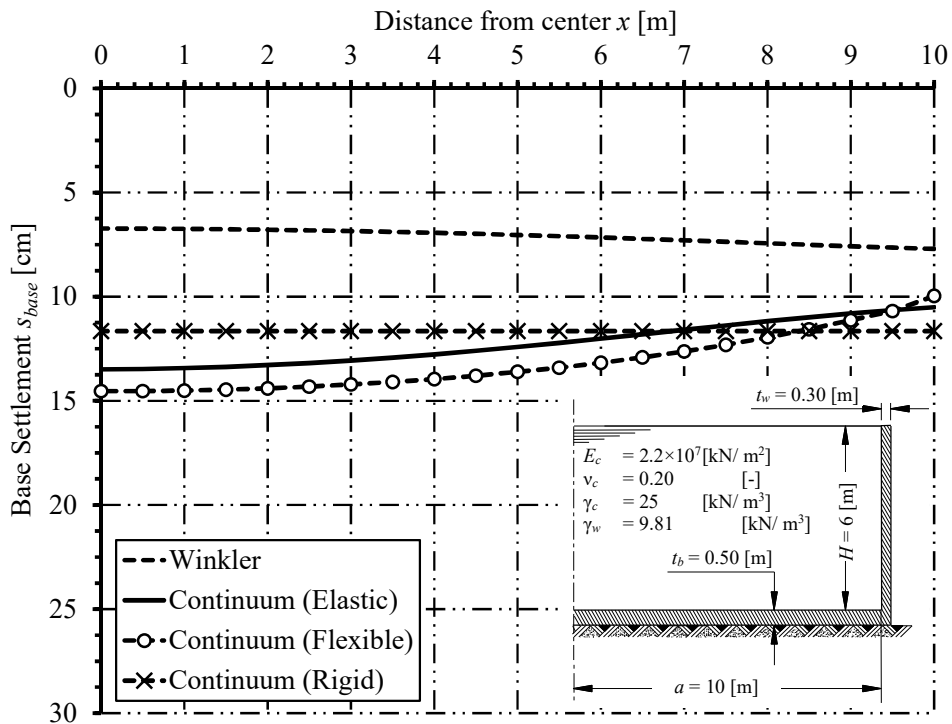


Figure 5.10 Variations of the base settlement s_{base} for different soil models

5.3.4 Radial moment across the base M_{base}

Variations of the radial moments in the base plate are shown in Figure 5.11. Bending moments resulting from *Winkler's* model and the simple assumption model are completely inaccurate if compared to those of the other soil models, because the soil parameters are not taken into consideration. The radial variations of bending moments in the base plate are totally reversed as shown in Figure 5.11. For the simple assumption model, the moment results at the edge and the center are smaller than the same results for the continuum model with difference values 67% and 57%, respectively. For *Winkler's* model, the moment results at the edge and at the center are smaller than the same results for the continuum model with differences 75% and 72% respectively.

5.3.5 Radial force across the base N_{base}

Figure 5.12 shows the radial force in the base. The radial force is compression in case of simple assumption model and tension in *Winkler's* model and continuum model. The values of the simple assumption model and *Winkler's* model are smaller than the continuum model values with the same difference 98%.

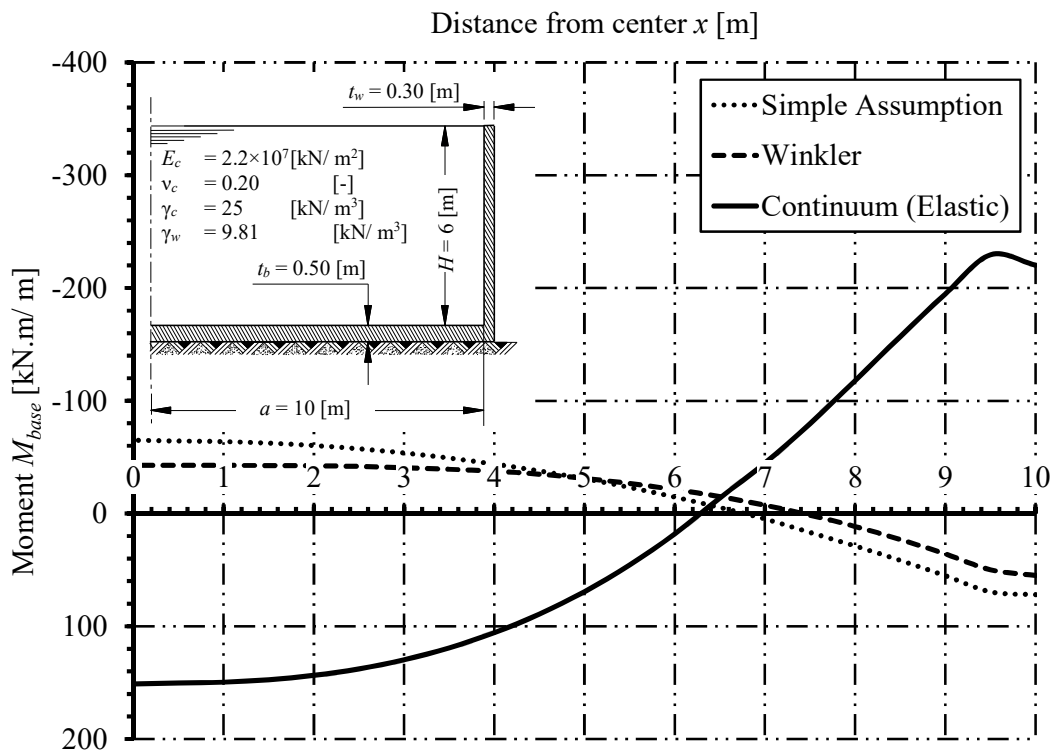


Figure 5.11 Variations of radial moment M_{base} for different soil models

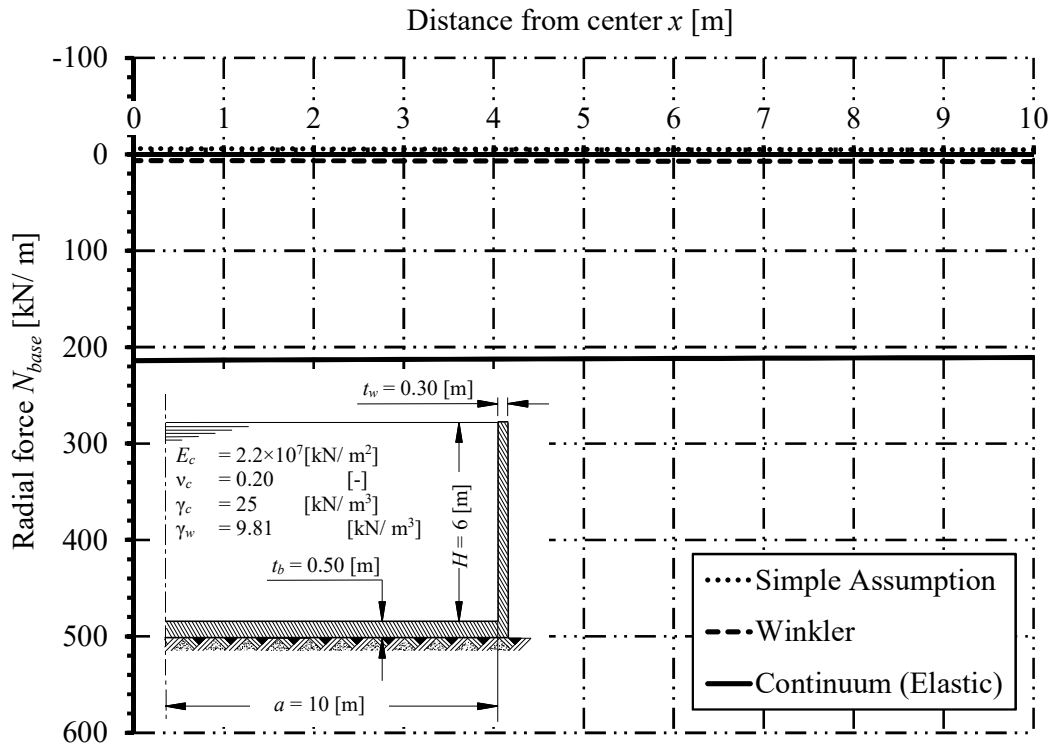


Figure 5.12 Radial force across the base N_{base}

5.3.6 Meridional moment in the wall M_s

Figure 5.13 shows the variation of the meridional moment along the wall height. It is obvious that the moments in the wall resulting from *Winkler's* model and the simple assumption model are totally reversed when compared with the results of the layered continuum model. Consequently, designers are recommended to deal with the moment results of the simple soil models cautiously.

5.3.7 Tangential force in the wall N_θ

Variations of the tangential force along the wall height are shown in Figure 5.14. The tangential forces in the wall for the simple assumption and *Winkler's* models are mostly tension. For layered continuum model the tangential force varies considerably along the wall height, as shown in the figure. The maximum tension force in the simple assumption model and *Winkler's* models are bigger than that for the continuum model with differences 65% and 61% respectively.

5.3.8 Normal displacement in the wall w

Figure 5.15 shows the normal displacement. It has the same diagrams shape as the tangential force diagrams in the three cases of the analysis.

The above results indicate that the distribution of the contact pressure under the tank base plays a great rule in the distribution of the internal forces in the tank. For the analyzed tank geometry and soil properties, results of *Winkler's* model and simple assumption model are nearly the same. For quick results without soil information and without soil structure interaction between the tank base and soil medium, the simple assumption may be used and will give the same results of *Winkler's* model. The continuum model for elastic base can be used for more accurate results of the tank considering soil structure interaction effect.

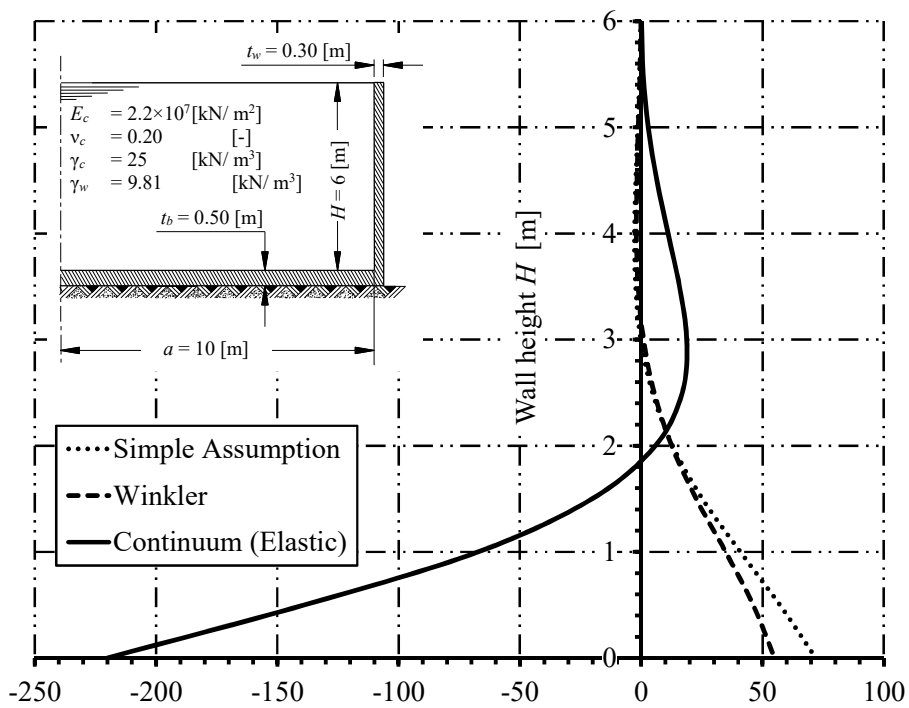
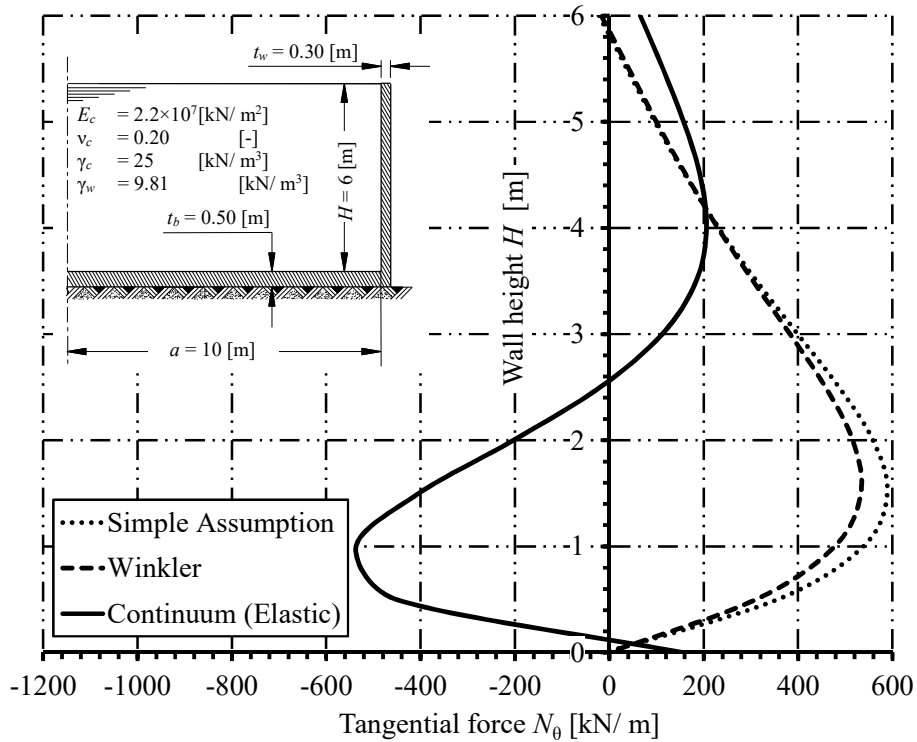
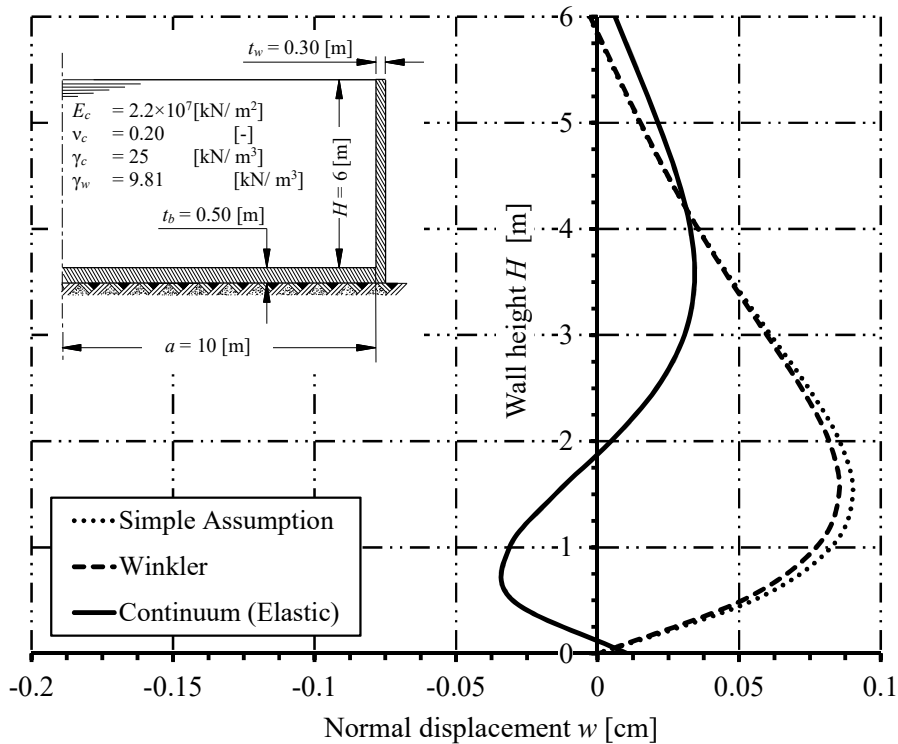


Figure 5.13 Variations of meridional moment M_s along the wall

Figure 5.14 Variations of tangential force N_θ along the wallFigure 5.15 Variations of normal displacement w along the wall

5.4 Effect of tank location in Port Said

The probable differences in the structural behavior of circular tanks arising from changing the site of construction at Port-Said is given in this section. The soil properties vary according to the construction zone, as given in Figure 5.2, Figure 5.4 and Figure 5.5. It should be noticed that the start and end of the main clay layer is located at depths 2 to 7 m, 12 to 15 [m], and 8.8 to 10.9 [m] below the ground surface, for zones-1, 2 and 3, respectively. All results given hereafter are obtained by the layered soil model, as it is the most realistic and effective, when compared with the other soil models. The geometric material properties of the tank are shown in Figure 5.16.

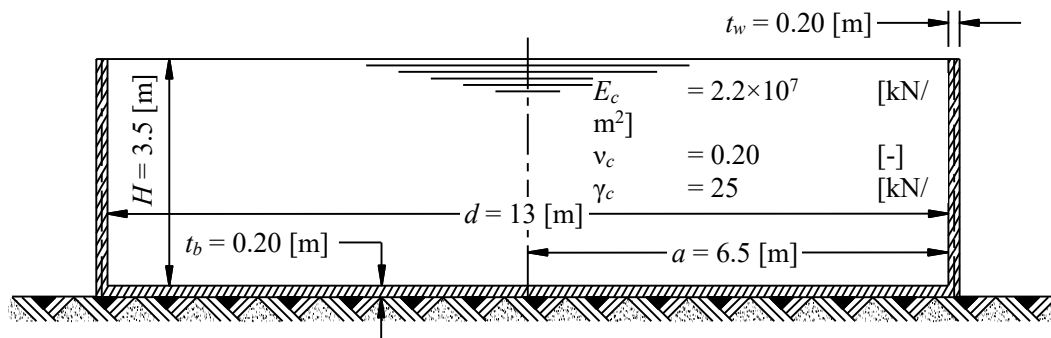


Figure 5.16 Geometry of the tank used to compare the results of tank location

The height of the tank is divided into 14 equal elements, each of 0.25 [m] and the base is divided into 26 equal elements, each of 0.20 [m]. The total elements number is 40 elements with 41 nodes as shown in Figure 5.17.

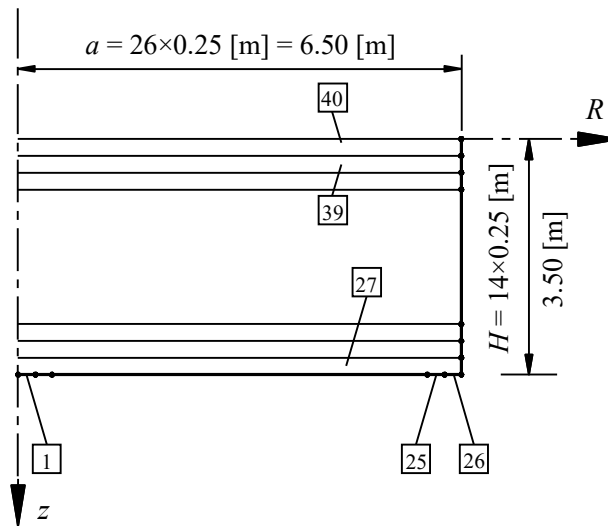


Figure 5.17 FE mesh of the tank used to compare the results of tank location

The contact pressure distribution under the circular base plate q is shown in Figure 5.18 for the three zones. The corresponding radial variations of the vertical displacements of the base plate, s_{base} , the moment in the base plate, M_{base} , and the radial force in the base plate N_{base} are shown in Figure 5.19, Figure 5.20 and Figure 5.21 respectively. Moreover, the corresponding distributions of the meridional moment, M_s , and tangential forces along the wall height, N_θ , are presented in Figure 5.22 and Figure 5.23 respectively.

5.4.1 Contact pressure q

The contact pressure at the center of the base in Zones-2 and 3 are bigger than the contact pressure in Zone-1 with difference of nearly 6% for the two values, where the clay- weak- layer get deeper in soil in Zone- 3 then Zone- 2 respectively.

5.4.2 Base settlement s_{base}

The deeper the effective clay layer from the ground surface, the higher the soil resistance for deformation, and so the settlement of the foundations get smaller. That is the explanation for the settlement curves distribution shown in Figure 5.19. The settlement at the center of the base in Zones- 2 and 3 are smaller than the settlement in Zone-1 with differences of 74% and 58% respectively; while at the edge, the differences become 78% and 64% respectively. On the other hand, the differential settlements in Zones-2 and 3 are smaller than the differential settlement in Zone-1 with differences 46% and 35% respectively.

5.4.3 Radial moment across the base M_{base}

Figure 5.20 shows the distribution of the radial moment along the base radius in the studied zones. The moment at the center of the base in Zones- 2 and 3 are smaller than the moment in Zone-1 with differences of 70% and 58% respectively. The wall-base joint, the differences become 58% and 40% respectively.

5.4.4 Radial force across the base N_{base}

Figure 5.21 shows the radial force along the base radius in the studied zones. The radial force along the base radius in Zones-2 and 3 are smaller than the radial force along the base radius in Zone-1 with differences of 48% and 34% respectively.

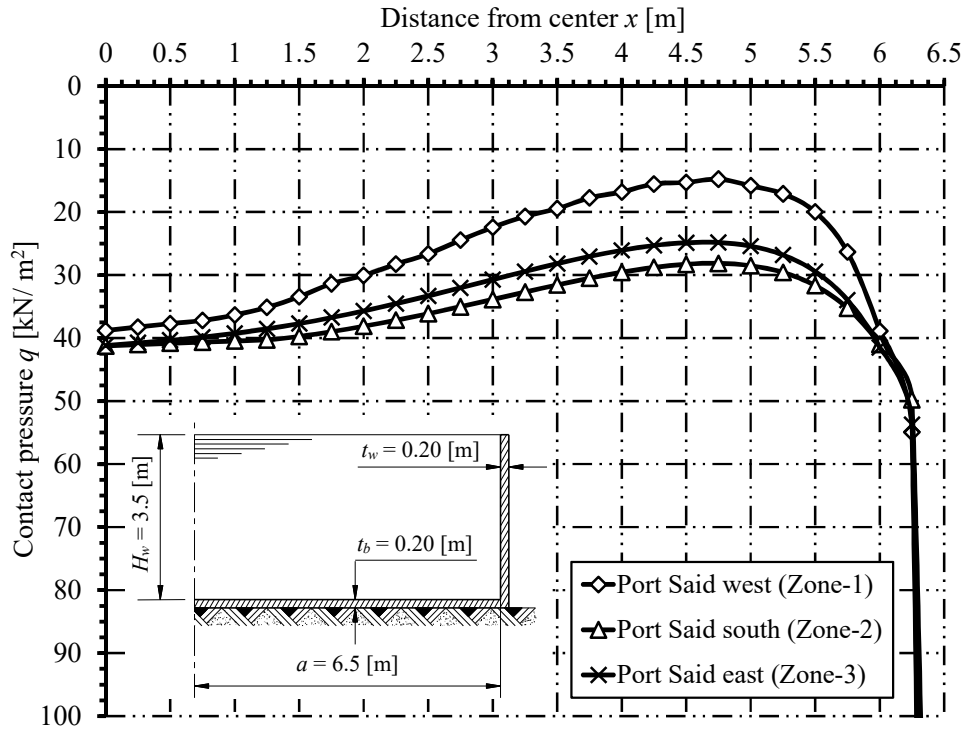


Figure 5.18 Variations of the contact pressure q below the tank for different zones

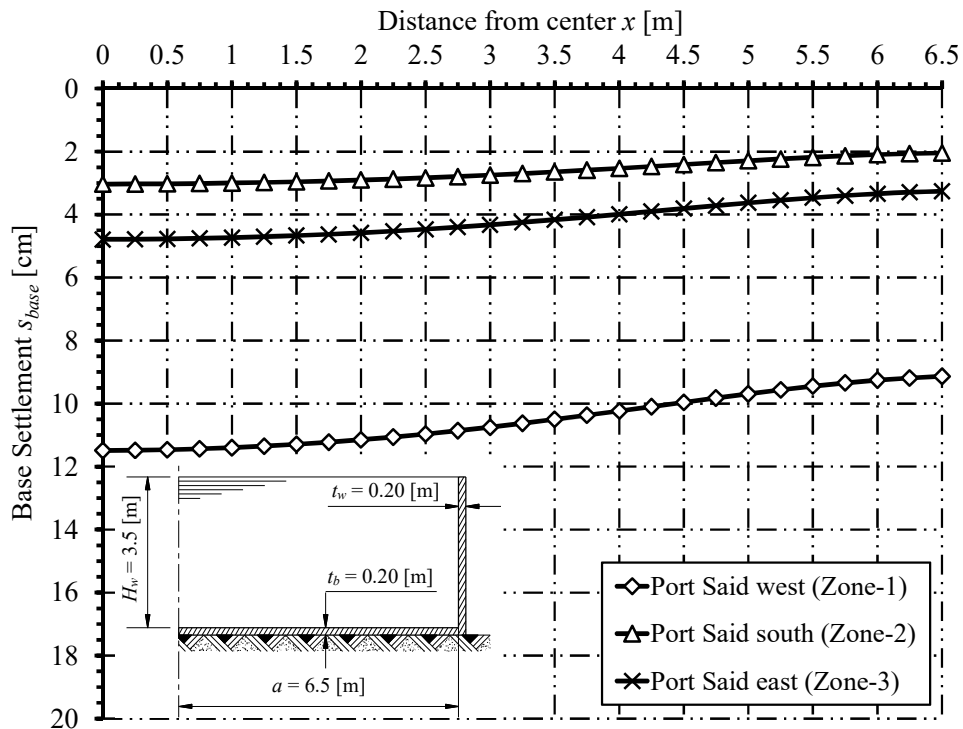
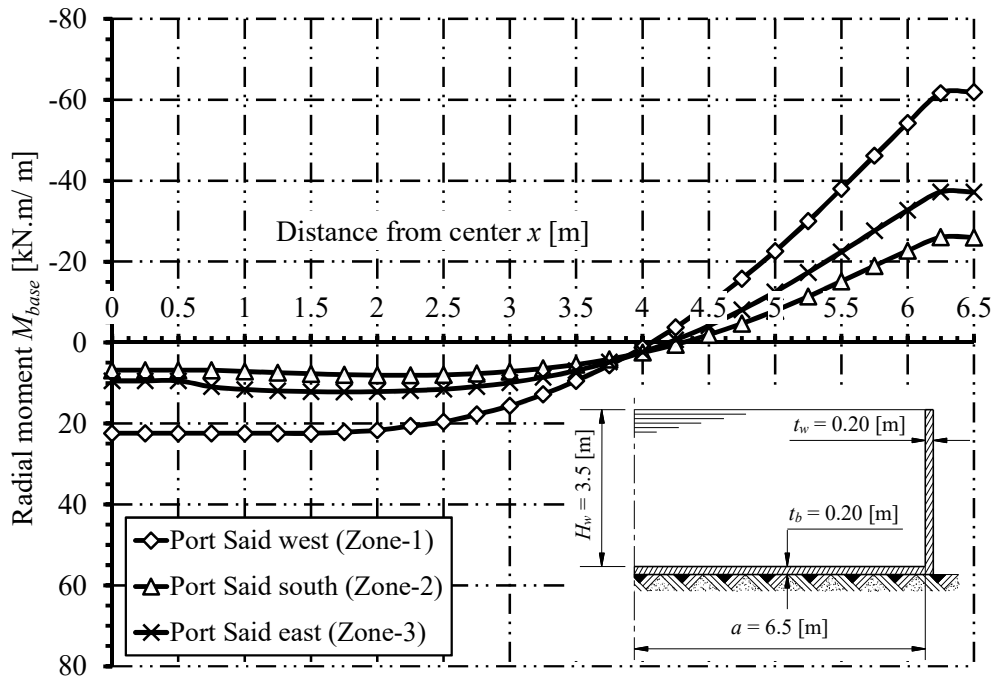
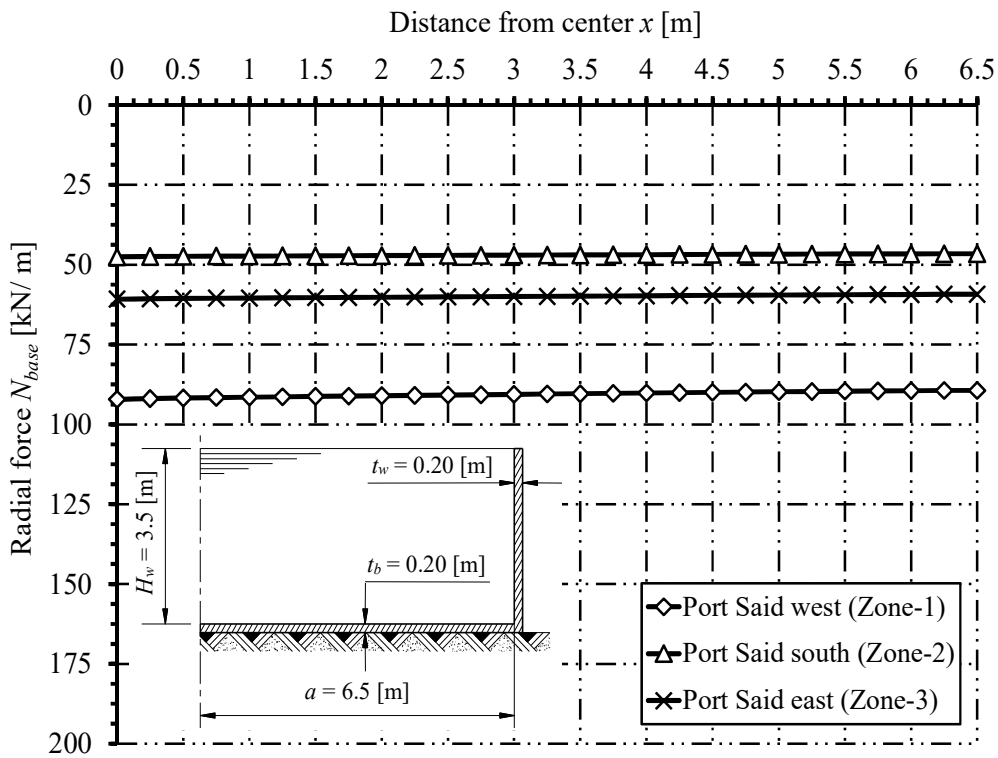


Figure 5.19 Variations of the base settlement s_{base} for different zones

Figure 5.20 Variations of the radial moment M_{base} for different zonesFigure 5.21 Variations of the radial Normal force N_{base} for different zones

5.4.5 Meridional moment in the wall M_s

Figure 5.22 shows the meridional moment along the wall height in the studied zones. The meridional moment at the wall-base joint – in water side- in Zones-2 and 3 are smaller than the moment in Zone-1 with differences of 58% and 40% respectively. The maximum meridional moments in air side are smaller in Zones-2 and 3 than the moment in Zone-1 with differences of 40% and 28%, respectively.

5.4.6 Tangential force in the wall N_0

As can be seen in Figure 5.23, the tangential force along the wall is led to be tension whenever the soil get stronger. The maximum compression force in the wall in Zones-2 and 3 are smaller than the tangential force in Zone-1 with differences of 80% and 56% respectively. In the tension zone, the maximum tension force in the wall in Zones-2 and 3 are bigger than the force in Zone-1 with differences of 18% and 5% respectively.

5.4.7 Normal displacement in the wall w

Figure 5.24 shows the normal displacement along the wall in the studied zones. It have the same diagrams as the tangential force diagrams. Accordingly, it can be said that from the structural point of view, Zone-2 (Port-Said South) is the most suitable place for the construction of circular cylindrical storage tanks and Zone-1 (Port-Said west) is the worst of the three zones.

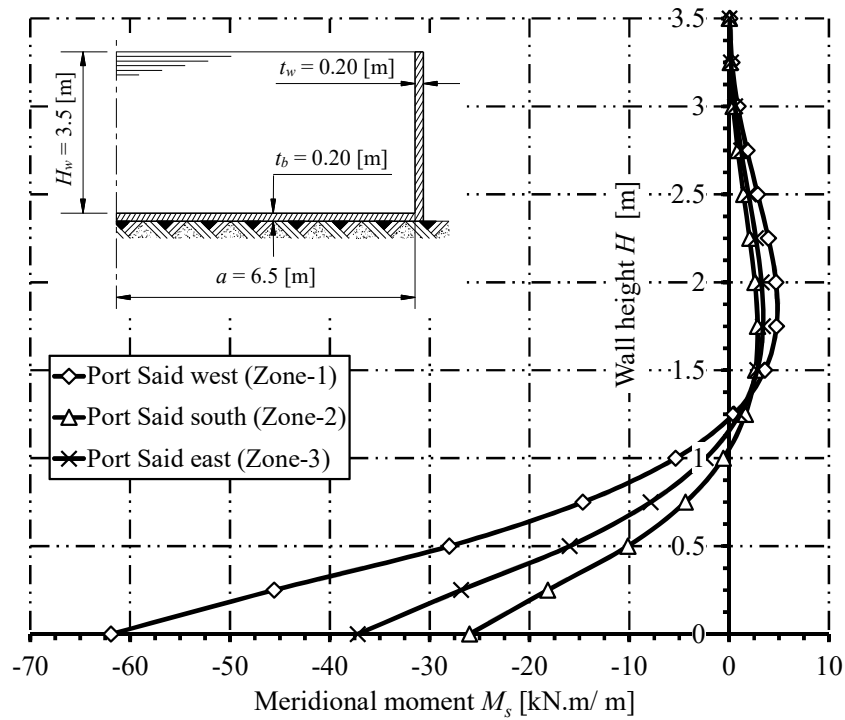


Figure 5.22 Variations of meridional moment M_s along the wall for different zones

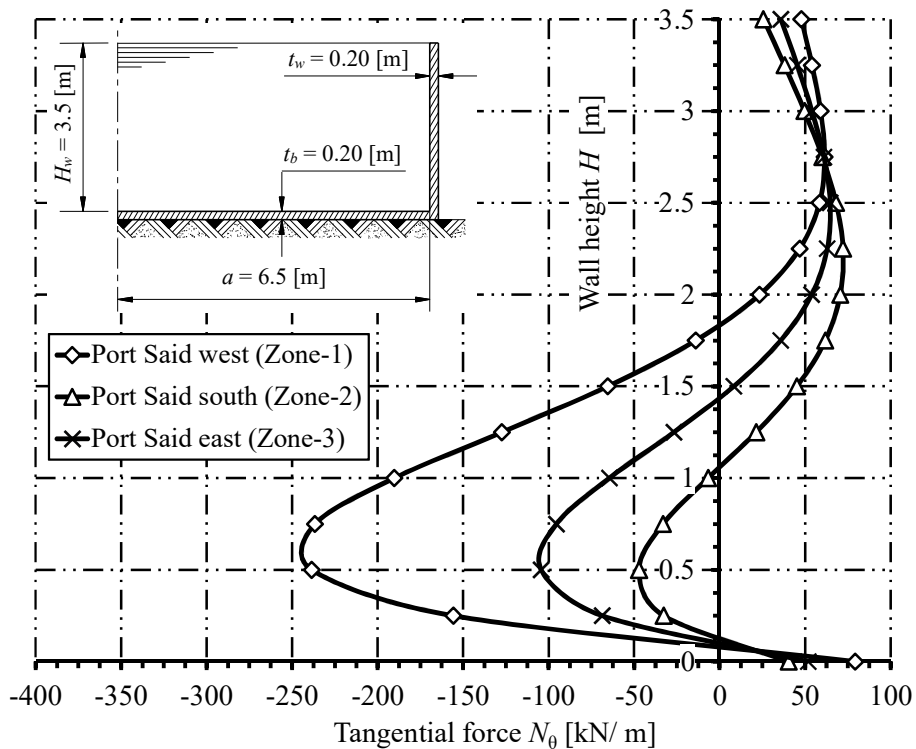


Figure 5.23 Variations of tangential force N_θ along the wall for different zones

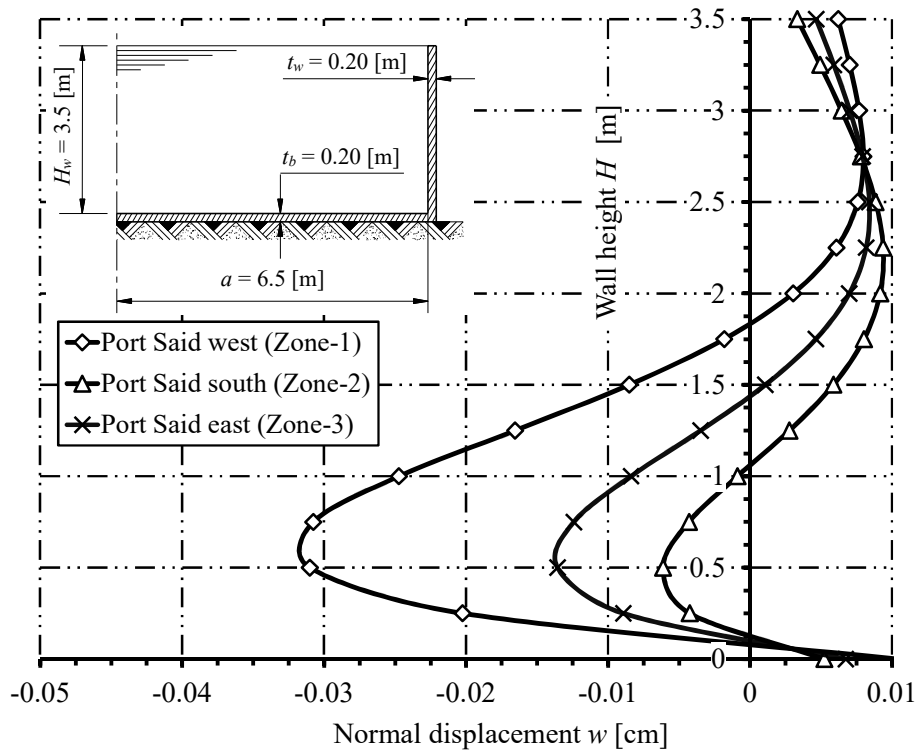


Figure 5.24 Variations of normal displacement w along the wall

5.5 Effect of the thickness of replacement layer on settlement

In this section, a study on the effect of varying the replacement layer thickness is presented. The replacement layer thickness increases from 2 to 4 [m]. The study is made on a group of tanks with radii 6, 8 and 10 [m] and with height to radius ratio of 0.5 and 1. This study is useful for identifying the safe dimensions of the tanks in the three zones under consideration in Port-Said so as not to exceed the maximum settlement allowed in clay soils -15 [cm]- according to table (4-3) the Egyptian Code of soil mechanics and foundations [11].

Figure 5.25 shows The effect of varying the replacement layer thickness H_{Rep} . in zone-1 on the settlements at the tank base center, for different height to radius ratios, H/a . For $H/a = 0.5$, increasing the replacement layer depth from 2 [m] to 3 [m] reduces the settlement at the center with 23% and 28% for radii 6 [m] and 8 [m], respectively. While increasing the replacement layer depth from 2 [m] to 4 [m] reduces the settlement at the center with 39% and 40% for radii 6 [m] and 8 [m], respectively. For $H/a = 1$, increasing the replacement layer depth from 2 [m] to 3 [m] reduces the settlement at the center with 11% and 24% for radii 6 [m] and 8 [m], respectively. While increasing the replacement layer depth from 2 [m] to 4 [m] reduces the settlement at the center with 31% and 38% for radii 6 [m] and 8 [m], respectively. Constructing tanks with diameters till 12 [m] and heights till 6 [m] in Zone-1 needs at least 2 [m] replacement to get acceptable values within the ECP limited settlement in clay (15 [cm]). The reduction rate of settlement

becomes smaller as the thickness of replacement layer gets larger. It can also be seen that the effectiveness of the replacement soil is much more pronounced as the height to radius ratio of the tank, H/a , gets larger. This is attributed to the fact that the vertical displacement at the center of base plate is much larger as the H/a ratio increases.

Figure 5.26 shows The effect of varying the replacement layer thickness H_{Rep} in zone-2 on the settlements at the tank base center, for different height to radius ratios, H/a . From the figure, it's obvious that increasing the thickness of the replacement layer has a very slight effect on the settlement, where the clay layer lies at 12 [m] deep from the ground surface.

Figure 5.27 shows The effect of varying the replacement layer thickness H_{Rep} in zone-3 on the settlements at the tank base center, for different height to radius ratios, H/a . For $H/a = 0.5$, increasing the replacement layer depth from 2 [m] to 3 [m] reduces the settlement at the center with 7, 6 and 4 [%] for radii 6, 8 and 10 [m], respectively. While increasing the replacement layer depth from 2 [m] to 4 [m] reduces the settlement at the center with 13, 12 and 7 [%] for radii 6, 8 and 10 [m], respectively. For $H/a = 1$, increasing the replacement layer depth from 2 [m] to 3 [m] reduces the settlement at the center with 5 and 4 [%] for radii 6 [m] and 8 [m], respectively. While increasing the replacement layer depth from 2 [m] to 4 [m] reduces the settlement at the center with 10 [%] for both radii 6 and 8, respectively.

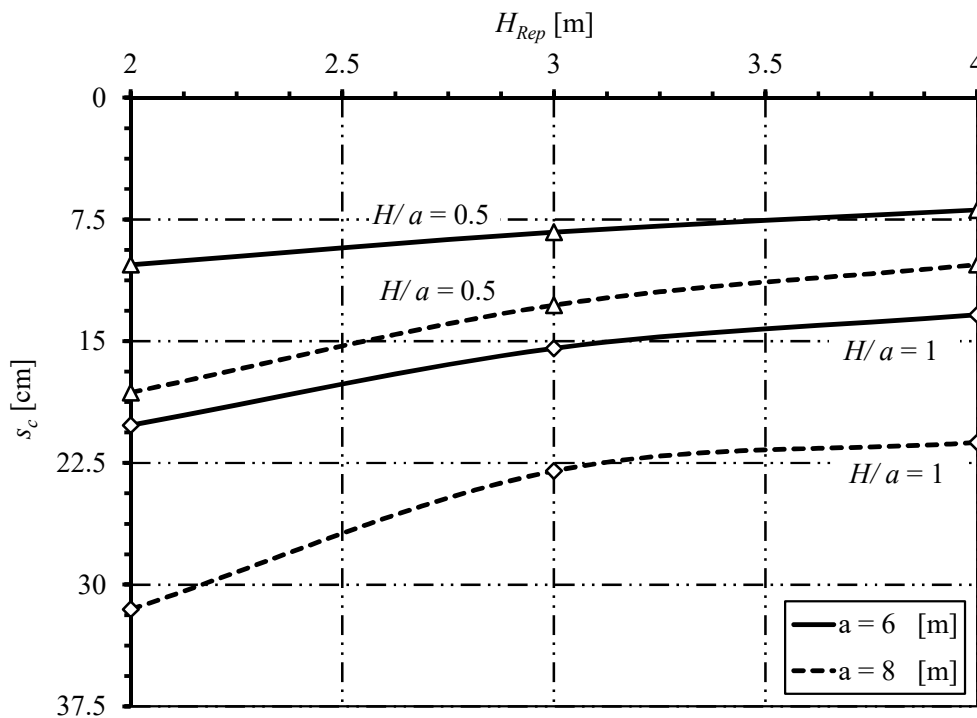


Figure 5.25 Effect of replacement thickness in Zone-1 on the variations of the settlement at base center s_c

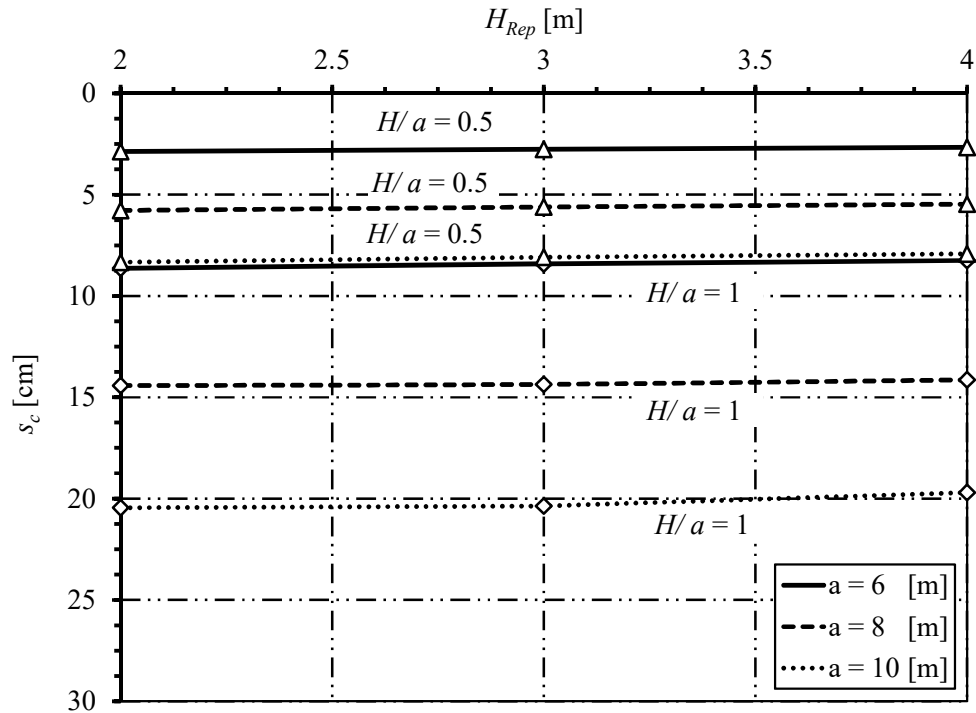


Figure 5.26 Effect of replacement thickness in Zone-2 on the variations of the settlement at base center s_c

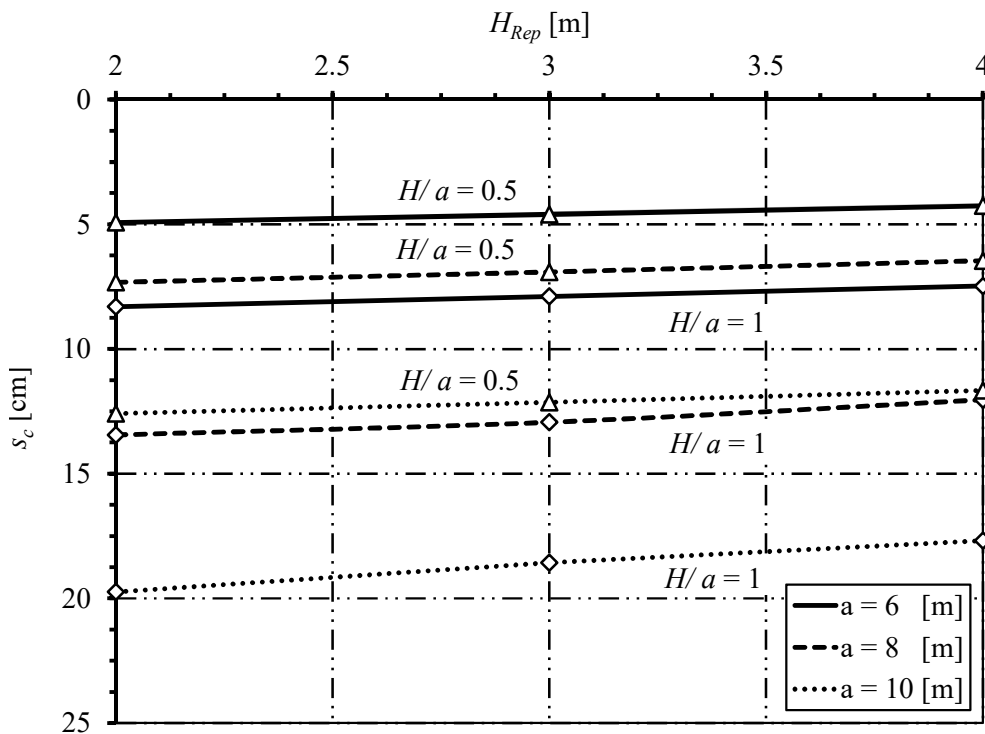


Figure 5.27 Effect of replacement thickness in Zone-3 on the variations of the settlement at base center s_c

Table 5.2, Table 5.3 and 0 show the maximum tank dimensions that are safe for settlement does not to exceed 15 [cm] at different zones of Port-Said.

Table 5.2 Maximum allowable safe dimension of tanks in zone-1

H/a [-]	$H_{Rep.}$ [m]	a_{max} [m]	H_{max} [m]
0.5	2	7	3.5
	3	9	4.5
	4	10	5
1	2	5	5
	3	6	6
	4	6	6

Table 5.3 Maximum allowable safe dimension of tanks in zone-2

H/a [-]	$H_{Rep.}$ [m]	a_{max} [m]	H_{max} [m]
0.5	2	15	7.5
	3	15	7.5
	4	15	7.5
1	2	8	8
	3	8	8
	4	8	8

Table 5.4 Maximum allowable safe dimension of tanks in zone-3

H/a [-]	$H_{Rep.}$ [m]	a_{max} [m]	H_{max} [m]
0.5	2	11	5.5
	3	11	5.5
	4	11	5.5
1	2	8	8
	3	8.5	8.5
	4	9	9

5.6 Effect of the roof condition on the flexural behavior of the tank

For the tank shown in Figure 5.28, three cases were considered for comparison, the tank is open at the top, the tank is covered with a flat roof and the last case the tank is covered with a spherical shell roof. The three cases are presented to study the flexural behavior of the tank wall and base in the three cases.

Consider the open tank geometry shown in Figure 5.16 and the tanks covered with flat or spherical roof geometry as shown in Figure 5.28. The tanks are considered to be constructed in Port Said south (zone-2). This problem is an axi-symmetrically circular cylindrical tank resting on a continuum layered soil medium. In this example, compressibility and consolidation parameters are used in the analysis according to the data of soil properties in zone-2.

The analysis of the tanks is carried out with simulating the tank elements by a thin shell element using finite element method. The three tanks are analyzed using the continuum model for layered soil medium to get more realistic results.

The height of the tank is divided into 14 equal elements, each of 0.20 [m] and the base is divided into 26 equal elements, each of 0.20 [m]. The flat floor is divided – as the base- into 26 equal elements, each of 0.20 [m], while the spherical roof is 0.14 [m] thick and is divided into 26 equal elements, each of 0.26 [m]. The total elements number is 40 elements with 41 nodes for the opened tank and 66 elements with 67 nodes for both the tanks covered with a spherical or flat roof as shown in Figure 5.29.

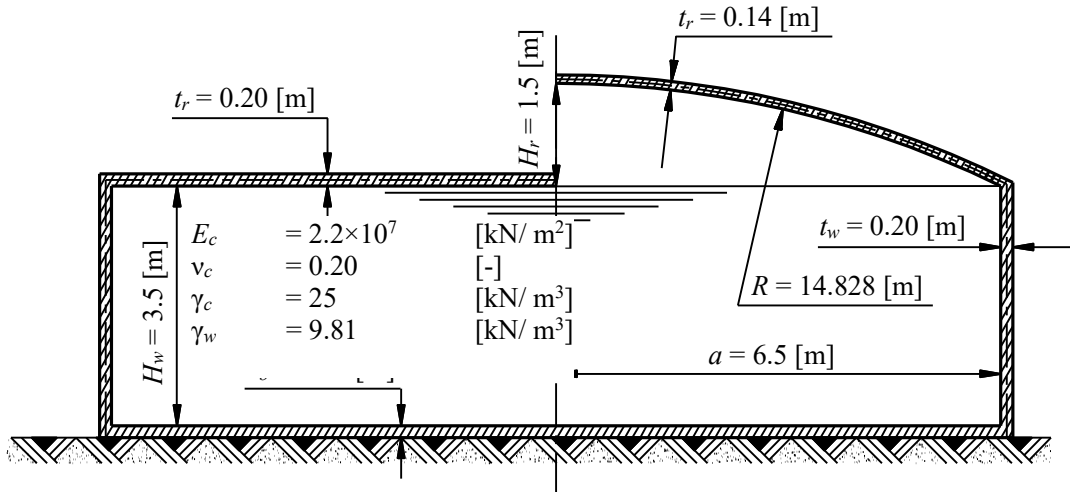


Figure 5.28 Tank covered with flat or spherical roof

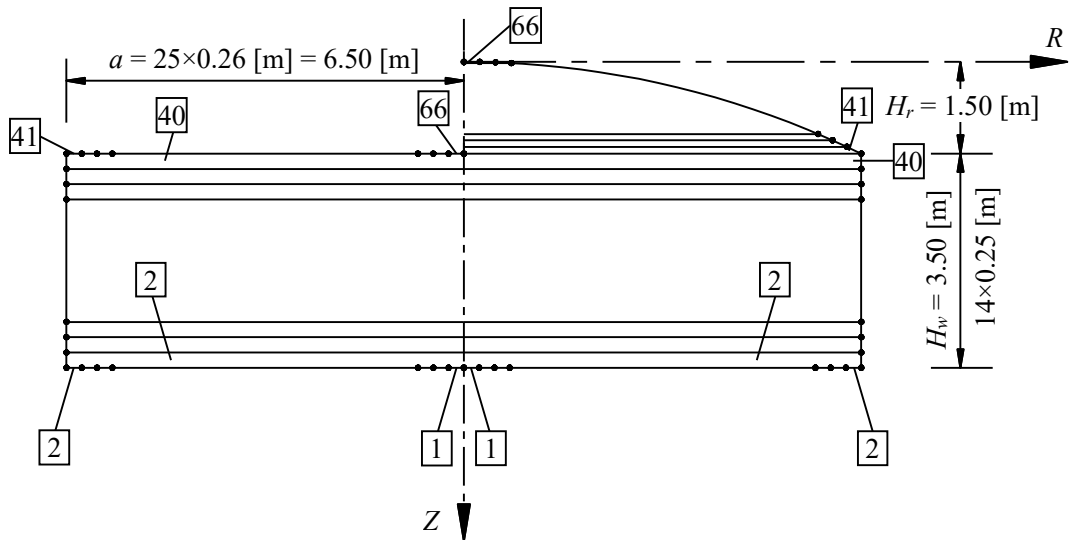


Figure 5.29 Finite element mesh of the two covered tanks

5.6.1 Contact pressure q

Figure 5.30 shows the contact pressure distribution below the base in the three cases. The contact pressure distribution below the three tanks are nearly identical.

5.6.2 Base settlement s_{base}

Figure 5.31 shows the base settlement in the three cases. The settlements of the tanks covered with flat and spherical roofs are bigger than the settlements of opened tanks with maximum difference of 6% and 4%, respectively. These differences are due to the weight of the tanks, where the tank with flat roof is the biggest in weight then the tank with spherical roof and finally the opened tank.

5.6.3 Moment across the base M_{base}

Figure 5.32 shows the moment along the base radius in the three cases. The moment curves in the three cases are identical.

5.6.4 Radial force across the base N_{base}

Figure 5.33 shows the radial force in the base of the three tanks. The radial force curves are also identical in the three cases.

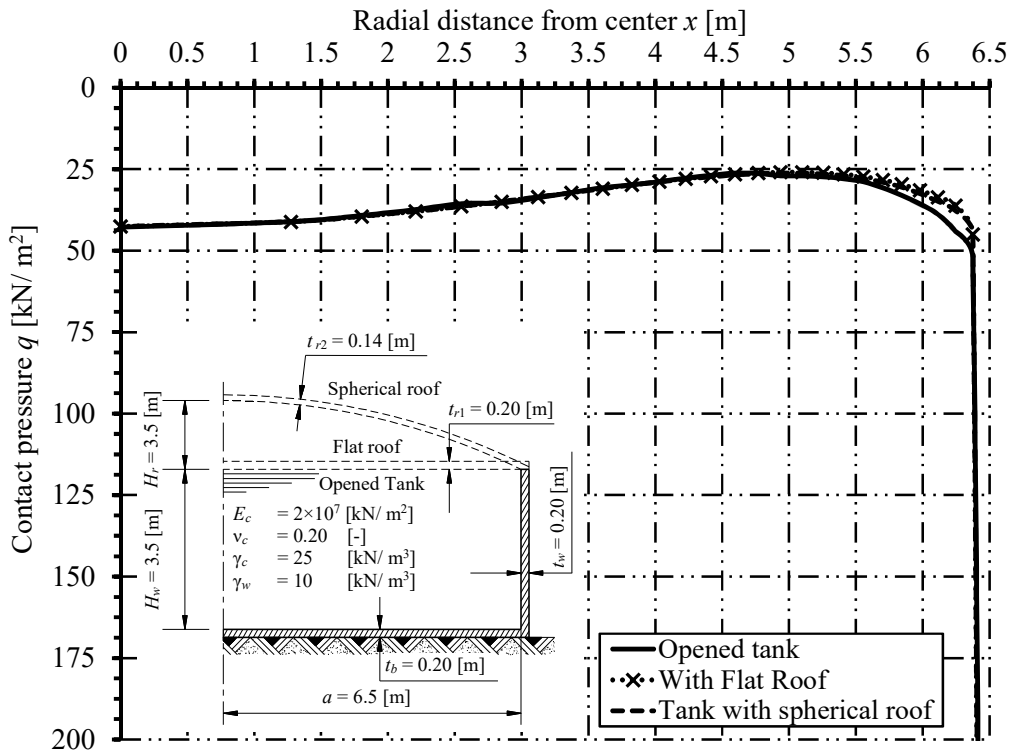


Figure 5.30 Contact pressure q distribution under the tank base

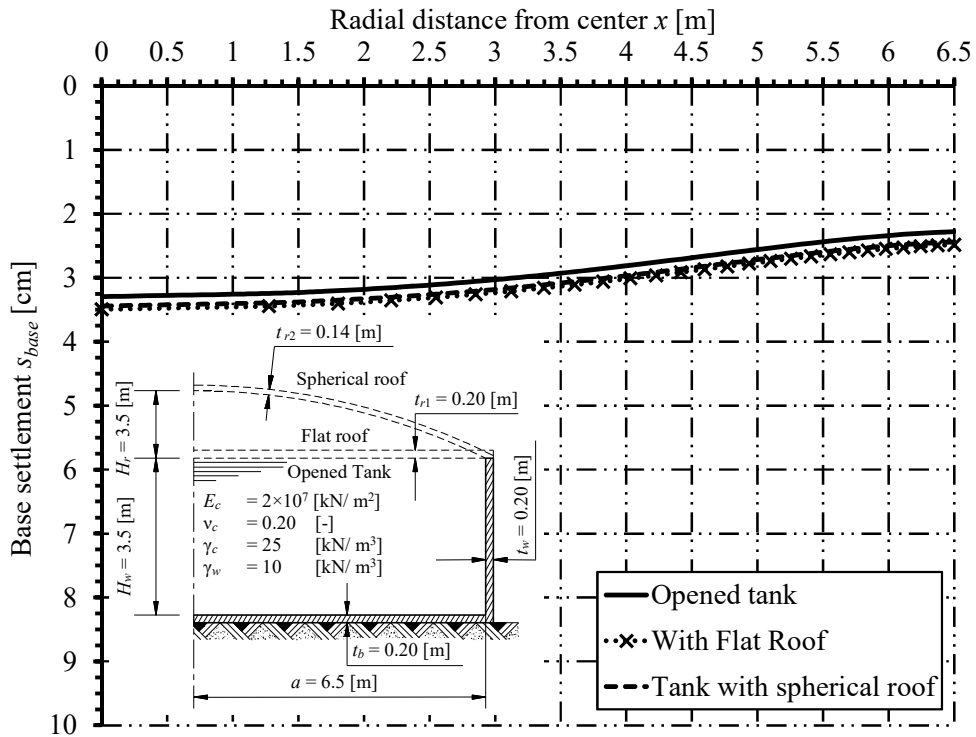


Figure 5.31 Settlement of the base s_{base}

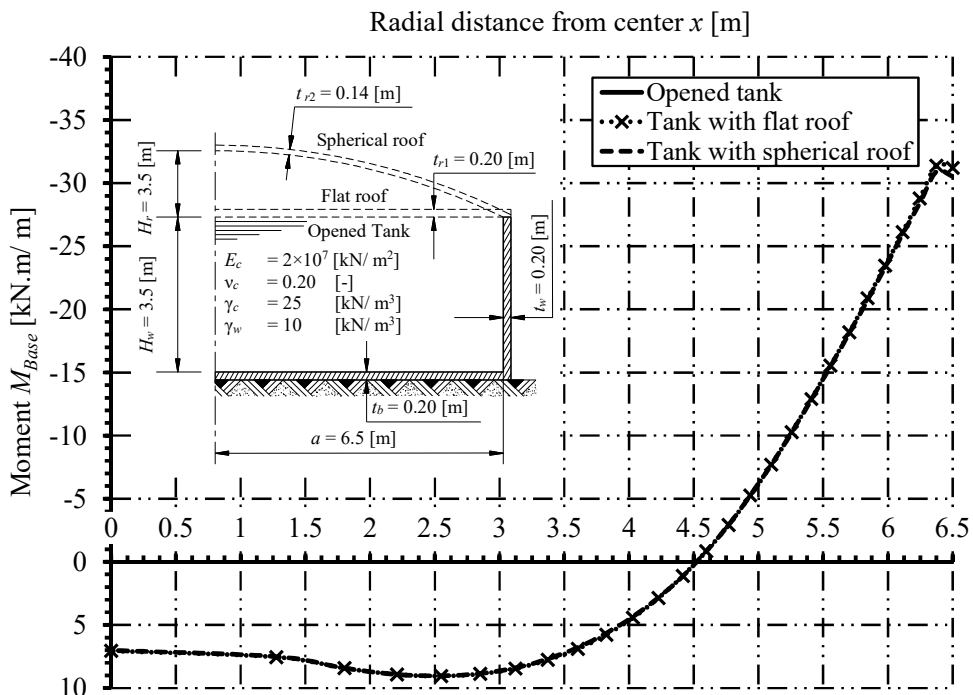


Figure 5.32 Moment across the base M_{base}

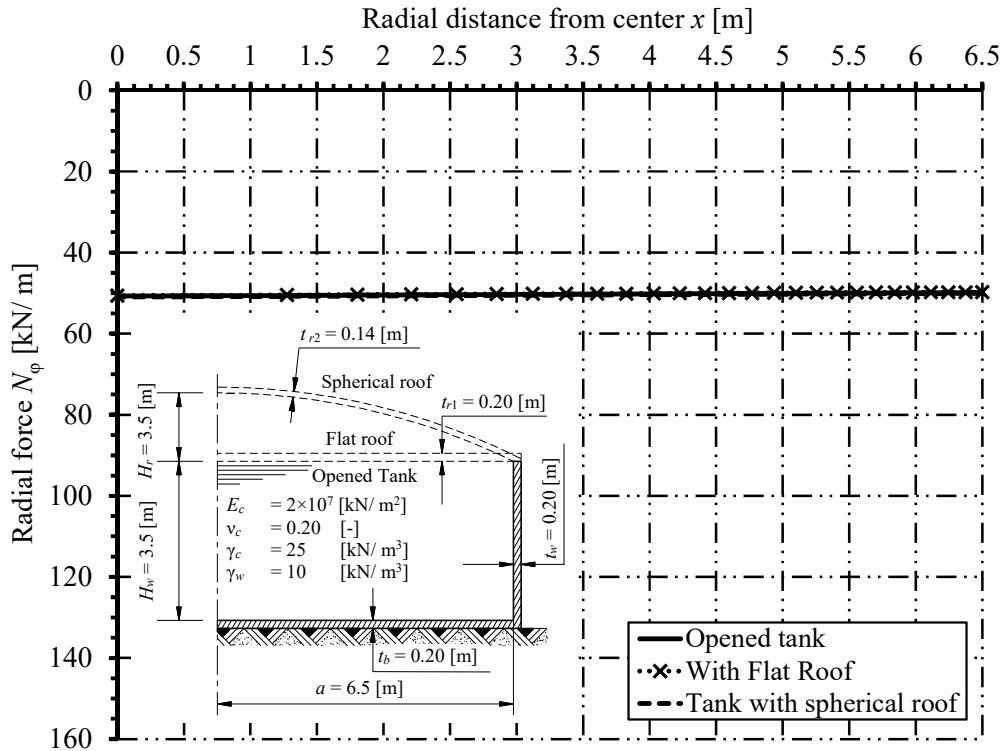


Figure 5.33 Radial force across the base N_{base}

5.6.5 Meridional moment in the wall M_s

Figure 5.34 shows the meridional moment along the wall in the three cases. The moment distribution along the wall is identical in the three cases till 57% of the height from the base. At the upper edge, the moment in the case of the spherical roof is smaller than the moment in the case of flat roof with a difference of 65%. This high drop in moment is due to the arch effect, where the effective internal forces are the normal forces, while the moment is very small.

5.6.6 Tangential force in the wall N_θ

Figure 5.35 shows the tangential force along the wall. In the compression zone, the tangential forces in the three cases are identical. In the tension zone, the tangential force in the tank covered with flat roof is the biggest, then in the tank covered with spherical roof and finally in the open tank.

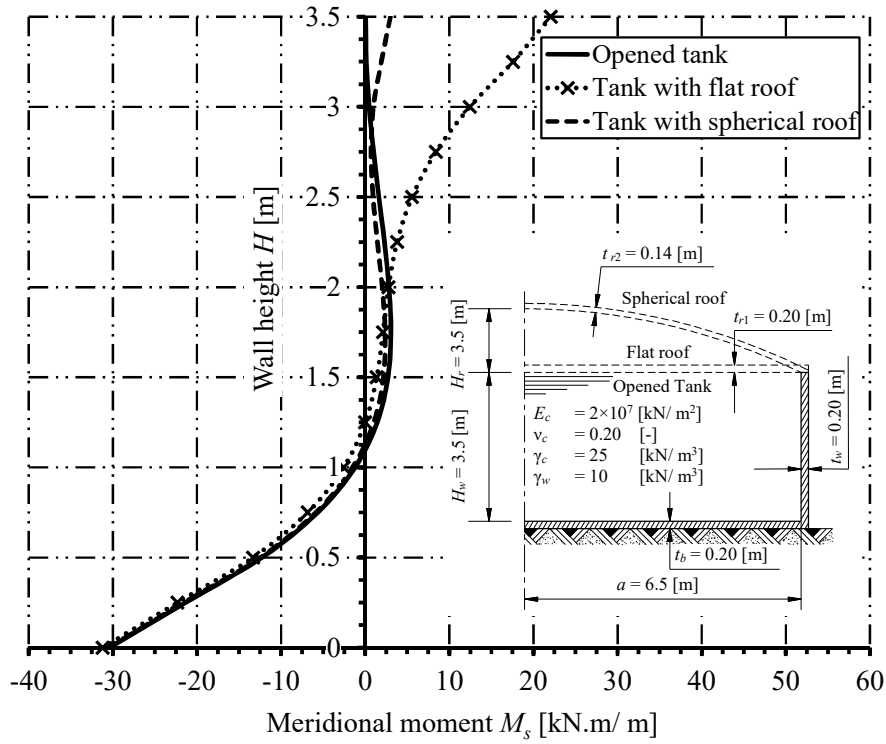


Figure 5.34 Meridional moment M_s along the wall height

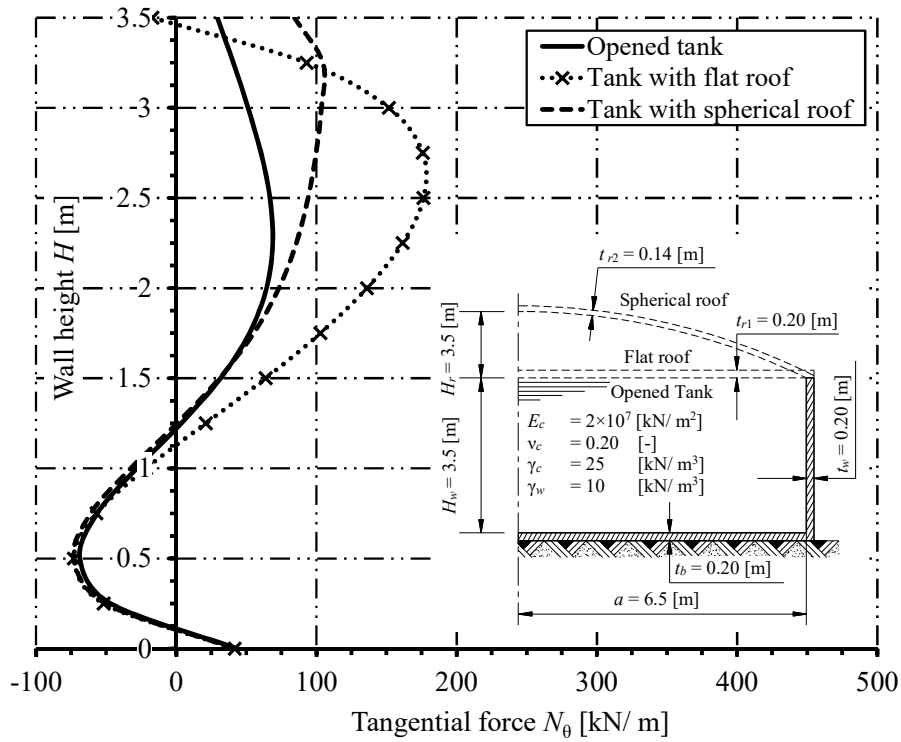


Figure 5.35 Tangential force N_θ along the wall height

5.6.7 Moment across the roof M_{Roof}

Figure 5.36 shows the roof moment distribution M_{Roof} for the two roof types either flat or spherical. For the flat roof, the moment values are smaller than the moment values of the base with difference of 29% at the edge and 50% at the center of the tank radius.

For the spherical roof, the moment is too small due to the arch effect. This moment distribution has the biggest value at the edge due to the connectivity between the wall and the roof. This value is smaller than the value of the base at the edge with difference 90%.

5.6.8 Membrane forces across the roof N_θ, N_ϕ

Figure 5.37 shows the membrane forces in the roof for the two roof types. For the flat roof, the membrane forces either the tangential forces N_θ or the radial forces N_ϕ are compression. The radial forces are bigger than the tangential forces with 51% at the edge, and then the difference is getting smaller until zero difference at 15% of the radius from the center. After that the radial forces are getting smaller than the tangential forces with difference of 72% at the center of the roof.

For the spherical roof, the tangential force is compression at 75% of the radius from the center. For the rest distance (25%) the tangential force is tension due to the connectivity between the wall and the roof. The maximum tension locates at the edge, while the maximum compression occurs at the center and is smaller with 19% from the maximum tension force. The maximum compression in the case of flat roof is bigger than the maximum compression in the spherical roof by 38%. The radial force in the spherical roof is compression along all the radius, with maximum value at distance 57% of the radius from the center.

5.6.9 Roof vertical displacement \bar{u}

Figure 5.38 shows the vertical displacement of the roof for the two covered types. For the flat roof, the displacement curve has the same shape as the settlement curve of the base. The maximum value occurs at the center, while the minimum value occurs at the edge with difference less than 35%.

For the spherical roof, the vertical displacement is almost linear along the radius and equal to the settlement at the edge of the tank base.

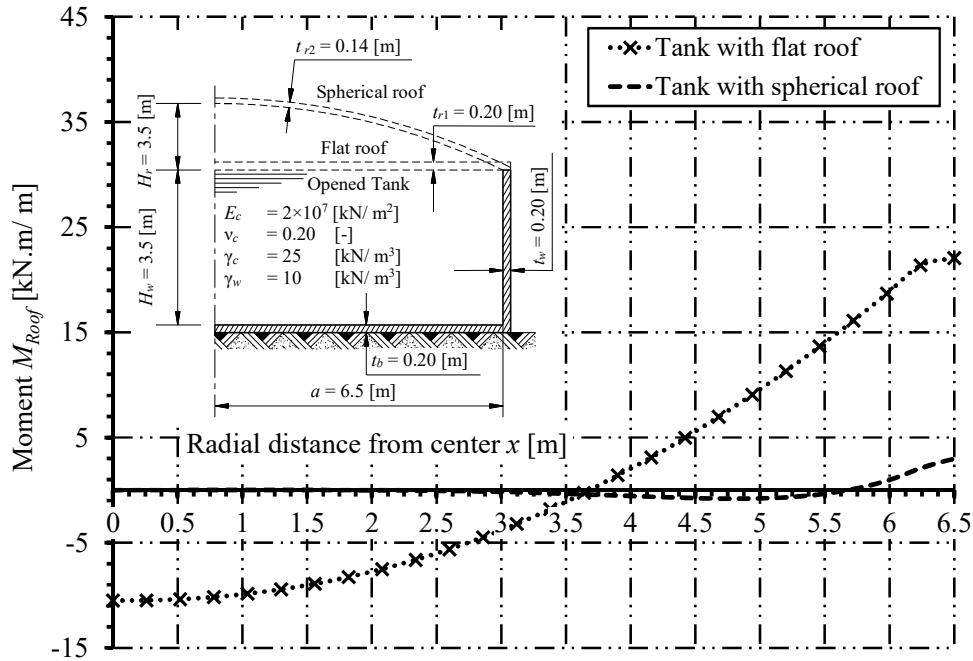


Figure 5.36 Moment across the roof M_{Roof}

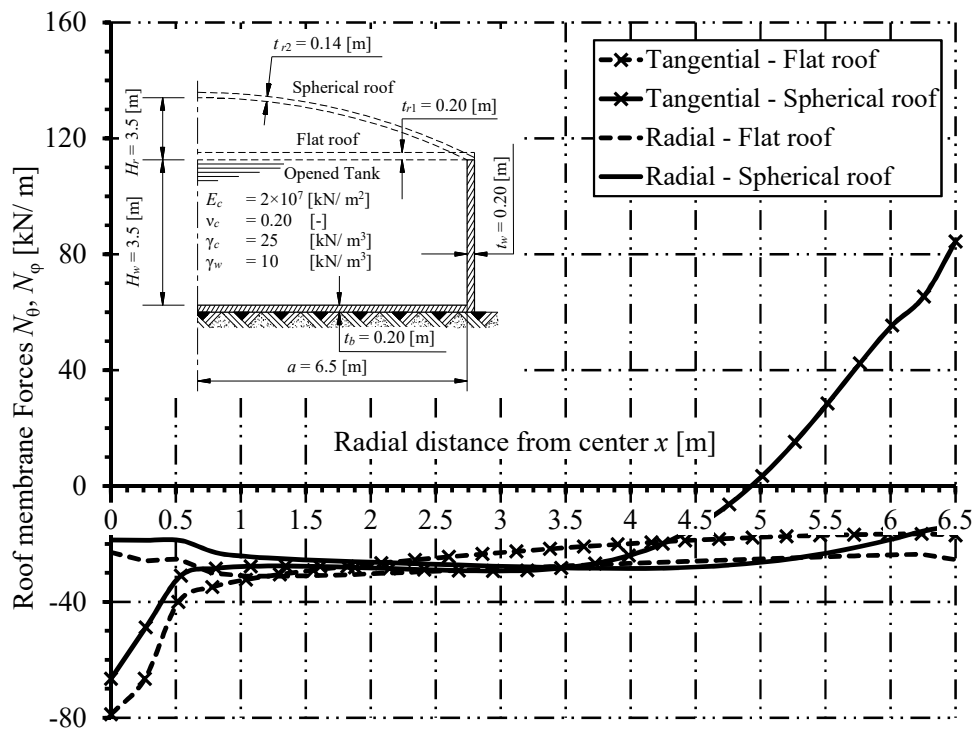


Figure 5.37 Membrane forces across the roof N_θ, N_ϕ

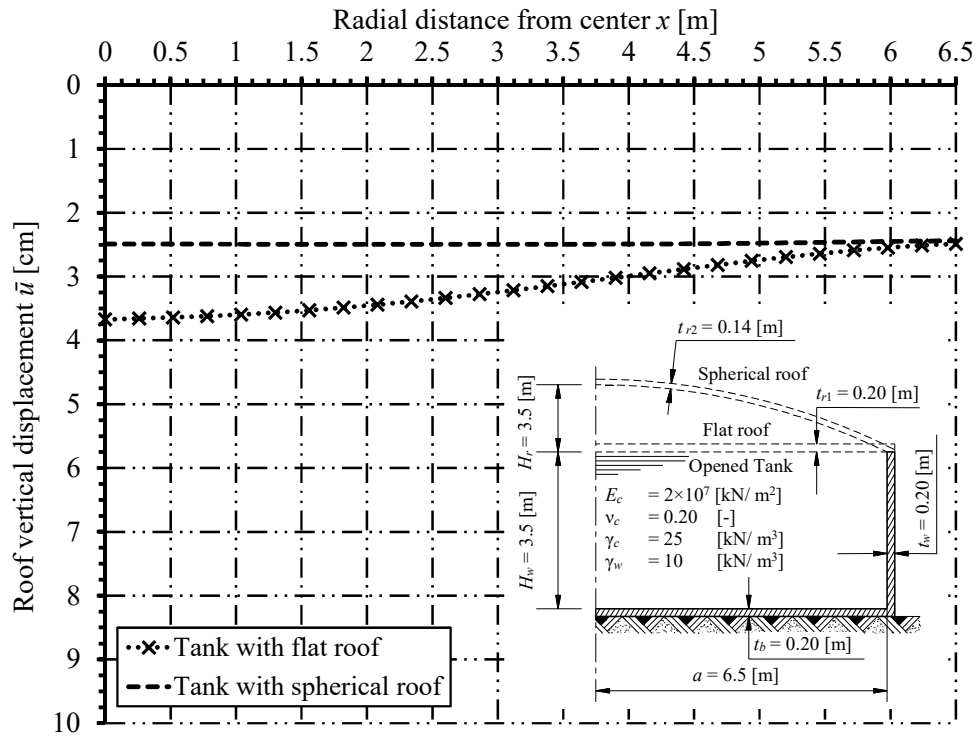


Figure 5.38 Vertical displacement of the roof \bar{u}

Chapter 6

6 Numerical analysis and discussions of cyclic loading

6.1 Introduction

This chapter presents a study on circular ground tanks under time dependent- and cyclic loading, where the analysis is considered as a time dependent problem. Two cases of loading are studied separately, namely: self-weight of the tank (DL), and the water pressure acting on the wall and base of the tank (LL). The nonlinear structural behavior of the tank is studied under the gradual application of the DL to simulate the construction phase, while the effect of LL is taken as a cyclic load problem. In the present analysis, the behavior of the soil during the consolidation process is considered either a linear, a bilinear or nonlinear behavior. Time dependent parameters of the tank model such as the duration of construction phase, periods of filling and emptying the tank, and the type of cyclic loading are studied, in addition to the structural parameters of the tank. The results of consolidation settlement, the degree of consolidation, and the excess pore water pressure with time are presented for different cases.

6.2 Tanks under time-dependent loading

In this section, the behavior of circular ground tanks during the construction phase is considered. Every study case is analyzed three times assuming different soil parameters. The assumed soil properties are taken corresponding to the actual properties and typical soil profiles covering three different zones at Port-Said (refer to chapter 5 for details). Two cases of loading are studied separately, namely: self-weight of the tank (DL), and the water pressure on the wall and base of the tank (LL). In the first case, the effect of the gradual application of self-weight of the tank on the settlement and the degree of consolidation is studied.

Consider the standard ground tank studied earlier in the previous chapters. Refer to Figure 6.1 and assume that the construction duration reaches 70 day, and that the loading is applied linearly starting from zero until it reaches the full dead load q_c at the finishing time t_c .

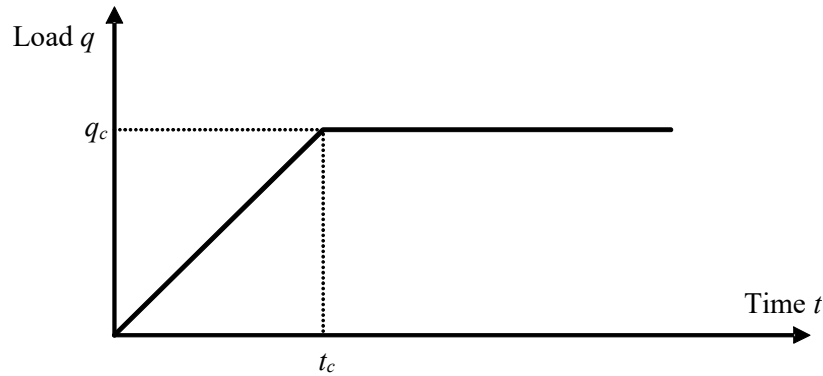


Figure 6.1 Loading scheme of the own weight

6.2.1 Change of the degree of consolidation due to self-weight of the tank

Figure 6.2, Figure 6.3, and Figure 6.4 show the variation of the degree of consolidation with time due to the gradual application of the self-weight of the tank for zones-1, 2, and 3, respectively. As shown in Figure 6.1, the load increases linearly starting from zero (at the start of construction), till it reaches its maximum value q_c at time t_c (at the end of tank construction), beyond which it remains constant. Figure 6.2 shows the relation between the degree of consolidation and time for linear analysis (clay layer properties are constant throughout the whole analysis). The results shown in Figure 6.2 are not affected by the variation of the tank self-weight. This can simply be understood with reference to equations (3.58) and (3.59) given earlier in chapter 3; that define the degree of consolidation U as the ratio between the current stress (or settlement) to its counterpart at the final state. From Figure 6.2, it can be seen that the fastest consolidation rate is observed in Zone-2 (Port Said south), while the slowest is encountered at Zone-3 (Port Said east).

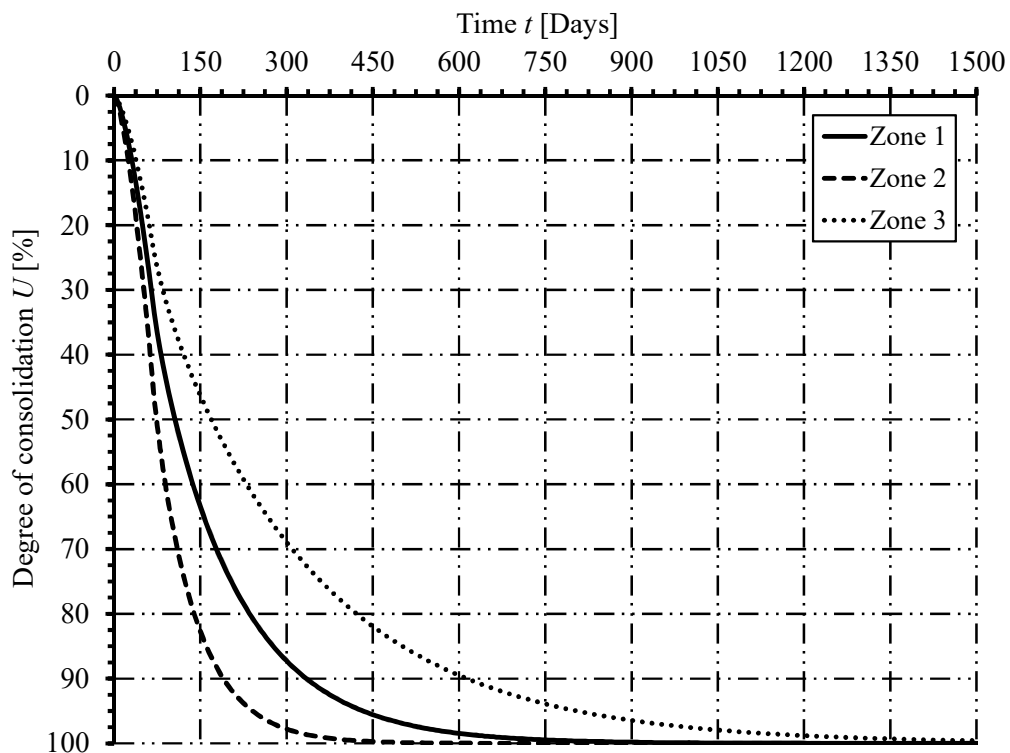
The relations between the degree of consolidation and time for nonlinear analyses U_p and U_s are shown in Figure 6.3 and Figure 6.4, respectively. At earlier time stages, the consolidation process is faster at Zone-2, if compared to the situation in the two other zones. The slowest consolidation rate is recorded at Zone-1. This is attributed to the considerable differences of the clay layer height as well as its properties for the different zones. Table 6.1 shows the time period required to reach the steady-state condition (SSC) in linear and nonlinear analyses and for the three different zones.

Table 6.1 The time period [days] required to reach *SSC*

Zone	Linear Analysis	Nonlinear analysis
1	2055	2700
2	1075	1205
3	3955	3010

6.2.2 Influence of self-weight of the tank on the settlement

Figure 6.5 shows the time variation of the clay layer settlement s_{co} , obtained by linear analysis, due to the gradual application of the self-weight of the tank according to the loading scheme shown in Figure 6.1; for zones-1, 2, and 3, respectively. In this case, the settlement s_{co} is calculated due to unit stress applied at the ground surface [1.0 kN/m^2]. Then, the settlement curves for zones-1, 2 and 3 are obtained by multiplying the unit load results by the load parameter q_c . If compared to the other two zones, the height of clay layer in Zone-1 is bigger, and the clay layer itself is closer to the ground surface. These are the reasons that the maximum settlement is encountered at Zone-1.

Figure 6.2 Degree of consolidation of linear analysis U with time

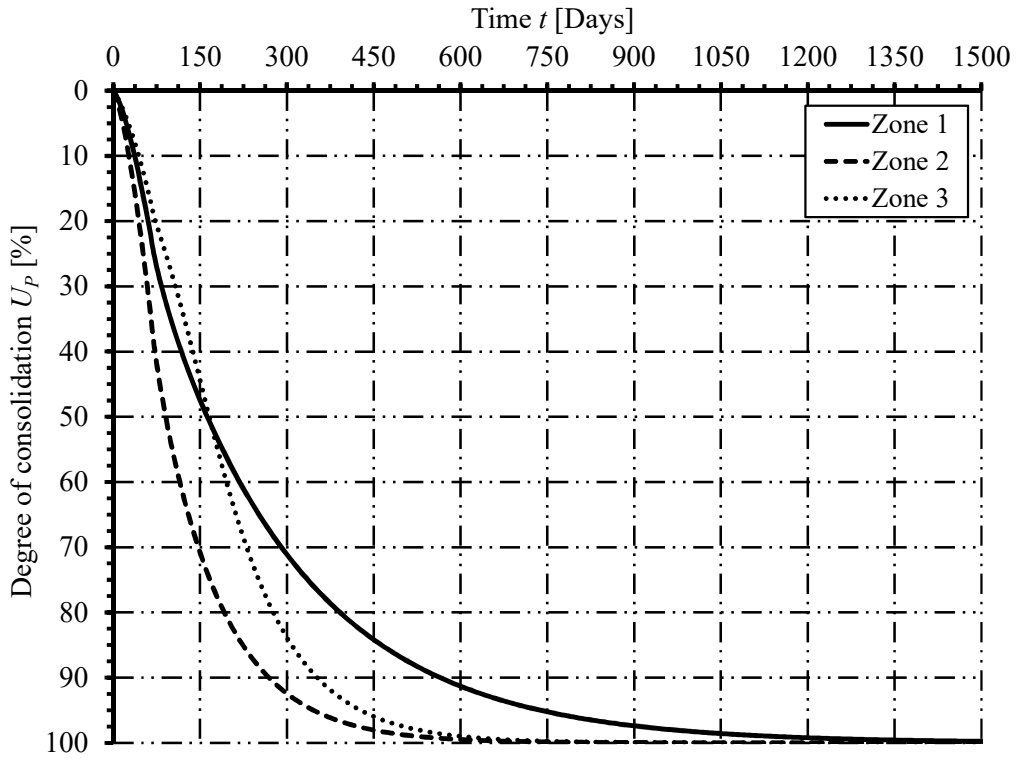


Figure 6.3 Degree of consolidation of nonlinear analysis U_p with time

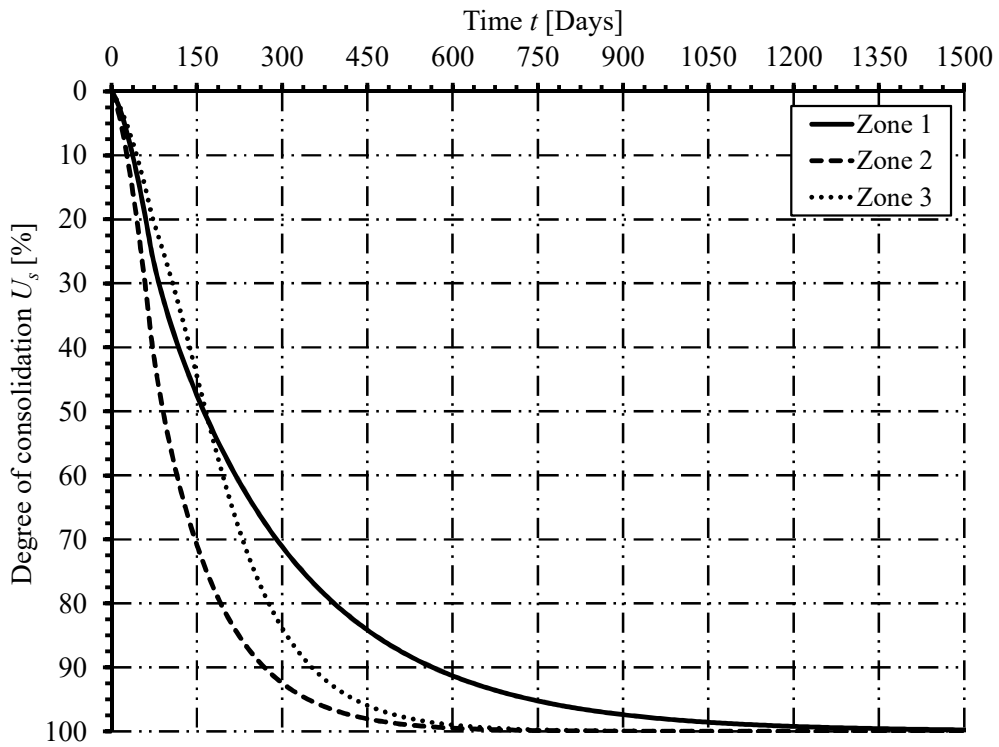


Figure 6.4 Degree of consolidation of nonlinear analysis U_s with time

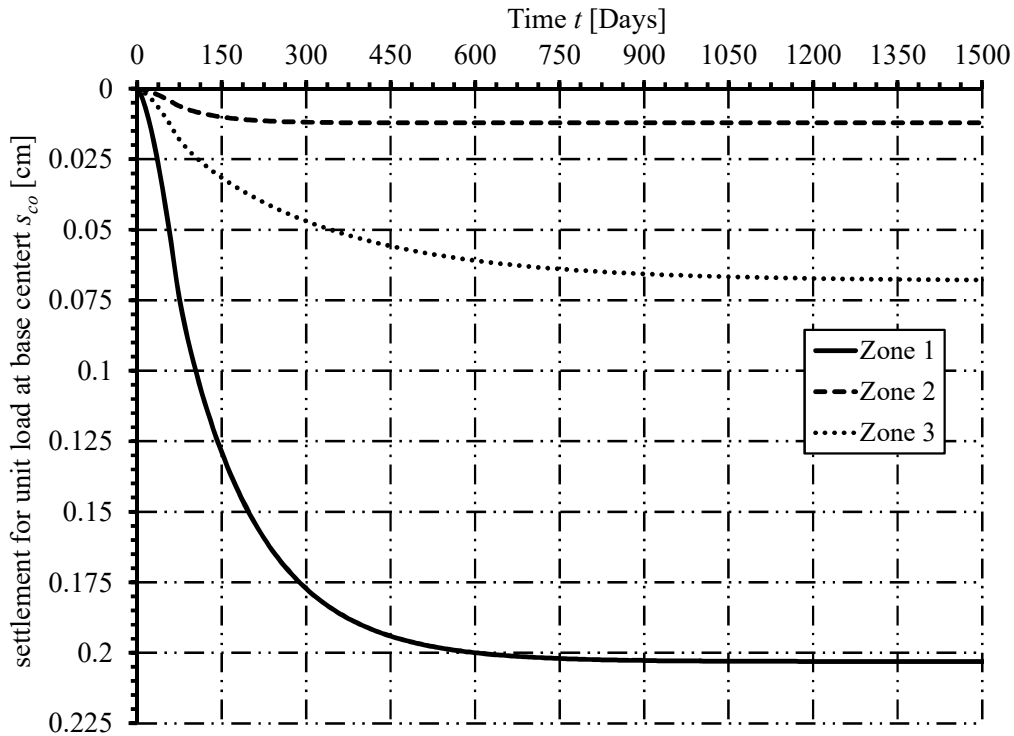


Figure 6.5 Time variation of linear settlement of the clay layer at the base center s_{co} due to unit load.

6.3 Tanks under cyclic loading

In this section, a parametric study is carried out to study the behavior of circular tanks subjected to cyclic loading. The interaction between the wall, base and the soil is taken into consideration. The assumed soil properties are taken corresponding to the actual properties and typical soil profiles covering three different zones at Port-Said (refer to chapter 5 for details). Load cycling is considered hereafter for the water pressure on the tank base and wall (LL) only, assuming that the final settlement resulting from the self-weight of the tank occurs during the construction phase (for simplicity).

The study of tanks under cyclic loading in this chapter is divided into 3 parts:

- 1- At first, a proposed model for circular tanks; for which the base is either fully-flexible or fully-rigid, is considered to explore the differences between the results of bilinear and nonlinear consolidation analyses for both hypotheses.
- 2- Secondly, a parametric study is carried out to study the effects of time parameters of the load on the degree of consolidation and settlement; for circular tanks with flexible and rigid bases.

- 3- Finally, a parametric study is carried out on a circular tank with elastic base taking soil-structure interaction into consideration. The internal forces are presented for the base and the wall for different Load-Time schemes.

6.3.1 Effect of filling and emptying tank with water

In the analysis, the hydrostatic pressure is considered as cyclic loads with load parameters as shown in Figure 6.6. There are three variables, i.e. t_o , α_o and β_o , that govern the consolidation process in one cycle as shown in Figure 6.6. t_o represents the time length of the load; α_o and β_o reflect the geometry properties of the load. Therefore, the consolidation behavior of the soil can be investigated by giving one of the variables different values while fixing the values of the other variables, as shown by the following discussions.

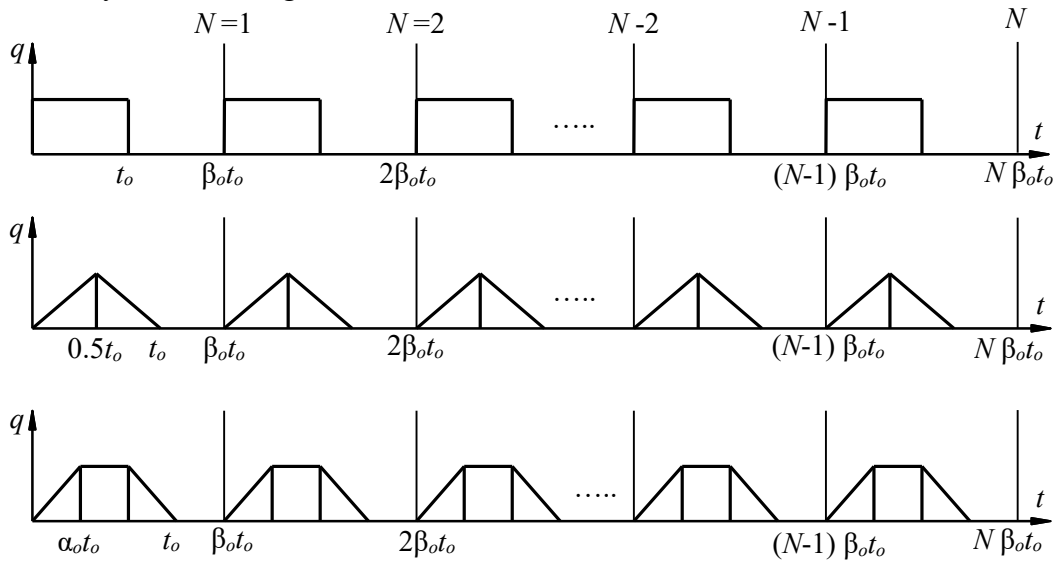


Figure 6.6 The main types of cyclic loading with variables t_o , α_o and β_o

Consider that the tank shown in Figure 6.7 is subjected to a hydrostatic cyclic load. The tank is assumed to be constructed in any of the three zones-1, 2, and 3, which was presented earlier in the previous chapters. The hydrostatic load intensity is taken as $34.33 \text{ [kN/m}^2\text{]}$. This load is considered as circular uniform load acting on the soil profile under consideration. To represent the process of filling and emptying the tank, the trapezoidal cyclic load scheme shown in Figure 6.6. is chosen; with the load parameters t_o , α_o and β_o as given in Table 6.2.

The data of the clay layers in zones-1, 2 and 3 required for cyclic loading analysis are given in Table 6.3 for bilinear consolidation, and in Table 6.4, Table 6.5 and Table 6.6 for nonlinear consolidation, for the three zones respectively.

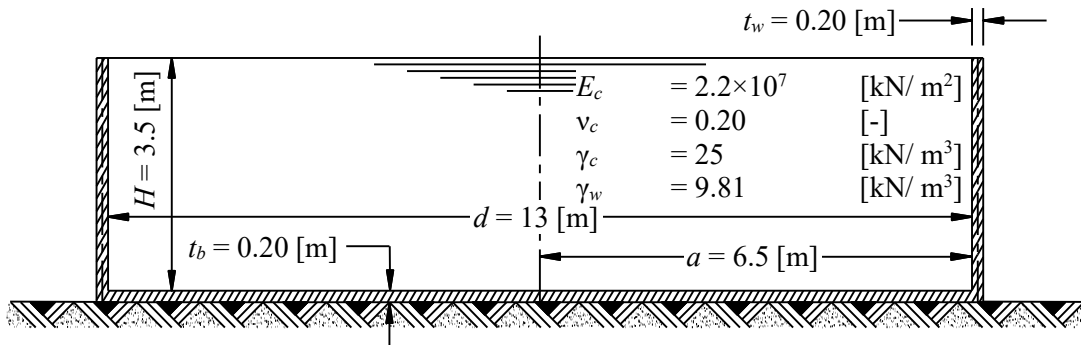


Figure 6.7 Geometry of the tank subjected to cyclic loading

Table 6.2 Cyclic loading properties

Loading and unloading parameter	α_o	=	0.008	[-]
Cycle parameter	β_o	=	1.328	[-]
Time length of the applied load	t_o	=	30.5	[Days]
Time length of loading and unloading	$\alpha_o t_o$	=	0.25	[Day]
Full cycle period	$\beta_o t_o$	=	40.5	[Days]
Load intensity	q	=	34.335	[kN/ m ²]

Table 6.3 Properties of clay layers for bilinear analysis under cyclic loading

Parameter	Zone-1	Zone-2	Zone-3
Layer thickness H [m]	5	3	2.1
Coeff. of volume change for loading m_v [m ² / kN]	0.00691	0.000914	0.000773
Coeff. of consolidation for loading C_v [m ² / year]	1.5	0.75	0.59
Coeff. of volume change parameter α [-]	0.23	0.164	0.071
Coeff. of consolidation parameter β [-]	0.23	0.164	0.071
Coeff. of volume change for reloading m_r [m ² / kN]	0.00159	0.00015	5.49×10^{-5}
Coeff. of consolidation for reloading C_{vr} [m ² / year]	6.5	4.57	8.26
Initial soil state [NC/ OC]	OC	OC	NC

Table 6.4 Properties of clay layer for nonlinear analysis under cyclic loading at Zone-1

Sub layer number i [-]	Sub layer thickness h [m]	Over-consolidation ratio OCR [-]	Coeff. of consolidation for loading C_v [m ² /year]	Coeff. of volume change parameter α [-]	Coeff. of consolidation parameter β [-]	Coeff. of consolidation for reloading C_{vr} [m ² /year]
1	1	1.685	1.5	0.23	0.345	4.351
2	1	1.654	1.5	0.23	0.340	4.415
3	1	1.541	1.5	0.23	0.322	4.660
4	1	1.419	1.5	0.23	0.302	4.966
5	1	1.274	1.5	0.23	0.278	5.394

Table 6.5 Properties of clay layer for nonlinear analysis under cyclic loading at Zone-2

Sub layer number i [-]	Sub layer thickness h [m]	Over-consolidation ratio OCR [-]	Coeff. of consolidation for loading C_v [m ² /year]	Coeff. of volume change parameter α [-]	Coeff. of consolidation parameter β [-]	Coeff. of consolidation for reloading C_{vr} [m ² /year]
1	0.6	1.776	0.75	0.164	0.265	2.83
2	0.6	1.712	0.75	0.164	0.257	2.91
3	0.6	1.653	0.75	0.164	0.250	3.00
4	0.6	1.597	0.75	0.164	0.243	3.09
5	0.6	1.546	0.75	0.164	0.236	3.18

Table 6.6 Properties of clay layer for nonlinear analysis under cyclic loading at Zone-3

Sub layer number i [-]	Sub layer thickness h [m]	Over-consolidation ratio OCR [-]	Coeff. of consolidation for loading C_v [m ² /year]	Coeff. of volume change parameter α [-]	Coeff. of consolidation parameter β [-]	Coeff. of consolidation for reloading C_{vr} [m ² /year]
1	0.7	0.999	0.59	0.071	0.071	8.26
2	0.7	0.945	0.59	0.071	0.068	8.71
3	0.7	0.896	0.59	0.071	0.065	9.15

6.3.2 Tanks with flexible or rigid base located at Zone-1 under cyclic loading

Assume that the tank under consideration is constructed in Zone-1 (Port Said west) with the load parameters as given in Table 6.2. The data of the main clay layer located in Zone-1, required for both bilinear and nonlinear cyclic load analyses are given in Table 6.3 and Table 6.2, respectively. As the clay layer in this zone is OC at load beginning, so the behavior of the clay is elastic. Figure 6.8 shows the variation of average degree of consolidation with time for both type of analyses. The clay layer reached *SSC* after a total of 59 and 95 cycles for bilinear and nonlinear consolidation; respectively. At the steady-state condition, the maximum value of the average degree of consolidation in bilinear consolidation is slightly bigger than its counterpart in nonlinear one. Figure 6.9 shows the settlement at the center of the flexible base for both bilinear and nonlinear consolidation of the clay layer. At the steady-state condition, the maximum settlement of the bilinear consolidation is 47% bigger than that of the nonlinear consolidation.

Figure 6.11 shows the distribution of the excess pore water pressure with time along the height of the clay layer. The Y-axis reads the depth from the top surface of clay as a ratio of the total height of clay layer. On the other hand, the X-axis gives the excess pore water pressure as a ratio of the weight of total capacity of the tank. The pressure distributions due to loading are shown with solid lines, while those resulting after the unloading phase are shown as dashed lines. The figure shows also the distribution of initial excess pore water pressure along the clay layer height. It is clear from Figure 6.11 that the excess pore water pressure vanishes at the top and bottom surfaces of the clay layer, due to the existence of permeable sandy layers therein. At the loading phases, the excess pore water pressure decreases with load cycling. It is also clear that the excess pore water pressure at the loading phase gets smaller with load cycling. At the steady-state condition, excess pore water pressure at the layer center reaches a constant value of 26% of its initial value. On the other hand, the pressure in the negative side for the unloading phase gets bigger with load cycling until it becomes constant at *SSC*. At the center of clay layer this ratio reaches a constant value of 74 % of its initial value before loading.

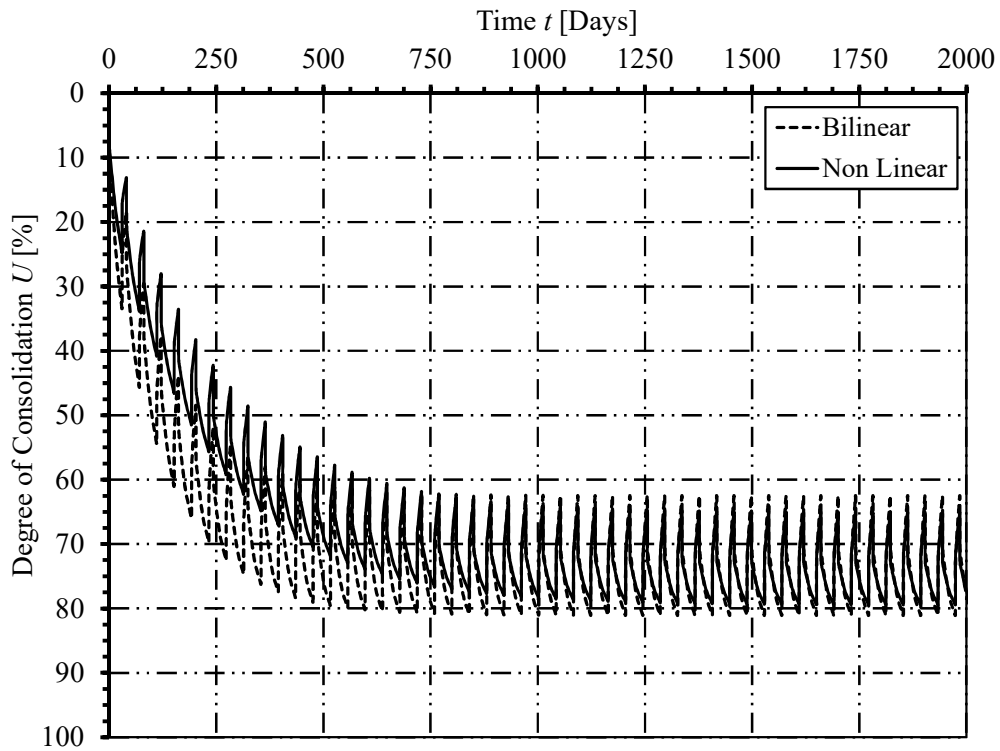


Figure 6.8 Degree of consolidation U in Zone-1

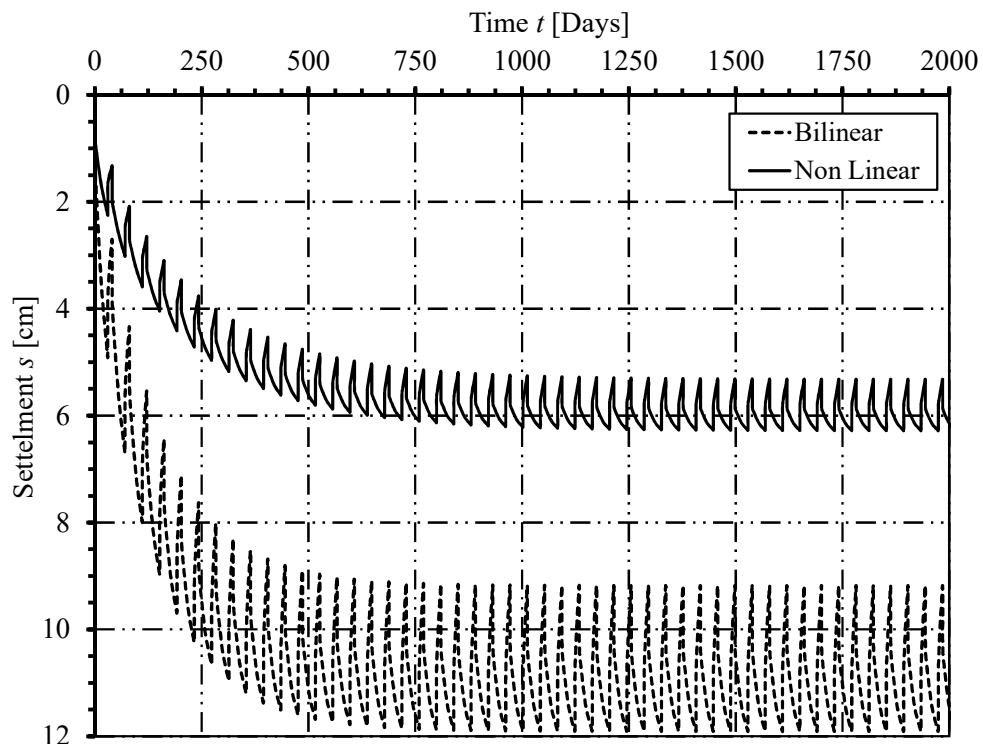


Figure 6.9 Settlement s at the center of the flexible base in Zone-1

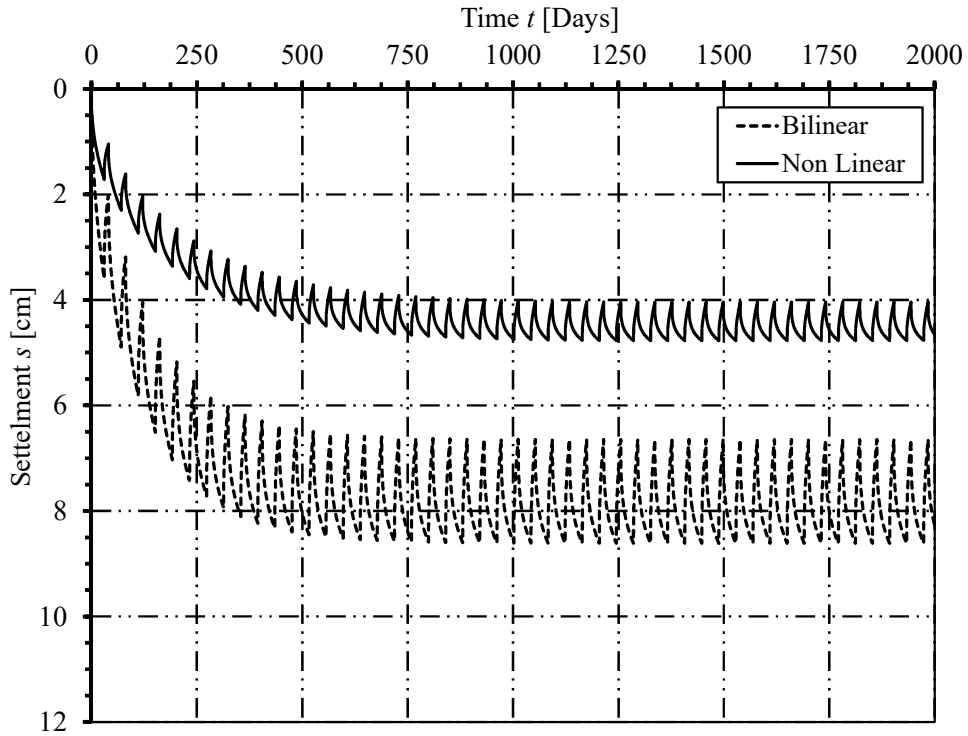


Figure 6.10 Settlement s at the characteristic point of the flexible base in Zone-1

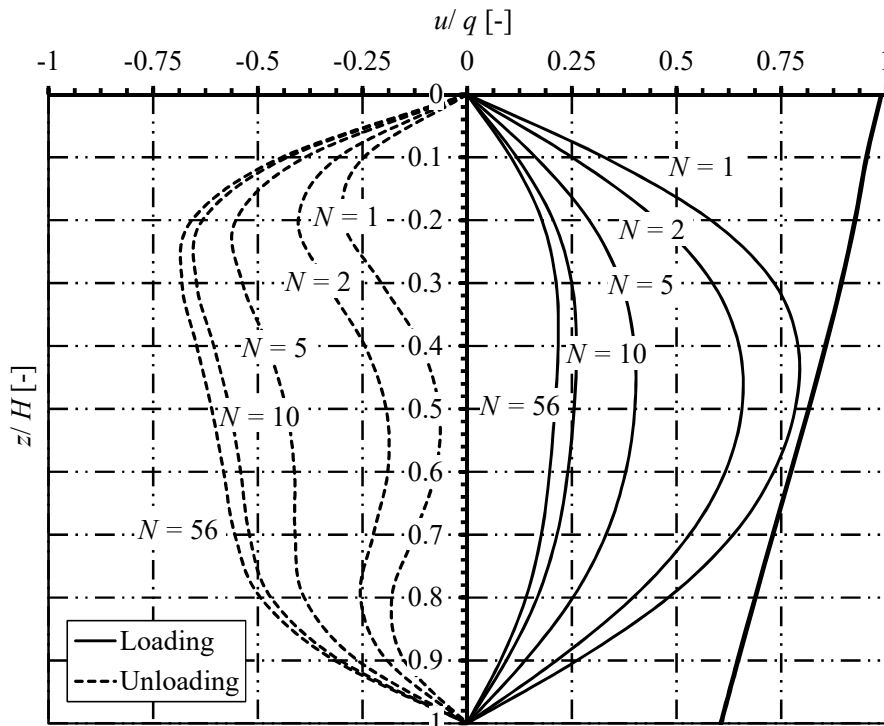


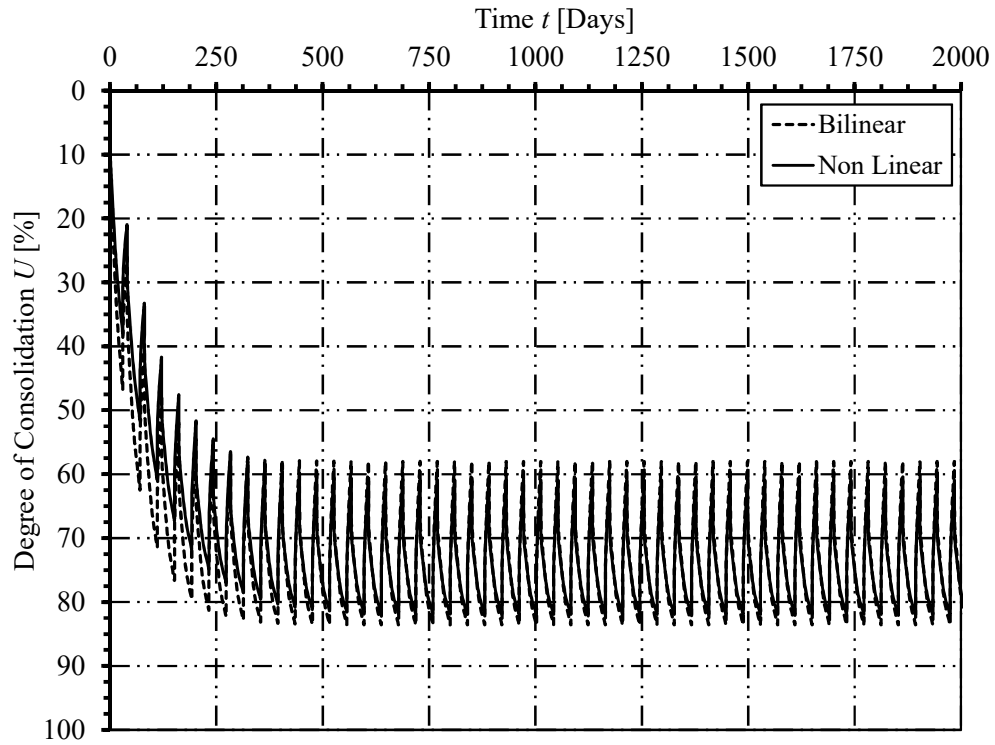
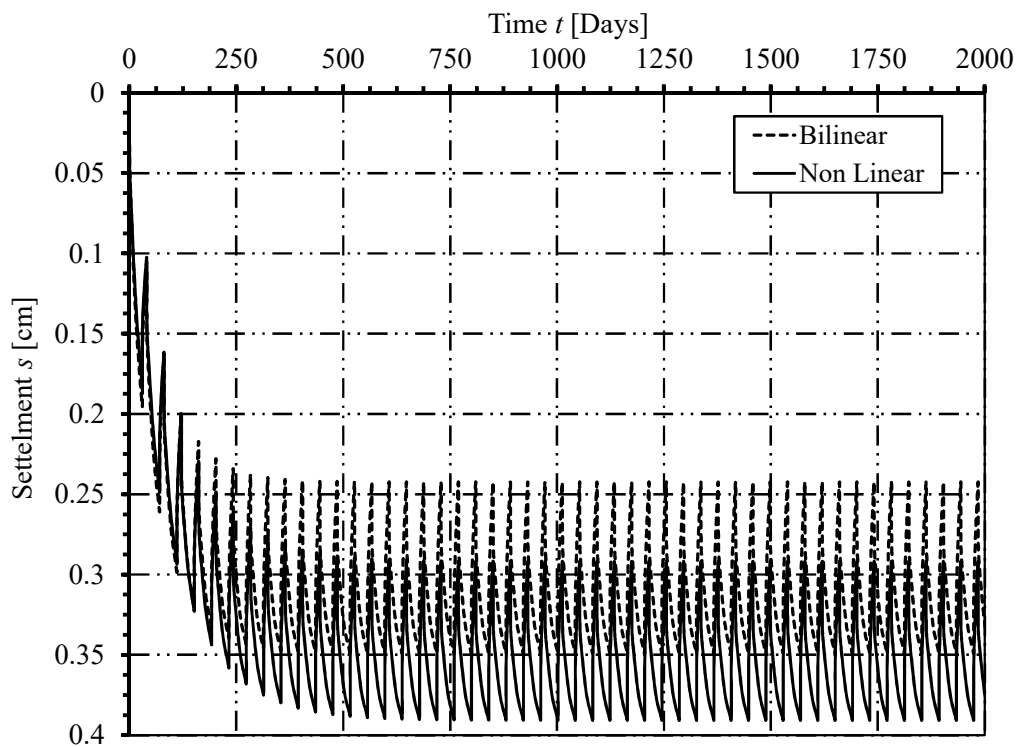
Figure 6.11 Isochrones for excess pore water pressure u with time in Zone-1

6.3.3 Tanks with flexible or rigid base located at Zone-2 under cyclic loading

For a tank constructed in Zone-2, the analysis data of the clay layer are given in Table 6.3 and Table 6.5. The clay layer in this zone is OC at the load beginning, therefore the behavior of the clay is also elastic. Figure 6.12 shows the variation of the bilinear and nonlinear average degree of consolidation with time. The clay layer needs 31 and 44 cycles with bilinear and nonlinear consolidation; respectively; to reach the steady-state condition. At the steady-state condition, the maximum value of the average degree of consolidation in bilinear consolidation is slightly bigger than its counterpart in nonlinear consolidation.

Figure 6.13 shows the time variations of settlement at the center of the flexible base for bilinear and nonlinear analyses due to the clay layer consolidation. At the steady-state condition, the maximum settlement for nonlinear consolidation is 12% bigger than that obtained by the bilinear consolidation. This difference rises to 15 % at the characteristic point, as shown in Figure 6.14.

Figure 6.15 shows the distribution of the excess pore water pressure with time along the height of the clay layer. The Y-axis reads the depth from the top surface of clay as a ratio of the total height of clay layer. On the other hand, the X-axis gives the excess pore water pressure as a ratio of the weight of total capacity of the tank. The distribution due to loading is shown with solid lines, while those resulting after the unloading phase are shown as dashed lines. The figure shows also the distribution of initial excess pore water pressure along the clay layer height. It is clear from Figure 6.15 that the excess pore water pressure vanishes at the top and bottom surfaces of the clay layer, due to the existence of permeable sandy layers therein. It is also clear that the excess pore water pressure at the loading phase gets smaller with load cycling. At the steady-state condition, excess pore water pressure at the layer center reaches a constant value of 25% of its initial value. On the other hand, the pressure in the negative side for the unloading phase gets bigger with load cycling until it becomes constant at SSC. At the center of clay layer this ratio reaches a constant value of 77 % of its initial value before loading.

Figure 6.12 Degree of consolidation U in Zone-2Figure 6.13 Settlement s at the center of the flexible base in Zone-2

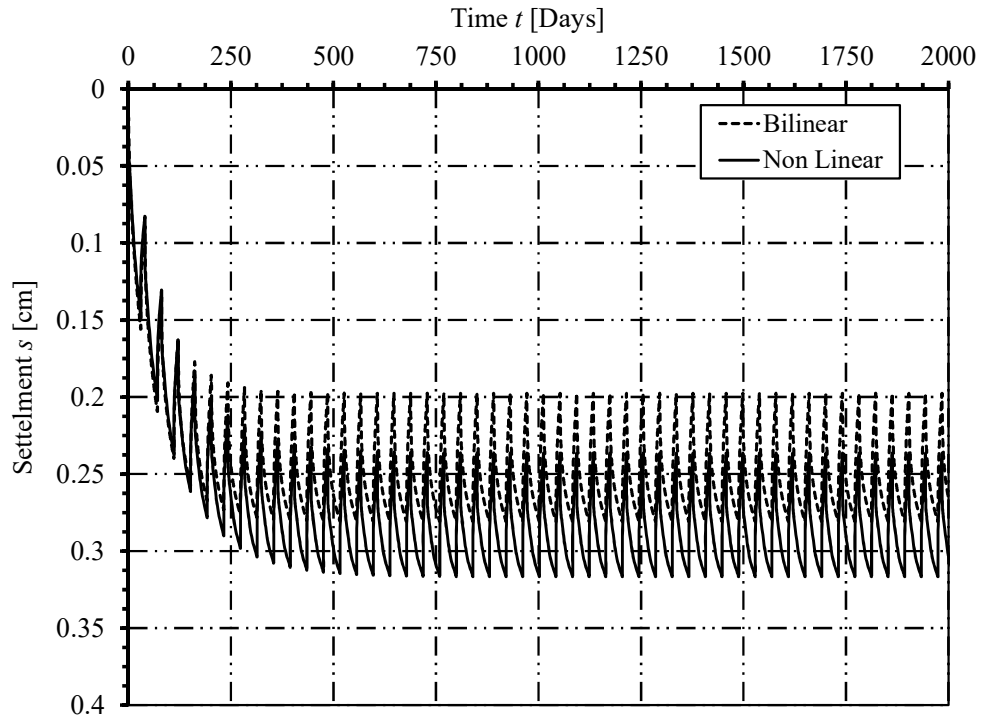


Figure 6.14 Settlement s at the characteristic point of the flexible base in Zone-2

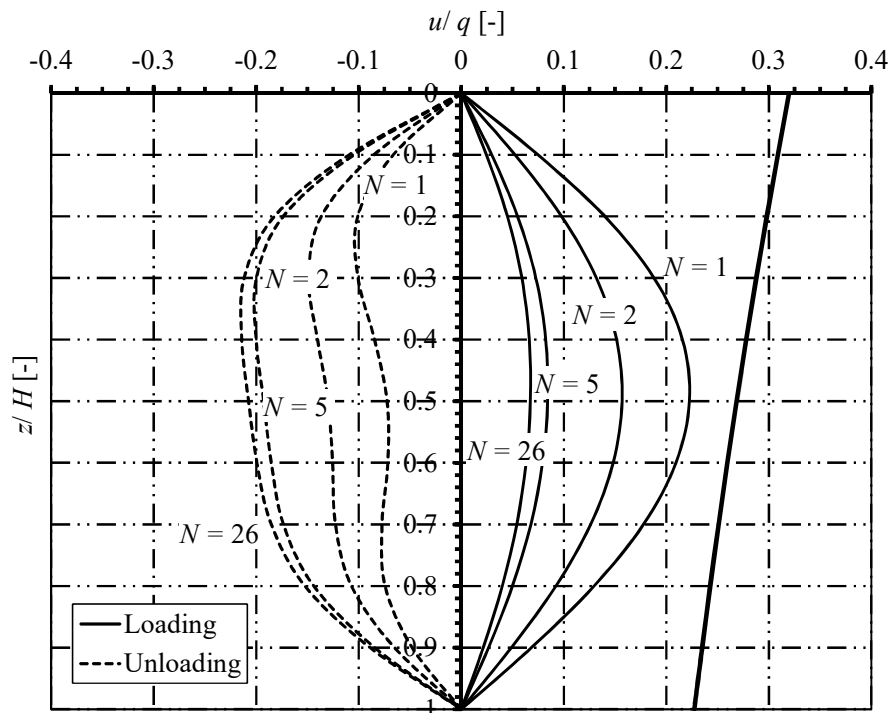


Figure 6.15 Isochrones for excess pore water pressure u with time in Zone-2

6.3.4 Tanks with flexible or rigid base located at Zone-3 under cyclic loading

For a tank constructed in Zone-3 (Port Sad east), the analysis data of the clay layer are given in Table 6.3 and Table 6.6. The clay layer in this zone is NC at the load beginning, therefore the behavior of the clay is plastic. Figure 6.16 shows the time variation of the average degree of consolidation for both bilinear and nonlinear analyses. From the figure, it is obvious that the behavior in both analyses is almost unchanged as the two curves are coinciding; as the OCR in nonlinear consolidation reaches 1.0 approximately. Figure 6.17 shows the time variations of settlement at the center of the flexible base for bilinear and nonlinear analyses due to the clay layer consolidation. At the steady-state condition, the maximum settlement for nonlinear consolidation is 7% bigger than that obtained by the bilinear consolidation. This difference rises to 9 % at the characteristic point, as shown in Figure 6.18.

Figure 6.19 shows the distribution of the excess pore water pressure with time along the height of the clay layer. At the loading phases, the excess pore water pressure gets smaller with load cycling. At the steady-state condition, excess pore water pressure at the layer center reaches a constant value of 13% of its initial value. On the other hand, the pressure in the negative side for the unloading phase gets bigger with load cycling until it becomes constant at *SSC*. At the center of clay layer this ratio reaches a constant value of 67 % of its initial value before loading.

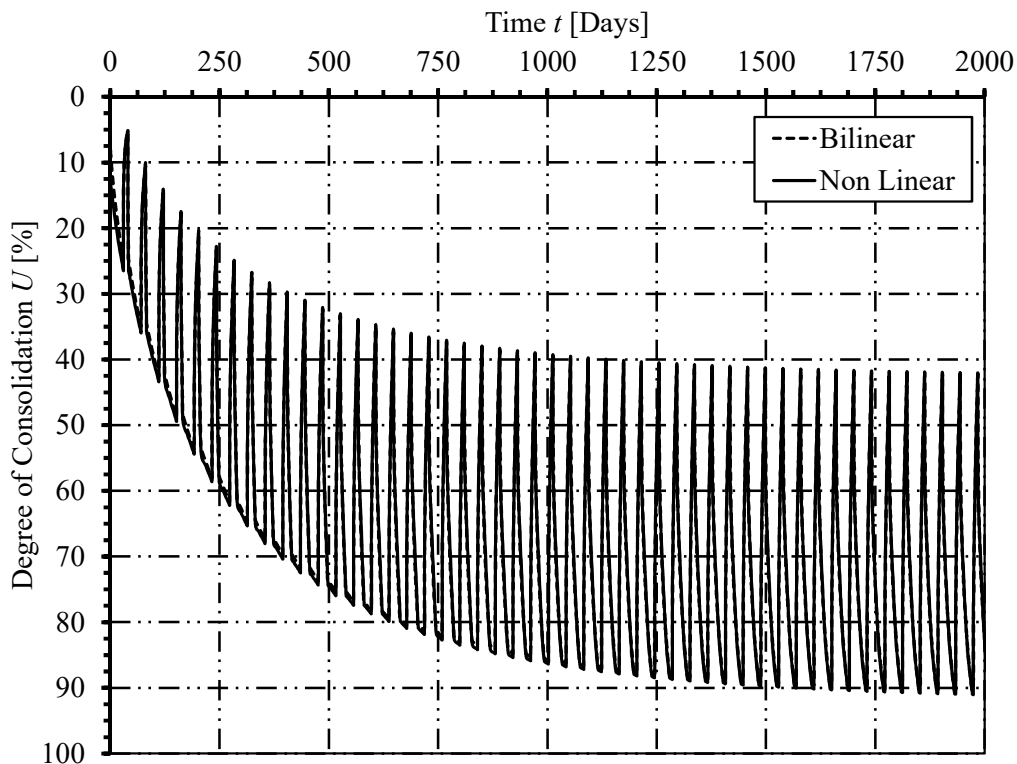


Figure 6.16 Degree of consolidation U in Zone-3

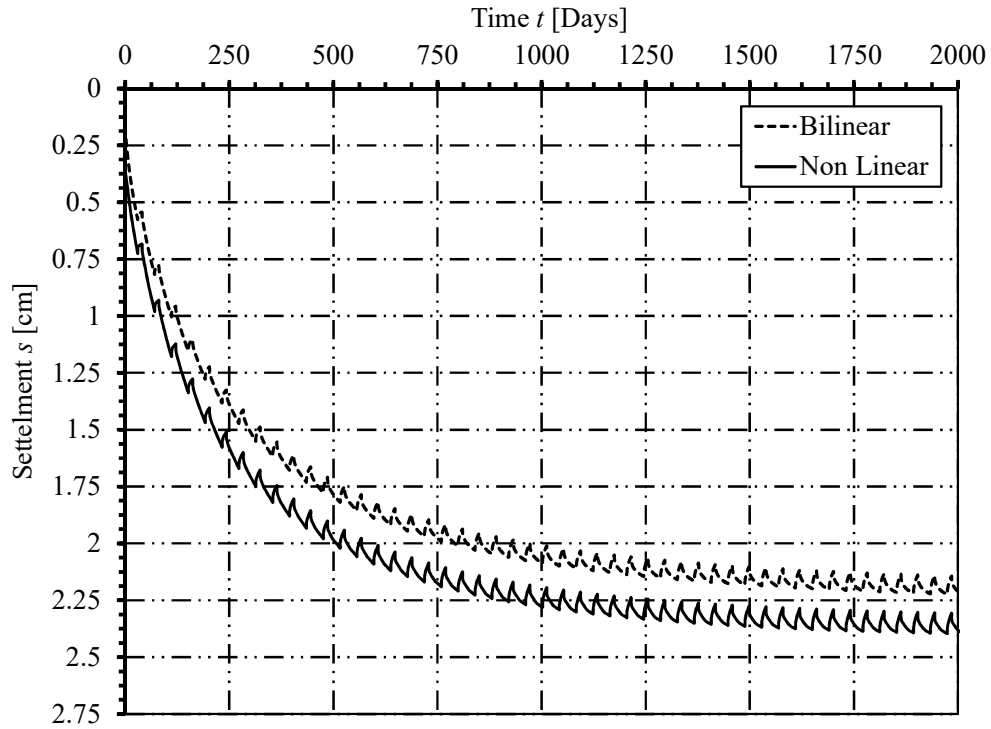


Figure 6.17 Settlement s at the center of the flexible base in Zone-3

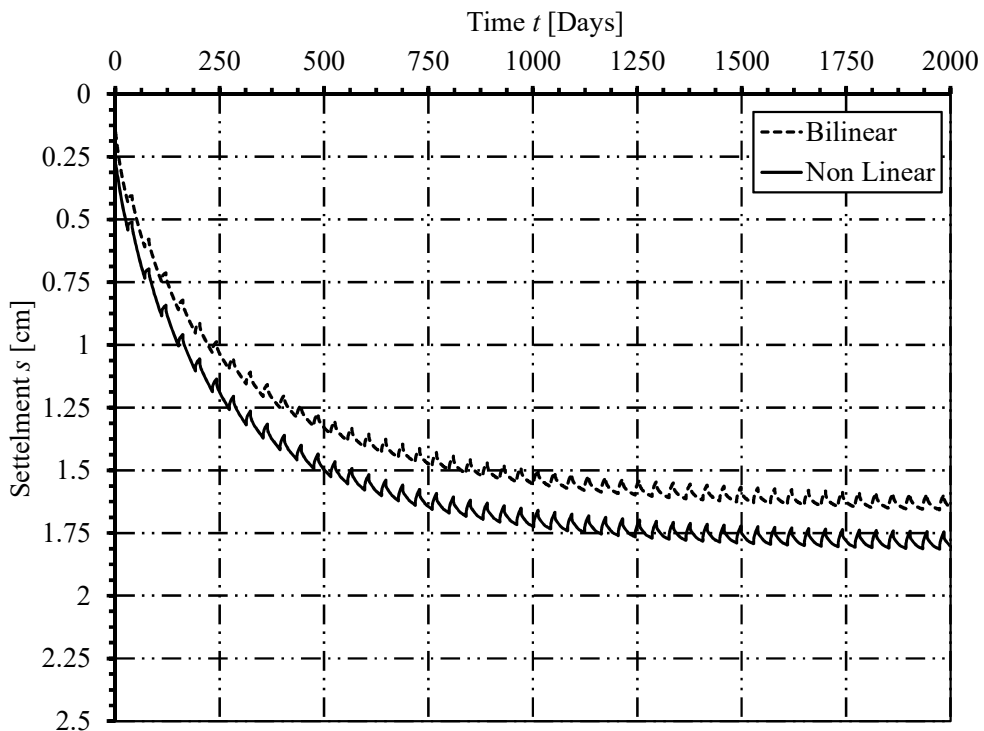


Figure 6.18 Settlement s at the characteristic point of the flexible base in Zone-3

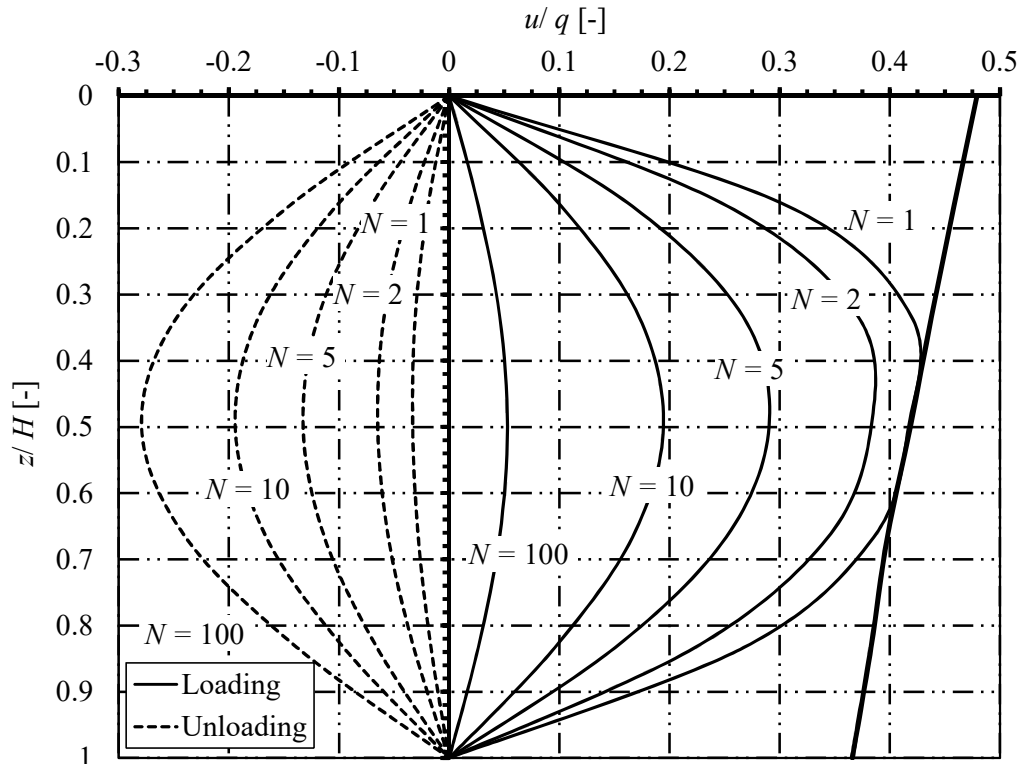


Figure 6.19 Isochrones for excess pore water pressure u with time in Zone-3

6.3.5 Comparison between the behaviors in the three zones

In this section, the results of the tank behavior resulting from the bilinear consolidation analysis are compared for the three zones under consideration. Figure 6.20 shows the time variation of the average degree of consolidation for the main clay layers in zones-1, 2 and 3. As explained before, the clay layers in zones-1 and 2 are OC, while that in Zone-3 is NC. As illustrated in Figure 6.20, the clay layer in Zone-3 starts NC and then changes between NC and OC with filling and emptying cycles till reaching SSC after more than 60 cycle (more than 2400 days). Any further load cycling would never affect either the tank or the clay layer behavior. The clay layers in zones-1 and 2 are initially OC and they stay in the same state till reaching SSC after 59 and 31 cycles (2390 and 1256 days) respectively. The maximum degree of consolidation at SSC for zones-1, 2 and 3 were found to be 81.03%, 83.53% and 90.660 %, respectively, while the corresponding minimum values were 62.56%, 58.05% and 42.370%, respectively. A maximum difference of about 54 % in the average degree of consolidation was found in Zone-3 (Port Said east), where the clay is plastic.

Figure 6.21 shows the time-settlement curves at the center of the base for a unit load, while Figure 6.22 shows the corresponding results at the characteristic point. From the figures, it can be seen that the settlement is maximum in Zone-1 (Port Said west). In fact, the clay layer at Zone-1 is closer to the ground surface and it is also of a bigger height, if compared to its counterparts in the other couple of zones.

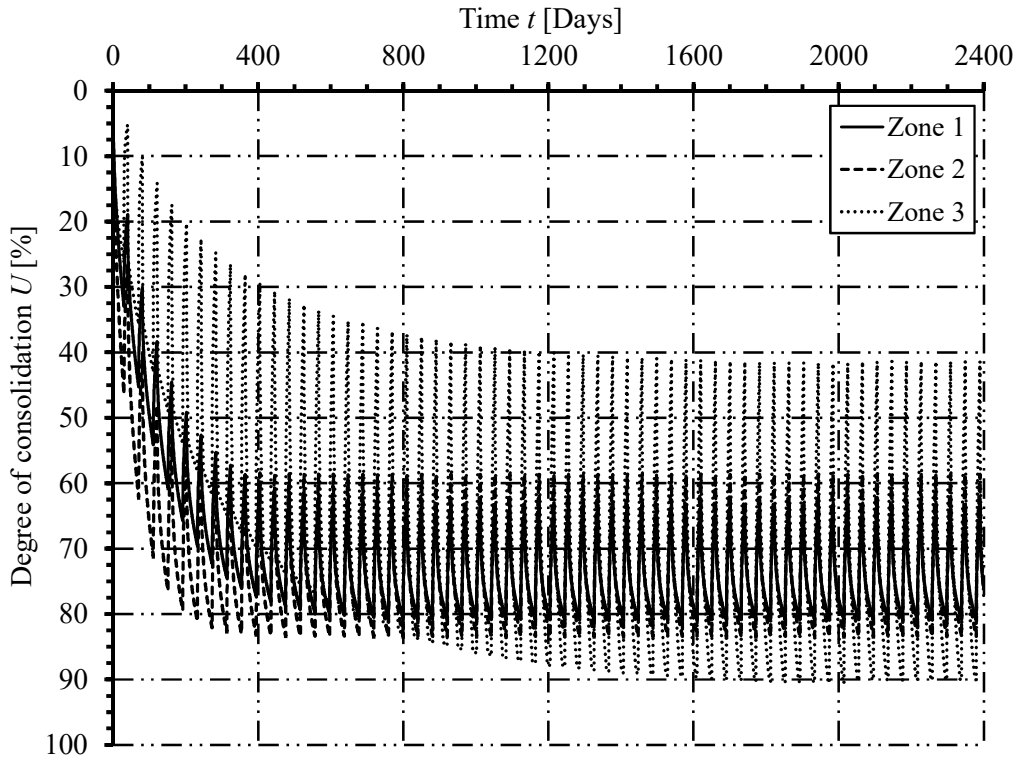
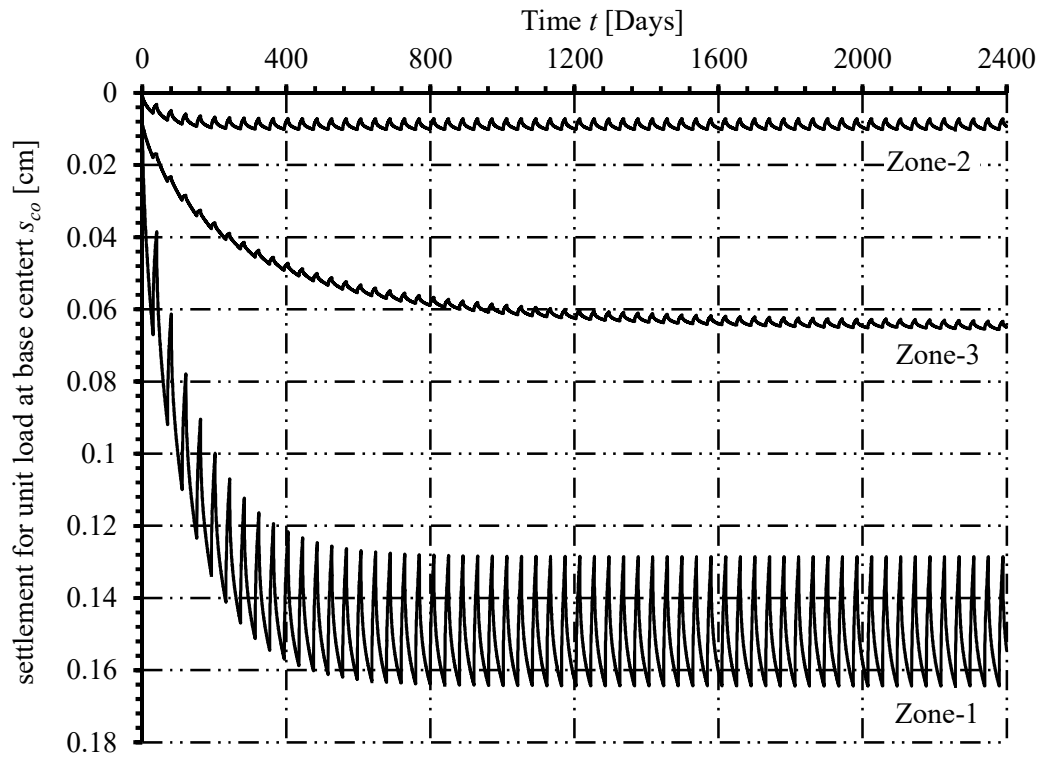
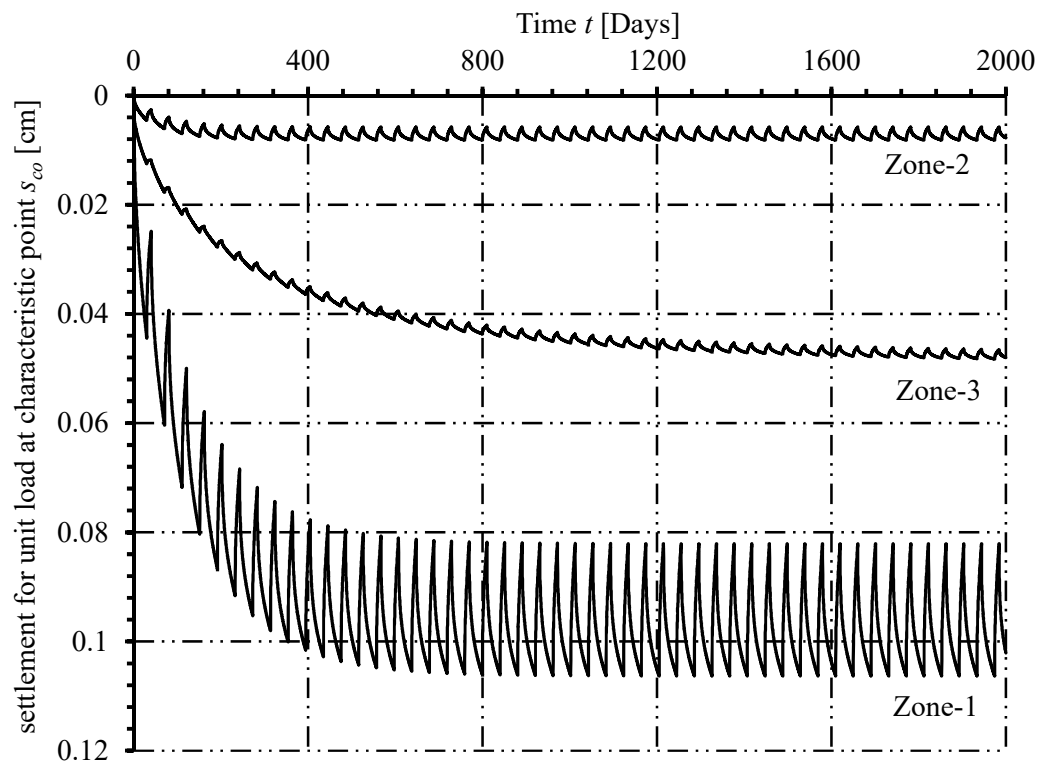


Figure 6.20 Bilinear degree of consolidation U in Zones under consideration

Figure 6.21 Bilinear settlement s_{co} at the flexible base centerFigure 6.22 Bilinear settlement s_{co} at the characteristic point

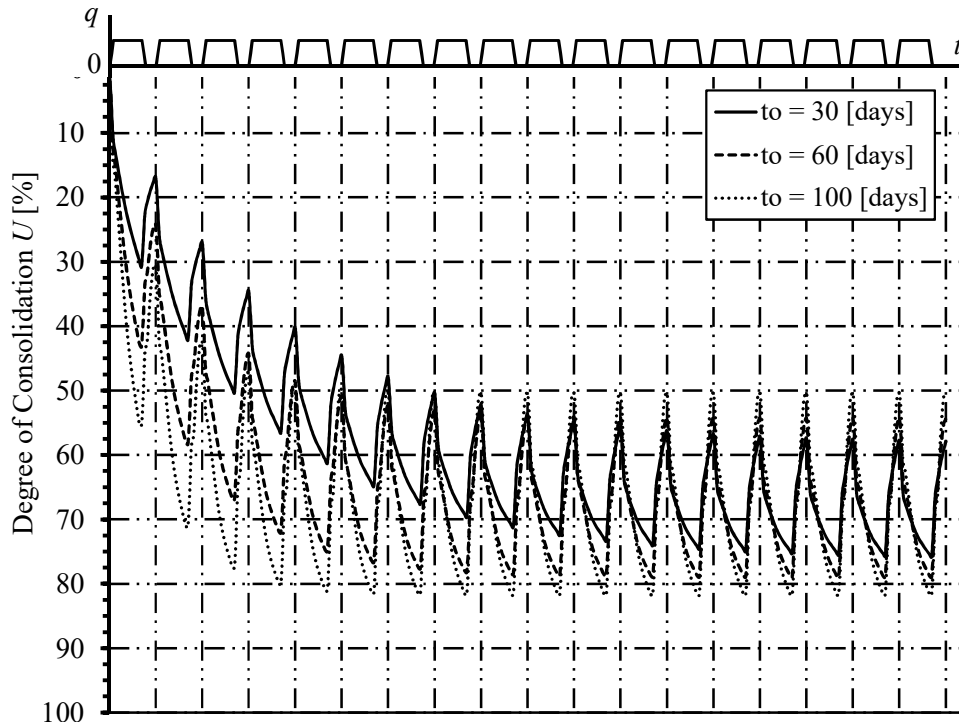
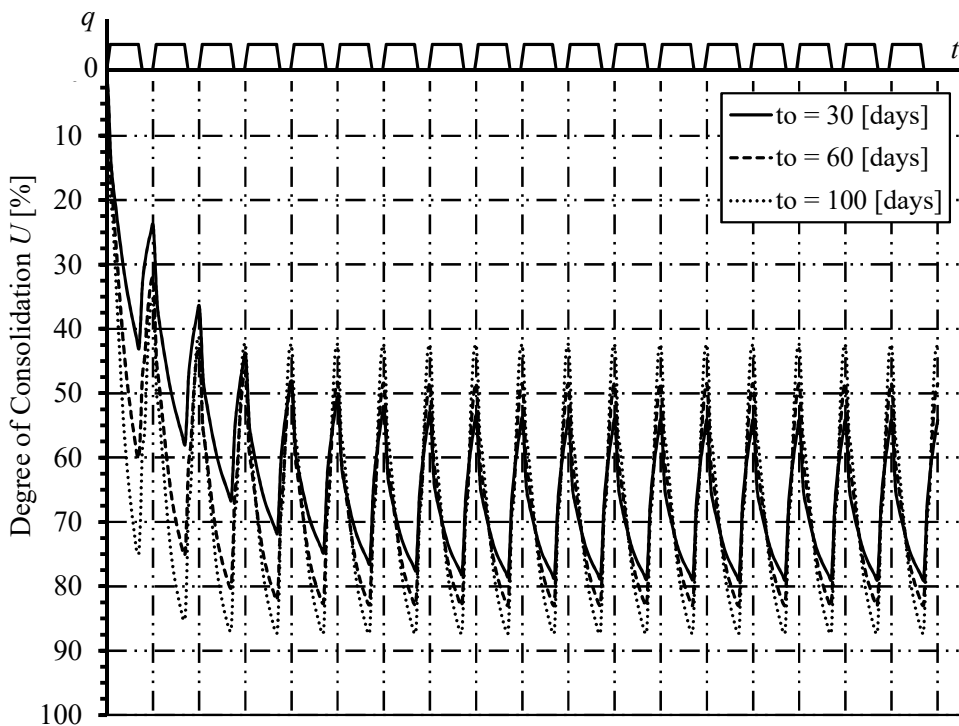
6.3.6 Effect of varying the loading period t_o

Figure 6.23, Figure 6.24 and Figure 6.25 show the variations of bilinear average degree of consolidation with the time t_o in zones-1, 2 and 3, respectively corresponding to a trapezoidal cyclic loading scheme (refer to Figure 6.1) with $q = 1$ [kN/ m²], $a = 6.5$ [m], $\alpha_o = 0.1$, $\beta_o = 1.3$, and $t_o = 30, 60$ and 100 [days]. On the other hand, Figure 6.26, Figure 6.27 and Figure 6.28 show the corresponding time variations of settlement at the center of the flexible base. It should be noted that the x-axis in all figures from Figure 6.23 to Figure 6.40 reads the time as multiples of the complete loading cycle, as it is displayed graphically on the axis. Table 6.7 gives the effect of loading period t_o on the behavior of the top clay layer at the three zones under consideration. It is clear that the number of loading cycles required to reach *SSC* becomes smaller, as well as the degree of consolidation and settlement become greater, as the loading period t_o gets longer.

Table 6.7 Effect of loading period t_o on clay layer behavior

	Loading period t_o [Days]	Zone-1 (Port Said west)	Zone-2 (Port Said south)	Zone-3 (Port Said east)
N^* [Cycles]	30	59	34	> 60 cycle
	60	31	15	56
	100	20	10	44
$U^*_{max.}$ [%]	30	76.26	79.01	85.7
	60	78.99	82.97	95.7
	100	81.78	87.31	99.06
$s^*_{max.}$ [cm]	30	0.3262	0.0120	0.0667
	60	0.3379	0.0124	0.0744
	100	0.3499	0.0130	0.0771

where N^* , $U^*_{max.}$, $s^*_{max.}$ are the number of cycles needed to reach *SSC*, the maximum bilinear degree of consolidation at *SSC* and the maximum bilinear settlement at the center of the flexible base at *SSC*, respectively.

Figure 6.23 Influence of t_o on the degree of consolidation U in Zone-1Figure 6.24 Influence of t_o on the degree of consolidation U in Zone-2

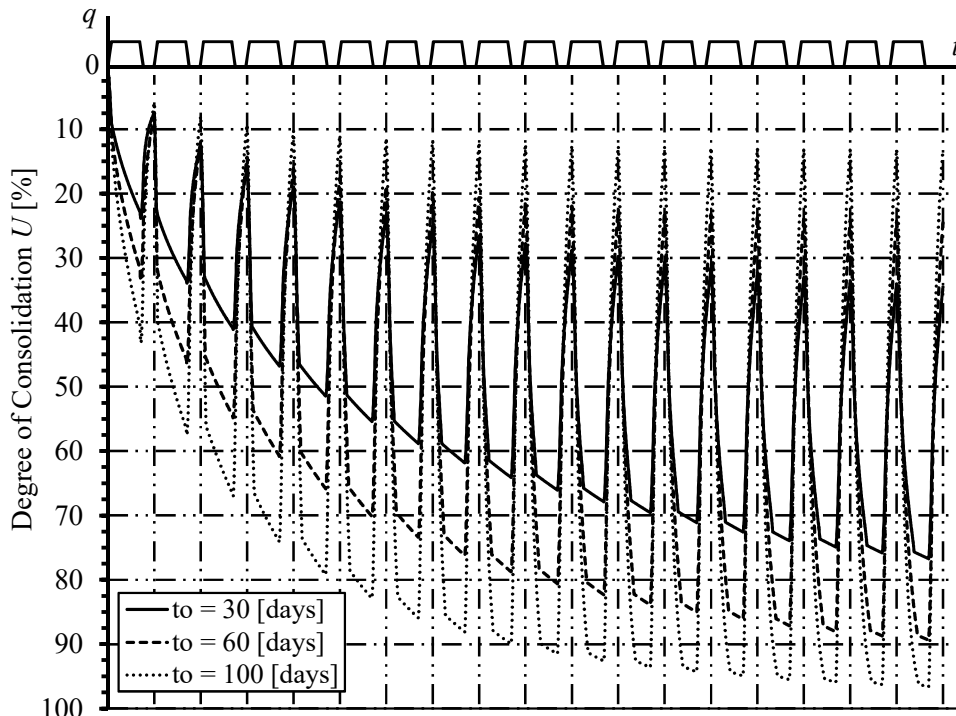


Figure 6.25 Influence of t_o on the degree of consolidation U in Zone-3

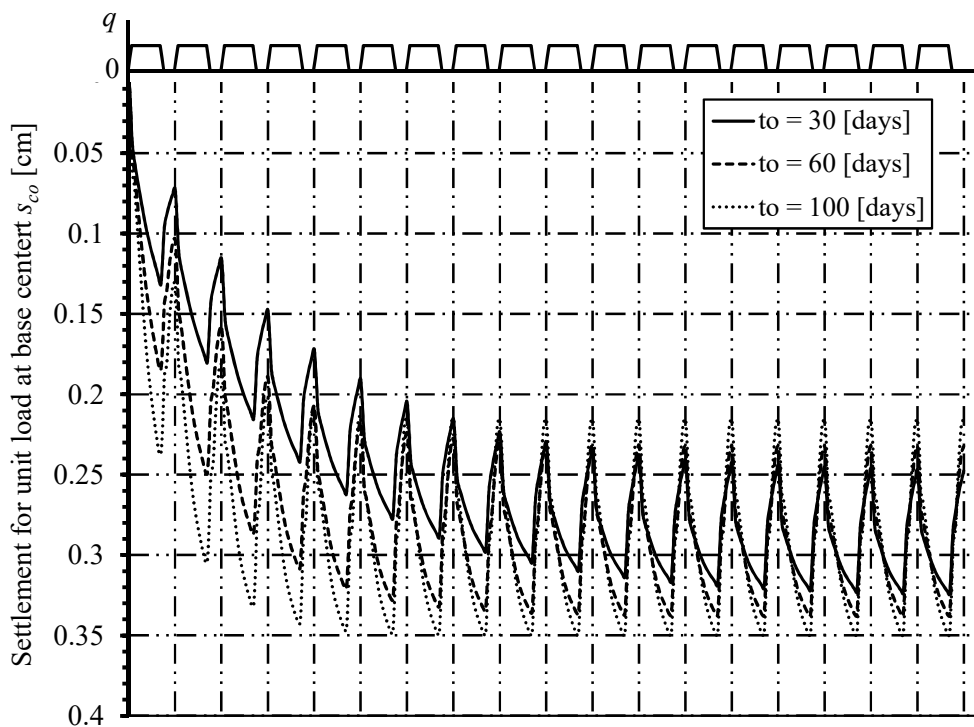


Figure 6.26 Influence of t_o on the settlement s_{co} at the flexible base center in Zone-1

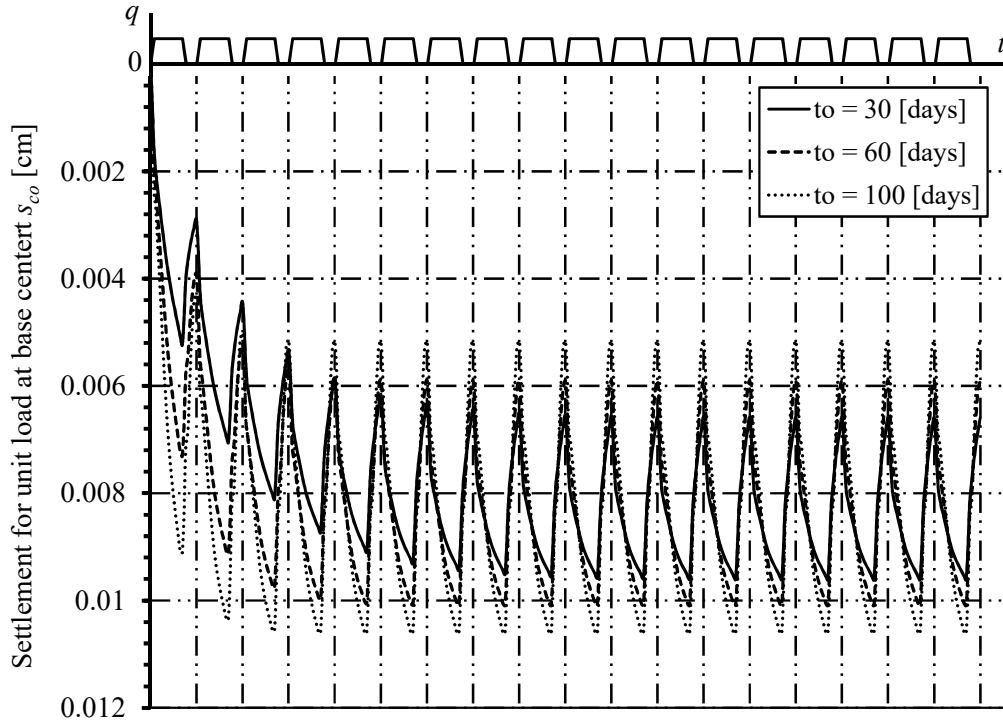


Figure 6.27 Influence of t_o on the settlement s_{co} at the flexible base center in Zone-2

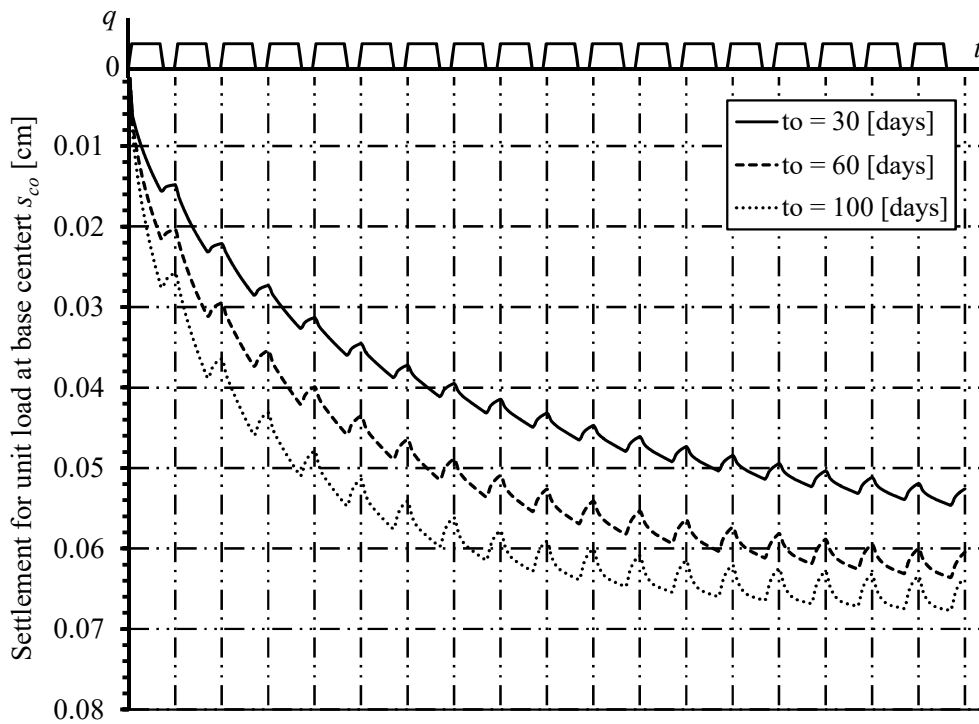


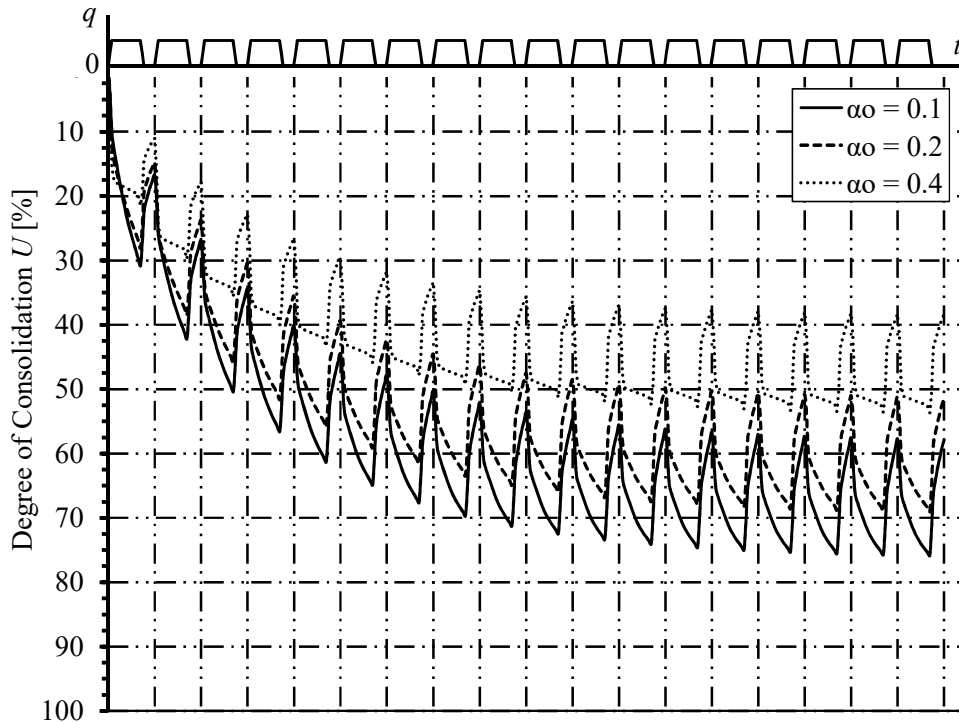
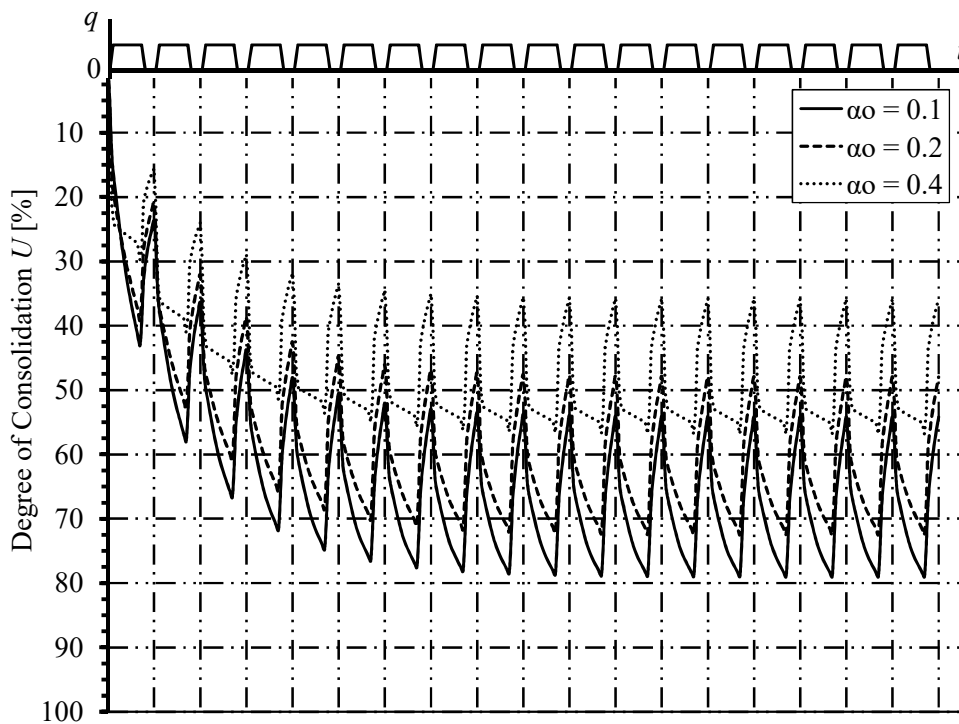
Figure 6.28 Influence of t_o on the settlement s_{co} at the flexible base center in Zone-3

6.3.7 Effect of varying the parameter α_o

Figure 6.29, Figure 6.30 and Figure 6.31 show the variations of bilinear average degree of consolidation with the factor α_o in zones-1, 2 and 3, respectively corresponding to a trapezoidal cyclic loading scheme with $q = 1$ [kN/ m²], $a = 6.5$ [m], $t_o = 30$ [days], $\beta_o = 1.3$, and $\alpha_o = 0.1, 0.2$ and 0.4 . On the other hand, Figure 6.32, Figure 6.33 and Figure 6.34 show the corresponding time variations of settlement at the center of the flexible base. Table 6.8 gives the effect of the factor α_o on the behavior of the top clay layer at the three zones under consideration. It was stated earlier that the factor α_o represents the rate of loading or unloading of the cyclic load. It can be seen from Table 6.8 that the number of loading cycles required to reach SSC at zones 1 and 2 is slightly affected by the change of α_o . However, it decreases considerably at Zone-3 (Port Said east) as α_o increases. It is also clear from Table 6.8 that the degree of consolidation and settlement get smaller, almost equally, in all zones as α_o gets bigger.

Table 6.8 Effect of parameter α_o on clay layer behavior

	Parameter α_o [-]	Zone-1 (Port Said west)	Zone-2 (Port Said south)	Zone-3 (Port Said east)
N^* [Cycles]	0.1	59	34	> 60
	0.2	58	32	> 60
	0.4	57	30	> 60
$U^*_{max.}$ [%]	0.1	76.26	79.01	85.70
	0.2	69.41	72.46	83.07
	0.4	53.99	56.84	66.98
$s^*_{max.}$ [cm]	0.1	0.3262	0.0120	0.0667
	0.2	0.2969	0.0110	0.0647
	0.4	0.2309	0.0086	0.0521

Figure 6.29 Influence of α_0 on the degree of consolidation U in Zone-1Figure 6.30 Influence of α_0 on the degree of consolidation U in Zone-2

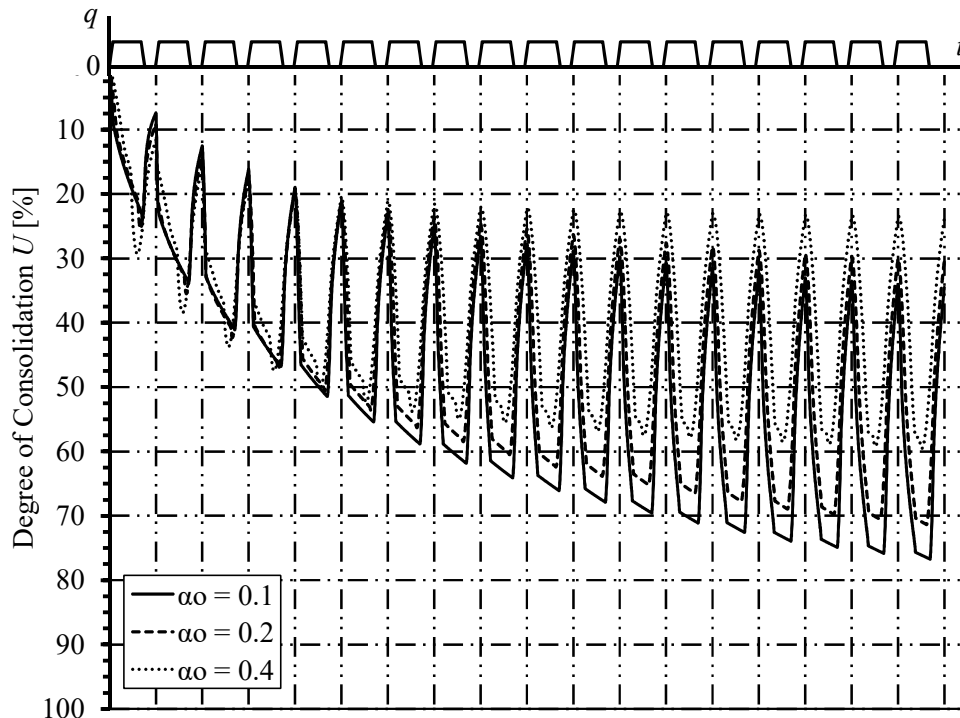


Figure 6.31 Influence of α_0 on the degree of consolidation U in Zone-3

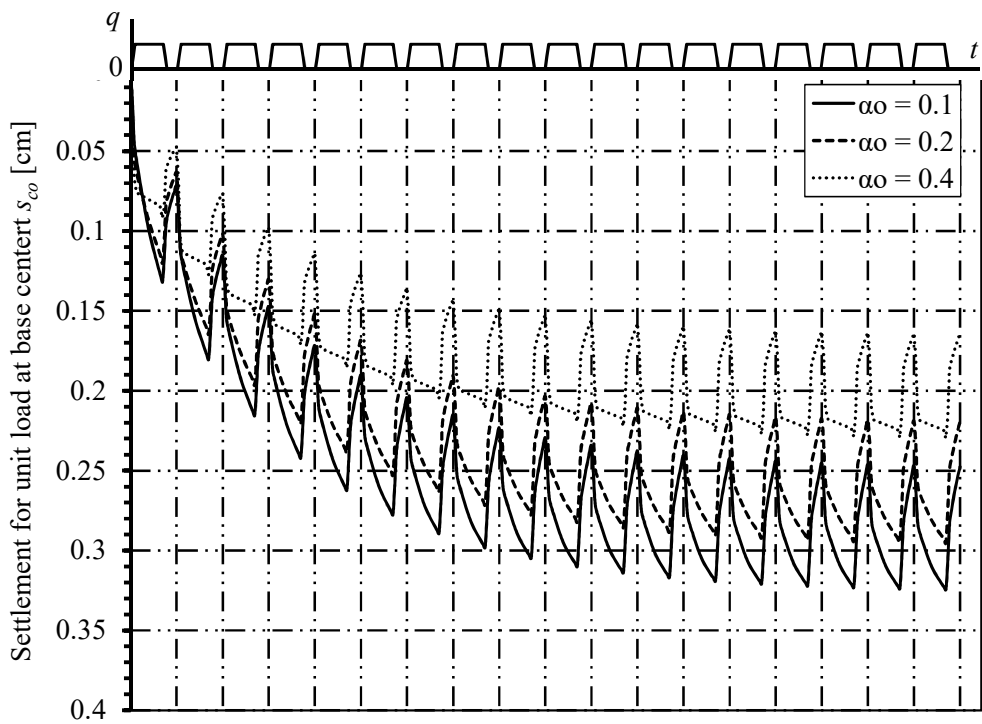


Figure 6.32 Influence of α_0 on the settlement s_{co} at the flexible base center in Zone-1

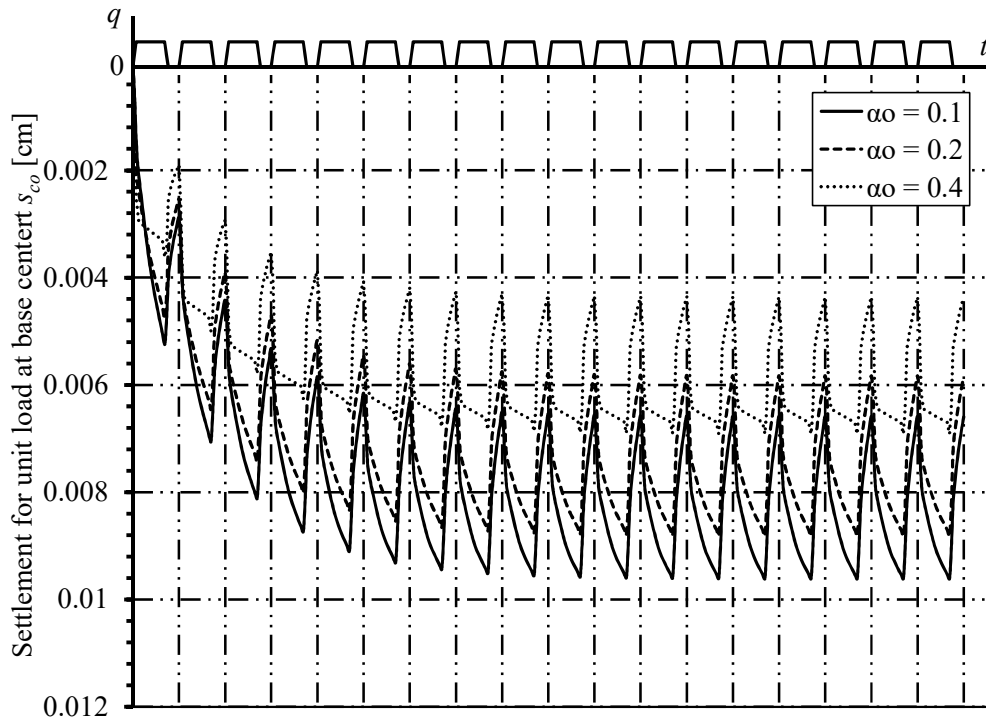


Figure 6.33 Influence of α_o on the settlement s_{co} at the flexible base center in Zone-2

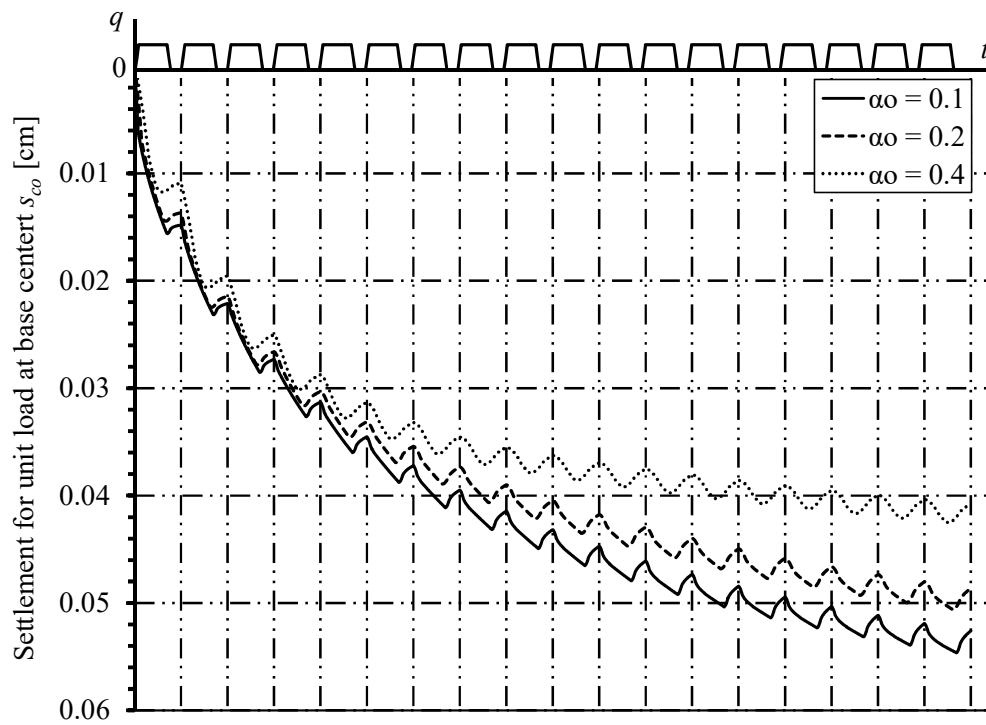


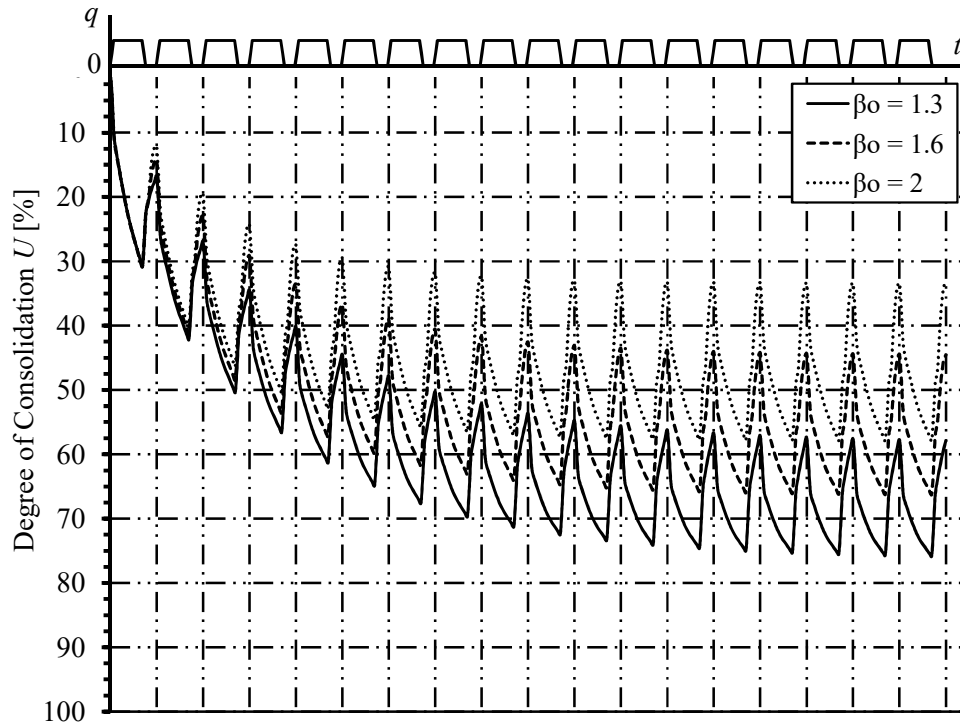
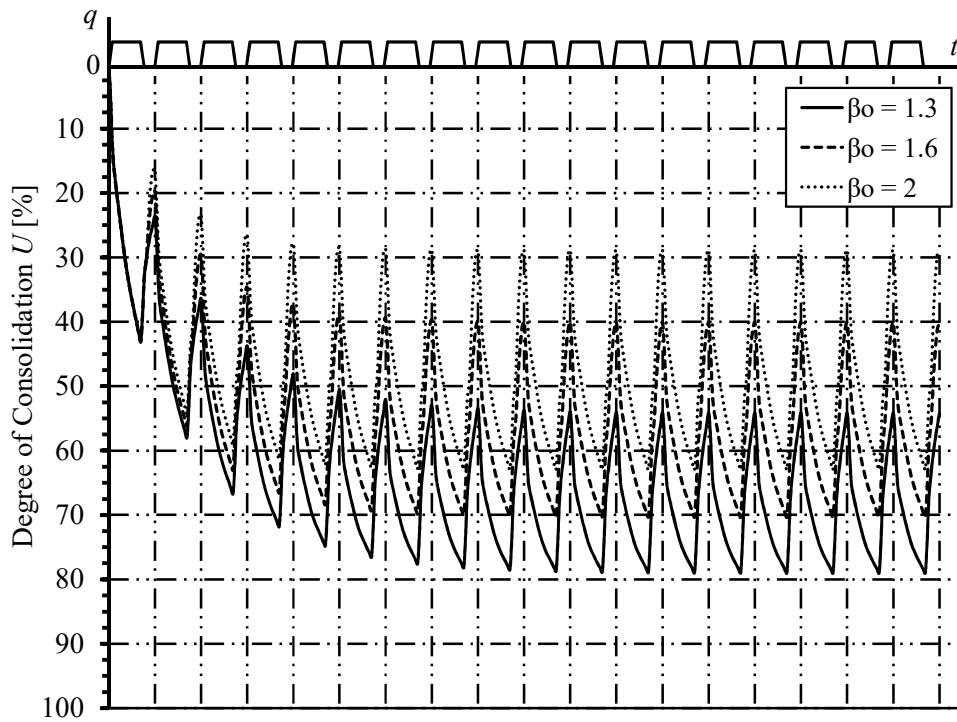
Figure 6.34 Influence of α_o on the settlement s_{co} at the flexible base center in Zone-3

6.3.8 Effect of varying the parameter β_o

Figure 6.35, Figure 6.36 and Figure 6.37 show the variations of bilinear average degree of consolidation with the factor α_o in zones-1, 2 and 3, respectively corresponding to a trapezoidal cyclic loading scheme with $q = 1$ [kN/ m²], $t_o = 30$ [days], $\alpha_o = 0.1$, and $\beta_o = 1.3, 1.6$ and 2.0 . On the other hand, Figure 6.38, Figure 6.39 and Figure 6.40 show the corresponding time variations of settlement at the center of the flexible base. Table 6.9 gives the effect of the factor β_o on the behavior of the top clay layer at the three zones under consideration. The factor β_o represents the duration of a complete loading cycle (including both filling and emptying stages). It can be seen from Table 6.9 that the number of loading cycles required to reach SSC, as well as the degree of consolidation and settlement for all zones decrease significantly as β_o increases.

Table 6.9 Effect of parameter β_o on clay layer behavior

	Parameter β_o [-]	Zone-1 (Port Said west)	Zone-2 (Port Said south)	Zone-3 (Port Said east)
N^* [Cycles]	1.3	59	34	> 60
	1.6	48	24	> 60
	2.0	46	19	> 60
$U^*_{max.}$ [%]	1.3	76.26	79.01	85.70
	1.6	66.37	70.34	84.39
	2.0	57.91	62.96	81.45
$s^*_{max.}$ [cm]	1.3	0.3262	0.0120	0.0667
	1.6	0.2839	0.0107	0.0657
	2.0	0.2477	0.0096	0.0634

Figure 6.35 Influence of β_0 on degree of consolidation U in Zone-1Figure 6.36 Influence of β_0 on degree of consolidation U in Zone-2

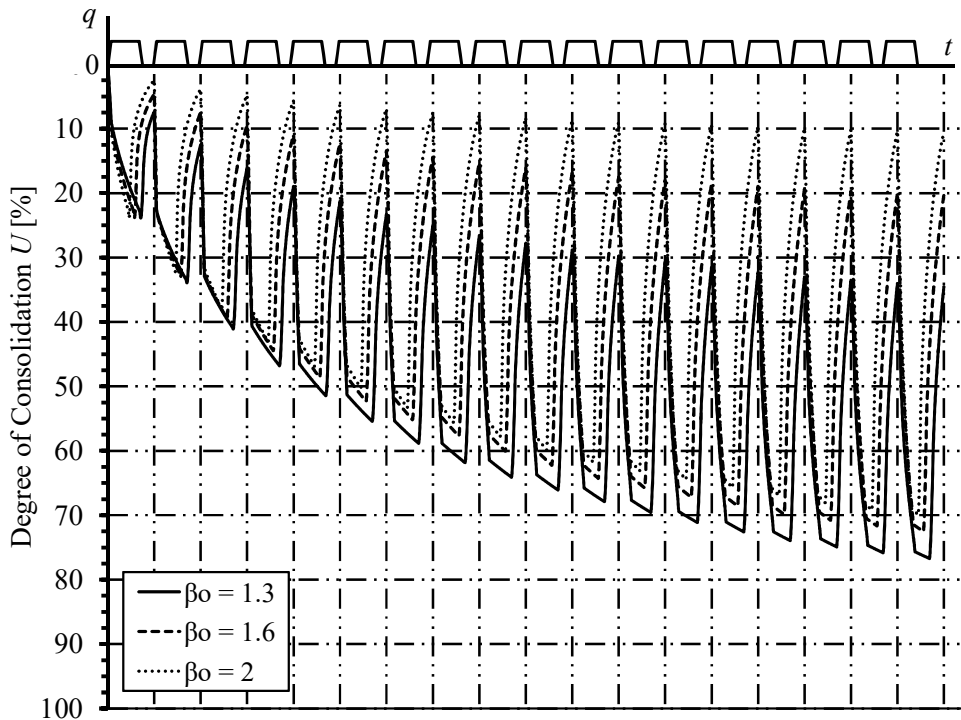


Figure 6.37 Influence of β_0 on degree of consolidation U in Zone-3

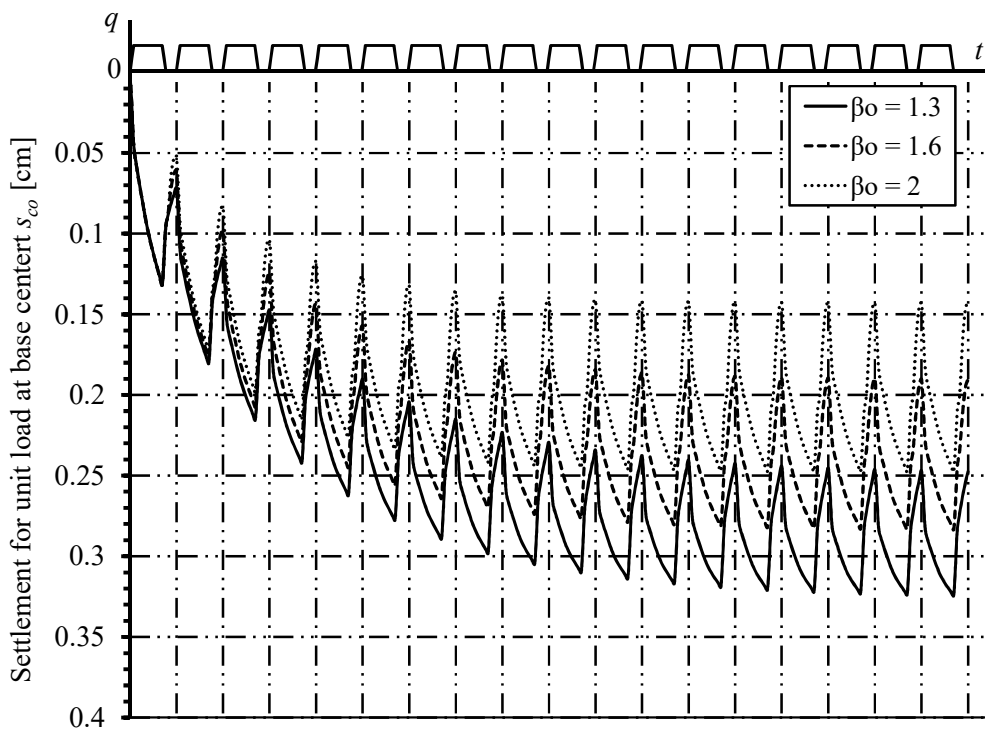


Figure 6.38 Influence of β_0 on the settlement s_{co} at the flexible base center in Zone-1

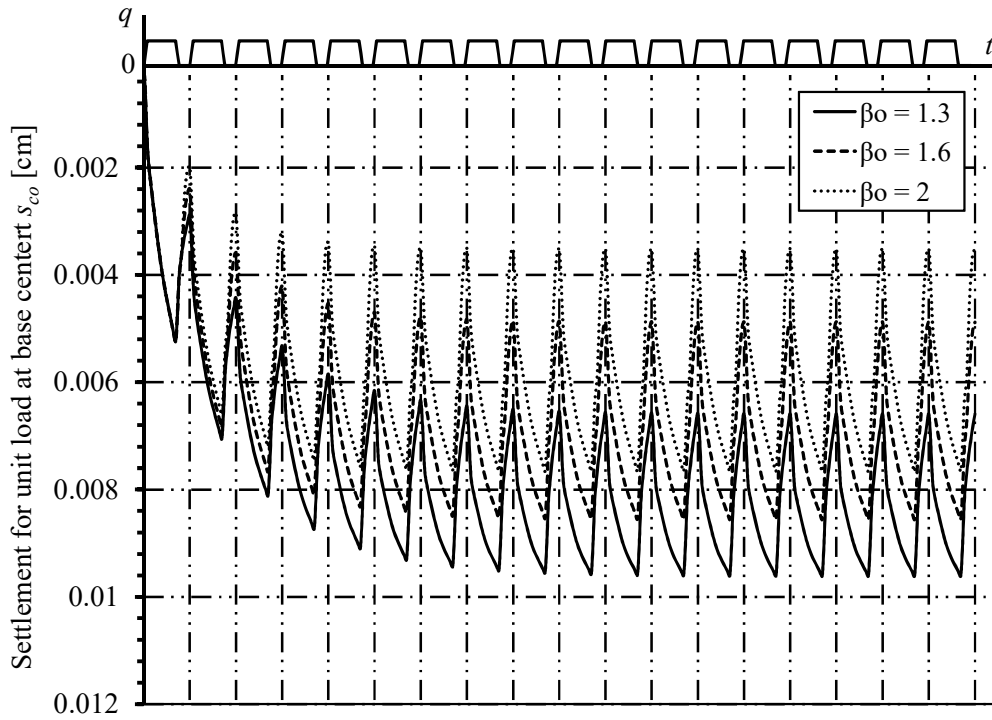


Figure 6.39 Influence of β_0 on the settlement s_{co} at the flexible base center in Zone-2

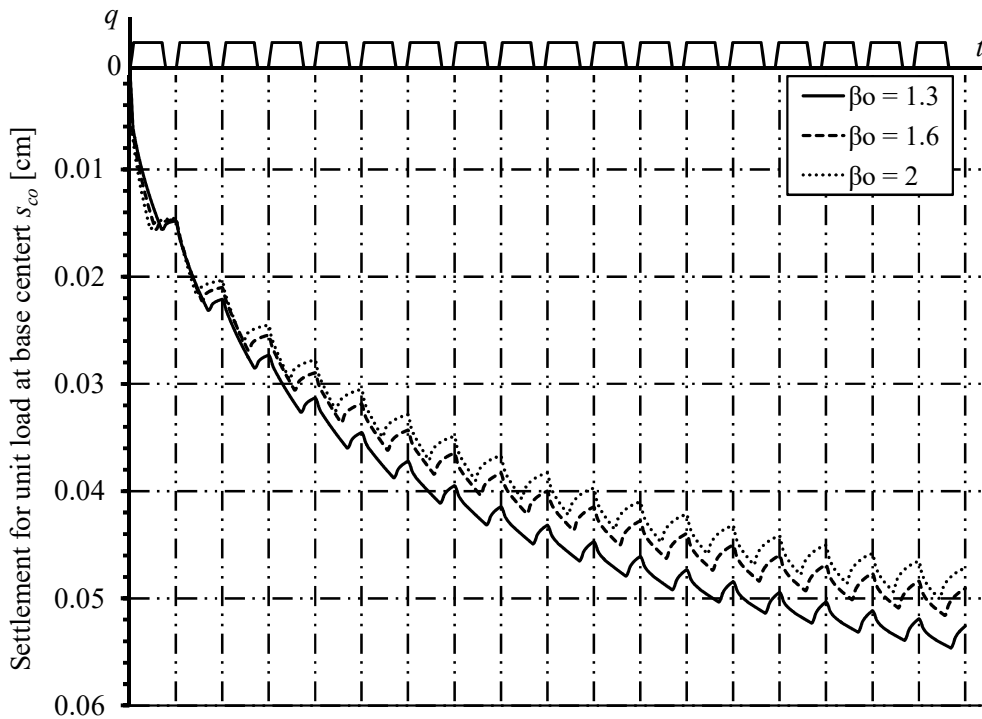


Figure 6.40 Influence of β_0 on the settlement s_{co} at the flexible base center in Zone-3

6.3.9 Behavior of a circular tank with elastic base under cyclic loading

Assume that the tank shown in Figure 6.7 is constructed in Zone-1 (Port Said west). Zone-1 has a top 5 [m] thick clay layer located at 2.0 [m] below the ground surface. The properties of clay for bilinear consolidation under cyclic loading are given in Table 6.3. Assume that a cyclic load as presented in 0 is applied. For simplicity, the factor α_0 is assigned to zero herein. In other words, it will be assumed that the cyclic load scheme would be rectangular, as shown in Figure 6.41. In this case, the loading phase is taken as 30 [days] long, while the no-loading phase is taken as 10 [days] long as shown in the figure. The results given hereinafter are obtained based on LL only, as the self-weight of tank will be neglected. The time is divided into small intervals; each of 0.5 [day], while the soil depth is divided into sub-layers; each of 1 [m]. The tank wall is divided into 14 equal elements of 0.25 [m] thick, whereas the base is divided into 26 ring elements of equal areas. The results of the main clay layer only are presented after 1, 5, 10 loading cycles, as well as after reaching the *SSC*. The analysis results under static loading are also presented for the sake of comparison. The static loading results represent the study case where the tank is assumed to be full permanently.

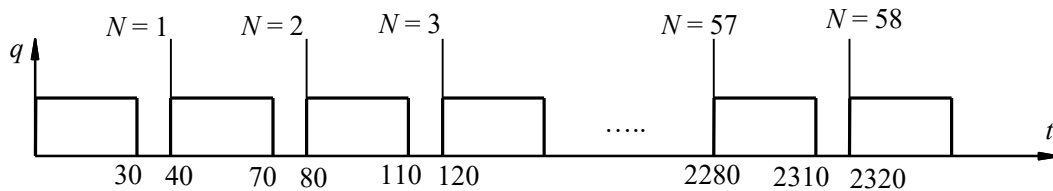


Figure 6.41 Load-Time scheme used in Zone-1

6.3.9.1 Contact pressure q

Figure 6.42 shows the radial variations of contact pressure under the tank base plate after 1, 5, 10 loading cycles, as well as after reaching the *SSC*. From the figure, it's obvious that the contact pressure does not affected by load cycling. Moreover, the contact stress distribution is almost the same for both static and cyclic loading.

6.3.9.2 Base settlement s_{base}

Figure 6.43 shows the radial variation of settlements under the tank base plate after 1, 5, 10 loading cycles, as well as after reaching the *SSC*. The settlement all over the tank base increases will load cycling, with a decreasing rate, until reaching its maximum at *SSC*. The *SSC* is reached after 58 loading cycles. In this case, the ratio of the settlement at the center after reaching *SSC* to its initial value after one loading cycle is about 260%. The maximum settlement at the tank center due to static loading is 24% higher than its counterpart resulting from cyclic loading at the *SSC*.

6.3.9.3 Radial moment across the base M_{base}

Variations of the radial moments in the base plate are showing Figure 6.44. The maximum moment at the edge after reaching *SSC* is about 30 [%] of the static loading result, while at the center of base plate, the moment at *SSC* is about 55 [%] of the static loading result.

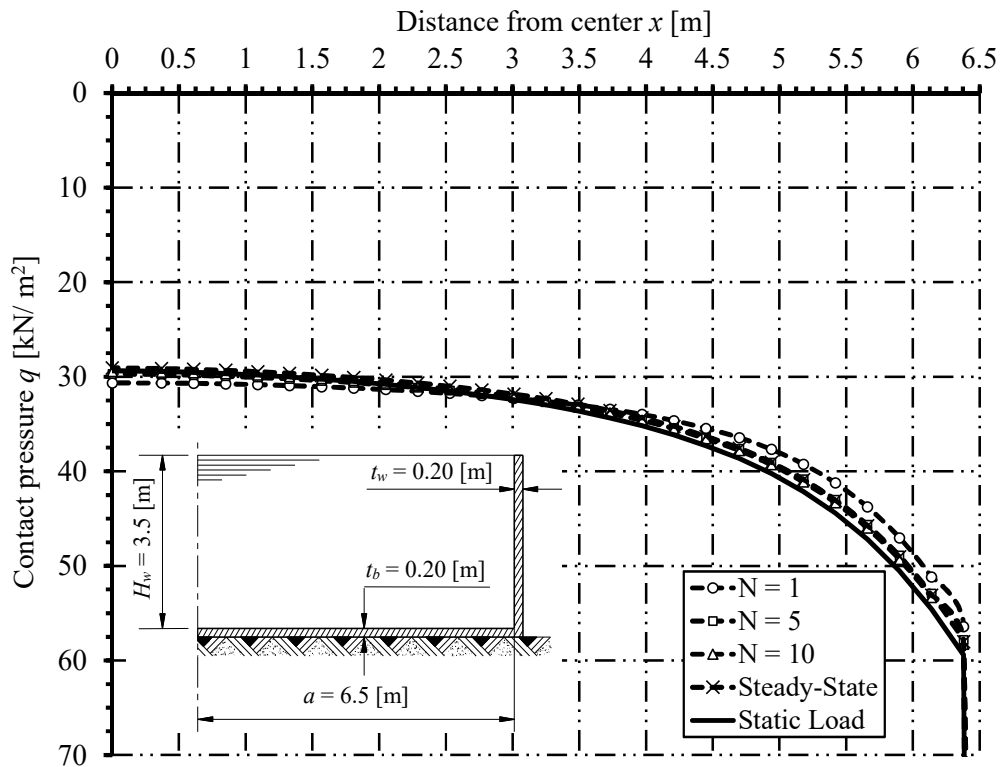


Figure 6.42 Variations of the contact pressure q

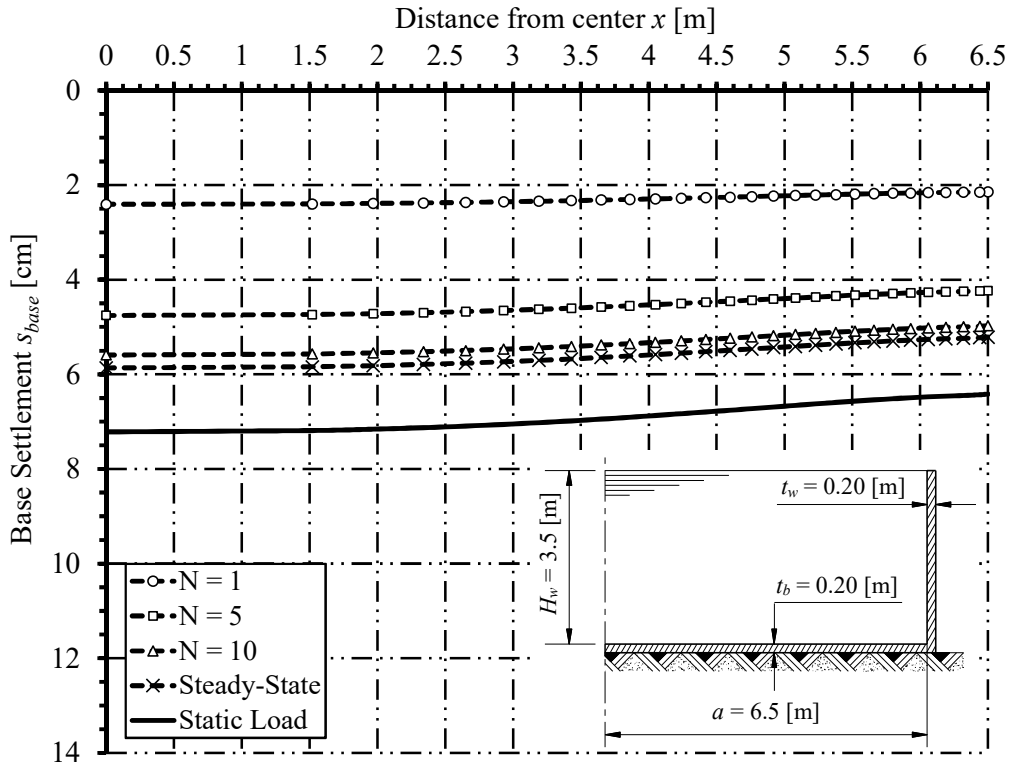


Figure 6.43 Variations of the base settlement s_{base}

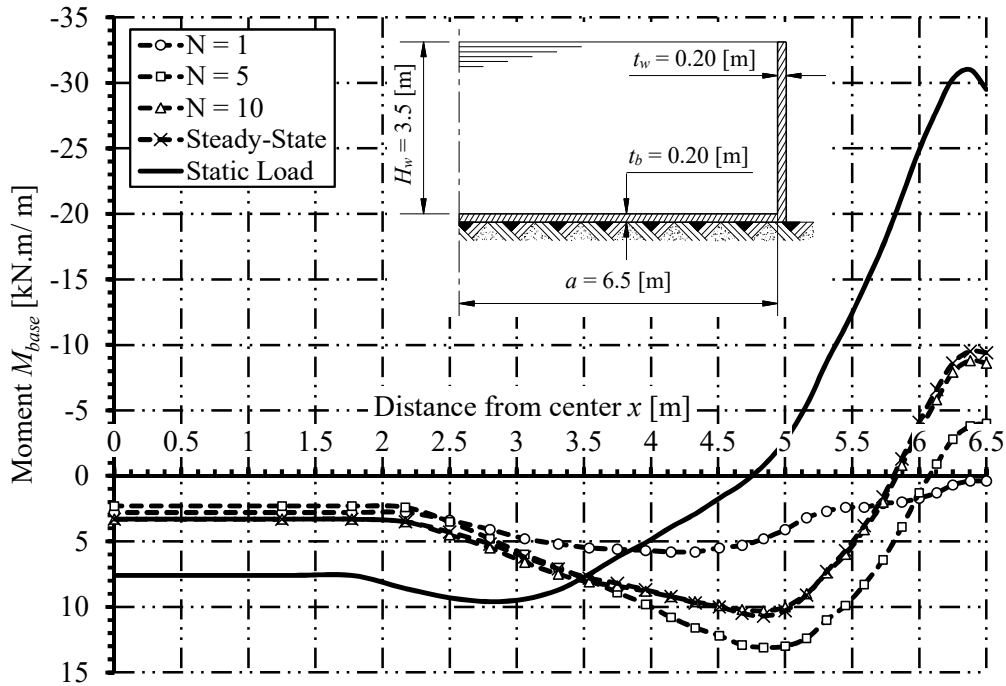


Figure 6.44 Variations of radial moment M_{base}

6.3.9.4 Radial force across the base N_{base}

Variations of the radial force distribution in the base plate are shown Figure 6.44. The radial forces after reaching SSC is about 30 [%] of the static loading result.

6.3.9.5 Meridional moment in the wall M_s

Variations of the meridional moments along the wall height are shown Figure 6.46 . The meridional moment at the air side reaches its maximum after one loading cycle, and its 20% bigger than its counterpart under static loading. The meridional moments at the air side decrease with further load cycling, and the maximum meridional moment at the air side after reaching SSC is about 80 [%] of the static loading result.

6.3.9.6 Tangential force in the wall N_θ

Distributions of the tangential force along the wall height are shown Figure 6.47 . The tangential force in the wall reaches its maximum after one loading cycle, and it reaches 90% higher than its counterpart under static loading. The maximum tangential force in the wall decrease with further load cycling, and the maximum force resulting after reaching SSC is about 70 [%] of its counterpart resulting after one loading cycle.

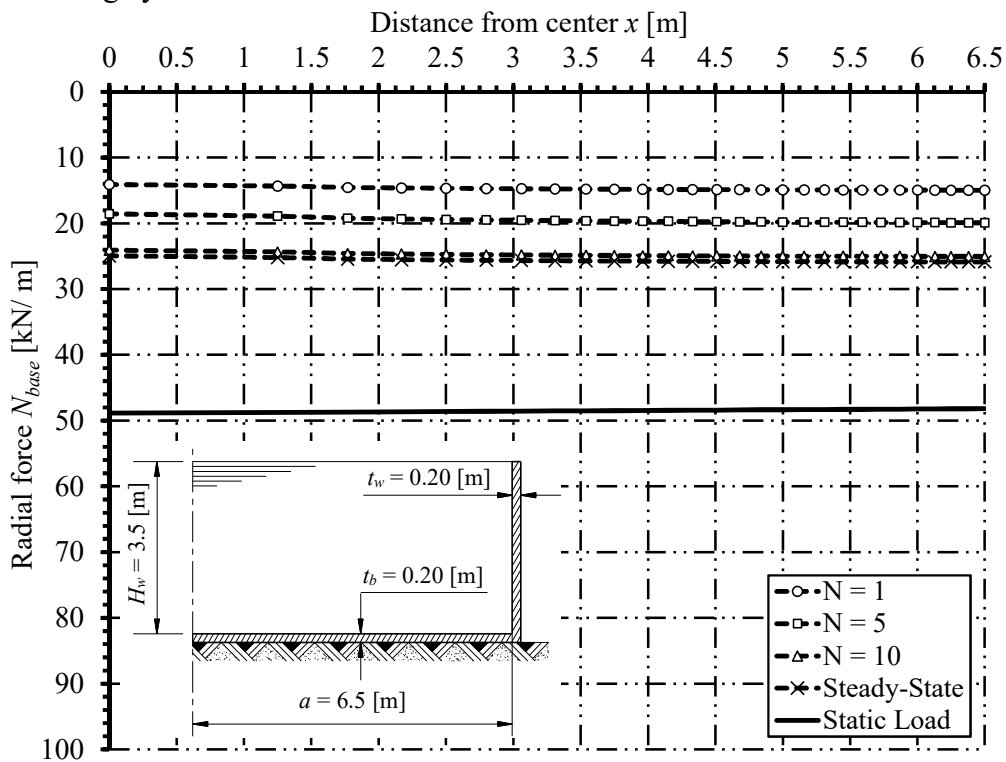


Figure 6.45 Radial force across the base N_{base}

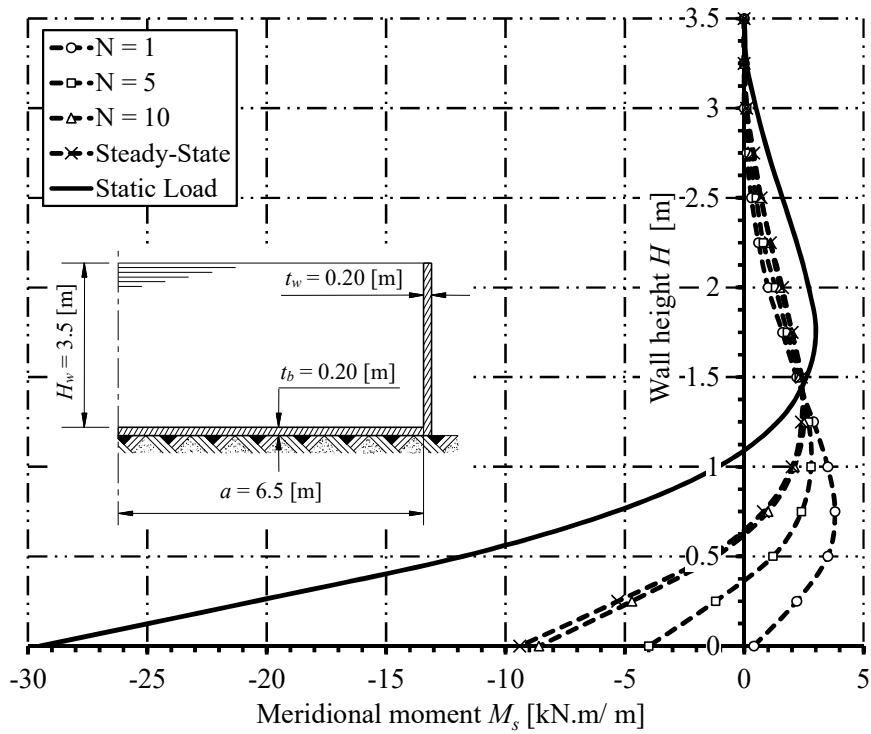


Figure 6.46 Variations of meridional moment M_s along the wall

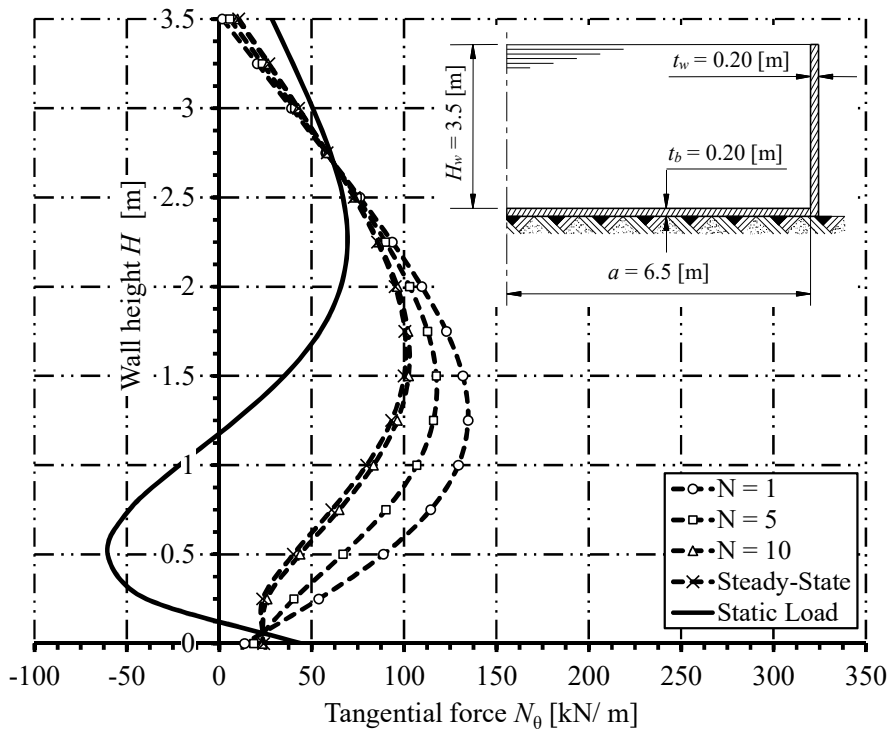


Figure 6.47 Variations of tangential force N_0 along the wall

6.3.10 The effect of changing Load-Time scheme on the internal forces

Consider the tank presented in Figure 6.7 is subjected to four different Load-Time schemes. Figure 6.48 shows the Load-Time scheme parameters for rectangular cyclic loading. The data of the four Load-Time schemes are presented in Table 6.10. The results of the internal forces in the four cases were compared to study the effect of period length and loading phase length on the internal forces.

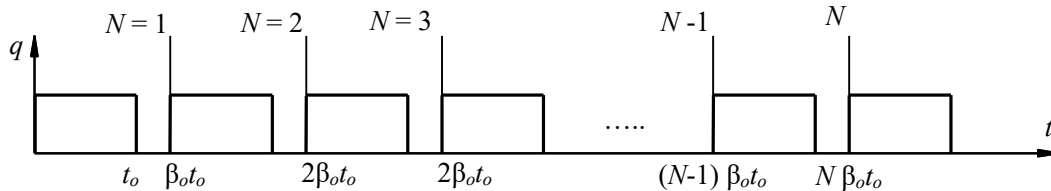


Figure 6.48 Load-Time scheme for rectangular cyclic loading

Table 6.10 Data of the Load-Time schemes for analysis

Load-Time scheme NO.	Loading period t_o [Days]	No-Loading period $\beta_o t_o$ [Days]
1	30	10
2	90	10
3	180	10
4	365	10

6.3.10.1 Contact pressure q

Figure 6.49 shows the radial variations of contact pressure under the tank base plate for different Load-Time schemes and for static loading. The contact stress distribution is almost the same for both static and cyclic loading as explained before.

6.3.10.2 Base settlement s_{base}

Figure 6.50 shows the radial variation of settlements in the base plate. The results of the settlements represent 81.26, 94.19, 97.39 and 99.54 [%] of the static loading result for Load-Time schemes 1, 2, 3 and 4, respectively. These ratios are the same as the average degree of consolidation ratios. The ratios increase with increasing the loading period, while the no-loading period is constant in all schemes.

6.3.10.3 Radial moment across the base M_{base}

Variations of the radial moments in the base plate are shown in Figure 6.51. The results of the moment at the edge represent 31.86, 46.10, 56.61 and 71.19 [%] of the static loading result for Load-Time schemes 1, 2, 3 and 4, respectively.

6.3.10.4 Radial force across the base N_{base}

Figure 6.52 shows the radial force distribution in the base with different Load-Time schemes. The results of the radial force represent 51.09, 62.04, 69.32 and 79.40 [%] of the static loading result for Load-Time schemes 1, 2, 3 and 4, respectively.

6.3.10.5 Meridional moment in the wall M_s

Figure 6.53 shows the variation of the meridional moments along the wall height with different Load-Time schemes. The results of the maximum meridional moment in the air side represent 67.67, 73.33, 80.00 and 86.67 [%] of the static loading result for Load-Time schemes 1, 2, 3 and 4, respectively.

6.3.10.6 Tangential force in the wall N_θ

Variations of the tangential force along the wall height with different Load-Time schemes are shown in Figure 6.54. The results of the maximum tensile force represent 144.66, 130.58, 121.74 and 112.52 [%] of the static loading result for Load-Time schemes 1, 2, 3 and 4, respectively. As seen in the figure, the tension zone goes smaller, while the compression zone expands.

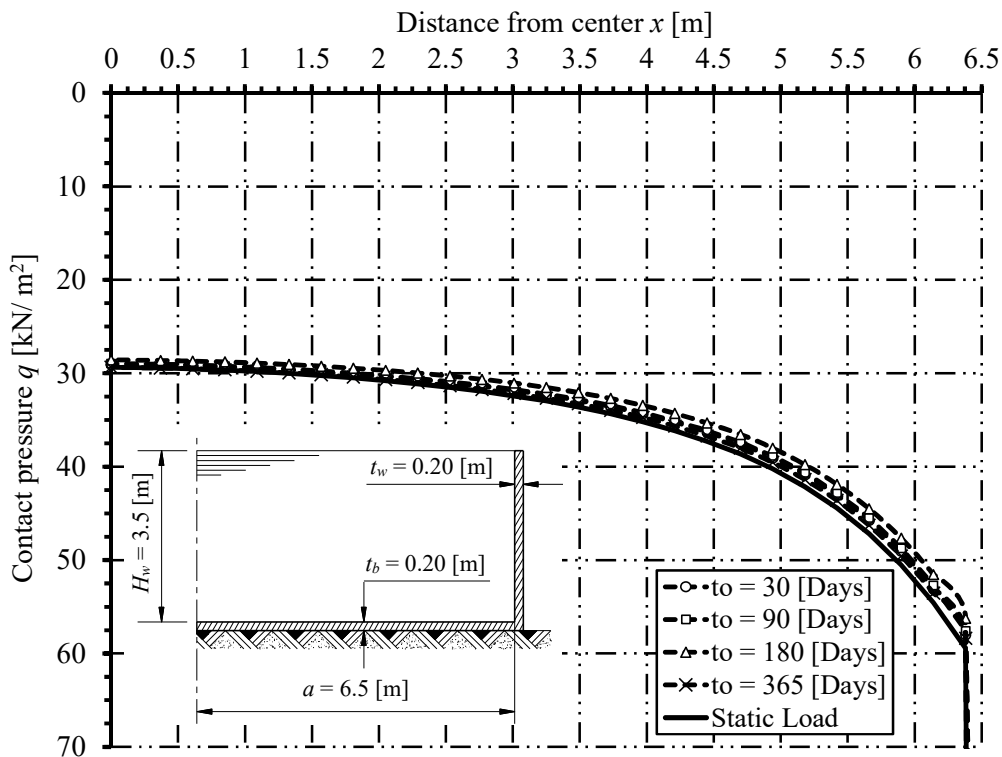


Figure 6.49 Variations of the contact pressure q at SSC for different Load-Time schemes

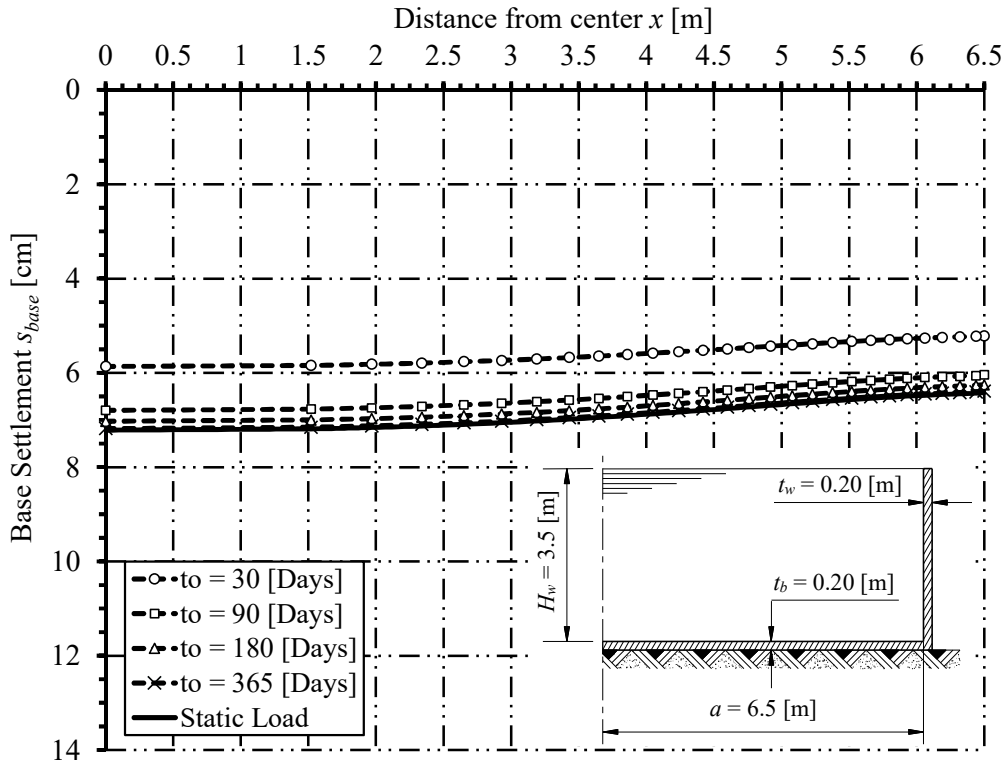


Figure 6.50 Variations of the base settlement s_{base} at SSC for different Load-Time schemes

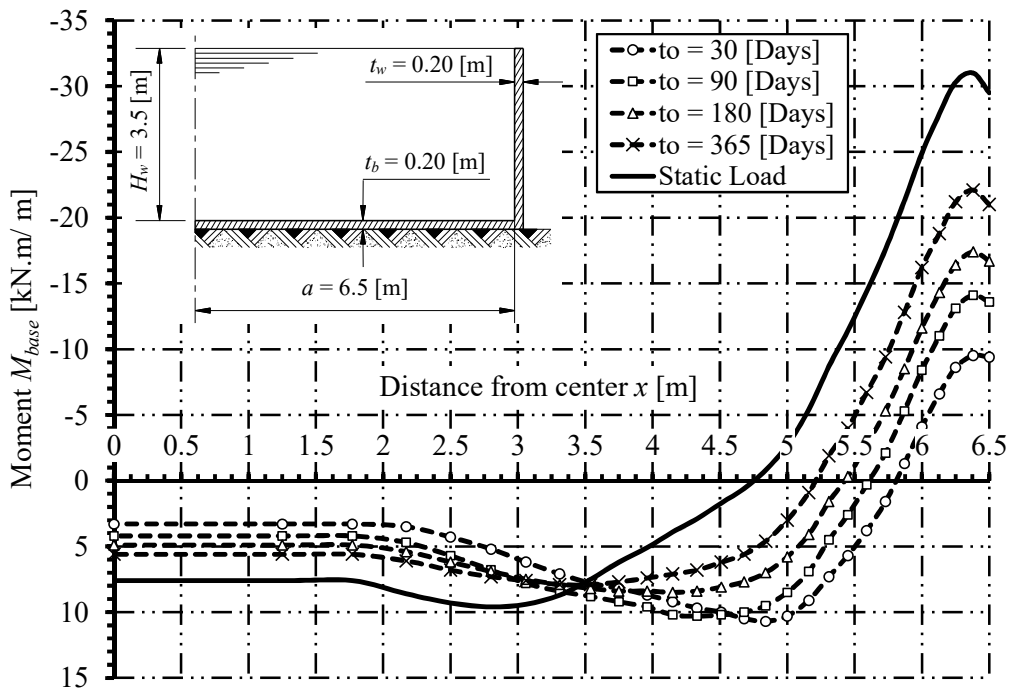


Figure 6.51 Variations of radial moment M_{base} at SSC condition for different Load-Time schemes

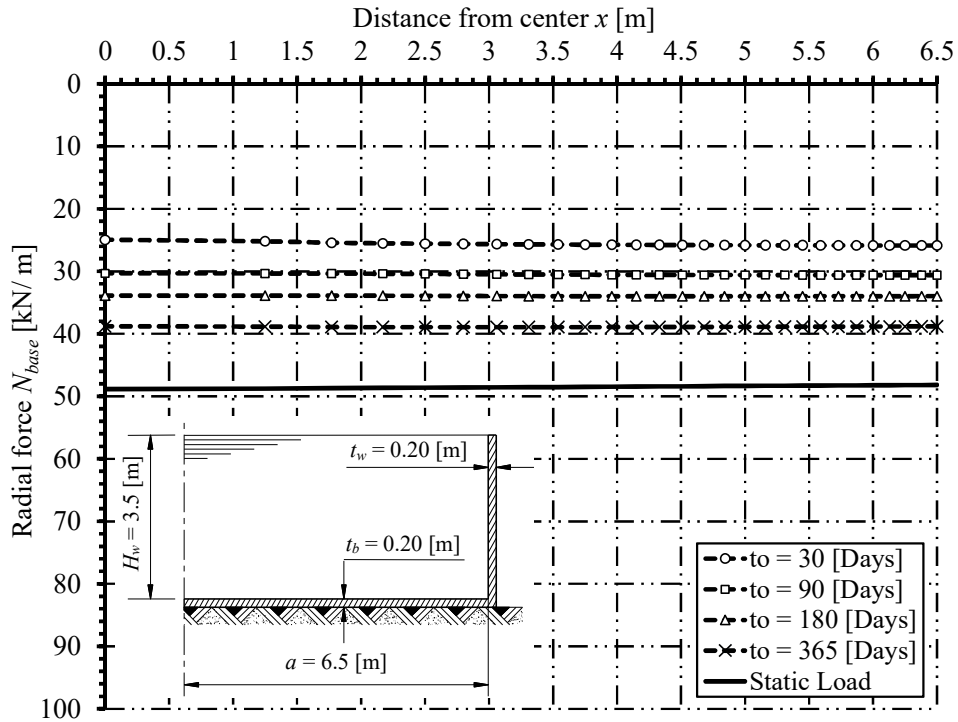


Figure 6.52 Radial force across the base N_{base} at SSC condition for different Load-Time schemes

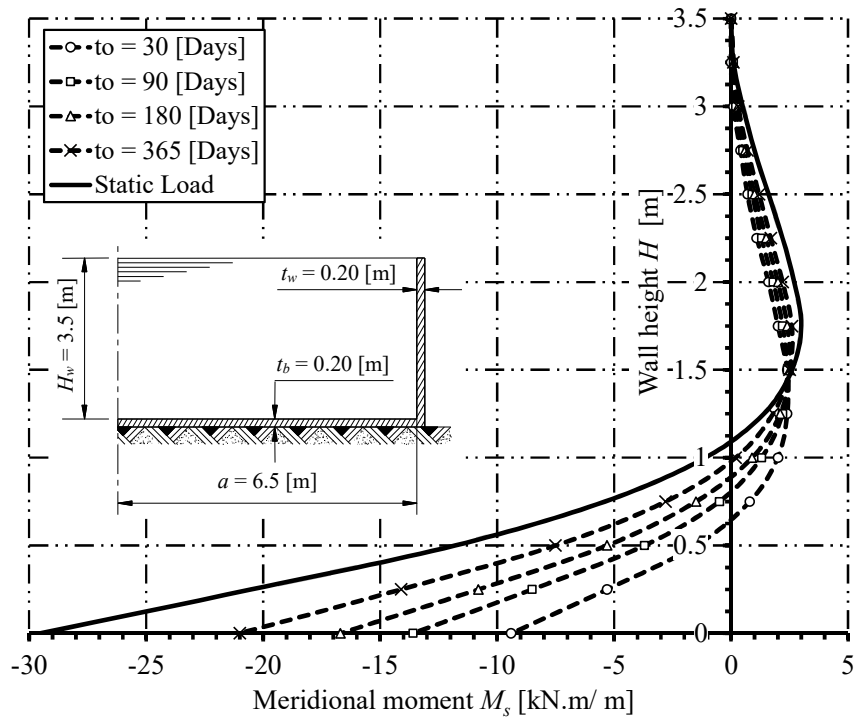


Figure 6.53 Variations of meridional moment M_s along the wall at SSC for different Load-Time schemes

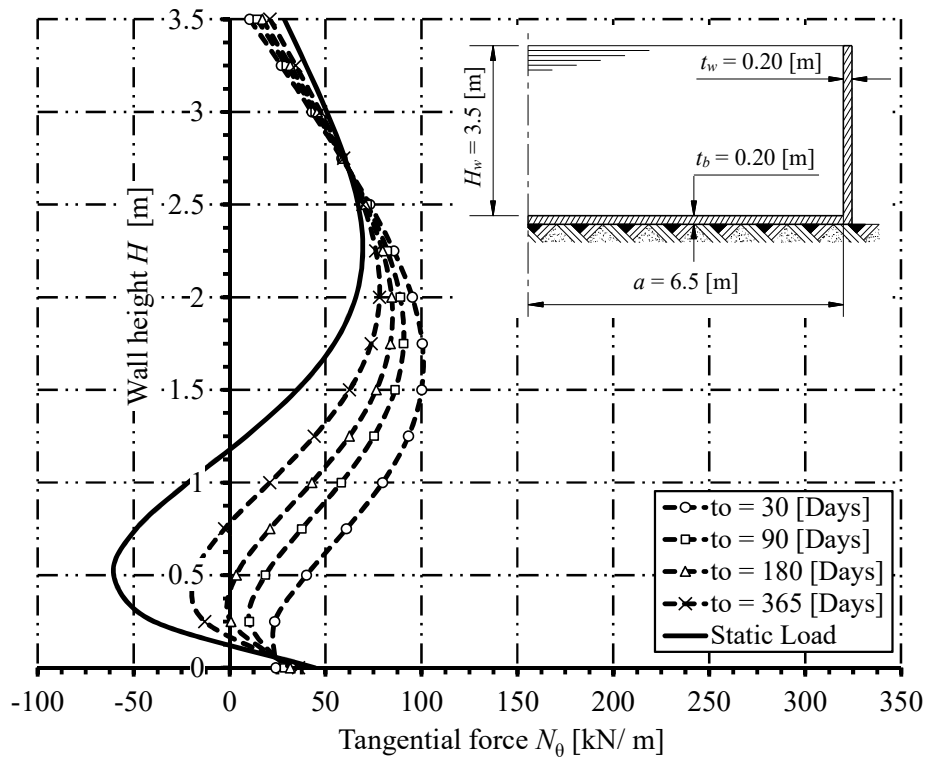


Figure 6.54 Variations of tangential force N_θ along the wall at SSC for different Load-Time schemes

Chapter 7

7 Conclusions and recommendations

7.1 Summary

The presence of clay layers under the ground surface causes a great foundation settlement. A special type of structures which may be subjected to a static or cyclic loading and can be constructed on clay layers is circular ground tanks. Tanks are commonly used for industrial liquid storage and water treatment plants. The great problem which may occur here is the time-dependent loading and settlement considering full compatibility between the structure and the soil. Therefore, a numerical analysis based on finite element method using a cylindrical finite element shell is presented. The analysis is capable of modeling circular cylindrical tanks resting on layered soil medium with real subsoil physical constants. In the proposed mathematical model, the axi-symmetry of the problem is exploited to transform the problem from a 3-D problem to a 2-D problem to save in memory and time required for calculations. In the analysis, the performance of the soil during the consolidation process is considered as linear, bilinear and nonlinear.

In addition, a numerical modification is carried out on the semi-analytical solution of *Toufigh/ Ouria* (2009) to be applicable for multi-layered soil subjected to any variable stress along the depth of the soil using layer equation method (*LEM*) of *Herrmann/ El Gendy* (2014). The developed solution is used for normally or overconsolidated clays subjected to any type of cyclic loading. It takes into account the structure rigidity with the subsoil layers at any cyclic period. Besides, the actual contact pressure under the tank can be obtained at any cyclic period. The solution is applied for water tanks as a structure subjected to cyclic loading. Base of the tank may be considered as rigid, elastic or flexible. For analyzing the base of the tank as elastic base, full compatibility between the structure and subsoil elements, wall, base and subsoil, is accounted for.

Time-dependent parameters of the tank model such as construction time, periods of filling and emptying tanks and types of cyclic loadings are studied with structural parameters of the tank. As a practical application for the developed analysis, a parametric study was carried out to study the behavior of cylindrical tanks under different variables and conditions using real soil data from real sites. To achieve this task, three different areas are suitable for constructing storage tanks located in Port Said were considered. The study presented guidelines and diagrams for cylindrical tanks that may be used in Port-Said area under static or cyclic loading.

7.2 Conclusions from the analysis of tanks under static loading

The study presented guidelines and diagrams for cylindrical tanks that may be used in Port-Said area. The following conclusions could be drawn from the studies carried out:

- 1- Throughout the design process, it is not recommended to rely on a simplified soil models such as the simple assumption or *Winkler's* models, as they may lead to inaccurate results. Designers are strongly recommended to adopt a more realistic soil model such as layered soil models.
- 2- Comparing the suitable zones for constructing circular storage concrete tanks in Port-Said, the southern industrial zone was found to be the most appropriate zone all over Port-Said for the construction of circular ground tanks, whereas the west zone that contains most of the petroleum facilities was found to be the worst; from a structural point of view. It's found that the farther the effective clay layer from the ground surface, the higher the soil resistance for deformation and stresses.
- 3- The existence of roof, whether flat or spherical, doesn't have any effect on the structural behavior of the base. However, the condition of the tank roof has a great influence on the internal forces and deformations of the wall.
- 4- In a static analysis of a ground tank, the internal forces and settlement due to LL are computed directly at the final settlement. Therefore, those results can be considered as limits that would never be reached throughout a cyclic load analysis unless the average degree of consolidation becomes 100%.

7.3 Conclusions from the analysis of tanks under cyclic loading

The following main conclusions could be drawn from the studies carried out on ground circular tanks under cyclic loading:

- 1- An effective numerical model for analyzing circular ground tanks under time dependent and cyclic loading is presented. The proposed model is capable to represent layered soil with realistic conditions and variable stress distributions along the height of clay layers. Moreover, it can take account for the soil-structure interaction between the tank base and underlying soil. The tank base can be taken either a flexible, rigid, or elastic base.
- 2- Tanks resting on NC clay layers need much more loading cycles to reach the steady-state condition, if compared to those underlain by OC clay. This can be attributed to the fact that the tank situation in the latter case is actually closer to the steady state condition, which by its nature exists in the OC range.
- 3- The degree of consolidation is constant for any load in bilinear consolidation analysis for the same load-time scheme.
- 4- The longer the duration of applied cyclic load t_o , the fewer the number of cycles required for reaching the stable steady-state condition. In this case, the average degree of consolidation, the settlement, as well as the resulting internal forces are higher.
- 5- As the rate of loading and unloading becomes slower (i.e. as α_o gets smaller), the average degree of consolidation for any loading cycle gets bigger and the stable-state is reached faster.
- 6- For shorter loading periods (i.e. as β_o gets smaller), the resulting degree of consolidation, settlement and internal forces are higher and the stable-state condition is reached faster.
- 7- As the number of loading cycles increases, the resulting average degree of consolidation and settlement increases, until the steady- state condition is reached. In this case, further loading cycles will not affect the analysis results.
- 8- The resulting bending moment distribution along the wall height or the base of tank differs substantially according to the nature of loading; whether a static or cyclic loading.
- 9- The contact pressure is not affected by cycling loading. Moreover, the contact pressure distribution is almost the same for both static and cyclic loading.

7.4 Recommendations for future works

In this thesis, tanks under static and cyclic loading were studied. The scope for future studies may also include:

- 1- Short-period cyclic loading as earthquakes and ocean waves on coastal tanks.
- 2- More comprehensive non-linear consolidation by varying all consolidation parameters with time and depth.
- 3- Tanks on deep foundations under cyclic loading.
- 4- Elevated tanks under cyclic loading.
- 5- Underground tanks under cyclic loading.
- 6- Rectangular tanks under cyclic loading.

References

- [1] *Abbaspour, M.* (2014). "An investigation of consolidation process under triangular cyclic loading by numerical and experimental analysis". EJGE, Vol. 19, Bund. F.
- [2] *Ahrens, H. and Winselmann, D.* (1984): "Eine iterative Berechnung von Flächengründungen nach dem Steifemodulverfahren". Finite Elemente Anwendungen in der Baupraxis Verlag W. Ernst & Sohn, München.
- [3] *ANSYS software* (2009): User's manual for revision 5.4. Volume I-IV, software analysis system, Inc. 200 P.
- [4] *Bakhoun, M.* (1992): "Structural Mechanics". Cairo, Egypt.
- [5] *Booker, J. R. and Small, J. C.* (1983): "The analysis of liquid storage tanks on deep elastic foundation". Int. J. Numer. Anal. Methods Geomech. 7, 187-207.
- [6] *Consulting engineering office* (2012), "Geotechnical report for East Port Said Harbor", Port Said, Egypt.
- [7] *Conte, E. and Troncone, A.* (2006), "One-dimensional consolidation under general time-dependent loading", Can. Geotech. J., 43(11), 1107-1116.
- [8] *Conte, E. and Troncone, A.* (2007), "Nonlinear consolidation of thin layers subjected to time-dependent loading", Can. Geotech. J., 44(6), 717-725.
- [9] *Das, B. M.* (1997): "Advanced soil mechanics", 2nd ed., USA, Taylor & Francis.
- [10] *Davis, E.H. and Raymond, G.P.* (1965), "A non-linear theory of consolidation", Geotechnique, 15(2), 161-173.
- [11] *ECP 202-2001* (2007), Egyptian code of soil mechanics and foundation engineering, Housing and Building Research Center.
- [12] *El Gendy M.* (2014): "Computer Analysis of Foundations: Theory for the calculation of shallow foundations by *ELPLA*". GEOTEC Software Inc., Egypt.
- [13] *El Gendy M. and El Gendy A.* (2015): "Analysis and Design of Slab Foundations by FE-Method- Program *ELPLA 10*". GEOTEC Software Inc., Canada.

-
- [14] *El Gendy, M.* (2003): "Numerical Modeling of Rigid Circular Rafts on Consolidated Clay Deposits". Int. Workshop on Geotechnics of Soft Soils-Theory and Practice. Vermeer, Schweiger, Karstunen & Cudny (eds.).
- [15] *El Gendy, M.* (2006): "Developing stress coefficients for raft-deformation on a thick clay layer". Vol. 41, No. 3, September 2006, pp. 73-108. Scientific Bulletin, Faculty of Engineering, Ain Shams University, Cairo, Egypt.
- [16] *EL Mezaini, N.* (2006): "Effects of soil-structure interaction on the analysis of cylindrical tanks". Practice periodical on structural design and construction, Vol. 11, No. 01, Pages 50 -57.
- [17] *Ghali, A.* (2000): "Circular storage tanks and silos – 2nd edition", by E & FN spon – 11 New Fetter Lane, London EC4P 4EE.
- [18] *Golder Associates* (1979), "Port Said Urban land reclamation design study", Port Said, Egypt.
- [19] *Grafton, P. E. and Strome, D. R.* (1963): "Analysis of Axis-Symmetric Shells by the Direct Stiffness Method," AIAA Journal, Vol. 1, No. 10, pp. 2342-2347.
- [20] *Graßhoff, H.* (1955): "Setzungsberechnungen starrer Fundamente mit Hilfe des kennzeichnenden Punktes". Der Bauingenieur, S. 53-54.
- [21] *Hanna, D., Sivakugan, N., and Lovisa, J.* (2013). "Simple approach to consolidation due to constant rate loading in clays." Int. J. Geomech. 10.1061/ (ASCE) GM.1943-5622.0000195, 193–196.
- [22] *Hauso, A.* (2014): "Analysis methods for thin concrete shells of revolution", M.Sc. Thesis, Faculty of Engineering, Norwegian University of Science and Technology.
- [23] *Hemsley, J. A.* (1998): "Elastic analysis of raft foundations", Thomas Telford Ltd, 1 Heron Quay, London.
- [24] *Herrmann, R. and El Gendy, M.* (2014), "A layer equation method for 1-D consolidation under time-dependent reloading", Ain Shams Engineering Journal Volume 5, Issue 4, Pages 1043–1057.
- [25] *Hibbitt, Karlsson and Sorenson* (2008): "ABAQUS 6.8: A computer software for finite element analysis", *Hibbitt, Karlsson and Sorenson Inc.*, Rhode Island, USA.

- [26] *Itasca consulting group. FLAC* (2011): "Fast Lagrangian Analysis of Continua", Minneapolis, MN, US.
- [27] *Kany, M.* (1974): "Berechnung von Flächengründungen", 2. Auflage Verlag Ernst & Sohn, Berlin.
- [28] *Kany, M., El Gendy M. and El Gendy A.* (2008): "Analysis and Design of Slab Foundations by FE-Method- Program *ELPLA 9.2*". GEOTEC Software, Zirndorf, Germany.
- [29] *Kukreti, A. & Siddiqi, Z.* (1997): "Analysis of fluid storage tanks including foundation-superstructure interaction using differential quadrature method". *Appl. Math. Modeling* 1997, 21:193-205, April.
- [30] *Kukreti, A., Zaman, M. and Issa, A.* (1993): "Analysis of fluid storage tanks including foundation-superstructure interaction". *Appl. Math. Modelling* 1993, Vol. 17, December.
- [31] [Mathworld.wolfram.com](http://mathworld.wolfram.com)
- [32] *Melerski, E. S.* (1991), "Simple elastic analysis of axisymmetric cylindrical storage tanks", *Journal of Structural Engineering*, Vol. 117, No. 11, Pages 3239-3260.
- [33] *Melersky, E.* (2006): "Design analysis of beams, circular plates and cylindrical tanks on elastic foundations – 2nd edition". Taylor & Francis group, London, UK.
- [34] *Mistriková, Z & Jendželovský, N* (2012): "Static analysis of the cylindrical tank resting on various types of subsoil", *Journal of civil engineering and management*, Vol. 18(5): 744-751.
- [35] *Mobarak, W.* (2010): "Effect of Tie Girders on Piled Footing in Port Said", M.Sc. Thesis, Faculty of Engineering, Suez Canal University.
- [36] *Monideepa, P., Sahu, R.B. and Biswas, S.K.* (2010): "An analytical study consolidation of soft clay under cyclic loading", Thesis paper for master degree, civil engineering department, Jadavpur university, Kolkata, India.
- [37] *NEXIS software* (2006): Software manual. 174 P.
- [38] *Nishida, Y.* (1956): "A brief note on compression index of soils". *Journal of SMFE Div., ASCE*, July, p 1027 (1-14).

-
- [39] *Ohde, J.* (1942): "Die Berechnung der Sohldruckverteilung unter Gründungskörpern Der Bauingenieur". Heft 14/16, S. 99-107 - Heft 17/18 S. 122-127.
- [40] *Ouria, A., and Toufigh, M. M.* (2008). "An approximate solution for consolidation of inelastic clays under rectangular cyclic loading." *J. App. Sci.*, 8(11), 2075–2082.
- [41] *Ouria, A., Desai C. S. and Toufigh, V.* (2015): "Disturbed State Concept–Based Solution for Consolidation of Plastic Clays under Cyclic Loading", *Int. J. Geomech.*, Vol. 15(1), 04014039.
- [42] *Pelli, F. and Carletti, A.* (1998): "Characterization of soft deposits in the Eastern Nile Delta", *Proceedings 1st Int. Conf. on Site Characterization – ISC'98*, Atlanta, USA, Vol. 1, pp. 257-262.
- [43] *Pelli, F. and Rossanese, A.* (2000): "Settlements of an Instrumented Landfill on Soft-Delta Soil with Vertical Wick Drains", *International Conference on Geotechnical & Geological Engineering – GeoEng 2000-*, Melbourne, Australia, November 2000.
- [44] *Percy, J. H., Pian, T. H. H., Klein, S., and Navaratna, D. R.* (1965): "Application of matrix displacement method to linear elastic analysis of shells of revolution." *AIAA Journal*, Vol. 3, No. 11, pp. 2138-2145.
- [45] *Razouki, S. S., Bonnier, P., Datcheva, M. and Schanz, T.* (2013): "Analytical solution for 1D consolidation under haversine cyclic loading", *Int. J. Numer. Anal. Meth. Geomech.*, DOI: 10.1002/nag.2188.
- [46] *Reda, A.*(2009): "Optimization of Reinforced Concrete Piled Raft", M.Sc. Thesis, Faculty of Engineering, Suez Canal University.
- [47] *Rockey, K. C., Evans, H. R., Griffiths, D. W. and Nethercot, D. A.* (1975): "The Finite Element Method- A Basic Introduction For Engineers", by Crosby Lockwood Staples, London.
- [48] *Samangany, A.Y., Naderi R., Talebpur M. H. and Shahabi H.* (2013): "Static and Dynamic Analysis of Storage Tanks Considering Soil-Structure Interaction", *International Research Journal of Applied and Basic Sciences*, Vol. 6(4), 515-532, 2013.
- [49] *Selvadurai, A.* (1979): "Elastic Analysis of Soil-Foundation Interaction" Elsevier Scientific Publishing Company, Amsterdam/ Oxford/ New York.

- [50] *Szilard, R., Ziesing and Pickhardt* (1986): "Basic- Programme für Baumechanik und Statik". Wilhelm Ernst und Sohn Verlag für Architektur und technische Wissenschaften, Berlin.
- [51] *Terzaghi, K., Peck, R.B. and Mesri, Gh.* (1996), "Soil mechanics in engineering practice", 3rd Ed., John Wiley, New York.
- [52] *Timoshenko, S. & Woinowsky-Krieger S.* (1959): "Theory of plates and shells". McGraw- Hill Book Co. Singapore.
- [53] *Toufigh, M.M., and Ouria, A.* (2009). "Consolidation of inelastic clays under cyclic loading." *Soil. Dyn. Earthquake Eng.*, 29(2), 356–363.
- [54] *Ventsel, E. and Krauthammer, T.* (2001): "Thin Plates and Shells: Theory, Analysis and Applications". Marcel Dekker, INC., New York.
- [55] *Vichare, S. & Inamdar, M.* (2010): "An analytical solution for cylindrical concrete tank on deformable soil", *International journal of advanced structural engineering*, Vol. 2, No. 1, Pages 71-93, Islamic Azad university, south Tehran branch.
- [56] *Wilson E. L., and Habibullah A.* (2003): "Structural Analysis Program *SAP* 2000, User's manual, Computers and Structures, Inc., Berkeley, California, U.S.A.
- [57] *Wilson, N. E., and Elgohary, M. M.* (1974). "Consolidation of clays under cyclic loading." *Can. Geotech. J.*, 11(3), 420–433.
- [58] www.wolframalpha.com/entities/plane_curves.
- [59] *Xie, K., Tian, Qi. and Dong, Y.* (2006), "Nonlinear analytical solution for one-dimensional consolidation of soft soil under cyclic loading", *J. Zh. Univ. Sci.*, 7(8), 1358-1364.
- [60] *Ya-Yuan Hu* (2010): "Long-term settlement of soft subsoil clay under rectangular or semi-sinusoidal repeated loading of low amplitude", *Canadian Geotechnical Journal* (47): 1259-1270.
- [61] *Yazdani, H. and Toufigh, M.M.* (2012), "Nonlinear consolidation of soft clays subjected to cyclic loading - Part I: theory", *Geomech. Eng.*, 4(4), 229-241.
- [62] *Yazdani, H. and Toufigh, M.M.* (2012), "Nonlinear consolidation of soft clays subjected to cyclic loading - Part II: Verification and application", *Geomech. Eng.*, 4(4), 243-249.

-
- [63] *Zaman, M. and Koragappa, N.* (1989): "Analysis of tank-foundation-half-space interaction using an energy approach". *Appl. Math. Modelling*, Vol. 13, February.
- [64] *Zhuang, Y., Xie, K. and Li, X.* (2005), "Nonlinear analysis of consolidation with variable compressibility and permeability", *J. Zh. Univ. Sci.*, 6(3), 181-187.
- [65] *Zhuang, Y. C. and Xie, K.* (2005): "Study on one-dimensional consolidation of soils under cyclic loading with varied compressibility", *J Zhejiang Univ. Sci.*,(6A): 141–7.
- [66] *Zienkiewicz, O. C. and Cheung, Y. K.* (1965): "Plates and Tanks on Elastic Foundations - an Application of Finite Element Method". *International Journal of Solids Structures* Vol. 1, pp. 451-461, Pergamon.
- [67] *Zienkiewicz, O. C. and Cheung, Y. K.* (1967): "The Finite Element Method in Structural and Continuum Mechanics". Berkshire, England, by McGraw-Hill Publishing Company Limited.
- [68] *Zienkiewicz, O. C. and Taylor, R. L.* (1967): "The Finite Element Method – Vol. 2: Solid Mechanics". Berkshire, England, by McGraw-Hill Publishing Company Limited.
- [69] *Zingoni, A.* (1997): "Shell Structures in Civil and Mechanical Engineering". Thomas Telford publisher, Thomas Telford services Ltd, 1 Heron Quay, London E14 4JD.

"سلوك الخزانات تحت التحميل الاستاتيكي والدوري"

ملخص الرسالة

تعتبر عملية الإنشاء في مشاريع الهندسة المدنية على التربة الانضغاطية المشبعة مثل الطين والطيني أمر لا مفر منه. المشكلة الكبرى التي تواجه الإنشاء على هذا النوع من التربة هو هبوط التدعيم، والذي يعد ظاهرة معتمدة على الزمن. أثناء عملية التدعيم تحدث تغيرات لخصائص التربة والتحميل المعتمد على الزمن مثل التحميل الدوري مما يؤثر على معدل وقيمة الهبوط.

غالباً ما تؤثر الأحمال الدورية على طبقات الطين أسفل المنشآت المعرضة لظروف تحميل وتفريغ مثل خزانات المياه الأرضية. أحد المشاكل التي تظهر في هذه الحالة هي مشكلة التحميل والهبوط المعتمدين على الزمن مع الأخذ في الاعتبار التوافق التام بين المنشأ والتربة. كذلك احتمالات حدوث شروخ في الخزانات مما يتنافى مع الغرض من إنشائها. لهذا السبب تم تقديم تحليل عددي مبني على نموذج عناصر محددة لقشريات أسطوانية لدراسة وتحليل الخزانات الدائرية المصنوعة من الخرسانة المسلحة. التحليل قادر على تمثيل خزانات دائرية تتركز على وسط من تربة متعددة الطبقات. بالإضافة إلى ذلك، تم وضع حل عددي لتربة متعددة الطبقات معرضة لإجهادات متغيرة التوزيع بعمق التربة. في أثناء التحليل، يكون تمثيل سلوك التربة أثناء عملية التدعيم إما خطي، أو شبه خطي، أو غير خطي. قاعدة الخزان يمكن اعتبارها جاسنة أو مرنة أو لينة. عند تحليل قاعدة الخزان كأساس مرن، يؤخذ في الاعتبار التوافق التام بين العناصر الإنشائية وتربة التأسيس.

كتطبيق عملي للتحليل المطور، أجريت دراسة بارامترية لدراسة سلوك الخزانات تحت المتغيرات والظروف المختلفة باستخدام بيانات التربة لجسات حقلية لمواقع حقيقية. هذه الدراسة تقدم المبادئ التوجيهية والمخططات للخزانات الدائرية المعرضة لأحمال ساكنة أو دورية والتي يمكن استخدامها في الأماكن التي تحتوي على مثل هذا النوع من التربة.

الرسالة هي دراسة علمية في موضوع التفاعل التبادلي بين المنشآت والتربة الطينية وتحتوي على سبعة أبواب على النحو التالي:

الباب الأول:

يحتوي على مقدمة عن البحث، والغرض منه، ومكوناته، مع عرض مشكلة الخزانات المرتكزة مباشرة على التربة.

الباب الثاني:

يعرض هذا الباب ملخص للأبحاث السابقة المتاحة عن هذا الموضوع، ويقدم فكرة عامة عن: نظريات تحليل القشريات المتماثلة محورياً، وتمثيل التفاعل التبادلي بين الأساس والتربة، ومراحل تطور تحليل القواعد الدائرية والخزانات المرتكزة على التربة، وأخيراً تدعيم الطين تحت تأثير الأحمال المرتبطة بالزمن والأحمال الدورية.

الباب الثالث:

يحتوي هذا الباب على النماذج الرياضية المستخدمة والتي تم تطويرها وتطبيقها في هذا البحث. ويشمل نموذج العناصر المحددة للقشريات الرقيقة المتماثلة محورياً لتمثيل جدار وقاعدة الخزان. كما يشمل أيضاً نماذج تمثيل التربة في التحليل. وأخيراً نموذج التربة المستخدم في تحليل الخزانات تحت تأثير الحمل الدوري. وقد تم استخدام برنامج *ELPLA 10* في عمليات التحليل في هذه الرسالة، وذلك بعد ما قام الباحث بإدخال الإضافات المقترحة بالنموذج الرياضي إلى البرنامج، وتشمل نموذج العناصر المحددة للقشريات الرقيقة المتماثلة محورياً، ونموذج التربة المستخدم في تحليل الخزانات تحت تأثير الحمل الدوري.

الباب الرابع:

وفيه يتم دراسة مجموعة من الأمثلة والتطبيقات ومقارنة نتائج التحليل للنموذج المقترح في هذا البحث مع النتائج المنشورة بالأبحاث السابقة، وذلك للتحقق من دقة طرق التحليل المقترحة.

الباب الخامس:

يحتوي هذا الباب على عرض وتحليل النتائج الخزانات الواقعة تحت تأثير الأحمال الساكنة، وتم عرض النتائج في منحنيات وجداول توضح تأثير المتغيرات المختلفة.

الباب السادس:

يحتوي هذا الباب على عرض وتحليل النتائج الخزانات المستديرة تحت تأثير الأحمال الدورية، وتم عرض النتائج في صورة منحنيات وجداول للعديد من حالات الدراسة تحت تأثير المتغيرات المختلفة.

الباب السابع:

يشتمل على ملخص البحث وخلاصة ما تم التوصل إليه من نتائج والتوصيات للبحوث المستقبلية.

سلوك الخزانات تحت التحميل الاستاتيكي والدوري

رسالة مقدمة

للحصول على درجة الماجستير في الهندسة المدنية

إعداد

م / عمر محمد مسعد الجندي

أجيزت بواسطة

أ.د/ مصطفى كامل متولي زيدان

أستاذ الهندسة الإنشائية المتفرغ بكلية الهندسة، جامعة عين
شمس.

أ.د/ إبراهيم حسن علي القرش

أستاذ المنشآت المعدنية وعميد كلية الهندسة، جامعة قناة
السويس

أ.د/ كمال محمد حافظ إسماعيل

أستاذ ميكانيكا التربة والأساسات، وكيل كلية الهندسة
لشئون البيئة وخدمة المجتمع، جامعة قناة السويس.

د/ إبراهيم أحمد أحمد العربي

استاذ مساعد الهندسة الإنشائية بكلية الهندسة، جامعة
بورسعيد

2016

سلوك الخزانات تحت التحميل الاستاتيكي والدوري

رسالة مقدمة

للحصول على درجة الماجستير في الهندسة المدنية

إعداد

م / عمر محمد مسعد الجندي

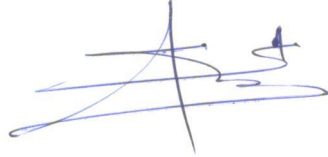
تحت إشراف

د/ إبراهيم أحمد أحمد العربي

أ.د/ إبراهيم حسن علي القرش

أستاذ مساعد الهندسة الإنشائية بقسم
الهندسة كلية الهندسة بجامعة بورسعيد

أستاذ المنشآت المعدنية بقسم الهندسة المدنية
عميد كلية الهندسة بجامعة قناة السويس





جامعة بورسعيد



كلية الهندسة
قسم الهندسة المدنية

سلوك الخزانات تحت التحميل الاستاتيكي والدوري

إعداد

عمر محمد مسعد الجندي

بكالوريوس الهندسة المدنية

كلية الهندسة، جامعة قناة السويس، 2008

رسالة مقدمة

للحصول على درجة الماجستير في الهندسة المدنية

تحت إشراف

د/ إبراهيم أحمد أحمد العربي

أستاذ مساعد الهندسة الإنشائية بقسم الهندسة
المدنية، كلية الهندسة بجامعة بورسعيد

أ.د/ إبراهيم حسن علي القرش

أستاذ المنشآت المعدنية بقسم الهندسة المدنية
عميد كلية الهندسة بجامعة قناة السويس

2016